

**Functional Characterization of Target Genes within Causal
Genomic Loci of Hepatocellular Carcinoma**

CHENG, Kit Chong Ibis

A Thesis Submitted in Partial Fulfilment of
the Requirements for the Degree of
Doctor of Philosophy
in
Anatomical & Cellular Pathology

The Chinese University of Hong Kong

May 2011

UMI Number: 3497767

All rights reserved

INFORMATION TO ALL USERS

The quality of this reproduction is dependent on the quality of the copy submitted.

In the unlikely event that the author did not send a complete manuscript and there are missing pages, these will be noted. Also, if material had to be removed, a note will indicate the deletion.



UMI 3497767

Copyright 2012 by ProQuest LLC.

All rights reserved. This edition of the work is protected against unauthorized copying under Title 17, United States Code.



ProQuest LLC.
789 East Eisenhower Parkway
P.O. Box 1346
Ann Arbor, MI 48106 - 1346

Abstract of thesis entitled:

Functional Characterization of Target Genes within Causal Genomic Loci of Hepatocellular Carcinoma.

Submitted by: CHENG, Kit Chong Ibis

for the degree of Doctor of Philosophy in Anatomical And Cellular Pathology

at The Chinese University of Hong Kong (January 2011)

Abstract

Hepatocellular carcinoma (HCC) is a highly malignant tumor that is associated with a high incidence of cancer morbidity and mortality. Elucidation of genomic aberrations of HCC holds much importance in understanding the molecular basis that underlies the disease causation and progression. Extensive research on HCC has by now revealed a number of key genomic aberrations but, for most of these loci, the underlying cancer-related gene(s) remains unknown.

In this thesis, array-based comparative genomic hybridization (array-CGH) was deployed to define target genes within HCC-associated chromosomal regions. The first part of my study focused on mapping the homozygous deletions (HDs) in HCC. Though infrequent, HD screening has been widely utilized to define tumor suppressor genes (TSGs) in cancers. A panel of HCC cell lines was systematically examined for the presence of HDs. Array-CGH identified 6 HD regions, amongst which *CRYLI* (located on chr.13q12.11) displayed most common down-regulations in primary HCC tumors. Significant associations could also be drawn between repressed *CRYLI* and advanced tumor staging, increased tumor size and shorter disease-free patient survival ($P \leq 0.037$). Moreover, HD on *CRYLI* could be detected

in 36% of HCC cases with *CRYL1* down-regulations. Examination of other inactivating mechanisms suggested histone deacetylation and promoter hypermethylation to be likely inactivating events as well. Re-expression of *CRYL1* in SK-HEP1 cell line induced profound inhibition on cellular proliferation and cell growth ($P \leq 0.002$). By Annexin V staining, *CRYL1* restoration readily increased pro-apoptotic cells with an induction of PARP cleavage. Flow cytometry further revealed *CRYL1* could prolong the G₂-M phase, possibly through interrupting the Cdc2/cyclin B path.

Array-CGH also defined candidate proto-oncogenes within 2 causal amplified regions in HCC, chr.8q24 and chr.1q21-q22. In resolving affected genes at chr.8q24, distinctive gains of *BOP1* was further established in primary HCC tumors, where frequent *BOP1* up-regulations in tumors compared to adjacent non-tumoral liver ($P < 0.0001$) was identified. Increased *BOP1* expression correlated with advanced HCC staging ($P = 0.004$), micro-vascular invasion ($P = 0.006$) and shorter overall and disease free survival of patients ($P < 0.02$). siRNA-mediated suppression of *BOP1* in HCC cell lines showed significant inhibition on cell invasion ($P < 0.003$) and migration ($P < 0.05$), whereas overexpression of *BOP1* in immortalized hepatocyte cell line, L02, showed increase cellular invasiveness and cell migratory rate ($P < 0.0001$). Evident regression of the Epithelial-to-Mesenchymal Transition (EMT) phenotype was readily identified in *BOP1* knockdown cells, where re-expressions of epithelial markers (E-cadherin, cytokeratin 18 and γ -catenin) and down-regulation of mesenchymal markers (fibronectin and vimentin) were found. It was found that *BOP1* likely stimulates actin stress fibers assembly through RhoA activation.

Amplification of chr.1q21-22 is also an aberration frequently detected in HCC. Copy number gains of the *GEF-H1* gene ranked the most frequent event from array-

CGH. *GEF-H1* up-regulation was significantly correlated in patients with advanced HCC staging ($P = 0.048$), presence of micro-vascular invasion ($P = 0.049$) and shorter overall and disease free survival of patients ($P < 0.03$). Similar to *BOPI*, functional examinations of *GEF-H1* suggested profound inhibitory effects on cell motility ($P < 0.035$) and invasiveness ($P < 0.003$) in cell lines studied. Upon *GEF-H1* depletion, re-expression of epithelial markers (E-cadherin, cytokeratin 18, α -catenin and γ -catenin) and down-regulations of mesenchymal markers (N-cadherin, fibronectin and vimentin) were also readily observed. In addition, reduced active form of GTP-RhoA together with its downstream effectors including cleaved ROCK1 and phosphorylated MLC2 were also found in *GEF-H1* depleted cells.

The similarities in functional behaviours of *BOPI* and *GEF-H1* might have implications in the fundamental biology of HCC tumorigenesis. It is known that HCC is a highly aggressive tumor often associated with intra- and extra-hepatic metastasis. The finding of 2 causal changes to be closely associated with cell migration and invasiveness may have implications in the metastatic potentials of HCC cells being predisposed earlier on from genomic events.

摘要

肝細胞癌 (HCC) 是一種具有高發病率和高死亡率特徵的高度惡性腫瘤。

剖析 HCC 中染色體異常對於理解其起因和發展的分子機制有著重要作用。隨著對 HCC 的深入研究，一系列關鍵的染色體異常位點已被發現，但是潛在於其中大部份異常位點的癌癥相關基因仍有待進一步研究。

在本論文中，使用陣列比較基因組雜交技術 (array-CGH) 探尋與 HCC 相關染色體區域中的目的基因。本研究的第一部份主要是描述 HCC 的純合性缺失 (HD)。儘管 HD 發生率不高，但在癌癥研究中，HD 篩選已被廣泛應用於確認腫瘤抑制基因 (TSG)。本研究首先使用 array-CGH 系統性地檢查了一組 HCC 細胞株中基因組 HD 存在的情況，並識別了 6 個 HD 區域。其中 *CRYLI* (位於 13 號染色體 q12.11) 的表達下調在原發性 HCC 中最為常見，而且它的表達下調與腫瘤的進展分期 (第三期)，增大的腫瘤體積及較短的無病生存期有著顯著相關性 ($P \leq 0.037$)。另外，在 *CRYLI* 表達下調的 HCC 中，36% 的病例發現 *CRYLI* 的位點帶有 HD。本研究更發現，組蛋白去乙酰化和啟動子的超甲基化亦可能是導致 *CRYLI* 表達下調的原因。在 SK-HEP1 細胞中過表達 *CRYLI* 可抑制細胞增殖和生長 ($P \leq 0.0015$)。膜聯蛋白 (Annexin V) 染色的結果表明 *CRYLI* 的重新表達能夠促進細胞凋亡，這與它能誘導 PARP 蛋白剪切有關。此外，流式細

胞儀分析進一步發現 *CRYL1* 的表達能夠延長細胞的 G₂-M 期，可能是通過影響 Cdc2/cyclin B 的信號通路。

同時，本論文亦通過 array-CGH 分析探討可能存在於兩個 HCC 染色體擴增區域(chr.8q24 和 chr.1q21-q22)中的原癌基因。在分析位於 chr.8q24 上的異常基因時，發現 *BOPI* 有著很明顯的拷貝數增加，並進一步證實 *BOPI* 在原發性 HCC 中顯著上調 ($P < 0.0001$)。統計分析表明 *BOPI* 的高表達與 HCC 的進展分期(第三期) ($P = 0.004$)，微血管侵犯 ($P = 0.006$)，和較短總生存期及無病生存期 ($P < 0.02$) 顯著相關。在 HCC 細胞系中運用 siRNA 下調 *BOPI* 的表達能夠明顯抑制細胞的侵襲 ($P < 0.003$)及遷移能力 ($P < 0.05$)。在永生化肝細胞株 L02 中，高表達 *BOPI* 亦能夠顯著增加細胞侵襲性及遷移能力 ($P < 0.0001$)。*BOPI* 基因被抑制的細胞的上皮細胞間質轉化 (Epithelial-to-Mesenchymal Transition (EMT)) 現象明顯減弱，表現為上皮性標記物 (E-cadherin, cytokeratin 18 和 γ -catenin) 的表達上調及間質性標記物 (fibronectin 和 vimentin) 的表達下調。*BOPI* 可能是透過活化 GTP-RhoA，從而促進肌動蛋白應力纖維的聚合。

Chr.1q21-22 的擴增也是 HCC 中一種很常見的基因異常。在 array-CGH 分析中，*GEF-H1* 基因拷貝數的增加在該異常染色體區域中最高為常見。*GEF-H1* 表達的上調與 HCC 病人的腫瘤分期(第三期) ($P = 0.048$)，微血管侵襲 ($P =$

0.049)，和較短總生存期及無病生存期 ($P < 0.03$) 顯著相關。與 *BOP1* 的功能相類似，*GEF-H1* 表達下調證實能夠持續抑制細胞的遷移 ($P < 0.035$) 和侵襲能力 ($P < 0.005$)。在 *GEF-H1* 缺失的情況下，亦觀察到 EMT 現象的減弱包括上皮性標記物 (E-cadherin, cytokeratin 18 和 γ -catenin) 的表達上調及間質性標記物 (N-cadherin, fibronectin 和 vimentin) 的表達下調。另外，在 *GEF-H1* 缺失的細胞中，活化形式的 GTP-RhoA 及其下游的效應子包括 ROCK1 的剪切體和磷酸化的 MLC2 均被發現表達有所減少。

BOP1 與 *GEF-H1* 功能上的相似提示了這兩者在 HCC 的發展中有著重要的功能。眾所周知，HCC 是高度侵襲性的腫瘤，常伴有肝內及肝外的轉移。這兩個基因的異常均被證實與細胞的遷移和侵襲能力有著密切的關係，暗示了其可能賦予 HCC 早期癌細胞轉移的潛能。

Acknowledgement

First, I would like to express my deepest thanks to my thesis supervisor, Prof Nathalie Wong for her patient guidance throughout my PhD training. I am grateful for the opportunities provided, these not only help me to develop the right attitude and responsibility in my daily work, but also enhance my critical thinking on scientific matters. I truly thank for all the time and effort she spent on supervising me.

I would like to acknowledge all the past and present laboratory members for making the working environment friendly and interactive that I really enjoy every moment in the laboratory. Many thanks to Dr Arthur KK Ching, Dr Erwin TC Chan, Dr Amy KY Chung, Dr KP Lei, Dr. Queenie WL Wong, Dr JH Chu, Dr WK Ip, Ms Priscilla TY Law, Mr CC Lau, Ms Emily PS Pang, Mr. Bruce CK Tsang, Mr Alfa HC Bai, Mr Wilson KC Leung, Mr Gary JW Chen, Ms PS Li and Ms Vanessa TI Fung, Ms Effic M He, Ms Navy LY Wong and Ms Joyce BS Yuen for their help and support during my study. Special thanks go to Dr Anthony WH Chan for his help in collecting patients' clinical data. I would also like to show my thanks towards the professors, lecturers and all the supporting staff at the Department of Anatomical and Cellular Pathology and Cancer Centre at PWH, who have assisted and helped me a lot throughout these years.

Last but not least, I would like to express my deepest gratitude to my beloved family members, Ting-Fai Cheng, and friends for all their mortal support and encouragement especially during difficult times.

Publications

Publications arising from thesis

1. Cheng IK, Ching AK, Chan TC, Chan AW, Wong CK, Choy KW, Kwan M, Lai PB, Wong N. Reduced *CRYLI* expression in hepatocellular carcinoma confers cell growth advantages and correlates with adverse patient prognosis. *J Pathol* 2010. **220**:348-60.
2. *Chung KY, *Cheng IK, Ching AK, Chu JH, Lai PS, Wong N. Over-expression of *BOP1* correlates with metastatic potential and poor prognostic outcome in hepatocellular carcinoma. *Hepatology* 2011. [*Epub ahead of print*]
3. Cheng IK, Lai KB, Tseung CK, Ching AK, Lai PS, Wong N. Frequent over-expression of *GEF-H1* promotes EMT and enhances cell motility in hepatocellular carcinoma. [manuscript in preparation]

Table of content

Abstract	II
摘要	V
Acknowledgement	VIII
Publications	IX
Table of content	X
List of Figures	XIV
List of Tables	XVII
Abbreviations	XVIII
CHAPTER 1 INTRODUCTION	1
1.1 ETHIOLOGICAL FACTORS	7
1.1.1 <i>Liver cirrhosis</i>	10
1.1.2 <i>Hepatitis B viral infection (HBV)</i>	11
1.1.3 <i>Hepatitis C viral infection (HCV)</i>	15
1.1.4 <i>Chronic alcohol consumption</i>	19
1.1.5 <i>Aflatoxin B1 exposure</i>	20
1.1.6 <i>Male gender</i>	23
1.1.7 <i>Obesity, Type 2 Diabetes and Non-Alcoholic Steatohepatitis (NASH)</i>	24
1.2 CHROMOSOMAL ABERRATIONS	26
1.2.1 <i>Gain of chr. 1q</i>	30
1.2.2 <i>Gain of chr. 8q</i>	32
1.3 STUDY AIMS	34
CHAPTER 2 MATERIALS AND METHODS	36
2.1 MATERIALS.....	37
2.1.1 <i>Chemicals and Reagents</i>	37
2.1.2 <i>Buffers</i>	39
2.1.3 <i>Cell Culture</i>	40

2.1.4	<i>Nucleic Acids</i>	41
2.1.5	<i>Enzymes</i>	42
2.1.6	<i>Equipments</i>	42
2.1.7	<i>Kits</i>	43
2.1.8	<i>Antibodies</i>	44
2.1.9	<i>Softwares</i>	45
2.1.10	<i>Web Resources</i>	45
2.2	CELL LINES.....	46
2.3	PATIENTS.....	48
2.4	ARRAY-CGH.....	49
2.4.1	<i>Preparation of genomic DNA</i>	49
2.4.2	<i>Restriction enzyme digestion and genomic DNA labeling</i>	50
2.4.3	<i>Hybridization and washing</i>	50
2.4.4	<i>Feature extraction and data analysis</i>	51
2.5	PCR VALIDATION OF HD GENES.....	55
2.6	EXPRESSION ANALYSIS BY QUANTITATIVE RT-PCR.....	58
2.6.1	<i>Total RNA extraction from cell lines and tumors</i>	58
2.6.2	<i>qRT-PCR analysis for gene expression</i>	58
2.7	FUNCTIONAL ANALYSIS.....	63
2.7.1	<i>Evaluation of transfection efficiency of the HCC cell lines</i>	63
2.7.2	<i>Sub-cloning</i>	67
2.7.3	<i>Cycle sequencing</i>	70
2.7.4	<i>Cell viability (MTT) and cell proliferation assays (BrdU-incorporation)</i>	72
2.7.5	<i>Colony formation assay</i>	73
2.7.6	<i>Apoptosis assay</i>	73
2.7.7	<i>Cell-cycle analysis</i>	74
2.7.8	<i>Invasion and migration assay</i>	75
2.7.9	<i>Wound healing assay</i>	76
2.8	IMMUNO-FLUORESCENT IMAGING.....	77
2.9	WESTERN BLOT.....	79
2.10	NORTHERN BLOT.....	81
2.11	METHYLATION-SPECIFIC PCR (MSP).....	82
2.12	5-AZA-2'-DEOXYCYTIDINE (5-AZA) AND TRICHOSTATIN A (TSA) TREATMENTS.....	84

2.13	GTPASE ACTIVITY ASSAYS OF RHOA, RAC1 AND CDC42.....	85
2.14	STATISTICAL ANALYSIS	86
CHAPTER 3	ARRAY-CGH DEFINES HOMOZYGOUS DELETIONS IN HCC AND CRYL1 AS A NOVEL TUMOR SUPPRESSOR GENE	87
3.1	INTRODUCTION	88
3.2	RESULTS	90
3.2.1	<i>Array-CGH defined HD regions</i>	90
3.2.2	<i>Functional effects of CRYL1</i>	99
3.2.3	<i>Effect of CRYL1 on cell-cycle</i>	101
3.2.4	<i>Inactivating mechanisms of CRYL1</i>	105
3.3	DISCUSSION	109
CHAPTER 4	BOP1 PLAYS AN ONCOGENIC ROLE IN HCC BY PROMOTING EMT	113
4.1	INTRODUCTION	114
4.2	RESULTS	116
4.2.1	<i>BOP1 is frequently up-regulated in HCC</i>	116
4.2.2	<i>Prognostic value of BOP1</i>	120
4.2.3	<i>Functional role of BOP1 in cell migration and invasion</i>	123
4.2.4	<i>BOP1 promotes HCC cell motility through EMT induction</i>	127
4.3	DISCUSSION	135
CHAPTER 5	FREQUENT OVER-EXPRESSION OF GEF-H1, ON CHR.1q22, PROMOTES EMT AND ENHANCES CELL MOTILITY IN HCC	138
5.1	INTRODUCTION	139
5.2	RESULTS	143

5.2.1	<i>GEF-H1 is frequently up-regulated in HCC</i>	143
5.2.2	<i>Prognostic value of GEF-H1</i>	147
5.2.3	<i>Functional studies of GEF-H1 upon GEF-H1 depletion by siRNA</i>	151
5.2.4	<i>GEF-H1 depletion restores the epithelial phenotype of HCC cells through reversing EMT process</i>	156
5.2.5	<i>GEF-H1 depletion abolishes Rho pathway activation and inhibits stress fibre formation</i>	162
5.3	DISCUSSION	168
 CHAPTER 6 CONCLUSIONS AND PROPOSED FUTURE STUDIES....		173
 CHAPTER 7 REFERENCES		176

List of Figures

Figure 1.1	Global incidence and mortality rate of HCC.....	4
Figure 1.2	Incidence and mortality frequency of top 10 cancers in Hong Kong in year 2007.....	5
Figure 1.3	Worldwide distribution of liver cancer incidence estimated in year 2008.....	6
Figure 1.4	Schematic representation of liver carcinogenesis.....	8
Figure 1.5	Representative photographs of pathologic section of liver.....	9
Figure 1.6	Hepatitis B Virus.....	14
Figure 1.7	Hepatitis C Virus.....	18
Figure 1.8	Metabolic conversion of aflatoxin B1 to the 8,9-epoxide and subsequent DNA adduct formation.....	22
Figure 1.9	Summary of CGH imbalances in HCC.....	28
Figure 1.10	Proposed evolutionary changes in the HCC carcinogenetic pathway.....	29
Figure 2.1	Procedural overview of array-CGH.....	53
Figure 2.2	Representative Cy3 and Cy5 labeled microarray images of HCC cell line HKCI-1.....	54
Figure 2.3	Agarose gel (1%) electrophoresis of total RNAs from HCC cell lines.....	61
Figure 2.4	Transfection efficiency of Hep3B, SK-HEP1 and L02 cell lines.....	65
Figure 3.1	Array-CGH analysis on SK-HEP1 and HKCI-9.....	93
Figure 3.2	Genomic validation of homozygous deleted candidates.....	94
Figure 3.3	Examples of Amp/Cycle Graph from qRT-PCR analysis.....	95
Figure 3.4	Relative expression of candidate HD genes.....	96
Figure 3.5	Frequent down-regulation of <i>CRYLI</i> in HCC cell lines and primary tumors.....	97
Figure 3.6	Frequent down-regulation of <i>CRYLI</i> in HCC cell lines and primary tumors.....	98
Figure 3.7	Functional effects of <i>CRYLI</i> on cell growth and proliferation..	100
Figure 3.8	Functional effects of <i>CRYLI</i> on cell-cycle arrest.....	103
Figure 3.9	Functional effects of <i>CRYLI</i> on apoptotic pathway.....	104

Figure 3.10	Genomic loss of <i>CRYLI</i>	107
Figure 3.11	Epigenetic inactivation of <i>CRYLI</i>	108
Figure 4.1	Array CGH analysis on chr.8q24.....	117
Figure 4.2	Over-expression of <i>BOP1</i> in HCC.....	118
Figure 4.3	Clinicopathologic correlations of <i>BOP1</i> expression in HCC...	119
Figure 4.4	Clinicopathologic correlations of <i>C-MYC</i> expression in HCC..	121
Figure 4.5	Functional effects of <i>BOP1</i> on Hep3B cell migration and invasion.....	124
Figure 4.6	Functional effects of <i>BOP1</i> on HKCI-9 cell migration and invasion.....	125
Figure 4.7	Ectopic expression of <i>BOP1</i> in immortalized liver cell line, L02.....	126
Figure 4.8	Effect of <i>BOP1</i> on rRNA maturation in HCC.....	130
Figure 4.9	<i>BOP1</i> promotes HCC motility through EMT.....	131
Figure 4.10	<i>BOP1</i> reduces the expression of cytokeratin 18.....	132
Figure 4.11	<i>BOP1</i> induced stress fibre formation.....	133
Figure 4.12	<i>BOP1</i> induces stress fibres formation and HCC motility through RhoA.....	134
Figure 5.1	Genetic map of YAC and PAC clones on chr.1q21-q25.....	141
Figure 5.2	Mapping analysis on HCC cases displaying chr.1q21-22 amplicon.....	143
Figure 5.3	Array-CGH analysis of chromosome 1 on Primary HCC.....	145
Figure 5.4	<i>GEF-HI</i> is frequently up-regulated in HCC.....	146
Figure 5.5	Kaplan-Meier analysis of <i>GEF-HI</i> expression in HCC.....	149
Figure 5.6	<i>GEF-HI</i> expression of Hep3B and SK-HEP1 cells in knockdown experiments.....	152
Figure 5.7	mRNA suppression of <i>GEF-HI</i> inhibits the cell invasiveness and cell migratory ability in Hep3B and SK-HEP1.....	153
Figure 5.8	Wound healing assay suggested mRNA suppression of <i>GEF-HI</i> inhibits cell migratory ability in Hep3B and SK-HEP1.....	154

Figure 5.9	mRNA suppression of <i>GEF-H1</i> does not affect the cell viability and cell proliferation in Hep3B and SK-HEP1.....	155
Figure 5.10	Western blot of EMT markers upon <i>GEF-H1</i> depletion.....	158
Figure 5.11	Immuno-fluorescence images of mesenchymal markers in <i>GEF-H1</i> knockdown experiment.....	159
Figure 5.12	Immuno-fluorescence images of epithelial markers in <i>GEF-H1</i> knockdown experiment.....	160
Figure 5.13	Decreased in mRNA and protein levels of E-cadherin transcription repressors were observed in Hep3B and SK-HEP1 cells upon <i>GEF-H1</i> depletion by qRT-PCR.....	161
Figure 5.14	The effect on GTPase guanine nucleotide binding status of RhoA, Rac1 and Cdc42 upon <i>GEF-H1</i> depletion in Hep3B and SK-HEP1.....	165
Figure 5.15	The effect on the downstream effectors of RhoA in Hep3B and SK-HEP1 upon <i>GEF-H1</i> depletion.....	166
Figure 5.16	Inhibition of stress fibre formation upon <i>GEF-H1</i> depletion....	167
Figure 5.17	Regulation of RhoA activity through GEF-H1 (RhoGEF) and DLC1 (RhoGAP).....	172

List of Tables

Table 2.1	Cell lines studied in various Chapters.....	47
Table 2.2	Primer sequences for the candidate HD targets as defined by array-CGH.....	56
Table 2.3	Primer sequences for exons 1 to 9 of <i>CRYLI</i>	57
Table 2.4	TaqMan assays for genes expression analysis by qRT-PCR....	62
Table 2.5	Transfection efficiency of cell lines.....	66
Table 2.6	Primer sequences for <i>CRYLI</i> and <i>BOPI</i> sub-cloning.....	69
Table 2.7	Primer sequences for <i>CRYLI</i> and <i>BOPI</i> cycle sequencing.....	71
Table 2.8	Primary antibodies for immune-fluorescence microscopy.....	78
Table 2.9	Primary antibodies for Western blot.....	80
Table 2.10	Primer sequences for MSP on <i>CRYLI</i> promoter region.....	83
Table 3.1	Candidate homozygous deleted targets as defined by array-CGH.....	92
Table 4.1	Multivariate Cox regression analysis of <i>BOPI</i> and <i>C-MYC</i> expressions in HCC.....	122
Table 5.1	Candidate genes showing frequent copy number gain from array-CGH analysis.....	144
Table 5.2	Clinicopathological correlations of <i>GEF-HI</i> expression in HCC.....	148
Table 5.3	Multivariate Cox regression analysis of <i>GEF-HI</i> expression in HCC.....	150

Abbreviations

°C	Degree Celsius
Array-CGH	Array-based Comparative Genomic Hybridization
AJCC	American Joint Committee on Cancer
AL	Allelic loss
ATCC	American Type Culture Collection
bp	Basepair
BrdU	5-bromo-2'-deoxyuridine
cDNA	Complementary DNA
CDS	Coding sequence
Chr.	Chromosome
cm	centimetre
Ct	Threshold cycle
Cy3	Cyanine 3
Cy5	Cyanine 5
DAPI	4',6-diamidino-2-phenylindole
DNA	Deoxy- ribonucleic acid
dNTP	Deoxy-nucleotide Trisphosphate
dUTP	Deoxy-uracil Trisphosphate
<i>E.coli</i>	Escherichia coli
ECL	Enhanced chemiluminescence
EMT	Epithelial-to-Mesenchymal Transition
EtBr	Ethidium bromide
FISH	Fluorescence <i>in situ</i> hybridization
FITC	Fluorescein isothiocyanate
GAPDH	Glyceraldehyde-3-phosphate dehydrogenase
GFP	Green fluorescence protein
HBV	Hepatitis B virus
HCC	Hepatocellular carcinoma
HCV	Hepatitis C virus
HD	Homozygous deletion
hr	Hour
JCRB	Japanese Collection of Research Bioresources
kb	Kilobase
kDa	Kilo dalton
M	Molar
mA	Milliampere
Mb	Megabase
mg	Milligram
min	Minute
ml	Milliliter
mM	Millimolar
mm	Millimetre

mRNA	Messenger ribonucleic acid
MTT	3-[4,5-dimethylthiazol-2-yl]-2,5-diphenyl tetrazolium bromide
ng	Nanogram
nM	Nanomolar
nm	Nanometre
nt	Nucleotide
ORF	Open reading frame
PCR	Polymerase chain reaction
PI	Propidium iodide
qPCR	Quantitative polymerase chain reaction
qRT-PCR	reverse transcription polymerase chain reaction
RNA	Ribonucleic acid
rpm	Rotation per minute
rRNA	Ribosomal RNA
RT	Reverse transcription
SDS-PAGE	Sodium dodecyl sulfate polyacrylamide gel electrophoresis
sec	Second
siRNA	Small interfering RNA
TRITC	Tetramethylrhodamine isothiocyanate
TSG	Tumor suppressor gene
U	Unit activity
V	Volt
µg	Microgram
µJ	Microjoule
µl	Microliter
µM	Micromolar

Chapter 1

Introduction

1. INTRODUCTION

Hepatocellular carcinoma (HCC) accounts 85-90% of all primary liver cancers and is one of the most common malignancies worldwide (El-serag HB *et al*, 2007). It currently ranks the third most common cause of cancer-related deaths (Ferlay J *et al*, 2010) (Figure 1.1). HCC is also considerably more common in men than women with an incidence ratio of 2.4:1 (Ferlay J *et al*, 2010). In Hong Kong, HCC is the fourth common cancer and the third leading cause of cancer mortalities (Figure 1.2). There is a male to female ratio of 3.4:1, with an incidence to mortality ratio is 1:0.85 (HK Cancer registry 2007, Hospital Authority). Despite recent advances in the diagnosis and treatment of HCC, the disease prognosis remains dismal with overall survival rate of 3-5%.

The adverse clinical prognosis is largely attributed to the majority of patients not being diagnosed in time for curative surgery. By the time of clinical presentation, most HCC tumors are in the advanced inoperable stages (Teo EK *et al*, 2001). Both intrahepatic and extrahepatic metastases are major factors contributing to the inferior prognosis in HCC patients. The lethality of HCC also stems in part from its resistance to the existing anticancer agents, a lack of biomarkers that can detect early disease and underlying liver disease that limits the use of chemotherapeutic drugs. Multikinase inhibitor sorafenib with antiangiogenic and antiproliferative properties is the first agent to demonstrate a statistically significant improvement in overall survival of HCC patients (from 7.9 months to 10.7 months) (Llovet JM *et al*, 2008; Di Lorenzo G *et al* 2010). However, surgical tumor resection or liver transplantation remains the most effective treatment option for HCC, but few patients are suitable for operative intervention.

The HCC incidence has a distinct geographic distribution (Figure 1.3). More

than 80% of the HCC cases occur in developing countries especially in Southeast Asia and sub-Saharan Africa. However, HCC incidence has been shown to rise in Western countries where the incidence rates increased by more than 2-fold between 1985 and 2002 (El-serag HB *et al*, 2007).

The approval of sorafenib as the first effective drug for HCC represents a milestone in HCC treatment, however, the short patient survival rate (~11 months) still urges for a better understanding on the liver tumorigenesis and development of more efficacious therapies based on target identifications from improved molecular genetic studies.

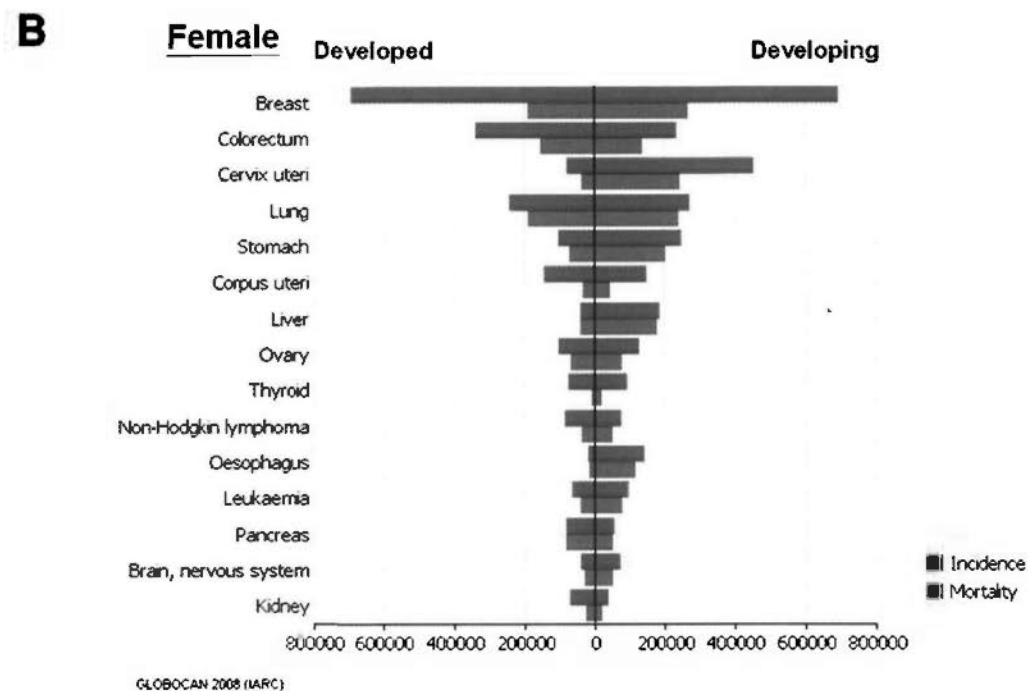
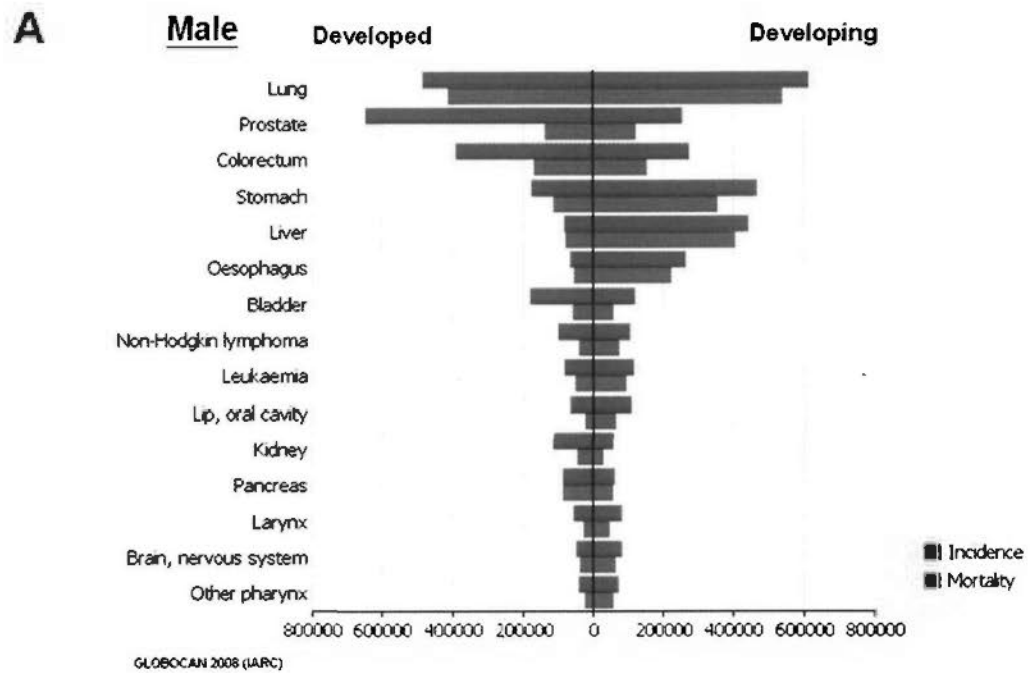
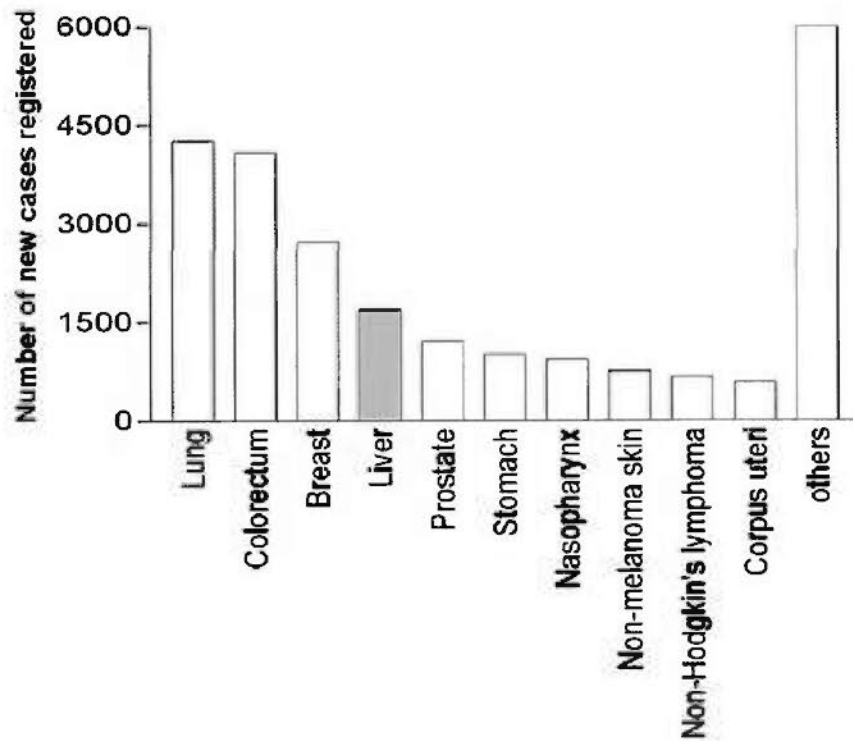


Figure 1.1 Global incidence and mortality rate of HCC

Estimated numbers (thousands) of new cancer cases (incidence) and deaths (mortality) in male (A) and in female (B) in developed and developing regions of the world in 2008 (GLOBOCAN2008).

A 10 most common Cancers in Hong Kong (2007)



B 10 major causes of cancer death in Hong Kong (2007)

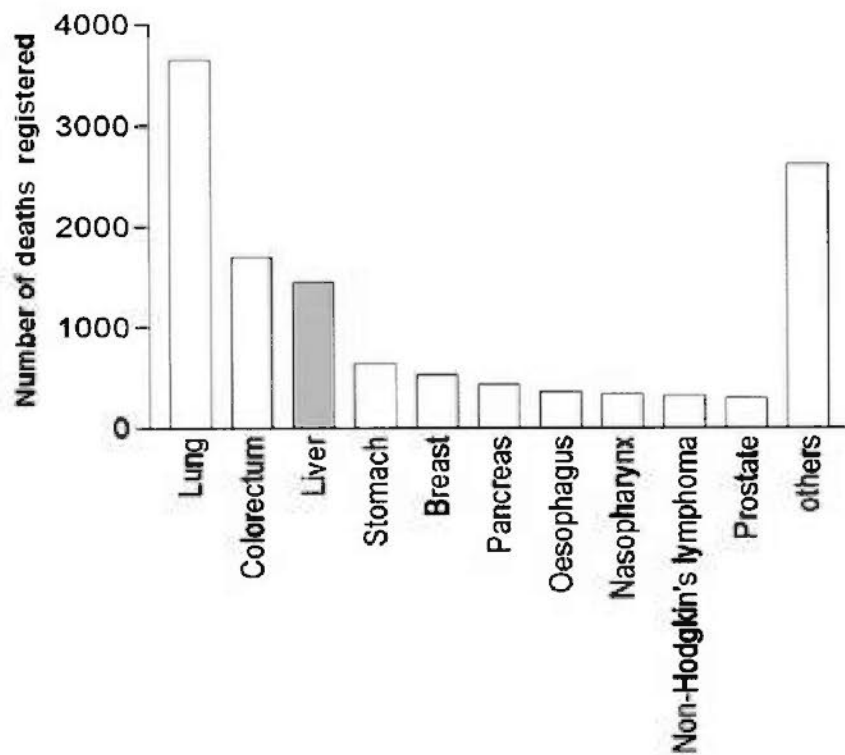


Figure 1.2 Incidence and mortality frequency of top 10 cancers in Hong Kong in year 2007

Information obtained from The Hong Kong Cancer Registry, Hospital Authority.

**Estimated age-standardized incidence rate per 100,000
Both sexes. all ages**

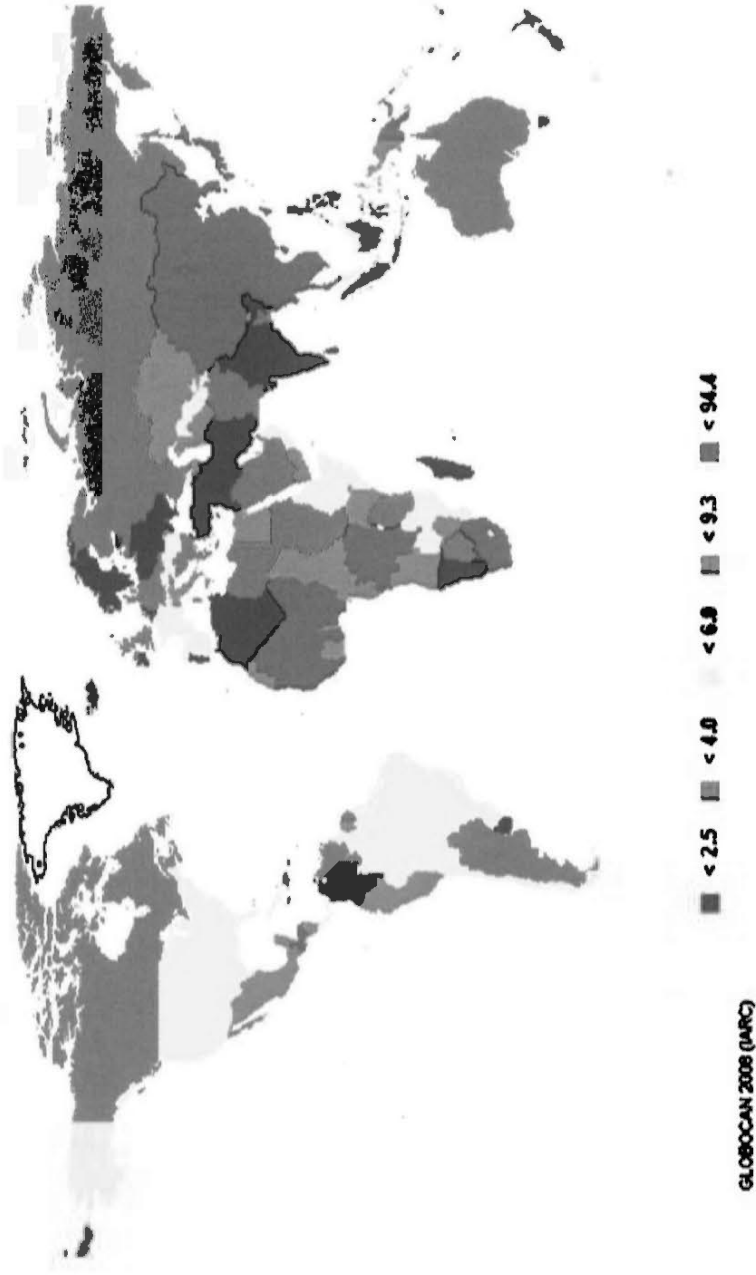


Figure 1.3 Worldwide distribution of liver cancer incidence estimated in year 2008 (GLOBOCAN2008)

1.1 ETHIOLOGICAL FACTORS

Hepatocarcinogenesis is believed to be a multistep process (Feo F *et al*, 2009) (Figure 1.4). In the majority of HCC cases (70-90%) arises in a background liver disease of either chronic hepatitis or cirrhosis, characterized by the progressive accumulation and interplay of genetic alterations causing aberrant growth, malignant transformation of liver parenchymal cells forming foci of altered hepatocytes (FAH). Subsequently, dysplastic nodules are observed and ultimately HCC which can be further classified into well differentiated (WD), moderately differentiated (MD) and poorly differentiated (PD) where the last of which represents the most malignant form of primary HCC (Figure 1.5).

Undoubtedly, the best way to prevent development of HCC is the effective prevention of risk factors leading to chronic liver injury which underlines HCC development. The most prominent factors associated with HCC include chronic hepatitis B and C infections, chronic alcohol consumption, aflatoxin B1 contaminated food, non-alcoholic steatohepatitis, obesity and type 2 diabetes. In addition, gender also influences the risk of HCC, with males accounting for a larger fraction of cases.

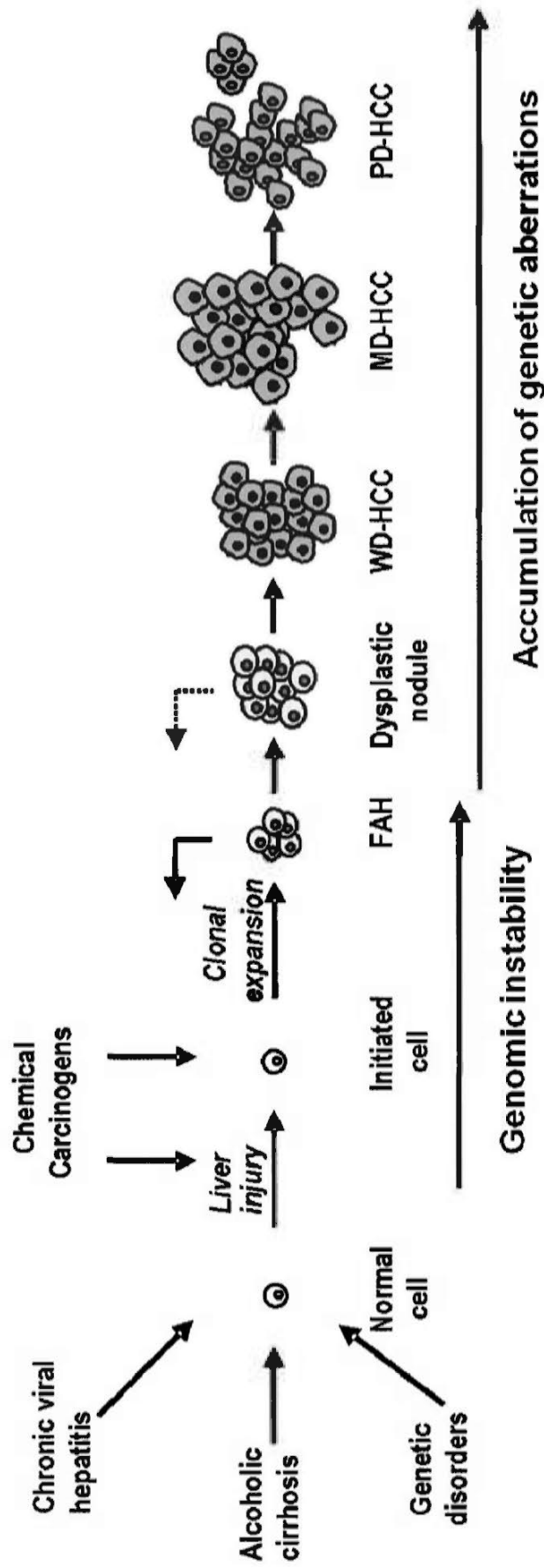


Figure 1.4 Schematic representation of liver carcinogenesis

Persistent liver injury due to hepatitis viral infections, acute alcoholic consumption, carcinogens exposure and genetic alterations accumulations induces genomic instability and initiates liver cell malignant transformation. Clonal expansion of initiated cells leads to the development of foci of altered hepatocytes (FAH), some of which can undergo phenotypic reversion (remodelling; reverse arrows). Accumulation of genetic damage leads to the development of autonomously growing dysplastic nodules which progress to well differentiated (WD), moderately differentiated (MD) and poorly differentiated (PD) invasive HCC.

Figure adapted from Feo F *et al.*, 2009.

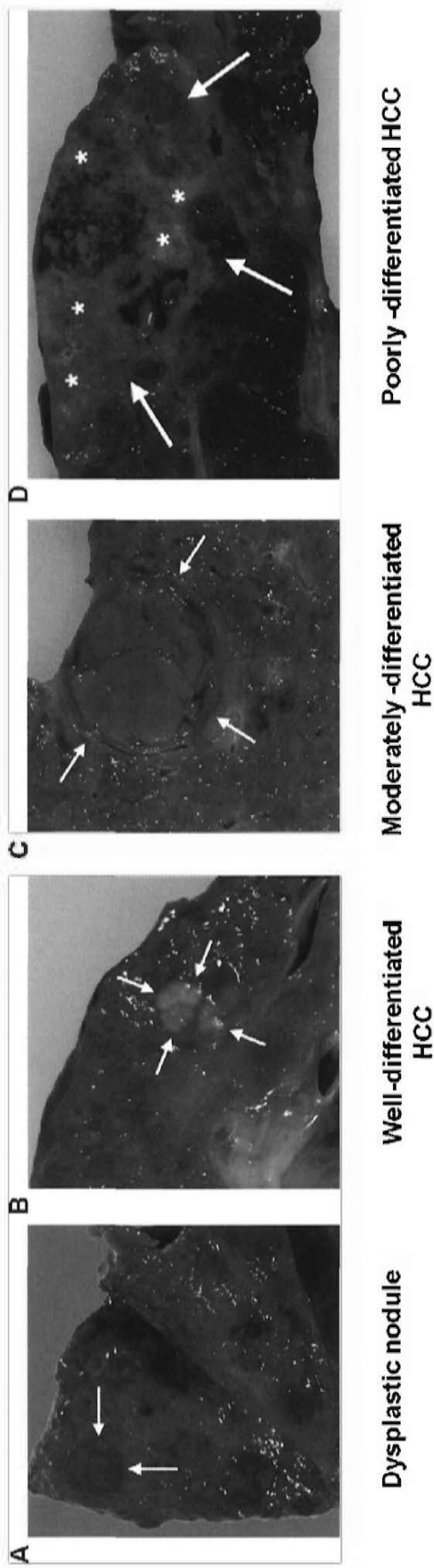


Figure 1.5 Representative photographs of pathologic section of liver

- (A) Dysplastic nodule: a well-defined 12-mm nodule (arrows)
 - (B) Well-differentiated HCC: a well-defined 18-mm pale nodule (arrows)
 - (C) Moderately-differentiated: an encapsulated 28-mm nodule (arrows)
 - (D) Poorly-differentiated: an infiltrative mass (arrows)
- Figure adapted from Hanna RF *et al*, 2008.

1.1.1 Liver cirrhosis

Cirrhosis is the final stage of chronic diffuse liver disease, which is characterized by alteration of the normal liver architecture into structurally abnormal nodules of liver cells surrounded by fibrosis. Cirrhosis is present in about 70-90% of HCC patients and is thereby the largest single risk factor (Nordenstedt H *et al*, 2010).

During the progression of liver injury, hepatic stellate cells (HSCs) become activated, losing retinoid-containing lipid droplets and transforming into myofibroblast-like cells, which produce extracellular matrix and the induction of hepatic fibrosis (Okuno M *et al*, 2002). Unchecked progression of fibrosis ultimately leads to irreversible cirrhosis. The activated HSCs become responsive to both proliferative platelet-derived growth factor (PDGF) (Friedman SL *et al*, 1989; Pinzani M *et al*, 1996) and fibrogenic transforming growth factor β (TGF- β) cytokines (Matsuzaki K, 2009), which are up-regulated in fibrogenesis and modulate inflammatory signaling from infiltrating immune cells. Chronic inflammation leads to repetitive cell necrosis and subsequently regeneration by induction of cell proliferation. The inflammation-induced oxidative stress is an important co-factor since it facilitates DNA damage and genomic alterations (Röcken C *et al*, 2001). Additionally, the loss of cell-cell contacts and cell-matrix interactions in a cirrhotic liver further disrupts the intercellular homeostasis of regular regeneration processes.

1.1.2 Hepatitis B viral infection (HBV)

HBV is a non-cytopathic, partially double-stranded circular hepatotropic DNA virus classified as a member of the *Hepadnaviridae* family. The minus strand of HBV genome contains four partially overlapping open reading frames (ORF) encoding several viral proteins essential to its life cycle, including the viral surface envelope proteins (HBsAg) encoded by pre-S/S; viral nucleocapsid (HBcAg) or hepatitis B e antigen (HBeAg) encoded by pre-C/C; polymerase protein (pol) containing reverse transcriptase domain encoded by P; protein X (HBxAg) encoded by ORF-X (Figure 1.6).

Several lines of evidence support the direct involvement of HBV in the transformation process. First is the HBV genomic integration which presents in over 85-90% of HBV-related HCC and usually precedes the development of HCC. During chronic inflammation, enhanced DNA replication and DNA damage would promote the process of viral integration (Guerrero RB *et al*, 2005), which induces a wide range of genetic alterations within the host genome, including chromosomal deletions, translocations, production of fusion transcripts, amplification of cellular DNA and generalized genomic instability (Guerrero RB *et al*, 2005; Feitelson MA *et al*, 2007). Different integrated events occur near or within fragile sites or other cancer-associated regions of the human genome that are prone to instability in tumor development and progression. A recent large-scale analysis of HBV DNA integration sites in cellular DNA found a preference at sites regulating cell signaling, proliferation and viability (Murakami Y *et al*, 2005). Common gene targets of integration include telomerase reverse transcriptase (TERT) (Horikawa I *et al*, 2001), PDGF receptor β (PDGFR β) and mitogen activated protein kinase 1 (MAPK1) (Murakami Y *et al*, 2005). A large proportion of HCC have integrated HBV

sequences encoding HBx and/or truncated envelope pre-S2/S proteins, which both contribute to hepatocarcinogenesis.

Second, HBx transcriptional activity can alter several cytoplasmic signaling pathways, including protein kinase C (PKC), Janus kinase (JAK)/signal transducer and activator of transcription (STAT), phosphoinositide-3-kinase (PI3K), stress-activated protein kinase (SAPK)/c-Jun NH2-terminal kinase (JNK), ras-raf-MAPK, activator protein-1 (AP-1), AP-2, nuclear factor- κ B (NF- κ B), Smad and Mad-related protein (SMAD) and Wingless-type protein (WNT), and by binding to nuclear transcription factors, including cAMP response element binding (CREB), activating transcription factor 2 (ATF-2), OCT-1 and TATA box binding protein (TBP) (Feitelson MA *et al*, 2007; Feitelson MA *et al*, 2009).

Third, HBx also causes transcriptional repression of the *p53* gene (Lee SG *et al*, 2000) and interacts with p53 to inactivate several important p53-dependent activities, including apoptosis, cell-cycle regulation, DNA repair and tumor suppression (Kremsdorf D *et al*, 2006), therefore increasing cellular proliferation and survival and compromising DNA-damage checkpoints. The hepatocarcinogenic potential of HBx has been genetically validated in HBx transgenic mice, of which 90% develop HCC (Kim CM *et al*, 1991; Yu DY *et al*, 1999).

Suppression of HBV replication or even loss of HBsAg in the serum has resulted in a low risk to develop HCC (Fattovich G *et al*, 1997), whereas high HBV load has been confirmed as negative prognostic factor in several HCC studies (Liu CJ *et al*, 2006; Chen CJ *et al*, 2006; Yuen MF *et al*, 2009). An effective therapy with interferon delays or even prevents the development of cirrhosis and HCC in patients with chronic hepatitis B infection (Yang YF *et al*, 2009; Lin SM *et al*, 2007). In parallel, sustained virological response to therapy with nucleotides analogues is

believed to have a similar long-term effect on disease progression (Liaw YF *et al*, 2009). However, these anti-viral therapies are only effective in preventing HCC in a small proportion of patients (Sorrell MF *et al*, 2009; Tai AW *et al*, 2009). Moreover, sustained clearance of HBV may be difficult to accomplish, particularly among cirrhotic patients.

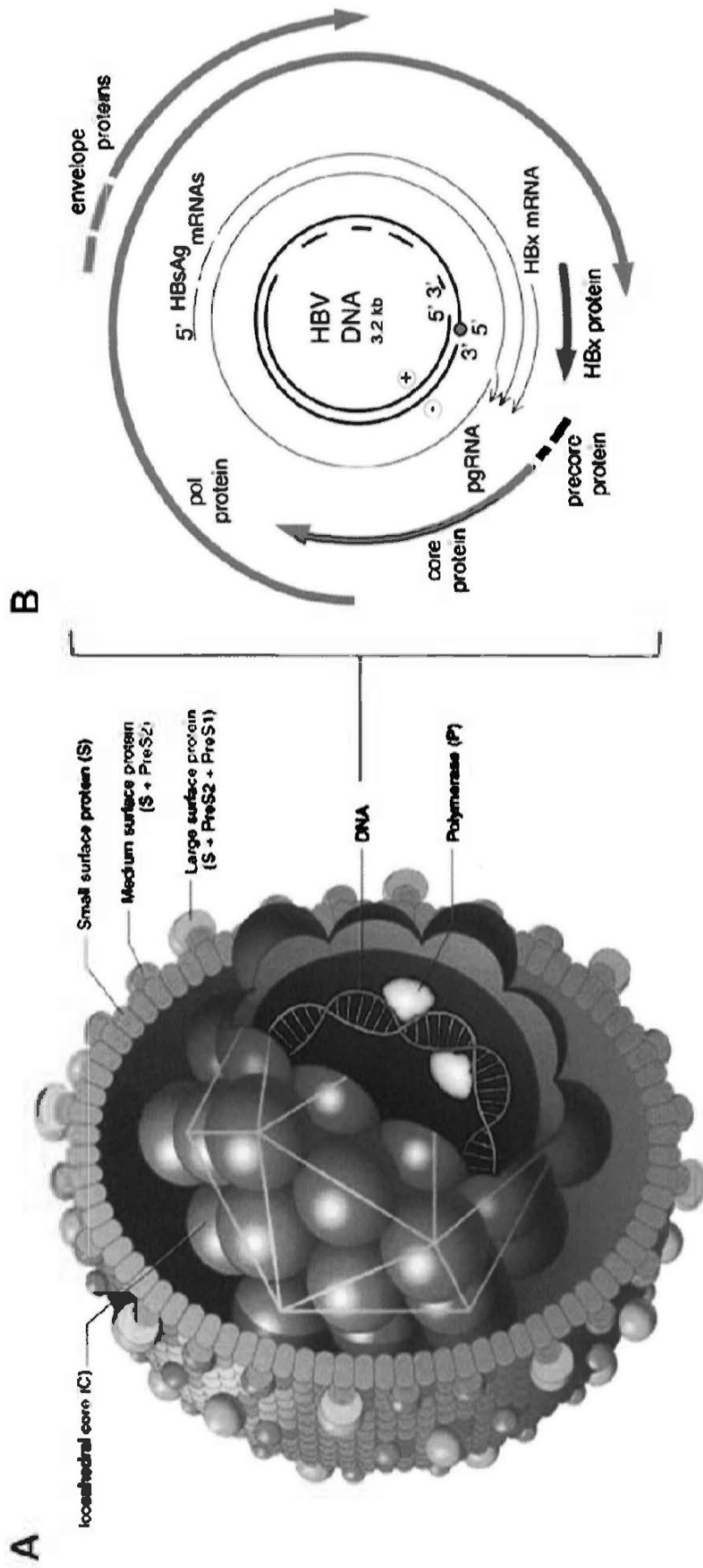


Figure 1.6 Hepatitis B Virus

(A) Model structure of HBV. (B) The genome of HBV. The partially double-stranded, circular DNA of HBV. Figure adapted from website of "The Hepatitis virus database" <http://www.ibibiobase.com/projects/hepatitis/index.htm>.

1.1.3 Hepatitis C viral infection (HCV)

HCV infection is a major HCC risk factor in Western countries and Japan. In which 44-66% and 80-90% of HCC cases with HCV infection were found in Italy and Japan respectively (Stroffolini T *et al*, 1999; Yoshizawa H *et al*, 2002). The wide spread of the HCV is mainly caused by contaminated blood donation, multiple use of syringes, the increase in intravenous drug abuse and sexual contact (Yoshizawa H *et al*, 2002). The risk for the development of HCC is 17-fold increased in HCV-infected patients (Donato F *et al*, 2002). HCV possesses two important clinico-biological distinctions from HBV that are relevant to hepatocarcinogenesis. First, HCV shows a higher propensity to yield chronic infection (10% of HBV cases versus 60-80% of HCV cases) (Rehermann B *et al*, 2005). This might relate to immune evasion by HCV quasi-species generated from high rates of replication errors (Rehermann B *et al*, 2005; Weiner A *et al*, 1995). The second key difference is the greater propensity of HCV to promote liver cirrhosis compared with HBV. About 5-10% of HCV-infected patients develop liver fibrosis that in dependency of host, environmental and viral factors may progress to liver cirrhosis after 10 years of infection, a frequency that is approximately 10-20-fold higher than HBV (Rehermann B *et al*, 2005).

HCV is a non-cytopathic virus of the *Flaviviridae* family. The HCV positive-stranded RNA genome contains only a single ORF which encodes 3 structural proteins including the core protein (C), envelope glycoproteins (E1 and E2); an ion channel protein (p7) and 6 non-structural proteins (NS2, NS3, NS4A, NS4B, NS5A and NS5B). The structural proteins are located at the N-terminus, whereas the non-structural proteins are situated at the C-terminal (Figure 1.7) (Moradpour D *et al*, 2007). The structural proteins are released from the polyprotein

by host signal peptidases that cleave signal peptides located between Core/E1, E1/E2, E2/p7, and p7/NS2 (Hijikata M *et al*, 1991; Lin C *et al*, 1994).

Since HCV is an RNA virus which is unable to reverse transcribe its genome and integrate it into the host genome. Instead, viral proteins and their evoked host responses contribute mostly to the viral oncogenic processes. Several HCV proteins have been reported to alter the regulation of cell proliferation and to be potentially oncogenic. The core protein has been reported to influence cell growth through diverse mechanisms including the activation of proto-oncogenes, *C-MYC* (Ray RB *et al*, 1995); inhibition of apoptotic activators, Fas and tumor necrosis factors- α (TNF- α) (Marusawa H *et al*, 1999); stimulation of growth factors, TGF- β and vascular endothelial growth factor (VEGF) (Taniguchi H *et al*, 2004; Shin JY *et al*, 2005; Battaglia S *et al*, 2009; Hassan M *et al*, 2009); and modulation of a tumor suppressor gene (TSG), p53 (Kasprzak A *et al*, 2008). Transgenic mice expressing the core protein develop HCC, indicating a direct part played by the core protein in this process (Moriya K *et al*, 1998). In addition to core, both NS3 and NS5A have been shown to interact with p53 and to suppress p53-mediated transcription activation and apoptosis (Ishido S *et al*, 1998; Majumder M *et al*, 2001; Deng L *et al*, 2006; Lan KH *et al*, 2002).

Recent studies revealed that HCV infection affects the cell-cycle regulating protein, retinoblastoma (Rb) which affects the cells in the G₁-S phase and inhibits transcription factor E2F (Watashi K *et al*, 2003; Edamoto Y *et al*, 2003). Both core and NS5B have been reported to reduce the abundance of pRb in hepatoma cell lines (Munakata T *et al*, 2005; Cho J *et al*, 2001). In particular, NS5B directly interacts with Rb to recruit the E3 ubiquitin ligase E6-associated protein (E6AP) which leads to ubiquitination and subsequent degradation of pRb (Huibregtse J *et al*, 2007). The

HCV sequence for binding was the same as the sequence previously reported in adenovirus and papilloma virus that bound the Rb gene (Whyte P *et al*, 1988; Dyson N *et al*, 1989; Lee JO *et al*, 1998).

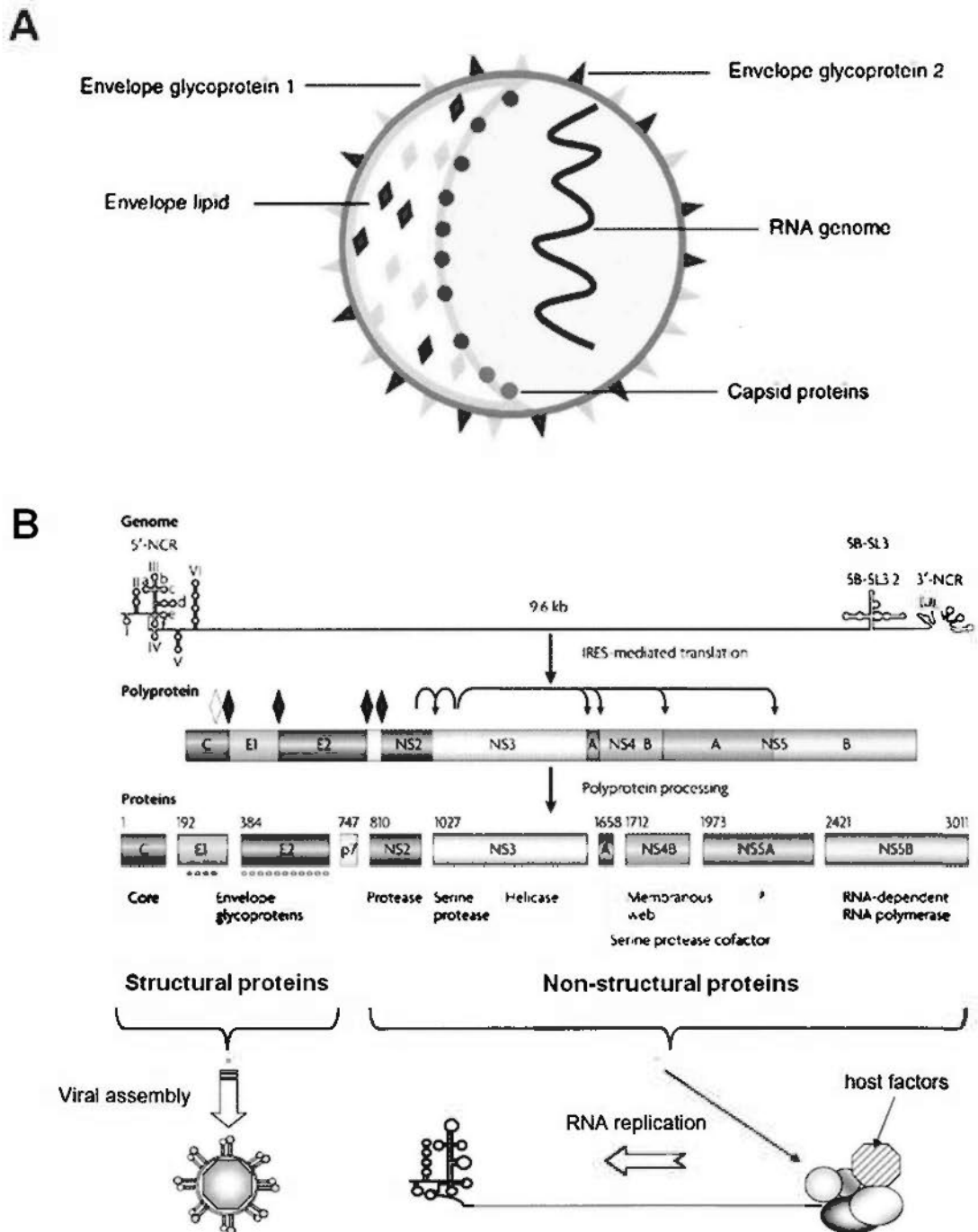


Figure 1.7 Hepatitis C Virus

(A) Model structure of HCV.

Figure adapted from website of "The Hepatitis virus database"
<http://www.ibiobiobase.com/projects/hepatitis/index.htm>.

(B) The genome of HCV. The 9.6 kb positive-strand RNA genome is schematically depicted at the top. Internal ribosome entry site (IRES)-mediated translation yields a polyprotein precursor that is processed into the mature structural and non-structural proteins. Diamonds and arrows indicate the cleavage sites by different peptidase.

Figure adapted from Moradpour D *et al*, 2007.

1.1.4 Chronic alcohol consumption

Chronic and excessive alcohol consumption is another major risk factor for developing liver cirrhosis and thereof HCC. This is mainly documented with respect to heavy intake of >50-70g/day for prolonged periods. In general, alcohol consumption is associated with a 2-fold increase of the individual risk for HCC development (Morgen TR *et al*, 2004), which increased up to 5- to 7-fold in cases of higher intake >80g/day for >10 years (Seitz HK *et al*, 2006). High consumption of alcohol leads to a fatty degeneration of hepatocytes, resulting in 30% in alcoholic liver fibrosis and in 10-20% in liver cirrhosis that is prone to the HCC development (Seitz HK *et al*, 2006; Becker U *et al*, 1996). Most researchers agree that it is the hepatic metabolism of ethanol rather than ethanol *per se* that underlies the mechanisms by which ethanol affects hepatocyte integrity.

1.1.5 Aflatoxin B1 exposure

Aflatoxin B1 (AFB1) produced by *Aspergillus flavus*, which is a mycotoxin, has been classified as a hepatic carcinogen. The toxin is usually found in spoiled food stuffs, such as grains, corns, peanuts and soya beans. AFB1 is metabolized in the liver to form an epoxide, which binds to the N7 position of specific guanines. This binding and formation of DNA adduct can lead to the transversion of G to T (Figure 1.8) (Smela ME *et al*, 2001; Miller E, 1978). Consequently, leading to heritable genetic changes that predispose to hepatic transformation (Smela ME *et al*, 2001; Essigmann JM *et al*, 1983). Of significance in HCC, the common mutational hotspot at which GC to TA transversion is prominent at the third position of codon 249 exon 7 of p53 gene (resulting in an Arg to Ser alteration in the p53 protein) (Smela ME *et al*, 2001; Essigmann JM *et al*, 1983; Puisieux A *et al*, 1991). This characteristic mutation in the p53 has been found in 30-60% of HCC in aflatoxin-endemic areas (Turner PC *et al*, 2002; Bressac B *et al*, 1991). Unlike HCV-induced and alcohol-induced hepatocarcinogenesis, there is no clear connection between AFB1 exposure and the development of cirrhosis, indicating that the mutational actions of this toxin might be the primary driver of HCC development. Previous evidence has revealed that 249 mutant promotes cell proliferation and inhibits the wild-type p53-mediated apoptosis and as a result, confers growth advantage to cancer cells (Ponchel F *et al*, 1994; Dumenco L *et al*, 1995; Wang XW *et al*, 1995; Tong WM *et al*, 2006).

Besides, a more detail study revealed that AFB1 binds preferentially to lysyl amino acid residues in histone proteins (Li ND *et al*, 1997) that has significant functional implications because histone has been reported to be the packaging material for DNA (Li ND *et al*, 1997; Stelolwagen RH *et al*, 1969). The effect of

AFB1 binding to histone is therefore similar to reaction elicited by acetylation in which the partial loosening of the histone-DNA bond that makes p53 accessible for damage and consequent degradation by specific proteases.

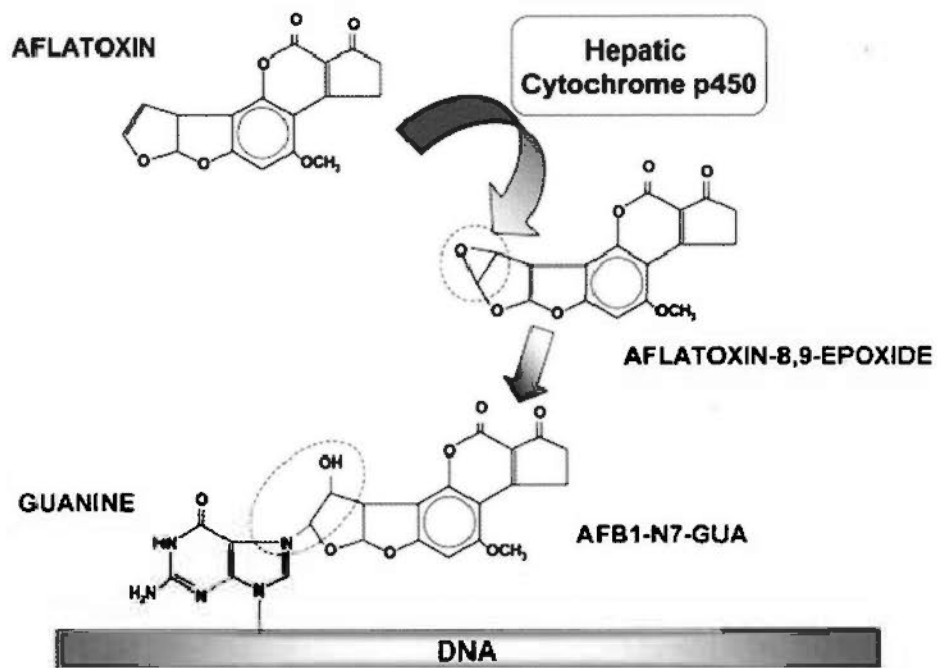


Figure 1.8 Metabolic conversion of aflatoxin B1 to the 8,9-epoxide and subsequent DNA adduct formation

AB1 is metabolized by cytochrome p450 to the 8,9-epoxide, which can subsequently react with a guanine base pair, most common form of DNA adduct formation. Figure adapted from McKillop IH *et al*, 2006.

1.1.6 Male gender

The increased risk for the male population in developing HCC has been proposed to be largely due to higher exposure to known risk factors, like alcohol consumption, tobacco smoking and higher rates of HBV and HCV viral infections. Moreover, certain studies on sex-specific hormones have demonstrated in animal model that male mice showed 2- to 8-fold increase in HCC development (Rudolph KL *et al*, 2000). These data support the hypothesis that androgen receptor (AR) poses an influence on HCC development. Knockout of AR expression in hepatocytes delayed the development of N',N'-diethylnitrosamine (DEN)-induced HCC, and decreased the number of tumors formation suggesting the active AR pathway in augmenting HCC risk (Ma WL *et al*, 2008). Moreover, an intriguing interaction between the specific viral protein of HBx protein and the androgen signalling pathway was recently established. The increased carcinogenic effect of HBx-enhanced AR activation was demonstrated by the anchorage-independent colony-forming assay and was suggested to be AR concentration-dependent manner (Chiu CM *et al*, 2007). Besides, several studies conducted in Taiwan reported on a positive association between increased circulating testosterone levels and HCC risk in HBV-infected men (Yu MW *et al*, 1993; Yu MW *et al*, 2001).

1.1.7 Obesity, Type 2 Diabetes and Non-Alcoholic Steatohepatitis (NASH)

Over the past few decades, the proportion of populations that are overweight or obese has increased substantially (Renehan AG *et al*, 2008; Larsson SC *et al*, 2008). In fact, excess bodyweight also seems to be an important risk factor for many cancers (Wolk A *et al*, 2001). For HCC, the increased body mass index (BMI) $>30\text{kg/m}^2$ has been associated with an increased risk of HCC development (Chen CL *et al*, 2008; Polesel H *et al*, 2009), especially in men whose liver cancer mortality rates were 5 times greater than those with a normal BMI (Calle EE *et al*, 2003).

Type 2 diabetes is an independent risk factor for HCC. The increased incidence of HCC among those with diabetes has ranged from 2- to 4-fold in different cohort studies (Harrison SA *et al*, 2006; El-Serag HB *et al*, 2006; Teoh NC *et al*, 2008). In addition, coexistent diabetes appears to increase the recurrence of HCC after potential curative therapy (Teoh NC *et al*, 2008). Type 2 diabetes and its associated hyperinsulinemia and hyper-insulin-like growth factor 1 (IGF-1) production, may also contribute to the formation of HCC (Smedile A *et al*, 2005). Diabetes appears to increase the odds of developing HCC through synergistic actions with other variables, such as viral hepatitis and alcohol (Donato F *et al*, 2006). A strong synergism between obesity and diabetes conveyed a 100-fold excess HCC risk with obesity in the context of either HBV or HCV infection (Nordenstedt H *et al*, 2010).

The most common liver diseases seen in patients with obesity and/or diabetes are non-alcoholic fatty liver disease (NAFLD) (Qian Y *et al*, 2005; Farrell GC *et al*, 2006; Fan JG *et al*, 2009). The clinicopathological spectrum ranges from simple steatosis to NASH. Simple steatosis has a relatively benign clinical course, but NASH has been proposed to be an important causative factor of HCC in recent years. The steadily increasing prevalence of obesity, coupled with diabetes and the

metabolic syndrome has put a very large proportion of population at risk of developing NASH and related cirrhosis, liver failure and HCC (Qian Y *et al*, 2005; Farrell GC *et al*, 2006; Bugianesi E *et al*, 2007; Larsson SC *et al*, 2008; Fan JG *et al*, 2009).

1.2 CHROMOSOMAL ABERRATIONS

HCC and other solid tumors develop and progress as a consequence of the stepwise accumulation of genomic alterations consequentially driving clonal selection. Some of the observed genomic alterations are widely shared among different tumor types, however, the association of the recurrent alterations is highly specific for each tumor type. Therefore, a comprehensive knowledge on the genomic alterations in a tumor type allows better understanding of the carcinogenesis process.

A number of studies on the chromosomal aberrations of HCC has been reported (Marchio A *et al*, 1997; Kusano N *et al*, 1999; Sakakura C *et al*, 1999; Wong N *et al*, 1999; Guan XY *et al*, 2000; Chang J *et al*, 2002; Niketeghad F *et al*, 2001; Shiraishi K *et al*, 2001; Balsara BR *et al*, 2001; Midorikawa Y *et al*, 2004). These comprehensive studies mainly derived from the conventional comparative genomic hybridization (CGH) analysis have been summarized by a meta-analysis based on 31 CGH studies of 785 HCC nodules. It was revealed that frequent gains on chromosome arms could be detected on chr.1q (57.1%), chr.6p (23.3%), chr.8q (46.6%) and chr.17q (22.2%), while losses were detected on chr.4q (34.3), chr.8p (38%), chr.13q (26.2%), chr.16q (35.9%), chr.17p (32.1%) (Moinzadeh P *et al*, 2005). A summary profile of CGH analysis on 47 HCCs from our group is shown in Figure 1.9, in which some recurrent genomic aberrant regions were highlighted.

Recently, expression imbalance map (EIM) has been applied to integrate the gene expression data and gene locus information of 31 HCC tissues in which the genomic loci concentrated with significantly up-regulated or down-regulated genes were mapped. The expression gains were revealed on chr.1q21-23 (74%), chr.8q13-21 (48%), chr.12q23-24 (41%), chr.17q12-21 (48%), chr.17q25 (25%) and chr.20q11 (22%) while the losses were detected on chr.4q13 (48%), chr.8p12-21

(32%), chr.13q14 (32%) and chr.17p13 (29%) (Midorikawa Y *et al*, 2004).

In order to acquire information on the genetic changes in HCC progression, a comprehensive analysis of the genomic alterations for each tumor with the known clinicopathological features is necessary. Comparison between HBV-positive and negative cases indicated that losses at chr.4q, chr.8p, chr.13q and chr.16q were positively correlated with HBV-positive cases, whereas only chr.8p loss was more frequent in HCV-positive cases. With regard to tumor histological grade, chromosomal losses at chr.4q and chr.13q were significantly associated with tumor dedifferentiation (Moinzadeh P *et al*, 2005). With regard to prognostic significance, losses on 8p and 13q have been implicated with unfavorable biologic behavior (Kusano N *et al*, 2002).

Besides, our group has previously demonstrated that the genetic aberrations accompanied by hepatocarcinogenesis occur in a specific order (Poon TC *et al*, 2006). By bioinformatic self-organizing tree algorithm (SOTA) analysis (Figure 1.10), unique patterns of significant chromosomal aberrations were derived. Three HCC subgroups organized in an evolutionary tree were identified. Gains of chr.1q21-23 and chr.8q22-24 appeared to be the earliest CGH events in HCC carcinogenesis.



Figure 1.9 Summary of CGH imbalances in HCC

Summary of gains and losses identified by CGH in 47 HCCs >3cm in diameter. Gains are shown on the right side of the chromosome ideogram and losses on the left. High-level gains are shown as thick lines. Each vertical line represents the affected chromosomal region seen in a single tumor specimen. Recurrent gains were represented in red boxes while the recurrent losses were represented in blue boxes. Figure adapted from Wong N *et al*, 1999.

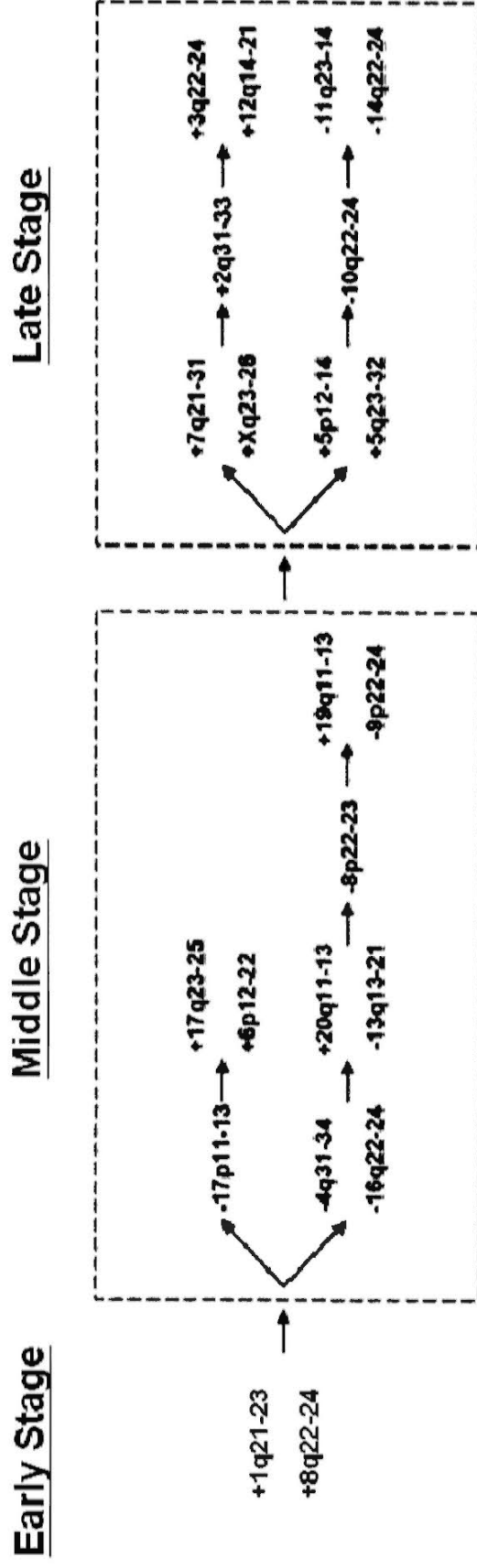


Figure 1.10 Proposed evolutionary changes in the HCC carcinogenetic pathway

The chromosomal imbalances, the minimal overlapping regions are presented. Figure adapted from Poon TC *et al*, 2006.

1.2.1 Gain of chr.1q

By CGH, our group and others have previously demonstrated that copy number gain of chr.1q is one of the most frequently detected alterations in HCC in which the gain of chr.1q could be detected in 46-86% of cases. Moreover, about 10% of HCC showed high copy number amplification on chr.1q (Marchio A *et al*, 1997; Kusano N *et al*, 1999; Sakakura C *et al*, 1999; Wong N *et al*, 1999; Guan XY *et al*, 2000; Chang J *et al*, 2002; Niketeghad F *et al*, 2001; Shiraishi K *et al*, 2001; Balsara BR *et al*, 2001; Midorikawa Y *et al*, 2004). Gains of chr.1q21-25 have been linked to a more aggressive phenotype with metastatic potential in renal clear cell carcinoma and squamous cell carcinomas of lung (Gronwald J *et al*, 1997; Petersen S *et al*, 2000). In ovarian cancer and neuroblastoma, chr.1q21-22 amplification has been suggested to be correlated with a drug-resistant phenotype (Kudoh K *et al*, 1999; Hirai M *et al*, 1999).

In HCC, several minimal amplifying regions (MAR) on chr.1q were mapped including chr.1q12-22 (Qin LX *et al*, 1999; Guan XY *et al*, 2000), chr.1q23.3-25.3 (Nishimura Y *et al*, 2005) and chr.1q24.2-1q43 (Nishimura Y *et al*, 2002). In an attempt to identify candidate oncogene(s) on chr.1q, our group has previously demonstrated the expression level of several candidate oncogenes including jumping translocation breakpoint (JTB), activates growth factor receptors to signaling pathway (SHC1), chaperonin containing TCP1 (CCT3) and coatmer protein complex alpha (COPA) on chr.1q21-22 were significantly over expressed in tumors compared with paired adjacent liver tissues (Wong N *et al*, 2003). By fluorescence *in situ* hybridization (FISH) and qRT-PCR analysis, cAMP responsive element binding protein 3-like 4 (CREB2L4), integrator complex subunit 3 (INTS3) and SNAP-associated protein (SNAPAP) were also found to be significantly

over-expressed in HCC tumors compared with the non-tumorous tissues (Inagaki Y *et al*, 2008).

In gene expression analysis, SHC1, CDC28 protein kinase regulatory subunit 1B (CKS1B), HCLS1 associated X-1 (HAX1) and CCT3 on chr.1q21-22 were highly expressed in HCC (Midorikawa Y *et al*, 2004). While in defining the recurrently altered regions (RARs), the expression of kinesin family member 14 (KIF14) (chr.1q32) and tropomyosin 3 (TPM3) (chr.1q21) was significant in primary HCC tumors (Kim TM *et al*, 2008).

Despite different mapping approaches in HCC, the functional effects of many candidate genes identified on chr.1q have not been well characterized so far. Except for a recently identified novel oncogene chromodomain helicase DNA binding protein 1-like (CHD1L) (on chr.1q21), which was demonstrated to possess oncogenic ability in increasing the colony formation in soft agar and tumorigenicity in nude mice (Ma NF *et al*, 2008). CHD1L was further characterized to be involved in the regulation of ARHGEF9-Cdc42 mediated Epithelial-to-Mesenchymal Transition (EMT) in HCC progression and metastasis (Chen L *et al*, 2010).

1.2.2 Gain of chr.8q

Besides HCC, gain of chr.8q is also frequently detected in different solid tumors including prostate (El Gammal AT *et al*, 2010), lung (Choi YW *et al*, 2007), esophagus (Kwong D *et al*, 2004), nasopharynx (Fang Y *et al*, 2001), ovary (Sham JST *et al*, 2002) and breast (Shadeo A, *et al*, 2006). By CGH analysis, 31-83% of HCC cases have been suggested to show copy number gain of chr.8q (Marchio A *et al*, 1997; Kusano N *et al*, 1999; Sakakura C *et al*, 1999; Wong N *et al*, 1999; Guan XY *et al*, 2000; Chang J *et al*, 2002; Niketeghad F *et al*, 2001; Shiraishi K *et al*, 2001; Balsara BR *et al*, 2001; Midorikawa Y *et al*, 2004). Our group and others have previously reported on recurrent chr.8q24 gains and emphasized on this sub-chromosomal region for its importance in cancer development and progression (Sakakura C *et al*, 1999; Kusano N *et al*, 1999; Niketeghad F *et al*, 2001; van Dekken H *et al*, 2003 Horlings HM *et al*, 2010).

One of the well-known proto-oncogenes *C-MYC* on chr.8q24 has been extensively studied. A role for *C-MYC* amplification has been postulated in the progression of human dysplastic nodules to HCC (Kaposi-Novak P *et al*, 2009). Besides, HCC developing in *C-MYC* transgenic mice undergo sustained regression, associated with re-differentiation of tumor cells, following inactivation of *C-MYC* transgene expression (Shachaf CM *et al*, 2004). Amplification and overexpression of *C-MYC* were correlated with HCC tumor size, tumor metastasis and recurrence (Kawate S *et al*, 1999; Wang Y *et al*, 2002; Takahashi Y *et al*, 2007). However, the clinical significance of *C-MYC* has been controversial as some have reported no significant correlation with clinicopathological features of HCC (Ikeguchi M *et al*, 2004; Chan KL *et al*, 2004).

Significant correlation was also found between elevated expression and

increased copy number of protein tyrosine kinase 2 (PTK2) (chr.8q24.3) and eukaryotic translation initiation factor 3 (EIF3S3) (chr.8q23.3). High expression of these 2 transcripts was found to be significantly associated with large tumor size and HBV infection (Okamoto H *et al*, 2003).

MicroRNA-151 (miR-151) located on chr.8q24.3 is frequently over-expressed in HCC tumors. Together with its host gene focal adhesion kinase (FAK), they were shown to correlate with intrahepatic metastasis of HCC. Also, it was found that miR-151 could augment HCC cell migration and invasion both *in vitro* and *in vivo* by directly targeting Rho GDP dissociation inhibitor (RhoGDI), leading to the activation of Rac1, Cdc42 and Rho GTPase (Ding J *et al*, 2010).

Although more and more candidate genes within the recurrent genomic aberrant regions have been identified, the precise roles of these genes in HCC tumorigenesis remain unclear. Due to the extensive and complex nature of chromosome aberrations, it is difficult for us to identify the biologically relevant alterations. The functional role of many identified genes has been minimal to date. To better elucidate the relationship between genomic aberrations and hepatocarcinogenesis, a comprehensive functional and mechanistic examination on gene characterization are needed to clarify their roles. This may eventually facilitate the development of more effective therapies against HCC.

1.3 STUDY AIMS

Genome-wide analysis can provide a comprehensive overview on the genomic aberrations of cancers. Our group has previously proposed a tumor progression model for human HCC based on the bioinformatics analysis of genomic CGH data on more than 150 patients (Poon TC *et al*, 2006). We found gains of chr.1q21-22 and chr.8q24 to be critical events associated with the development of HCC. Nevertheless, despite aberrant chromosomal changes may represent useful information that can be used in classifying the complex traits of HCC carcinogenesis, genomic data from CGH does not provide information on affected genes. In this thesis, in-depth investigations have been carried out to define and confirm target genes on chromosome regions for their role in liver tumorigenesis. In particular, focused analysis on chr.1q21-q22, chr.8q24, and the homozygously deleted regions in HCC has been accomplished.

The **first objective** of my study is to define cancer-associated genes within causal genomic loci of HCC by deploying the technique of high-resolution array-CGH. Specific emphasis was placed on mapping for novel TSGs within homozygous deleted chromosomal regions (Chapter 3) and identifying candidate oncogenes within common HCC amplicons, chr.1q21-22 and chr.8q24 (Chapters 4 and 5). Array-CGH analysis on primary HCC tumors and cell lines enabled the identification of a number of potential candidates. The **second objective** of my study is to ascertain clinical relevance and importance of identified genes in HCC. Validative analysis by quantitative PCR in an independent series of primary HCC tumor and corresponding adjacent non-tumoral liver was carried out. The verification of deregulated genes expression further led to the establishment of their prognostic values in association with clinicopathologic feature of tumors and survival of patients.

The **third objective** of my study is to characterize functional roles of defined genes, namely *CRYLI* (chr.13q12.11), *BOP1* (chr.8q24.3) and *GEF-H1* (chr.1q22), in HCC tumorigenesis. Ectopic expression and knockdown experiments were performed to establish their functional importance. Results obtained suggested that re-expression of *CRYLI* showed a strong inhibitory effects on HCC cell growth. Knocking down of *GEF-H1* or *BOP1* resulted in reduced cell migration and invasion. In my **fourth objective**, further elucidations of biological actions by which targeted genes exert their roles led to the delineation of potential mechanism. *CRYLI* was found to induce apoptosis and G₂-M phase cell-cycle arrest, whereas *GEF-H1* and *BOP1* exert their effects on cell motility and invasiveness through regulating RhoA pathway and the Epithelial-to-Mesenchymal Transition.

Chapter 2

Materials and Methods

2.1 MATERIALS

2.1.1 Chemicals and Reagents

Chemicals and Reagents	Company
40% Acrylamide/bis 29:1 Gel Solution	Bio-Rad Laboratories
Agarose, regular	USB Corporation
Alumin, from bovine serum (BSA)	Sigma-Aldrich Company
Ammonium persulfate (APS)	Sigma-Aldrich Company
Ampicillin Sodium salt	USB Corporation
Aprotinin	Sigma-Aldrich Company
5-Aza-2'-deoxycytidine	Sigma-Aldrich Company
Betadine solution	Mundipharma Laboratories
Bio-Rad Protein Assay (Bradford)	Bio-Rad Laboratories
Bromophenol blue	Sigma-Aldrich Company
Chloroform	Merck & Co., Inc
Crystal violet	Sigma-Aldrich Company
4',6-Diamidino-2-phenylindole (DAPI)	Sigma-Aldrich Company
Diethyl pyrocarbonate (DEPC)	Sigma-Aldrich Company
Dimethyl sulfoxide (DMSO)	Sigma-Aldrich Company
Ethylenediaminetetraacetic acid (EDTA)	Sigma Chemical Company
Ethanol	Merck & Co., Inc
Ethidium bromide	Sigma-Aldrich Company
Formaldehyde	Sigma-Aldrich Company
FuGENE®HD	Roche Diagnostics
Glycerol	Sigma-Aldrich Company
Glycine	Sigma-Aldrich Company
Hematoxylin Solution, Harris Modified	Sigma-Aldrich Company
Hi-Di™ Formamide	Applied Biosystems
Isopropanol	Merck & Co., Inc
LB agar	USB Corporation
LB broth	USB Corporation
Leupeptin	Sigma-Aldrich Company
Lipofectamine™ 2000	Gibco Invitrogen corporation
Methanol	Merck & Co., Inc
2-Mercaptoethanol	Sigma-Aldrich Company
Mountant for histology	Sigma-Aldrich Company
Nocodazole	Sigma-Aldrich Company

2.1.1 Chemicals and Reagents (con't)

Chemicals and Reagents	Company
Paraformaldehyde	Sigma-Aldrich Company
Pepstatin A	Sigma-Aldrich Company
Phenyl methyl sulfonyl fluoride (PMSF)	GE Healthcare
PhosSTOP	Roche Diagnostics
Precision Plus Protein™ Standards (Dual Colour)	BioRad Laboratories
Propidium iodide (PI)	Sigma-Aldrich Company
Protease Inhibitor Cocktail Tablets	Roche Diagnostics
RNase ZAP®	Ambion Inc
10% SDS solution	Ambion Inc
Sephadex™ G-50 Fine	GE Healthcare
Sigma H ₂ O	Sigma-Aldrich Company
Sodium citrate	Sigma-Aldrich Company
Sodium chloride (NaCl)	Sigma-Aldrich Company
Sodium deoxycholate	Sigma-Aldrich Company
Tetramethylrhodamine B isothiocyanate (TRITC)-labeled phalloidin	Sigma-Aldrich Company
Thiazolyl blue tetrazolium bromide (MTT)	Sigma-Aldrich Company
Trichostatin A (TSA)	Sigma-Aldrich Company
Triton X-100	Sigma-Aldrich Company
Trizma base	Sigma-Aldrich Company
TRIZOL® reagent	Gibco Invitrogen Corporation
Trypan blue	Gibco Invitrogen Corporation
Tween 20	Sigma-Aldrich Company
N,N,N',N'-tetramethylethylenediamine (TEMED)	Sigma-Aldrich Company
Vectorshield anti-fade reagent	Vector Laboratories,
Xylazine	Alfasan International BV

2.1.2 Buffers

Buffers	Company
Cell dissociation buffer (PBS-base)	Gibco Invitrogen Corporation
Phosphate buffer saline (PBS), pH7.4	Sigma-Aldrich Company
SSC solution (20X)	Ambion Inc.
siRNA buffer (5X)	Dharmacon, Thermo Fisher Scientific
Tris acetate EDTA buffer (TAE), pH7.4	Sigma-Aldrich Company
Tris borate EDTA buffer (TBE), pH7.4	Sigma-Aldrich Company
ULTRAhyb [®] -oligo hybridization buffer	Ambion Inc

Prepared buffers	Reagents
Electro-blotting Buffer (Western)	25mM Tris, 200mM glycine, 20% methanol (pH 8.3)
Laemmli sample buffer (5X) (Western)	60mM Tris-HCl, 2% SDS, 25% glycerol, 0.1% bromophenol blue, 5% 2-Mercaptoethanol
Lower Running Buffer (Western)	1.5M Tris-HCl (pH 8.8)
Running buffer (Western)	25mM Tris, 200mM glycine, 1% SDS (pH8.3)
Stripping buffer (Western)	65mM Tris-HCl, 2% SDS 100mM 2-Mercaptoethanol
Upper Stacking Buffer (Western)	1M Tris-HCl (pH 6.8)
RIPA Cell Lysis Buffer (Western)	20 mM Tris-HCl (pH7.4), 150mM NaCl, 1mM EDTA, 1mM EGTA, 0.1% SDS 1% Triton X-100, 1% sodium deoxycholate,
Tris buffered saline (TBS)	150mM NaCl, 50mM Tris, (pH 7.5)
Tris buffered saline tween (TBST)	150mM NaCl, 50mM Tris, 0.1% Tween, (pH 7.5)

2.1.3 Cell Culture

Reagents and culture flasks	Company
AIM-V	Gibco Invitrogen Corporation
DMEM	Gibco Invitrogen Corporation
Fetal bovine serum (FBS)	Gibco Invitrogen Corporation
Geneticin (G418)	Gibco Invitrogen corporation
L-Glutamine 200mM (100X)	Gibco Invitrogen Corporation
MEM Non-essential amino acids solution 10mM (100X)	Gibco Invitrogen Corporation
Opti-MEM®I Reduced Serum Medium	Gibco Invitrogen corporation
Penicillin-Streptomycin, liquid contains 10,000 units of penicillin and 10,000µg of streptomycin	Gibco Invitrogen Corporation
6.5mm Transwell® with 8.0µm Pore Polycarbonate Membrane Insert	Corning Incorporated
Matrigel Invasion Chambers in two 24-well plates, 8.0µm	Becton Dickinson
Trypsin-EDTA	Becton Dickinson
Tissue culture flask (150, 75, 25 cm ²)	Becton Dickinson
Tissue culture dish (150, 100, 60 mm)	Becton Dickinson
Tissue culture plate (96-, 24-, 12- and 6-well)	Becton Dickinson

2.1.4 Nucleic Acids

Nucleic Acids	Company
All custom designed primers/oligos	Gibco Invitrogen Corporation
BLOCK-iT Fluorecent Oligo	Gibco Invitrogen Corporation
Deoxynucleotide Trisphosphate Set, PCR grade	Boehringer Mannheim
1 kb Plus DNA Ladder	Gibco Invitrogen Corporation
Human Cot-1 DNA	Gibco Invitrogen Corporation
Human normal male DNA	Promega Biotech Co., Ltd
Human normal female DNA	Promega Biotech Co., Ltd
Human normal total liver RNA	Ambion Inc
Human normal total liver RNA	Clontech, Becton Dickinson
Human normal total liver RNA	Stratagene, Agilent Technologies
Human cDNA clone for BOP1	OriGene Technologies, Inc.
MGC clone for CRYL1	Invitrogen Corporation
ON-TARGET plus siGEF-H1	Dharmacon, Thermo Fisher Scientific
ON-TARGET plus siBOP1	Dharmacon, Thermo Fisher Scientific
ON-TARGET plus siRHOA	Dharmacon, Thermo Fisher Scientific
ON-TARGET plus siControl	Dharmacon, Thermo Fisher Scientific
Non-targeting Pool	
TaqMan probes (inventory)	Applied Biosystems
Green Fluorescence Protein expression vector (pEGFP-C2)	Clontech, Becton Dickinson
pcDNA3.1 (+)	Invitrogen Corporation

2.1.5 Enzymes

Enzymes	Company
AmpliTaq Gold DNA polymerase	Applied Biosystems
Pfu DNA polymerase	Stratagene, Agilent Technologies
Protease K	Qiagen
RQ1 RNase-free DNase	Promega Biotech Co., Ltd
RNase A	Roche Diagnostics
T4 DNA ligase	Invitrogen Corporation
T4 Polynucleotide Kinase (PNK)	GE Healthcare
<i>AluI</i>	Promega Biotech Co., Ltd
<i>EcoRI</i>	New England Biolabs
<i>HindIII</i>	New England Biolabs
<i>RsaI</i>	Promega Biotech Co., Ltd
<i>XhoI</i>	New England Biolabs

2.1.6 Equipments

Equipments	Company
ABI PRISM® 3100XL Genetic Analyzer	Applied Biosystems
Agilent Hybridization Owen Rotator	Agilent Technologies
Agilent Microarray Scanner	Agilent Technologies
Auto-radiograph	GE Healthcare
Centrifuge 5415R	Eppendorf International
CM3000-Cryostat	Leica Corporation
FACSCalibur System	Becton Dickinson
Gene Amp PCR System 9700	Applied Biosystems
ICYCLER IQ real time detection system	Bio-Rad Laboratories
Leitz DM RB fluorescence microscope	Leica Corporation
LSM 5 PASCAL	Carl Zeiss
ND-1000 UV-VIS Spectrophotomer	NanoDrop Technologies
Thermomixer 5435	Eppendorf International
Victor ³ ™ multilabel counter	Perkin Elmer

2.1.7 Kits

Kit	Company
Apoptosis Detection Kit	Becton Dickinson
BigDye Terminator Cycle Sequencing Kit	Applied Biosystems
Cell proliferation ELISA (BrdU) (colorimetric)	Roche Diagnostics
DNeasy Tissue Kit	Qiagen
ECL Western blotting detection reagents	GE Healthcare
ECL plus™ Western blotting detection reagents	GE Healthcare
EZ DNA Methylation-Gold™ Kit	Zymo Research Corporation
Genomic DNA Labeling Kit PLUS	Agilent Technologies
Oligo aCGH Hybridization Kit	Agilent Technologies
Oligo aCGH Hybridization Wash Buffer Kit	Agilent Technologies
One Shot® TOP10 Chemically Competent <i>E. coli</i>	Invitrogen Corporation
QIAamp DNA Mini Kit	Qiagen
QIAquick Gel purification Kit	Qiagen
QIAGEN® Plasmid Maxi Kit	Qiagen
QIAGEN® Plasmid Mini Kit	Qiagen
QIAquick PCR Purification Kit	Qiagen
Rho Activation Assay Kit	Upstate, Millipore Corporation
Rac1/Cdc42 Activation Assay Kit	Upstate, Millipore Corporation
SYBR Green PCR Reagents	Applied Biosystems
TaqMan Universal PCR master mix	Applied Biosystems
TaqMan® Reverse Transcription Reagents	Applied Biosystems

2.1.8 Antibodies

Primary/Secondary antibodies	Company
β-actin Mouse monoclonal	Sigma Chemical Company
BOP1 Rat monoclonal	Ascenion
E-cadherin Rabbit monoclonal	Cell Signaling Technology
E-cadherin Mouse monoclonal (IF)	Zymed, Invitrogen Corporation
N-cadherin Mouse monoclonal (IF)	Zymed, Invitrogen Corporation
N-cadherin Mouse monoclonal	Santa Cruz Biotechnology
α-catenin Rabbit polyclonal	Cell Signaling Technology
γ-catenin Rabbit polyclonal	Cell Signaling Technology
Cdc2 Mouse monoclonal	Santa Cruz Biotechnology
Cdc42 Rabbit monoclonal	Cell Signaling Technology
λ-crystallin Goat polyclonal	Santa Cruz Biotechnology
Cyclin B2 Mouse monoclonal	Santa Cruz Biotechnology
Cytokeratin 18 Mouse monoclonal	Dako
Fibronectin Rabbit polyclonal	Sigma-Aldrich Company
GAPDH Mouse monoclonal	Chemicon, Millipore Corporation
GEF-H1 Rabbit monoclonal	Cell Signaling Technology
Rac1/2/3 Rabbit polyclonal	Cell Signaling Technology
RhoA Rabbit monoclonal	Cell Signaling Technology
ROCK Rabbit monoclonal	Cell Signaling Technology
Cleaved ROCK Rabbit polyclonal	Millipore Corporation
MLC2 Rabbit polyclonal	Cell Signaling Technology
phosphor-MLC2 Mouse monoclonal	Cell Signaling Technology
Cleaved PARP Rabbit polyclonal	Cell Signaling Technology
Phalloidin-TRITC conjugate	Sigma-Aldrich Company
Vimentin Mouse monoclonal	Santa Cruz Biotechnology (sc-51721)
Vimentin Mouse monoclonal (IF)	Santa Cruz Biotechnology (sc-6260)
Mouse Alexa Fluor® 488	Invitrogen Corporation
Anti-rabbit conjugated HRP IgG	Santa Cruz Biotechnology
Anti-mouse conjugated HRP IgG	Santa Cruz Biotechnology
Anti-rat conjugated HRP IgG	Santa Cruz Biotechnology
Anti-goat conjugated HRP IgG	Santa Cruz Biotechnology

2.1.9 Softwares

Softwares	Company
Agilent Feature Extraction 9.1	Agilent Technologies
CGH Analytics 3.4	Agilent Technologies
CellQuest	Becton Dickinson
ABI PRISM® 3130 Genetic Analyzer Data Collection Software v1.1	Applied Biosystems
DNA sequencing analysis software v3.7	Applied Biosystems
Sequence Scanner v1.0	Applied Biosystems
LSM 5 PASCAL	Carl Zeiss
LSM Image Browser	Carl Zeiss
AxioVision LE Rel 4.5	Carl Zeiss
Adobe Photoshop CS ver 8.0	Adobe System Incorporation
GraphPad PRISM ver 3.02	GraphPad Software Incorporation
MedCalc® ver 11.0.1.0	MedCalc Software beba

2.1.10 Web Resources

Web Resources	URL
ExpASY Proteomics Server	http://www.expasy.ch/tools/sim-prot.html
MethPrimer	http://www.urogene.org/methprimer/index1.html
MultAlin	http://multalin.toulouse.inra.fr/multalin/multalin.html
National Centre for Biotechnology Information (NCBI)	http://www.ncbi.nlm.nih.gov/
NEBcutterv2.0	http://tools.neb.com/NEBcutter2/index.php
Primer3	http://frodo.wi.mit.edu/primer3/
UCSC Genome Bioinformatics	http://www.genome.ucsc.edu/

2.2 CELL LINES

Ten HCC cell lines HKCI-1, -2, -3, -6, -7, -9, -11, -C1, -C2 and -C3 were established previously from our laboratory. The early passages (passages 20-25) of the HKCI cell lines were employed. Two HCC cell lines SK-HEP1 and Hep3B were obtained from the American Type Culture Collection (ATCC, Rockville, MD). Huh7 cell line was acquired from the Japanese Collection of Research Bioresources (JCRB, Osaka, Japan). One immortalized normal human liver cell, L02 (Shanghai Institute of Cell Biology), was also included in the study of *BOP1* over-expression in HCC (Chapter 3). The cell lines studied in different Chapters have been summarized in Table 2.1

The series of HKCI cell lines were cultured in AIM-V medium supplemented with 10% fetal bovine serum (FBS), 1% L-Glutamine and 1% penicillin-streptomycin (Pang E *et al*, 2002). The culture condition for SK-HEP1, Hep3B, Huh7 and L02 was according to recommendations in Dulbecco's modified Eagle's medium (DMEM) containing 10% fetal bovine serum (FBS), 1% MEM non-essential amino acids, 1% penicillin-streptomycin (Gibco Invitrogen, Carlsbad, CA). All cultures were maintained in a humidified incubator at 37°C in an atmosphere of 5% CO₂.

Table 2.1 Cell lines studied in various Chapters

Chapter	Studied cell lines
<p>Chapter 3 Array-CGH defines homozygous deletion in HCC and <i>CRYLI</i> as a novel tumor suppressor gene</p>	<p>In-house established : HKCI-1, -2, -3, -6, -7, -9, -11, -C1, -C2 and -C3 ATCC : SK-HEP1 JCRB : Huh7</p>
<p>Chapter 4 <i>BOP1</i> plays an oncogenic role in HCC by promoting EMT</p>	<p>In-house established : HKCI-1, -2, -3, -9, ATCC : SK-HEP1 JCRB : Huh7 Shanghai : L02, immortalized normal liver cell line</p>
<p>Chapter 5 Frequent over-expression of <i>GEF-H1</i> on chr.1q22, promotes EMT and enhances cell motility in HCC</p>	<p>In-house established : HKCI-1, -2, -3, -6, -7, -9, -11, -C1, -C2 and -C3 ATCC : SK-HEP1 and Hep3B JCRB: Huh7</p>

ATCC : American Type Culture Collection
 JCRB : Japanese Collection of Research Bioresources

2.3 PATIENTS

Paired tumorous liver tissues and adjacent non-malignant livers were collected from HCC patients who underwent curative surgery for HCC at the Prince of Wales Hospital, Hong Kong. Informed consent was obtained from each of all patients recruited. A diagnosis of HCC was confirmed from histology examination. Relevant clinical and pathologic information were retrieved from the hospital database.

Sixty-six patient samples and 4 ultrasound-guided biopsies taken from patients who developed advanced inoperable HCC tumors were included in the study of *CRYL1* in Chapter 3 (median age 60, 86% male). They were predominantly HBV carriers (90%) with underlying liver cirrhosis indicated in 70% of the cases. According to the American Joint Committee on Cancer (AJCC) (6th edition) cancer staging criteria, 37 cases were classified as Stage T1, 13 cases as Stage T2 and 20 as Stage T3.

For the *BOP1* study in Chapter 4, tumorous and adjacent non-tumorous liver tissues were collected from 65 patients (median age 59; 88% male) in which 91% of them were chronic HBV carriers with identifiable cirrhosis in the non-tumorous liver indicated in 66% of the cases. The disease stage of tumors collected was classified 39 cases as Stage T1, 12 cases as Stage T2, and 14 cases as Stage T3.

In the *GEF-H1* study in Chapter 5, 100 patients (median age 56; 86% male) were recruited. Patients were also predominantly chronic HBV carriers (91%), and 70% of cases with cirrhosis. Sixty-four cases were graded as Stage T1, 17 cases as Stage T2, and 19 cases as Stage T3 according to AJCC staging.

2.4 ARRAY-CGH

Agilent human CGH microarray (Agilent Technologies, Santa Clara, CA) application uses a “two-colour” process to measure DNA copy number changes in an experimental sample relative to a reference sample labeled with Cy5-dUTP and Cy3-dUTP dyes respectively. Labeling reactions on 1µg of purified genomic DNA were performed and then hybridized to the array chip that contained unique oligonucleotides representing 43,000 probes at an average probe spatial resolution of ~35kb. The hybridized microarray chip was then scanned by the Agilent Microarray Scanner, and data analysis was performed by the Agilent Feature Extraction 9.1 followed by computation and normalization using CGH Analytics 3.4 software (Figure 2.1).

2.4.1 Preparation of genomic DNA

Genomic DNA of HCC biopsy samples (Biopsy-1, -2, -3) and cultured cells (12 HCC cell lines: HKCI-1, -2, -3, -6, -7, -9, -11, -C1, -C2, -C3, SK-HEP1 and Huh7) were extracted using DNeasy Tissue Kit (Qiagen, Valencia, CA). Tumorous liver tissues embedded in OCT compound were first sectioned by CM3000-Cyrostat (Leica, Wetzlar, Germany). Sectioned tissues were washed in cold PBS prior to centrifugation at 6000 rpm for 5 min. The tissue sections were then processed for DNA extraction following manufacturer’s protocol with addition of 4µl RNaseA (100mg/ml) after lysis buffer incubation. For cultured cell DNA preparation, 1×10^6 cells were washed with PBS and harvested. The cell pellets collected were further washed twice by PBS prior to lysis procedures according to the manufacturer’s protocol.

Sex matched normal genomic DNAs were purchased from Promega (Madison, WI) and all genomic DNA samples were stored at -20°C until use.

2.4.2 Restriction enzyme digestion and genomic DNA labeling

Two micrograms of high quality genomic DNA was digested with 5U of each restriction endonucleases, *AluI* and *RsaI*, in the presence of 2µg BSA for 2 hr at 37°C. The digested product was then used directly as a template for a genomic DNA labeling reaction using Agilent Genomic DNA labeling Kit PLUS (Agilent Technologies, Santa Clara, CA). Test and reference DNA samples were labeled with Cy5-dUTP and Cy3-dUTP respectively according to the manufacturer's protocol for 1 hr at 37°C. Labeled DNA were then purified using Microcon YM-30 filtration devices (Millipore, Bedford, MA).

2.4.3 Hybridization and washing

Appropriate Cy5 and Cy3 labeled DNA sample pairs were combined and then mixed with human Cot-1 DNA (Invitrogen, Carlsbad, CA). Prior to hybridization, the samples were heated at 95°C for 3 min and then incubated for 30 min at 37°C. The labeled target solutions were hybridized onto the microarray chip using Agilent Oligo aCGH Hybridization Kit (Agilent Technologies, Santa Clara, CA). The chips would then be secured in Hybridization Chamber and incubated at 65°C for 40 hr in the Agilent Hybridization Owen Rotator (20 rpm). The hybridized chips were disassembled by Oligo aCGH Wash Buffer 1 (Agilent Technologies, Santa Clara, CA) and further washed again by Wash Buffer 1 for 5 min and Oligo aCGH Wash Buffer 2 for 1 min (Agilent Technologies, Santa Clara, CA).

2.4.4 Feature extraction and data analysis

Microarray chips were scanned immediately using an Agilent Microarray Scanner. Representative Cy3 and Cy5 labeled microarray images of HCC cell lines HKCI-1 are shown in Figure 2.2. Data analysis was performed in the Agilent Feature Extraction 9.1 and CGH Analytics 3.4. Raw images acquired were analyzed and quantified by The Quality-Weighted Interval Score algorithm (ADM2) with a threshold value of 6.0 was used to compute and assist the identification of aberrations for a given sample. Fizzy zero correction was applied to all aberrant intervals identified in ADM2 analysis to avoid erroneous aberration calls when the errors were correlated. Putative chromosome copy number gain or loss was defined by intervals of two or more adjacent probes with \log_2 ratios suggestive of an amplification or a deletion when compared with the \log_2 ratios of adjoining probes.

The array-CGH profiles of the 12 HCC cell lines were analysed for mapping potential homozygous deleted genes (Chapter 3). A homozygous deletion (HD) was considered when a \log_2 ratio ≤ -3.0 was achieved.

The array-CGH profiles of 8 HCC samples that displayed chr.8q24 gains from early conventional CGH analysis were extracted and analysed for affected genes within this region (Chapter 4). The specimens included 6 cell lines (HKCI-1, -2, -3, -9, Huh7 and SK-HEP1) and 2 primary tumors. The copy number gain was defined by ≥ 1.8 -fold increase.

From early conventional CGH analysis, 9 HCC samples included 6 cell lines (HKCI-C1, -C2, -C3, -6, -9 and HKCI-11) and 3 primary tumors displayed chr.1q21-22 gain. The array-CGH profiles of these specimens were extracted and the candidate genes were selected when more than two-third of cases (i.e. ≥ 6 cases in a total of 9 cases studied) showed ≥ 1.8 -fold gain in copy number (Chapter 5).

All target regions identified by array-CGH were cross-checked with the Database of Genetic Variants Website to ensure the candidate genes did not reside within the copy number variants (CNV) regions.

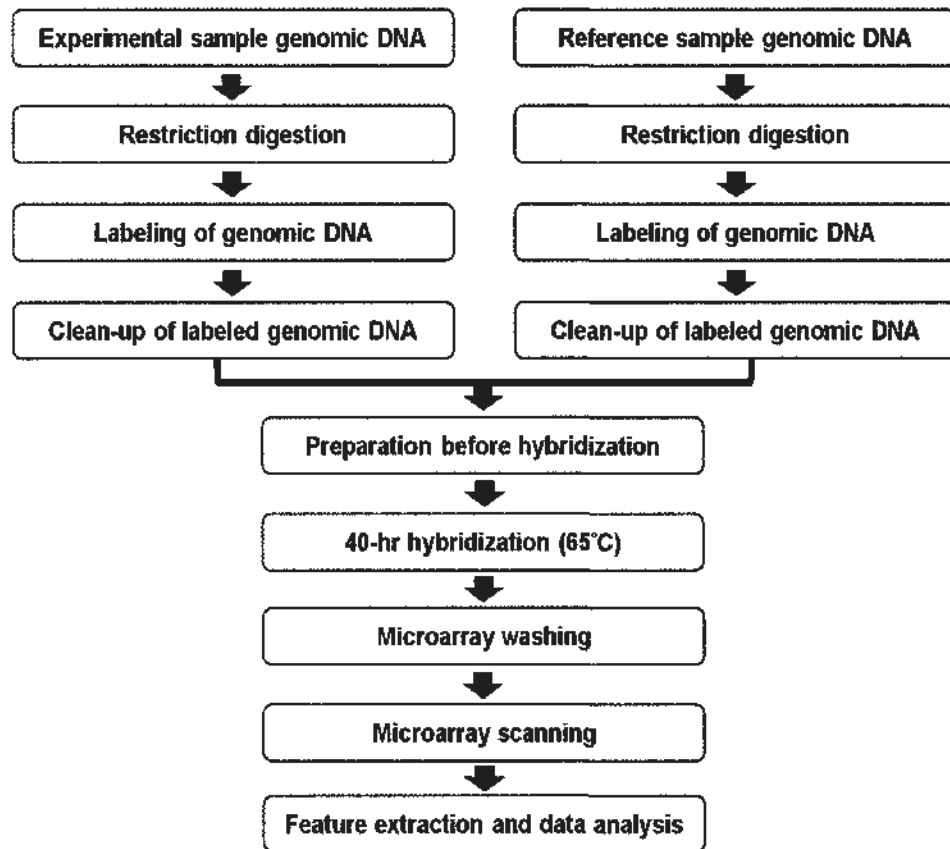


Figure 2.1 Procedural overview of array-CGH.

Adapted from the manual of Oligonucleotide Array-Based CGH for Genomic DNA Analysis, Agilent.

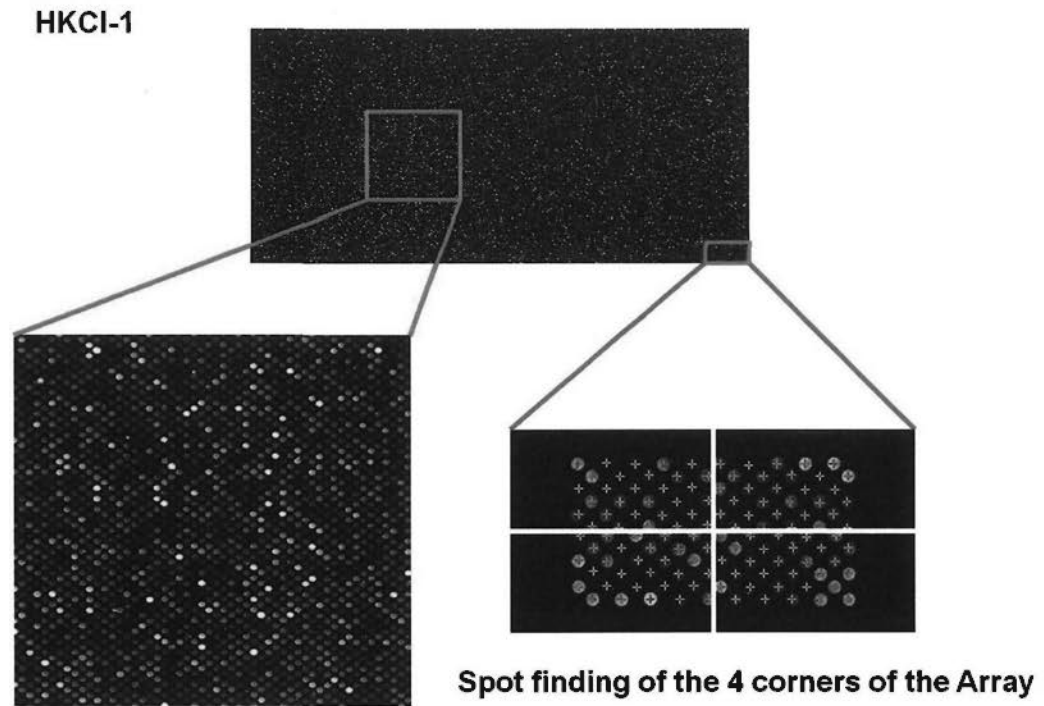


Figure 2.2 Representative Cy3 and Cy5 labeled microarray images of HCC cell line HKCI-1.

Yellow spots represent no copy number gain or loss of that genomic region in the test DNA (cell line or primary case) compared to the reference (normal liver DNA). Green spot corresponds to copy number loss in test sample, whereas red spot corresponds to copy number gain in test sample.

2.5 PCR VALIDATION OF HD GENES

The HD genes as defined from array-CGH were verified by PCR. Primer sets of 24 candidate genes were designed to amplify the flanking probe region (Table 2.2). One-hundred nanogram of DNA extracted by QIAamp DNA Mini Kit (Qiagen, Valencia, CA) was subjected to 35 cycles of PCR reactions with specific primers designed using AmpliTaq Gold DNA Polymerase (ABI, Foster City, CA). No template reaction mixture was served as negative control. The PCR products were separated on 1.5% agarose gels and visualized by ethidium bromide (EtBr) staining. Results obtained from 12 cell lines were compared to normal human liver controls.

In examining *CRYL1* for homozygously deleted exons, 100ng DNA from 25 HCC specimens (19 primary tumors and 6 cell lines) were subjected to qPCR analysis in SYBR Green PCR Reagents (ABI, Foster City, CA) using specific primers for exons 1-9 (Table 2.3). The emission signal was detected by iCycler IQ real time detection system (Bio-Rad, Hercules, CA). Ct values obtained from duplicate reactions were normalized against internal reference β -globin, and the copy number relative to the mean value obtained from 3 normal livers was determined by $2^{-\Delta\Delta Ct}$. An allelic loss (AL) was considered when a 2-fold reduction was achieved, and an HD was defined at ≥ 4 -fold reduction or when no visible band could be detected from gel electrophoresis.

Table 2.2 Primer sequences for the candidate HD targets as defined by array-CGH

HD location	Cell line	Gene Symbol	Primer sequences	T _m (°C)	Product size (bp)	
3q26.1	Huh7	SERPIN2	Forward: 5' CTGTTTATGGGAAGAGTGACAAATC 3' Reverse: 5' ACAGGCACAGTTTAAAAACAGAAAAG 3'	60.7	190	
		PDCD10	Forward: 5' AAATATTGCAGTGAATGAAGATTCC 3' Reverse: 5' AACACAGGATACATGACTGCATAGA 3'	60.7	157	
		SERPIN1	Forward: 5' GATAATAAGGAGATTTTCTTTCCAA 3' Reverse: 5' CCCACTCAAGATTGTCTAAAAATA 3'	57.6	152	
9p21.3	SK-HEP1	MTAP	Forward: 5' AAAAGACTAAATGCACATTTTATGG 3' Reverse: 5' TTAAAAAGCAAAAATTACCAACTCG 3'	62	110	
		CDKN2A	Forward: 5' GTAAACTGGGAGTATAATGGGCTCT 3' Reverse: 5' ACATATGTAACAAACCTGCACATTG 3'	62	154	
		CDKN2B	Forward: 5' TTAATTATCATACTCAGTGCCAGAT 3' Reverse: 5' AAGCAGGATTCGTACTTAAACATTG 3'	60.7	150	
11p15.4	HKCI-11	HBB	Forward: 5' CTGAGAACITCAGGGTGAGTCTATG 3' Reverse: 5' TACCCTGTACTTATCCCTTCCTA 3'	56	101	
		HBD	Forward: 5' GGAAGTCTTCTGATAACCATAAGA 3' Reverse: 5' CATTCTTTATTAGGCAGAAGCCATA 3'	56	110	
		HBG1	Forward: 5' AAGAACTTGTACATGGGAGTTCTG 3' Reverse: 5' ATGGGATTAATTTACCTCTTTAGG 3'	60	452	
13q12.11	SK-HEP1 and Huh7	TUBA2	Forward: 5' AGCTGAGTTTCACCTCCTAGAGTCA 3' Reverse: 5' TTTAAGGCCTATACTCACCAAGATG 3'	55.6	200	
	SK-HEP1	HSMPP8	Forward: 5' ACTTTCAGAGTAGCAGAAAGAGACAA 3' Reverse: 5' GGTATGTTCTGTGGGGGTTTGTA 3'	55.6	150	
		PSPC1	Forward: 5' GAAAGAGAGGAAAAAGAAAACCTCC 3' Reverse: 5' AATCCCCCAGAAAACAACTAAG 3'	55.6	102	
		ZNF237	Forward: 5' AACCTTATTTGTCTTGACCTCAG 3' Reverse: 5' GCAAACAGTAGAACTACCCCAAAT 3'	55.6	135	
		ZNF198	Forward: 5' ATAACTACAATGAAAGGAACCATT 3' Reverse: 5' GCTCCITTAGTAGGATTCTGTTTGTG 3'	62	119	
		GJB2	Forward: 5' TGCTGTCCTAATTTCTTTCACTT 3' Reverse: 5' ATGAAAGAACCAATGTTACCTTTA 3'	55.6	236	
		GJB6	Forward: 5' ATCTTTGAAGCAGCCTTATGTATG 3' Reverse: 5' CATAAAAATGGTAAACACGGTCTTC 3'	55.6	153	
		CRYL1	Forward: 5' GCATTTGACTATATTTTACAGCCAGT 3' Reverse: 5' ATTCAGAATAAGCGTTAGCAAAAATG 3'	55.6	152	
		TTC10	Forward: 5' TATGAATTAATGGAAAATCCCAGTC 3' Reverse: 5' CTCATAGTAATATTGAAATGCTTGAGA 3'	62	150	
		IL17D	Forward: 5' TTCTTAGAGTAACCAGGGATGATGA 3' Reverse: 5' TTCATGTGTCACTTCTGGAAGAC 3'	62	171	
		XPO4	Forward: 5' AGTTTTATTTAAAGACCCAGGGATG 3' Reverse: 5' AACCTGATATTCAGCCTATAACTGG 3'	55.6	165	
	17p13.1	HKCI-9	TP53	Forward: 5' TCAGATTCACCTTTTATCACCTTTCC 3' Reverse: 5' AATTGCAGGTAACACAGTCAAGAAG 3'	55.6	204
	17p11.2-12	HKCI-9	ADORA2B	Forward: 5' CTAATTAAGTTTGCCAGGCTTTCT 3' Reverse: 5' CAGACCCTCAAACCTACAAAACAT 3'	55.6	155
TTC19			Forward: 5' ATGTCAGGTAGGAAACCCATT 3' Reverse: 5' TGCTGATACCTTAAAGACAGACACTT 3'	57.6	150	
NCOR1			Forward: 5' GTCTGGAACAGGTTTCTGATTCTC 3' Reverse: 5' AACATTACAAACCTACAACCTACAGG 3'	57.6	150	
+ve control		β-globin	Forward: 5' GAAGAGCCAAGGACAGGTAC 3' Reverse: 5' CAACTTCATCCACGTTTACC 3'	60	268	

Table 2.3 Primer sequences for exons 1 to 9 of *CRYLI*

<i>CRYLI</i> Exon	Primer Sequences	Product size (bps)	T _m (°C)
1	Forward: 5' ACCCCACTCAGGGACCAAG 3' Reverse: 5' TTTACCTGCCAACGATCACC 3'	196	50
2	Forward: 5' TACAATCAATCTTTTCATCTTGCAG 3' Reverse: 5' AACACAGATGAATCTTGAGCACAT 3'	206	60
3	Forward: 5' CTTCCAGGTGAAACTCTATGACATT 3' Reverse: 5' AAATGTGACATCACAGATCCTCATA 3'	169	60
4	Forward: 5' TGGGCTTTATCTGTTTTAAATGTG 3' Reverse: 5' ACCCTCTACTGCTTCTTGATATTG 3'	178	60
5	Forward: 5' AAGATTTTTGCTCAGTTAGATTCCA 3' Reverse: 5' AGATGAGATAACAATCAATCCTCTGG 3'	169	60
6	Forward: 5' TCTCTCTCTCCTAAGGTGAATCC 3' Reverse: 5' CCTCGCTGATGATTGCATATTG 3'	195	60
7	Forward: 5' GTAGGAAGGAATCGTGTCTCCTAGT 3' Reverse: 5' CCATGACAACACTAAATAGAATGGA 3'	162	60
8	Forward: 5' CTGAATGCATTTCTGAGTTTGAATA 3' Reverse: 5' TACATACCTGGTTAACCTTCTCAGC 3'	194	60
9	Forward: 5' GCATTTGACTATATTTTACAGCCAGT 3' Reverse: 5' ATTCAGAATAAGCGTTAGCAAAATG 3'	152	60

2.6 EXPRESSION ANALYSIS BY QUANTITATIVE RT-PCR

The mRNA expression analyses of target genes in normal liver samples, HCC cell lines, HCC tumors and adjacent non-tumoral livers were performed using quantitative RT-PCR (qRT-PCR). The RNA from liver samples were first extracted and then transcribed into complementary DNA (cDNA) by reverse transcription (RT). qRT-PCRs were performed with different gene-specific TaqMan Probes (ABI, Foster City, CA).

2.6.1 Total RNA extraction from cell lines and tumors

The cells were first lysed with TRIzol.[®] reagent (Invitrogen, Carlsbad, CA) and the total RNA was extracted and precipitated by chloroform and isopropanol respectively according to the manufacturer's protocol. The RNA pellet was then washed with cold ethanol and air-dried for 15 min prior the resuspension in DEPC-treated water. The integrity of total RNA was also assessed by agarose gel electrophoresis. Representative gel photo of good quality RNA was shown in Figure 2.3. The total RNA was stored at -80°C until use.

2.6.2 qRT-PCR analysis for gene expression

Four micrograms of total RNA was first subjected to DNase treatment in a 50µl total volume containing 1U/µl RNase-free DNase and 5µl of DNase reaction buffer (Promega, Madison, WI) in order to eliminate the possible carryover of genomic DNA. Then 1µl of DNase-treated total RNA was subjected to PCR reaction

using primers targeting genomic β -globin gene to ensure there was no DNA contamination.

Two micrograms of DNase-treated RNA was subjected to RT reaction using the TaqMan® Reverse Transcription Reagents (ABI, Foster City, CA). A hundred-microliter reaction mixture contained 25 μ l of 80ng/ μ l DNase-treated total RNA, 10 μ l of 10X TaqMan RT buffer, 22 μ l of 25mM MgCl₂, 20 μ l of 10mM dNTP mixture, 5 μ l of 50 μ M random hexamers, 2 μ l of 20U/ μ l RNase inhibitor, and 2.5 μ l of 50U/ μ l MultiScribe™ Reverse Transcriptase. The reaction was performed as follows: 10 min at 25°C, 60 min at 37°C and 5 min at 95°C. All first strand cDNA was stored at -80°C until use.

Two microliters of first strand cDNA were added to 18 μ l PCR reaction mix containing 10 μ l Taqman® Universal PCR Master Mix with AmpErase UNG (ABI, Foster City, CA) and 1 μ l of 20X TaqMan probe (ABI, Foster City, CA). The reaction was performed in 96-well optical tray and the thermal cycling conditions were as follows: 50°C for 2 min, 95°C for 10 min, followed by 40 cycles of 95°C for 15 sec and 60°C for 1 min. The emission intensity was detected by the iCycler IQ detection system using fluorophore FAM490 (Bio-Rad, Hercules, CA). Threshold cycles were averaged from triplicate reactions. A no template reaction was included to serve as negative control. To adjust for variations in starting template, all gene expressions were normalized with internal reference gene, 18S rRNA. The fold change relative to the mean value obtained from 6-7 normal liver controls was determined by the $2^{-\Delta\Delta C_t}$ method.

Gene-specific TaqMan Assays for qRT-PCR examinations of 12 HD candidate genes (Chapter 3), *BOP1* and *C-MYC* expressions (Chapter 4) and *GEF-H1* and a panel of E-cadherin transcriptional repressors (Chapter 5) were shown

in Table 2.4. A relative gene expression ≤ 2 -fold was considered as down-regulation while ≥ 2 -fold as up-regulation.

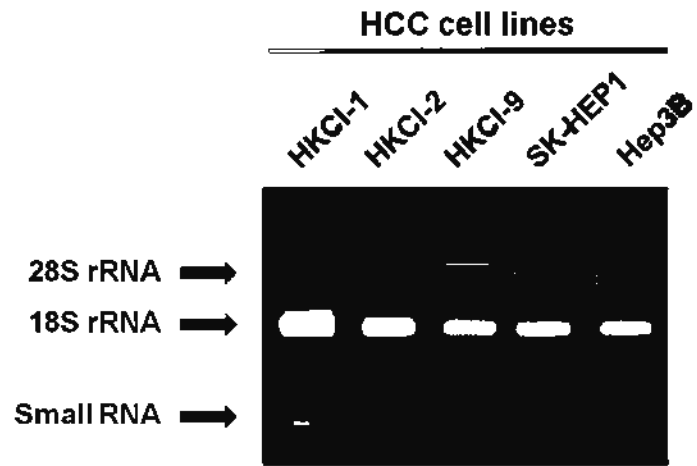


Figure 2.3 Agarose gel (1%) electrophoresis of total RNAs from HCC cell lines.

Table 2.4 TaqMan assays for genes expression analysis by qRT-PCR

Chapter 3	HD Location	Gene	TaqMan Gene Expression Assay
	9p21.3	MTAP	Hs00559618_m1
		CDKN2B	Hs00793225_m1
	13q12.11	HSMPP8	Hs00736882_m1
		ZNF237	Hs00383349_m1
		GJB2	Hs00955889_m1
		GJB6	Hs00917676_m1
		CRYL1	Hs00211084_m1
		XPO4	Hs00223803_m1
	17p13.1	TP53	Hs00153340_m1
	17p11.2-12	ADORA2B	Hs00386497_m1
		TTC19	Hs00214958_m1
		NCOR1	Hs00196920_m1
Chapter 4	Genomic Loci	Gene	TaqMan Gene Expression Assay
	8q21	BOPI	Hs00374884_m1
	8q24.21	C-MYC	Hs00905030_m1
Chapter 5		Gene	TaqMan Gene Expression Assay
	E-cadherin repressors	GEF-H1	Hs00190884_m1
		SNAL1 (SNAIL1)	Hs00195591_m1
		SNAL2 (SLUG)	Hs00950344_m1
		ZEB1	Hs00611018_m1
		ZEB2	Hs00207691_m1
		TWIST1	Hs00361186_m1
		TCF3	Hs01012685_m1
	Internal reference	18S rRNA	Hs99999901_s1

2.7 FUNCTIONAL ANALYSIS

2.7.1 Evaluation of transfection efficiency of the HCC cell lines

Transfection efficiencies of cell lines were evaluated by employing the FITC-labeled double stranded RNA (BLOCK-iT Fluorescent Oligo) (Invitrogen, Carlsbad, CA) or Green Fluorescence Protein expression vector (pEGFP-C2) (BD, Franklin Lakes, NJ). FITC or GFP signal from transfected cells were examined under fluorescence microscope at 24 hr post-transfection by LipofectamineTM 2000 (Invitrogen, Carlsbad, CA) or FuGENE®HD reagents (Roche, Penzberg, Germany). The transfected cells were fixed in 70% ethanol and re-suspended in PBS. The transfection efficiency was then quantified by the FITC or GFP fluorescence signal measured by flow cytometry analysis. Representative images and flow cytometry spectra of GFP-vector or FITC-Oligo transfected cells were shown in Figure 2.5. Altogether 4 cell lines (SK-HEP1, Hep3B, HKCI-9 and L02) had been transiently transfected with different siRNAs or gene expression plasmid in the following studies. Their corresponding transfection efficiencies were evaluated and shown in Table 2.5.

For the functional experiments of *CRYL1* in Chapter 3, pcDNA3.1-*CRYL1* or pcDNA3.1-vector was transfected into SK-HEP1 cells using Lipofectamine 2000 (Invitrogen, Carlsbad, CA) for 24 hr. In Chapter 4, siRNA against *BOP1* (LU-014065-01) or siControl (D001818-10) (Dharmacon, Lafayette, CO) was transfected into Hep3B cells (for 6 hr) or HKCI-9 cells (for 24 hr) using LipofectamineTM 2000. Whereas in over-expression experiments, L02 was transfected with pcDNA3.1-*BOP1* or pcDNA3.1-vector using FuGENE®HD (Roche, Penzberg, Germany) for 24 hr. In validation experiment of RhoA as downstream effector of

BOP1, siRNA against RhoA (LU-003860-00) or siControl (Dharmacon Lafayette, CO) was transfected into pcDNA3.1-vector or pcDNA3.1-*BOP1* expressing L02 cells using Lipofectamine 2000. In Chapter 5, siRNA against *GEF-H1* (LU-009883-00) or siControl (D001818-10) (Dharmacon, Lafayette, CO) was transfected into Hep3B or SK-HEP1 cells using LipofectamineTM 2000 for 6 hr and 24 hr respectively. From all the transfection carried out above, the cells were trypsinized, washed and seeded for various functional assays at 24 hr post-transfection.

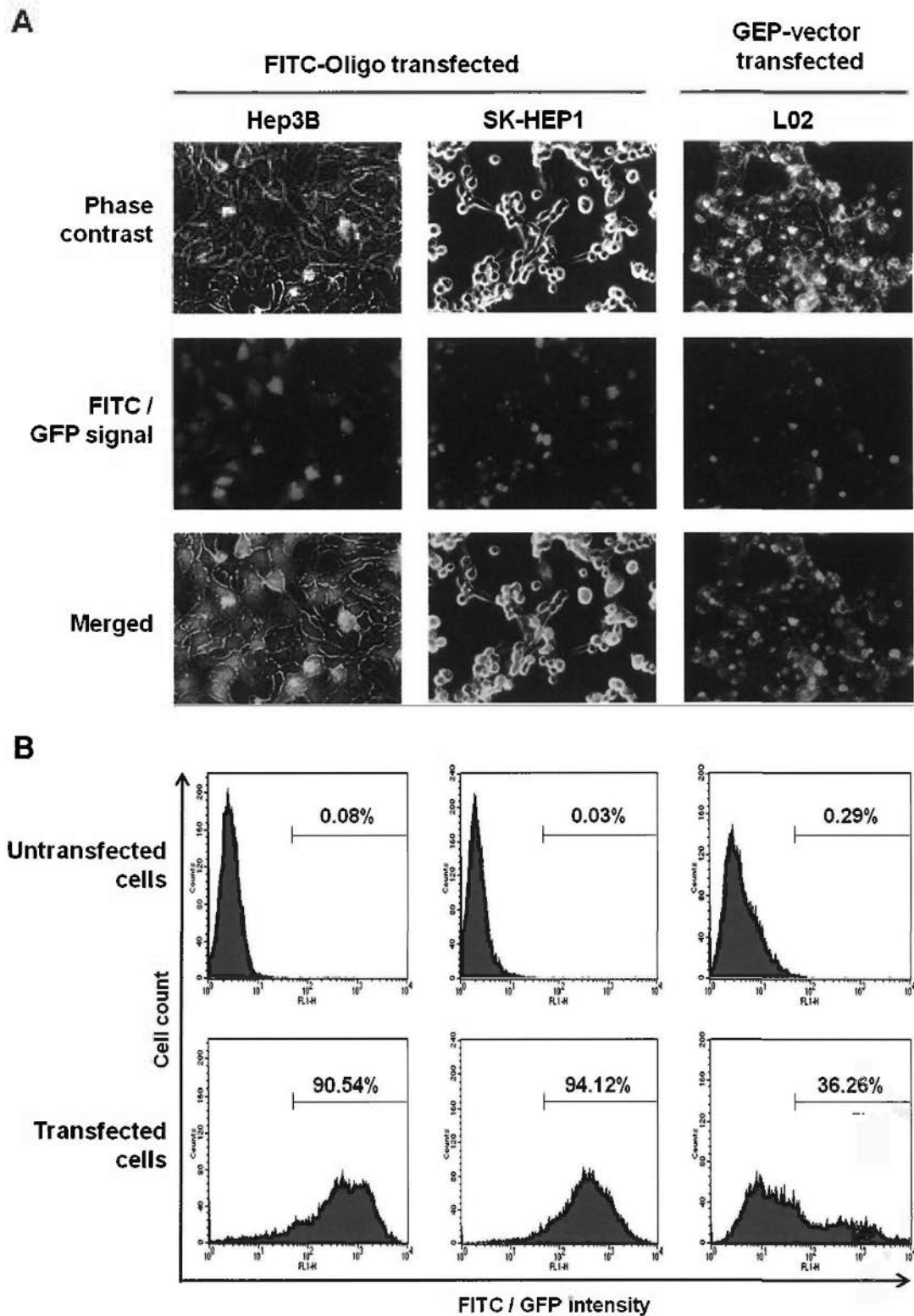


Figure 2.4 Transfection efficiency of Hep3B, SK-HEP1 and L02 cell lines

(A) Representative images of Hep3B, SK-HEP1 (transfected with FITC-oligos) and L02 (transfected with GFP-expression vector). FITC or GFP signals from transfected cells were examined under a fluorescence microscope at 24 hr post-transfection.

(B) Flow cytometry analysis showed the cell population relative to the FITC or GFP intensity. The shift of cell population to the right with higher FITC or GFP signals represented the transfected cells (transfection efficiency).

Table 2.5 Transfection efficiency of cell lines

Cell lines	Transfection reagent	Transfection of FITC oligos or GFP-vector	Transfection time	Transfection efficiency
SK-HEP1	Lipofectamine™ 2000	GFP-vector	24 hr	39.84%
SK-HEP1	Lipofectamine™ 2000	FITC-oligos	24 hr	94.12%
Hep3B	Lipofectamine™ 2000	FITC-oligos	6 hr	90.54%
HKCI-9	Lipofectamine™ 2000	FITC-oligos	24 hr	94.70%
L02	FuGENE®HD	GFP-vector	24 hr	36.26%

2.7.2 Sub-cloning

For constructing the gene expression vector, the cDNA clones containing the entire CDS of *CRYLI* (Image ID: 6451755) and *BOPI* (SC319330) were purchased from Mammalian Genomic Collection (MGC) (Invitrogen, Carlsbad, CA) and OriGene (Rockville, MD) respectively.

Specific primer-pairs were designed to amplify the gene coding sequences by *Pfu* DNA polymerase (Stratagene, Aligent, Cedar Creek, TX) (Accession No. of *CRYLI* CDS: BC071810; Accession No. of *BOPI* CDS: NM_015201) with the insertion of N-terminal and C-terminal linkers containing the appropriate restriction enzyme sites. Both the PCR products (insert) and pcDNA3.1 (vector) were double digested with corresponding restriction enzymes (NEB, Ipswich, MA) at 37°C overnight. The digested DNAs were then purified using QIAquick PCR Purification Kit (Qiagen, Valencia, CA). The insert was ligated to the pre-digested pcDNA3.1 vector (Invitrogen, Carlsbad, CA) in insert/vector molar ratio of about 10:1 by T4 DNA Ligase (Invitrogen, Carlsbad, CA) at 16°C overnight. Ligation product was heat shock transformed into TOP-10 *E.coli* cells (Invitrogen, Carlsbad, CA) at 42°C for 45 sec. Transformed cells were recovered in glucose-rich SOC medium at 37°C for 1 hr and then selected overnight on LB agar plate with Ampicillin (50µl/ml) (Sigma-Aldrich, St. Louis, MO). Ten colonies were picked for PCR to check for the presence of insert. Colonies with insert were inoculated in LB broth/Ampicillin (100µl/ml) for overnight and subjected to plasmid extraction using MiniPrep Kit (Qiagen, Valencia, CA). Plasmids were sequence verified prior to further investigative studies. Only plasmids with correct gene coding sequences were

subjected to large scale preparation using MaxiPrep Kit (Qiagen, Valencia, CA).
Subcloning primers for *CRYLI* and *BOPI* were listed in Table 2.6.

Table 2.6 Primer sequences for *CRYL1* and *BOP1* sub-cloning

Sub-cloning	Sequence (5'→3')	T_m (°C)
<i>CRYL1</i>		
(<i>EcoRI</i>) <i>CRYL1</i>-forward	GGTGGTGAATTCATGCTGTTTGCCAGTGGAGG	78.3
(<i>XhoI</i>) <i>CRYL1</i>-reverse	GGTGGTCTCGAGTCACTGGGGCTGCACTTGAC	79.9
<i>BOP1</i>		
(<i>HindIII</i>) <i>BOP1</i>-forward	CCCAAGCTTATGGCGGGTTCGCGGGGTGCG	81.6
(<i>EcoRI</i>) <i>BOP1</i>-reverse	CCGGAATTCCTAGGTGAAGAGGCGGACAGT	71.0

2.7.3 Cycle sequencing

The DNA sequencing was performed using the BigDye Terminator Cycle Sequencing Kit (ABI, Foster City, CA). In 15 μ l of sequencing reaction, 2 μ l of plasmid was mixed with 3.22 μ M primer, 2.25 μ l Sequencing buffer and 1.5 μ l Big Dye. The thermal cycling conditions were as follows: 1 min at 96°C for 10 sec, annealing at 50°C for 5 sec and extension at 60°C for 4 min. To remove unincorporated nucleotides, the sequencing PCR products were purified with SephadexTM G-50 (GE, Piscataway, NJ) fine column. Then 8 μ l of Hi-DiTM formamide (ABI, Foster City, CA) was added to the purified product and the DNA was denatured at 95°C for 5 min. The denatured DNA was chilled on ice for 5 min prior to the sequencing analysis by the automated ABI PRISM[®] 3100XL Genetic Analyzer (Foster City, CA).

The sequences were extracted and analysed by ABI PRISM[®] 3100 Genetic Analyzer Data Collection Software v1.1 and DNA sequencing analysis software v3.7 (ABI, Foster City, CA). The UCSC Blat search Genome and NCBI Basic Local Alignment Search were used for sequence alignment.

Table 2.7 Primer sequences for *CRYL1* and *BOP1* cycle sequencing

Cycle sequencing		Sequence (5'→3')	T _m (°C)
<i>CRYL1</i>	CRYL1 seq_1	ACTTCATCTCCTTTCTGATGTTTTTC	59.2
	CRYL1 seq_2	GAAAACATCAGAAAGGAGATGAAGT	59.2
	CRYL1 seq_3	ATCCTGTGAATCCGCCATA	58.9
	CRYL1 seq_4	CTCAATGCAGAAGGTATGTTAAGCT	60.2
<i>BOP1</i>	BOP1 seq_1	GATTGGGGATGAGTATGCGG	56.3
	BOP1 seq_2	CCCCTCCCTGGTGGAGAAGG	61.3
	BOP1 seq_3	GTGAATGTAGACCCTGAGGA	48.3
	BOP1 seq_4	CAGCCGGCCCGCTGGCTGGA	72.8
	BOP1 seq_5	TGACCTGGATCTTTCCACCA	54.8
	BOP1 seq_6	TAGAAGGCACAGTCGAGGCT	53.8

2.7.4 Cell viability (MTT) and cell proliferation assays (BrdU-incorporation)

Cell viability was assessed by a tetrazolium salt, 3-[4,5-dimethylthiazol-2-yl]-2,5-diphenyl tetrazolium bromide (MTT) assay. MTT is the substrate of succinate-tetrazolium reductase belonging to the mitochondrial respiratory chain and is active only in viable cells. In brief, cells were seeded in 96-well culture plate in 5 replicates (SK-HEP1, Hep3B and HKCI-9 were seeded at 2×10^3 cells/well while L02 was seeded at 3×10^3 cells/well). MTT (Sigma-Aldrich, St. Louis, MO) was added to each well at concentration of 500 μ g/ml and the cells were incubated for 2 hr. The reduced purple-colored formazan formed was then dissolved in 100 μ l dimethyl sulfoxide (DMSO) (Sigma-Aldrich, St. Louis, MO) and the absorbance was quantified by measuring at 570nm relative to the basal absorbance 630nm using the micro-plate reader Victor³™ multilabel counter (Perkin Elmer, Waltham, MA).

Cell proliferation was studied by the incorporation of thymidine analogs, 5-bromo-2'-deoxyuridine (BrdU) into the newly synthesized DNA of replicating cells (during the S-phase). BrdU (1X) labeling reagent provided in the Cell Proliferation ELISA, BrdU (colorimetric) Kit (Roche, Penzberg, Germany) was added to the cells seeded in 96-well plate in 5 replicates (at same density as in MTT assay). The cells in another 5 wells were cultured in normal medium without BrdU serving as background controls. After 2 hr incubation at 37°C, the cells were then fixed for 30 min with FixDenat solution which would denature the genomic DNA and exposed the incorporated BrdU for immune-detection. Peroxidase-conjugated anti-BrdU antibody (anti-BrdU-POD) was then added to the cells and incubated for 90 min. Anti-BrdU-POD is a mouse monoclonal antibody specifically recognizes BrdU and it shows no cross-reactivity with any endogenous cellular components

such as thymidine or uridine. It can therefore locate the BrdU label within the DNA. After washing 3 times with PBS, the substrate tetramethy-benzidine (TMB) was added and incubated for 2-5 min on shaker at 300 rpm in dark. Once the colour product was formed, 25µl of 1M H₂SO₄ was added to each well and incubated for an additional 1 min on shaker to stop further colour development. The reaction product was quantified by measuring the absorbance at 450 nm relative to background absorbance 690 nm.

For both MTT and BrdU assays, the experiments were carried out in every 24 hr basis for 6-7 consecutive days. The cell viability and cell proliferation were expressed as a percentage of maximum absorbance in a ratio between test and background control in 3 independent experiments.

2.7.5 Colony formation assay

pcDNA3.1-*CRYL1* or pcDNA3.1-vector transfected SK-HEP1 cells were seeded at 2x10⁴/well in 6-well culture plate. After 14 days of incubation in selective medium containing 1.5mg/ml G418 (Gibco Invitrogen, Carlsbad, CA), colonies were fixed and stained by 1% crystal violet (Sigma-Aldrich, St. Louis, MO) in methanol for 10 min followed by ddH₂O washing. Visible colonies containing >50 cells were scored, and results from duplicate assays were expressed as a mean from 4 independent experiments

2.7.6 Apoptosis assay

Annexin V is a Ca²⁺ dependent phospholipid-binding protein that has a high affinity for phosphatidylserine (PS) which will be translocated from the inner to the

outer leaflet of the plasma membrane in pre-apoptotic cells. Propidium iodide (PI) is a vital dye specially stains the dead cells and damaged cells with non-intact membrane. In combination of Annexin V and PI staining, pre-apoptotic and dead cell populations can be differentiated from viable cells.

Transfected SK-HEP1 at 4×10^5 cells were washed in cold PBS twice before being re-suspended in staining buffer containing PI and Annexin V conjugated with FITC in optimized ratio of 1:10 (Apoptosis Detection Kit; BD, Franklin Lakes, NJ). The cells were gently vortexed and incubated at room temperature for 15 min in dark. Four-hundred microlitres of 1X binding buffer was added to the stained cells prior the flow cytometry analysis. Double-labeled cells were immediately analyzed by the FACSCalibur System and CellQuest programme (BD, Franklin Lakes, NJ). Pre-apoptotic and dead cell populations were differentiated in different quadrants from viable cells. The mean ratios of dead cells and pre-apoptotic cells relative to viable cells were calculated from 3 independent assays.

2.7.7 Cell-cycle analysis

SK-HEP1 at 1×10^6 cells were transfected with either pcDNA3.1-*CRYL1* or pcDNA3.1-vector. On day 4 post-transfection, 50ng/ml nocodazole (Sigma-Aldrich, St. Louis, MO) was added and allowed to further incubate for 16 hr for synchronizing the cells at G₂-M phase. Nocodazole was then removed and the synchronized cells were gently dissociated by PBS. Further washed in PBS twice were essential for complete removal of the remaining drug. Cells in the density of 1×10^6 were re-seeded on 10cm culture dish and were harvested every 2 hr for up to 12 hr. Then the cells were re-suspended in 500 μ l PBS and immediately fixed in 4 ml of ice-cold 70% ethanol. The cells were left at -20°C overnight. Fixed cells were

centrifuged for 5 min at higher rpm (2000 rpm) in preventing sample loss after ethanol fixation as the cells would become flocculent. The cells were then incubated in 500µl staining solution containing RNase A (20µg/ml) (Roche, Penzberg, Germany), sodium citrate (1mg/ml), Triton X-100 (3mg/ml) and PI (10µg/ml) (Sigma-Aldrich, St. Louis, MO) for 15 min prior to flow cytometric analysis (BD FACSCalibur™, BD, Franklin Lakes, NJ). The average value of G₀-G₁, S and G₂-M phases were calculated from 4 independent experiments.

2.7.8 Invasion and migration assay

Cell migratory ability and metastatic potential were assessed by migration assay (Corning Inc., Corning, NY) and Matrigel Invasion Chamber (BD, Franklin Lakes, NJ) respectively. Both chambers consist of an 8µm pore size PET membrane while the Matrigel Invasion Chamber is additionally coated with a thin layer of MATRIGEL Basement Membrane Matrix on the PET.

The invasion and migration inserts were first allowed to rehydrate in plain DMEM for 2 hr at 37°C. Then the transfected cells re suspended in plain DMEM were seeded on the top of the invasion and migration inserts in the volume of 500µl and 200µl respectively. FBS supplemented DMEM (chemo-attractant) were added to the well, thus the lower side of the inserts was immersed in chemo-attractant. For invasion assay, transfected cells of Hep3B and HKCI-9 (8×10^4), SK-HEP1 (1×10^4) or L02 (2×10^4) were seeded and incubated for 5 days (Hep3B), 3 days (HKCI-9), 2 days (L02) or 1 day (SK-HEP1). For migration assay, 1×10^4 transfected cells (Hep3B, HKCI-9 and L02) or 0.5×10^3 (SK-HEP1) were seeded on transwell and incubated for 24 hr (Hep3B, HKCI-9 and SK-HEP1) or 48 hr (L02).

After incubation, the non-migrated/invaded cells were removed from the upper surface of the membrane by cotton swab. The invaded or migrated cells on the lower surface were then fixed in 100% methanol for 5 min and stained in Harris's haematoxylin (Sigma-Aldrich, St. Louis, MO) for 20 min. The inserts were subsequently rinsed with ddH₂O, immersed in 80% ethanol twice for 2 min and 100% ethanol twice for 2 min. After the dehydration process, the dried inserts were cut out and mounted on glass slide.

The >20 views were analysed under light microscope (400X) and the numbers of invaded and migrated cells were recorded. Each experiment was performed in duplicate inserts and the mean value expressed in the percentage from three independent experiments.

2.7.9 Wound healing assay

SK-HEP1 and Hep3B cells transfected with siGEF-H1 or siControl were seeded in 24-well culture plates in triplicate. When the cells reached 90% confluent, they were starved for 4 hr in plain DMEM. A straight sharp scratch of about 1mm width was applied in the middle of the well by p200 pipette tip followed by two times of PBS wash. The wound closure was monitored and images were recorded every 24 hr. Three independent experiments were performed.

2.8 IMMUNO-FLUORESCENT IMAGING

Transfected cells were seeded at a density of 2×10^4 onto a cover-slip (22 × 22 mm) placed in a 6-well plate for overnight. The cells were rinsed with PBS twice and fixed with 4% paraformaldehyde (Sigma-Aldrich, St. Louis, MO) for 15 min. Following the fixation, cells were gently washed twice with PBS for 5 min on a shaker, and permeabilized with 0.1% Triton X-100 (Sigma-Aldrich, St. Louis, MO) for 5 min. Cells were gently washed twice with PBS at room temperature for 5 min on a shaker. Goat serum (Invitrogen, Carlsbad, CA) was added to block the non-specific binding for 1 hr. The primary antibodies (E-cadherin, cytokeratin 18, N-cadherin and vimentin) were then added to cells and incubated for 3 hr at room temperature followed by PBS wash. Corresponding secondary antibody Alexo-Fluro® 488 (1:250; Invitrogen, Carlsbad, CA) was added and incubated for further 2 hr (Table 2.8). After final washing in PBS, the cell nuclei were counterstained with DAPI (Sigma-Aldrich, St. Louis, MO) in anti-fade solution (Vector Laboratories, Burlingame, CA). Images were captured using confocal microscope LSM 5 PASCAL (Carl Zeiss, Gottingen, Germany).

Specifically, filamentous actin (F-actins) was stained in 7.6 μ M of TRITC-labeled phalloidin (Sigma-Aldrich, St. Louis, MO) at room temperature for 20 min in dark. Phalloidin is a toxin from the toadstool *Amantia phalloides* that binds to actin (Cooper JA, 1987). Post-staining washes in PBS and DAPI counterstained were carried out as described above.

Table 2.8 Primary antibodies for immuno-fluorescence microscopy

Antibody	Source	Primary dilution	Secondary dilution	Company
E-cadherin	Mouse	1:100	1:250	Zymed, Invitrogen Corporation
Cytokeratin 18	Mouse	1:500	1:250	Dako
N-cadherin	Mouse	1:100	1:250	Zymed, Invitrogen Corporation
Vimentin	Mouse	1:250	1:250	Santa Cruz Biotechnology
TRITC-labeled Phalloidin	---	1:100000	1:250	Sigma-Aldrich Company

2.9 WESTERN BLOT

The cells with 80% confluence were rinsed with PBS and harvested by Cell Dissociation buffer (Gibco Invitrogen, Carlsbad, CA). The cells were then lysed in RIPA lysis buffer supplemented with protease inhibitors including 1mM PMSF (GE, Piscataway, NJ), 1X protease inhibitor cocktail (Sigma-Aldrich, St. Louis, MO), 1X pepstatin A (Roche, Penzberg, Germany). The lysate was incubated on ice for 15 min and centrifuged at 13,000 rpm at 4°C for 15 min. The protein concentration was determined by the standard curve plotted by the concentration gradient of BSA (Sigma-Aldrich, St. Louis, MO) in Bradford reagent (Bio-Rad, Hercules, CA).

Twenty micrograms of protein lysate mixed with Laemmli sample buffer was first boiled at 95°C for 5 min. According to the molecular weight of target protein, the proteins were separated on 8-15% of acrylamide gel. After separation, the SDS-PAGE gel was equilibrated in transfer buffer for 5-10 min to remove the salts and detergents in electrophoresis buffer. All the blotting paper and nitrocellulose membrane (GE, Piscataway, NJ) were also pre-wetted in transfer buffer. Then the proteins were transferred onto nitrocellulose membrane and the membrane was blocked in 5% non-fat milk or BSA in TBST at room temperature for 1 hr. The blot was incubated with primary antibody of the target protein diluted in appropriate concentration in milk or BSA at 4°C overnight with gently shaking. After washing the blot with TBST twice, corresponding HRP conjugated secondary antibody was added for further 1.5 hr incubation with agitation. The blot was washed twice in TBST and followed by addition of chemiluminescent HRP substrate, ECL reagents or ECL plus reagents (GE Healthcare). Probing against β -actin or GAPDH was used as the loading control in parallel to the experiment (Table 2.9).

Table 2.9 Primary antibodies for Western blot

	Antibody	Source	Primary dilution	Secondary dilution	Molecular Weight (kDa)	Company
<u>Chapter 3</u>						
	CRYL1	Goat	1:500	1:2000	35	Santa Cruz Biotechnology
Cell cycle	Cyclin B2	Mouse	1:1000	1:5000	51	Santa Cruz Biotechnology
	Cdc2	Mouse	1:1000	1:5000	34	Santa Cruz Biotechnology
Apoptotic pathway	Cleaved PARP	Rabbit	1:1000	1:5000	89	Cell Signaling Technology
Internal control	β -actin	Mouse	1:10000	1:20000	42	Sigma-Aldrich Company
<u>Chapters 4 and 5</u>						
	BOP1	Rat	1:100	1:500	90	Ascenion
Rho pathway	GEF-H1	Rabbit	1:1000	1:5000	120	Cell Signaling Technology
	ROCK1	Rabbit	1:1000	1:5000	160	Cell Signaling Technology
	Cleaved ROCK1	Rabbit	1:1000	1:5000	130/30	Millipore Corporation
	MLC2	Rabbit	1:500	1:1000	18	Cell Signaling Technology
	Phospho-MLC2	Mouse	1:500	1:1000	18	Cell Signaling Technology
	RhoA	Rabbit	1:1000	1:5000	21	Cell Signaling Technology
EMT pathway	Rac1/2/3	Rabbit	1:1000	1:5000	21	Cell Signaling Technology
	Cdc42	Rabbit	1:1000	1:5000	21	Cell Signaling Technology
	E-cadherin	Rabbit	1:1000	1:5000	135	Cell Signaling Technology
	Cytokeratin 18	Mouse	1:1000	1:5000	45	Dako
	α -catenin	Rabbit	1:1000	1:5000	100	Cell Signaling Technology
	γ -catenin	Rabbit	1:1000	1:5000	83	Cell Signaling Technology
	N-cadherin	Mouse	1:1000	1:5000	130	Santa Cruz Biotechnology
	Vimentin	Mouse	1:500	1:2000	57	Santa Cruz Biotechnology
	Fibronectin	Rabbit	1:1000	1:5000	220	Sigma-Aldrich Company
	Internal control	GAPDH	Mouse	1:25000	1:30000	37

2.10 NORTHERN BLOT

Ten micrograms of total RNA of Hep3B and HKCI-9 were resolved electrophoretically in 1.5% agarose gel with formaldehyde at constant voltage of 120V. The gel was equilibrated in 0.5X TBE (Sigma-Aldrich, St. Louis, MO) for 5 min. Then resolved RNA was capillary blotting onto the Nytran Plus nylon membrane (Schleicher & Schuell, Dassel, Germany) at 0.25mA for 1.5 hr. After blotting, RNA was fixed by UV cross linking at $1200 \times 10^{12} \mu\text{J}$ for 30 sec using a UV cross-linker (Stratagene, Agilent Technologies, Santa Clara, CA). A 40-mer oligonucleotide complementary to nt 68-108 of the human 5.8S rRNA (probe sequence: 5'-GCGTTCGAAGTGTCGATGATCAATGTGTCCTGCAATTCAC-3') was labeled with [γ - ^{32}P]-adenosine triphosphate (ATP) using Poly Nucleotide Kinase (PNK) (GE, Piscataway, NJ) incubated at 37°C for 1 hr and then incubated at 70°C for 10 min. Probe was purified by a SephadexTM G-50 fine column (GE, Piscataway, NJ) to remove unincorporated [γ - ^{32}P] -ATP.

Hybridization was performed in ULTRAhyb®-Oligo hybridization buffer (Ambion, Austin, TX) containing labeled probe at 42°C overnight. After post-hybridization washes in 2X SSC/0.1% SDS for 3 times at room temperature for 5 min, followed by 1X SSC/0.1% SDS wash at 42°C for 15 min, the blot was visualized by auto-radiography (GE, Piscataway, NJ).

2.11 METHYLATION-SPECIFIC PCR (MSP)

Genomic DNA at 500ng extracted from 12 cell lines and 40 primary tumors were subjected to bisulfite conversion by EZ DNA Methylation-Gold™ Kit (Zymo Research, Orange, CA) for the methylation status study of *CYRL1* promoter region. In brief, 130µl of bisulfite containing CT Conversion Reagent was added to 20µl of DNA samples and incubated in thermal cycler at 98°C for 10 min followed by 64°C for 2.5 hr. These incubations were mainly for the conversion of unmethylated cytosines to uracil while the methylated cytosines remained unchanged. The converted DNA mixed with 600µl of Binding Buffer were loaded into the Zymo-Spin™ IC column and centrifuged at 13,000 rpm. Desulphonation was carried out by adding 200µl of Desulphonation Buffer to the column and incubated at room temperature for 15 min. The column was then centrifuged at 13,000 rpm and the DNA was eluted by adding 50µl Elution Buffer. Two microlitres of the bisulfite treated DNA were subjected to PCR of 35 cycles. Specific primers were designed for amplifying the methylated and unmethylated regions of *CYRL1* promoter (Table 2.10).

Table 2.10 Primer sequences for MSP on *CRYLI* promoter region

<i>CRYLI</i> promoter region	Primer Sequences	Product size (bps)	T_m (°C)
Methylated primers	Forward: 5' AAGAAGGTTAGGAGTTAGGGTACGA 3' Reverse: 5' TACGAACTAAACGCAAAAACACTACG 3'	164	60
Unmethylated primers	Forward: 5' AAGAAGGTTAGGAGTTAGGGTATGA 3' Reverse: 5' TACAACTAAACACAAAACACTACAAC 3'	164	60

2.12 5-AZA-2'-DEOXYCYTIDINE (5-AZA) AND TRICHOSTATIN A (TSA)

TREATMENTS

Three HCC cell lines (HKCI-2, HKCI-C1 and HKCI-C2) were exposed to demethylating agent, 5-Aza (Sigma-Aldrich, St. Louis, MO), or histone deacetylase inhibitor, TSA (Sigma-Aldrich, St. Louis, MO), or the combination of both. Cell treated with 1 μ M of 5-Aza were cultured for 72 hr in line that fresh medium with 5-Aza was replenished to the cell in every 24 hr. For TSA treatment, 30 nM of TSA was added to cells for 24 hr. In combination treatment, cells were first treated with 1 μ M 5-Aza for 72 hr followed by 300nM TSA for an extra 24 hr while untreated cells were served as control along the experiments. Total RNA was extracted and the *CRYLI* expression was estimated by qRT-PCR from 3 independent experiments.

2.13 GTPASE ACTIVITY ASSAYS OF RHOA, RAC1 AND CDC42

Cultured cells (siRNA transfected SK-HEP1 and Hep3B cells; pcDNA3.1-Vector or pcDNA3.1-*BOP1* expressed L02 cells) at approximately 85-90% confluence were rinsed twice with ice-cold Tris-Buffered Saline (TBS). The cells were lysed by adding 500 μ l diluted Mg²⁺ lysis/Wash Buffer (MLB) provided in the Rho Activation Assay Kit or Rac1/Cdc42 Activation Assay Kit (Upstate, Millipore, Bedford, MA) containing 10% glycerol, 10 μ g/ml leupeptin and aprotinin (Sigma-Aldrich, St. Louis, MO). The lysed cell were incubated on ice for 15 min and followed by centrifugation at 14,000 \times g for 5 min at 4°C. The supernatant was aliquot into 500 μ l each and 20 μ g slurry of Rho Assay Reagent (Rhotekin Rho Binding Domain) or 10 μ g slurry of Rac1/Cdc42 Assay Reagent (PAK-1 PBD, agarose) was added. The reaction mixtures were gently rocked at 8 rpm for 2 hr at 4°C. Then the agarose beads were collected by centrifugation at 14,000 \times g for 1 min. After removing the supernatant, the beads were washed with 500 μ l MLB three times and re-suspended in 25 μ l (for RhoA pull down) or 40 μ l (for Rac1/Cdc42 pull down) of 2X Laemmli sampling buffer, then the beads were boiled for 5 min. SDS-PAGE and Western blot were performed and the amount of GTP bound RhoA, Rac1 and Cdc42 were compared to their total amount in whole cell lysate.

2.14 STATISTICAL ANALYSIS

The *CRYLI*, *BOP1* and *GEF-H1* expressions in tumors and non-tumoral liver were compared by paired *Student's t-test*. The unpaired *t-test* was used in comparing *BOP1* or *GEF-H1* expression in HCC cell lines with normal liver samples. Pair-wise comparisons (vector control and *CRYLI* transfected group; vector control and *BOP1* transfected group; siBOP1/siGEF-H1 and siControl transfected cells) in functional investigations were also conducted by paired *Student's t-test*.

The Mann-Whitney test was used to examine the *CRYLI* or *BOP1* or *GEF-H1* mRNA expression with clinicopathological features including tumor staging and the presence of microvascular invasions. The relation of *CRYLI* to tumor size was analysed by Pearson correlation.

The overall and disease-free survivals were calculated from the date of tumor resection to the time of first recurrence (disease-free survival) or death (overall survival) (both to a maximum of 120 months). Patients who were lost follow-up or died from causes unrelated to HCC were treated as censored events. Kaplan-Meier survival curves were constructed according to the mRNA expression of *CRYLI* or *BOP1* or *GEF-H1*, and the differences between groups were analyzed using the log rank test. Correlations with patient's overall and disease-free survival were also investigated by Cox regression using MedCalc (MedCalc Software, Mariakerke, Belgium).

A *P*-value of ≤ 0.05 was considered to be statistically significant. All statistical analyses were performed using GraphPad Prism 3.02 (GraphPad Software Inc., San Diego, CA).

Chapter 3

**Array-CGH defines homozygous
deletions in HCC and *CRYL1* as a
novel tumor suppressor gene**

3.1 INTRODUCTION

Extensive genomic research over the past decade has identified a number of causative genetic deletions in HCC as briefly described in section 1.2. Recent informatics analysis on the genomic data further highlighted allelic losses on chr.9p21-p22, chr.13q12-q13 and chr.17p13 as causal molecular events in the HCC tumorigenesis (Poon TC *et al*, 2006; Hertz S *et al*, 2008). For most of these loci, the underlying tumor suppressor genes (TSGs) remain unsure. Though infrequent, homozygous loss of genomic sequences has been used as a tag for the identification of novel TSGs. Somatically acquired homozygous deletion (HD) is one of the mechanisms through which TSGs are inactivated. Positional mapping for HDs in tumor cell lines have guided the localization of many important TSGs including *CDKN2A* (Kamb A *et al*, 1994), *SMAD4* (Hahn SA *et al*, 1996), *PTEN/MMAC1* (Li J *et al*, 1997), *FHIT* (Thiagalingam S *et al*, 1996), *DMBT1* (Mollenhauer J *et al*, 1997), *LIMD1* (Sharp TV *et al*, 2008). Since HDs have been instrumental in the identification of recessive cancer genes, fine mapping investigations have been attempted to study HCC-associated HDs in cell lines, which is a proven resource for the identification of cancer-related genes. Moreover, reports on HD screening in HCC have been minimal to date.

The recent availability of high-density mapping tool array-CGH permits high-throughput identifications of genomic variations. In this part of my study, array-CGH was deployed to provide a comprehensive view on DNA copy changes in HCC cells. Particular emphasis has been undertaken to define gene dose within regions of allelic losses (AL) that have been implicated in the liver tumorigenesis (Poon TC *et al*, 2006; Hertz S *et al*, 2008). This array study examined a panel of HCC cell lines that included a unique repertoire of in-house established cell lines at

their early passages (HKCI series) (Pang E *et al*, 2002; Wong N *et al*, 2005; Chan KY *et al*, 2005) and 2 established cell lines (SK-HEP1 and Huh7). HD can be difficult to discern in primary tumors because of confounding hybridization signals from non-neoplastic cells within the tumor. The use of early passages cancer cell lines can overcome the problem in being devoid of non-neoplastic cells and at the same time not associated with the development of additional genetic alterations from extended *in vitro* culture (Jones S *et al*, 2008). Based on array-CGH analysis, a high frequency of biallelic deletions in HCC was found and a number of novel candidate genes within these small interstitial regions of homozygous losses was highlighted. In particular, crystalline Lambda1 (*CRYLI*) located on chr.13q12 exhibited the most frequent down-regulations and correlated with unfavourable prognosis of HCC patients. It was further demonstrated that HD of *CRYLI* is common in HCC and this novel TSG plays a significant functional role in the liver tumorigenesis.

3.2 RESULTS

3.2.1 Array-CGH defined HD regions

A total of 12 HCC cell lines was subjected to array-CGH analysis according to procedure described in Chapter 2.4. Array-CGH mapping uncovered 6 HD regions in our panel of HCC cell lines analyzed as shown in Table 2.2. These HD regions including chr.3q26.1, chr.9p21.3, chr.11p15.4, chr.13q12.11, chr.17p13.1 and chr.17p11.2-12, encompassed an average loss of 0.53Mb. The chromosomal CGH profiles of several HD regions on chr.9, chr.13 and chr.17 were shown in Figure 3.1. The sharp moving averages displacing towards \log_2 ratio of ≤ -3.0 on the left side along the chromosomes corresponded to the HD regions. Within the 6 HD regions, 24 homozygously deleted genes were suggested (Table 3.1). PCR validations of these HD candidates were performed and a concordant genomic loss of 15 genes in the same cell line was found (Figure 3.2).

Confirmed biallelic deleted genes were further assessed for mRNA expression by qRT-PCR. The relative expression of 12 genes that resided on important genomic aberrations of HCC, namely chr.9p21.3, chr.13q12.11, chr.17p13.1 and chr.17p11.2-12, were prioritized for evaluation. qRT-PCR experiments using primers as described in section 2.5 corroborated a loss of gene expression in the same cell line that harboured the genomic HD, which in turn conferred reliability on the array-CGH results (Figure 3.3A). However, subsequent examination of gene deregulations in the remaining cell lines failed to indicate common down-regulations for most genes which may not be HCC specific, except for *CRYL1* which showed distinct frequent down-regulations (Figure 3.4).

To establish the incidence of *CRYLI* down-regulations in HCC, its mRNA and protein expression in primary tumors were further examined. By qRT-PCR, 53% of primary HCC (n=66) showed down-regulations of *CRYLI* relative to normal livers. A significant *CRYLI* repression was also detected in tumors relative to the corresponding non-tumoral liver (*paired t-test* $P = 0.0097$) (Figure 3.3B and Figure 3.5A). The same trend of *CRYLI* down-regulation was also observed in 13/20 pairs of HCC samples by Western blot analysis (Figure 3.5B). In addition, the level of *CRYLI* expression was inversely correlated with tumor size (n=66; $R = -0.306$; $P = 0.013$) (Figure 3.6A) and it was more frequently down-regulated in the advanced Stage T3 tumors ($P = 0.027$) (Figure 3.6B). Remarkably, lowered *CRYLI* expressions also correlated with a shorter disease-free patient's survival ($P = 0.037$) (Figure 3.6C).

Table 3.1 Candidate homozygous deleted targets as defined by array-CGH

HD location	HD size (Mbp)	Cell line	Gene Symbol	Genomic validation
3q26.1	0.381	Huh7	SERPIN2	-
			PDCD10	-
			SERPIN1	-
9p21.3	1.352	SK-HEP1	MTAP	+
			CDKN2A	-
			CDKN2B	+
11p15.4	0.026	HKCI-11	HBB	+
			HBD	+
			HBG1	+
13q12.11	1.196	SK-HEP1 and Huh7	TUBA2	-
		SK-HEP1	HSMPP8	+
			PSPC1	-
			ZNF237	+
			ZNF198	-
			GJB2	+
			GJB6	+
			CRYL1	+
			TTC10	-
			IL17D	-
			XPO4	+
17p13.1	0.005	HKCI-9	TP53	+
17p11.2-12	0.248	HKCI-9	ADORA2B	+
			TTC19	+
			NCOR1	+
+ve control			β-globin	-----

“+” = Confirmed Homozygous Deletion; “-” = Non-validatable Candidate

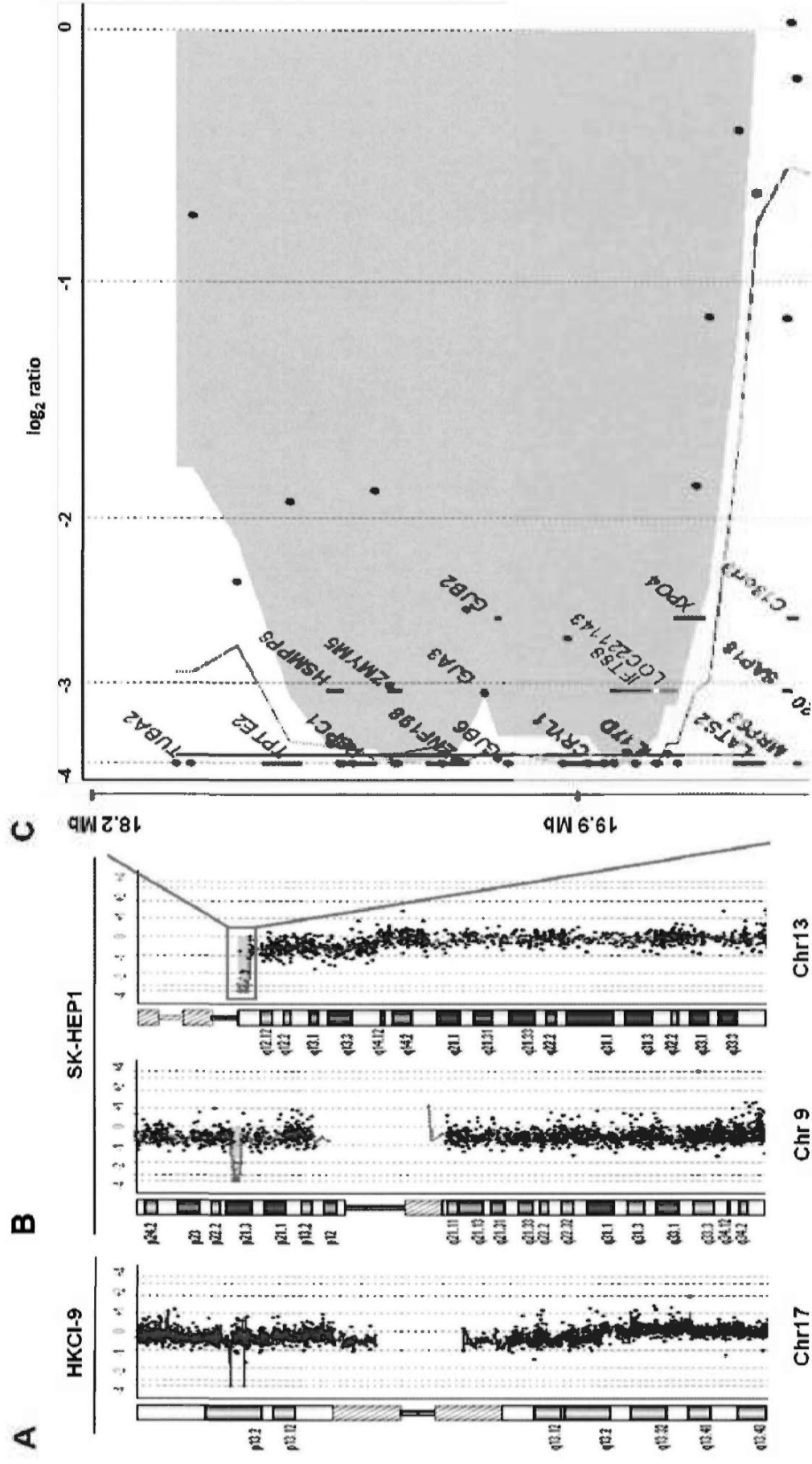


Figure 3.1 Array-CGH analysis on SK-HEP1 and HKCI-9

(A & B) Vertical profiles of chr.9, chr.13 and chr.17 were showed with a log₂ scale. The zero line represented the balanced region. Sharp moving averages displacing towards log₂ ratio of < -3.0 on the left side along the chromosomes corresponded to the HD regions.

(C) A high resolution profile of the homozygously deleted chr.13q12.11 locus was shown with the implicated candidate genes.

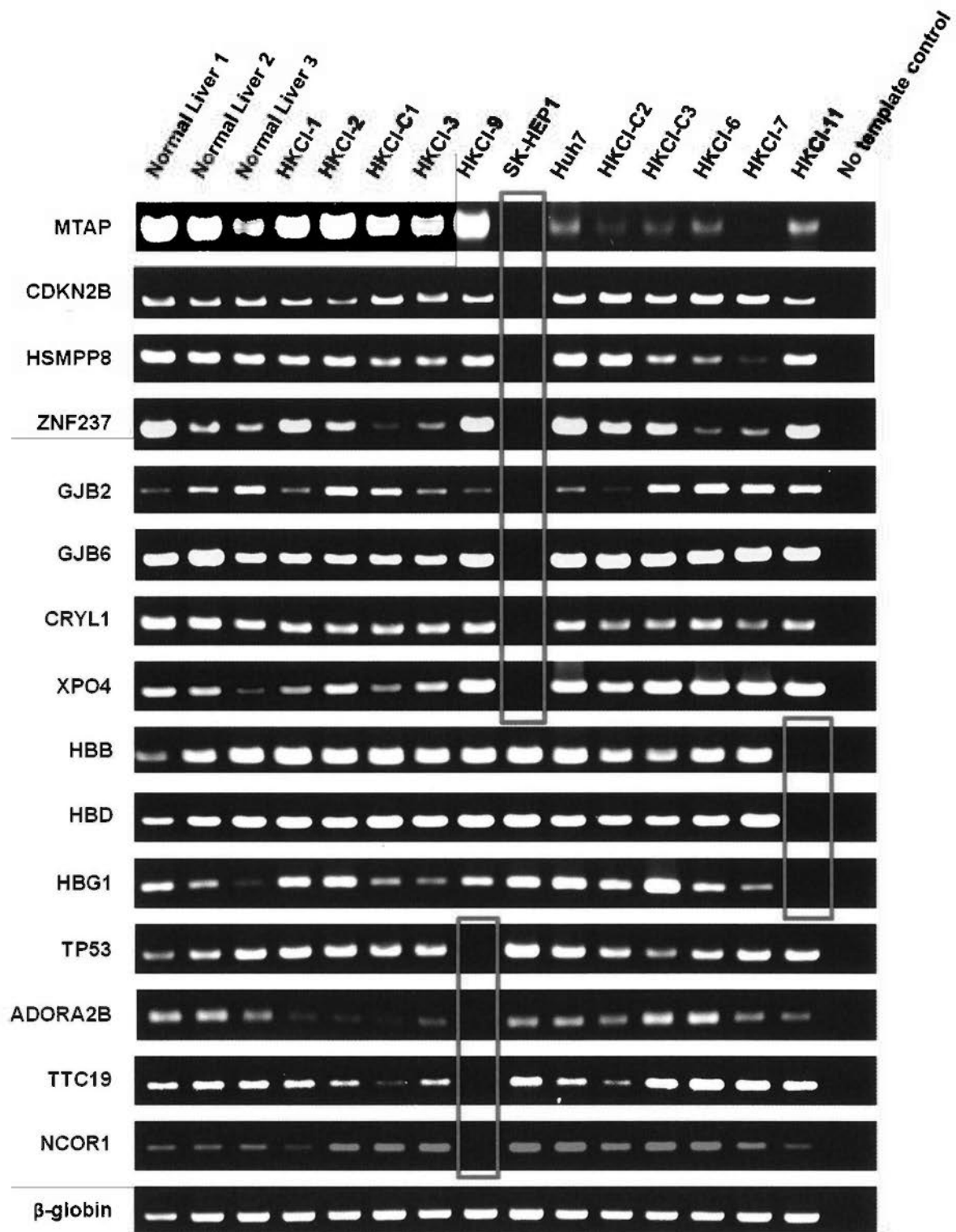


Figure 3.2 Genomic validation of homozygous deleted candidates

Primer pairs were designed in the proximity of array-CGH probe (Section 2.5). Biallelic genomic deletion was confirmed in 15 genes (highlighted in red boxes).

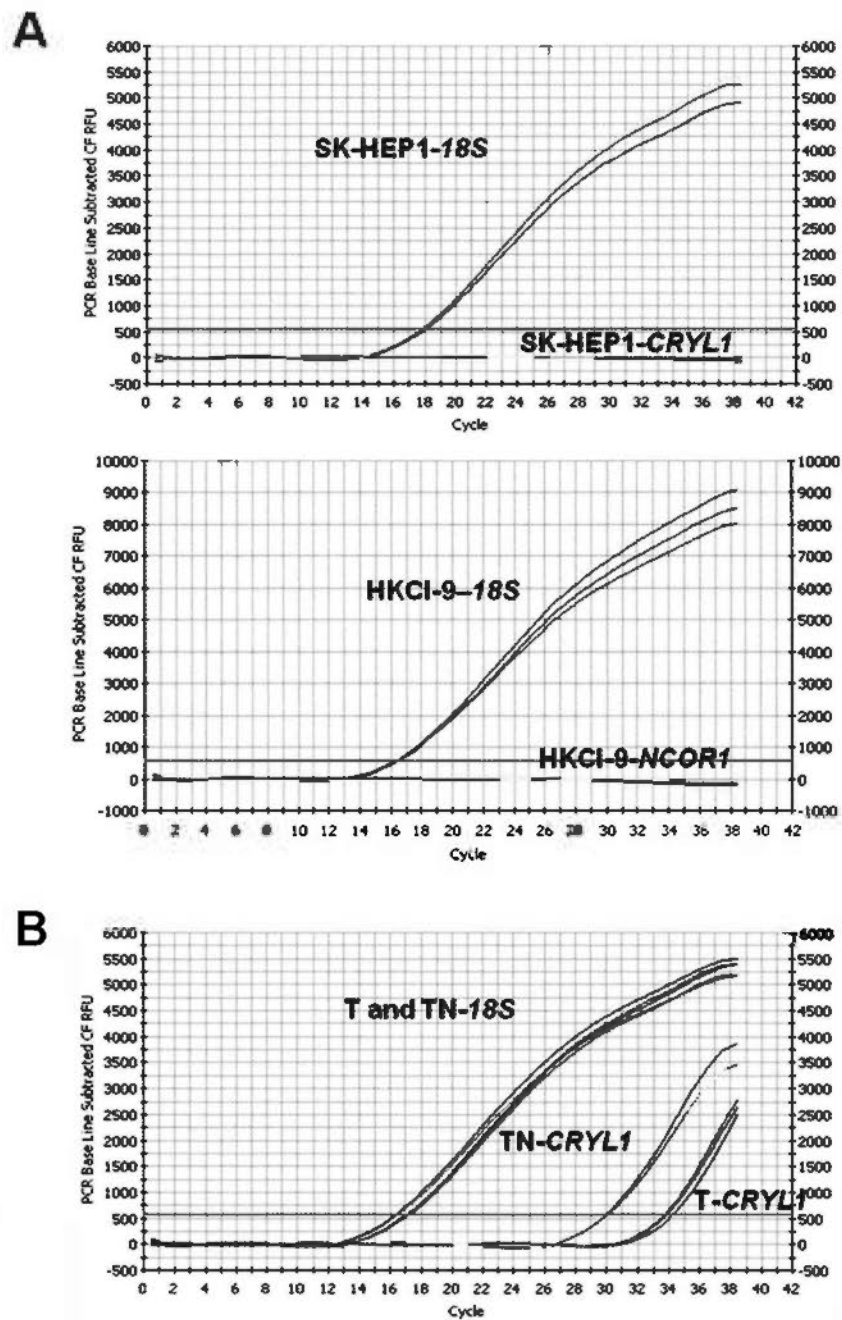


Figure 3.3 Examples of Amp/Cycle Graph from qRT-PCR analysis

(A) The qRT-PCR validations of HD genes for example *CRYL1* on SK-HEP1 and *NCOR1* on HKCI-9. (B) The qRT-PCR examination of *CRYL1* expression in a pair of representative HCC tumor sample with its adjacent non-tumoral liver sample.

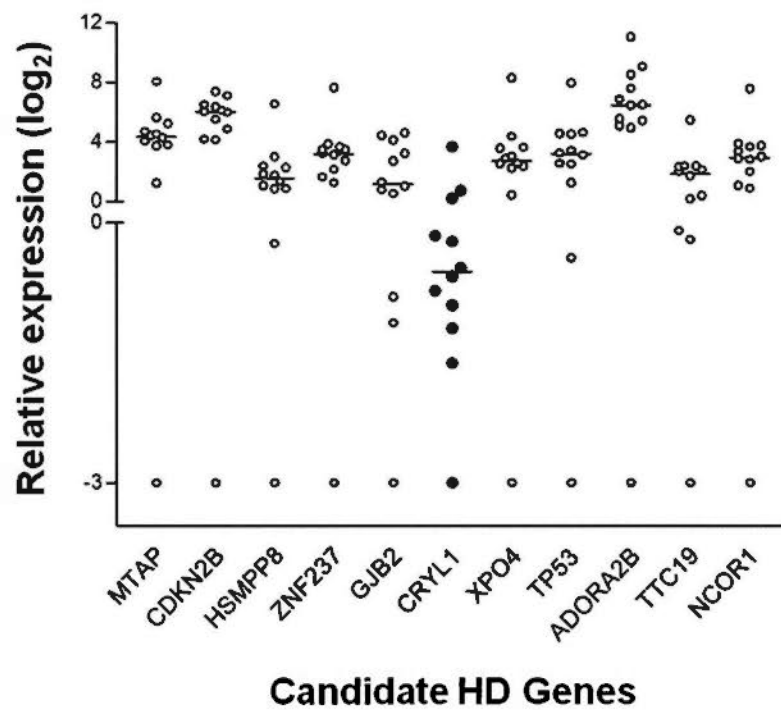
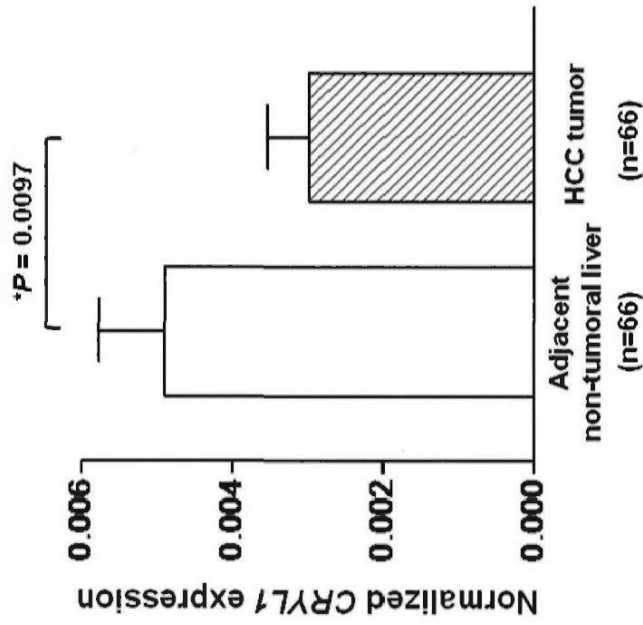


Figure 3.4 Relative expressions of candidate HD genes

The expressions of candidate HD genes were examined by qRT-PCR in 12 HCC cell lines. The expression levels (log₂) are plotted for each candidate. Among 11 genes studied, only *CRYL1* showed distinct down-regulations, where 5/12 cell lines (42%) displayed a fold reduction ranging from ~2-fold to negligible expression.

A qRT-PCR



B

Western Blot

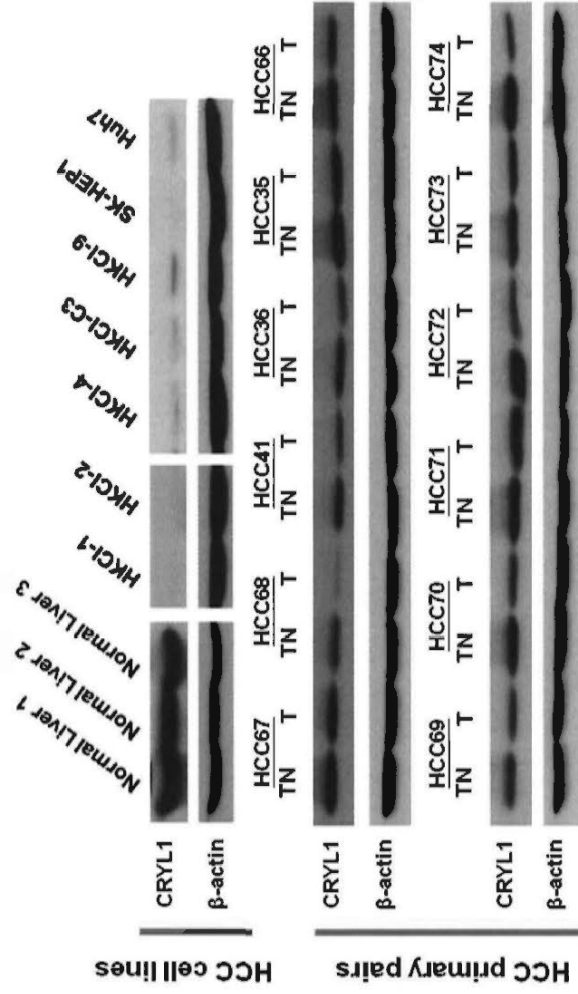


Figure 3.5 Frequent down-regulation of *CRYL1* in HCC cell lines and primary tumors

(A) Normalized *CRYL1* expression in 66 paired HCC tumors and adjacent non-tumoral livers shown. A significant down-regulation of *CRYL1* was found in tumors relative to its matching non-tumoral liver (*paired t-test). (B) Western blot analysis of *CRYL1* in 7/12 cell lines and 12/20 paired HCCs were shown. Significant *CRYL1* down-regulations were found in cell lines relative to normal livers and in primary tumors compared to its corresponding non-tumoral liver.

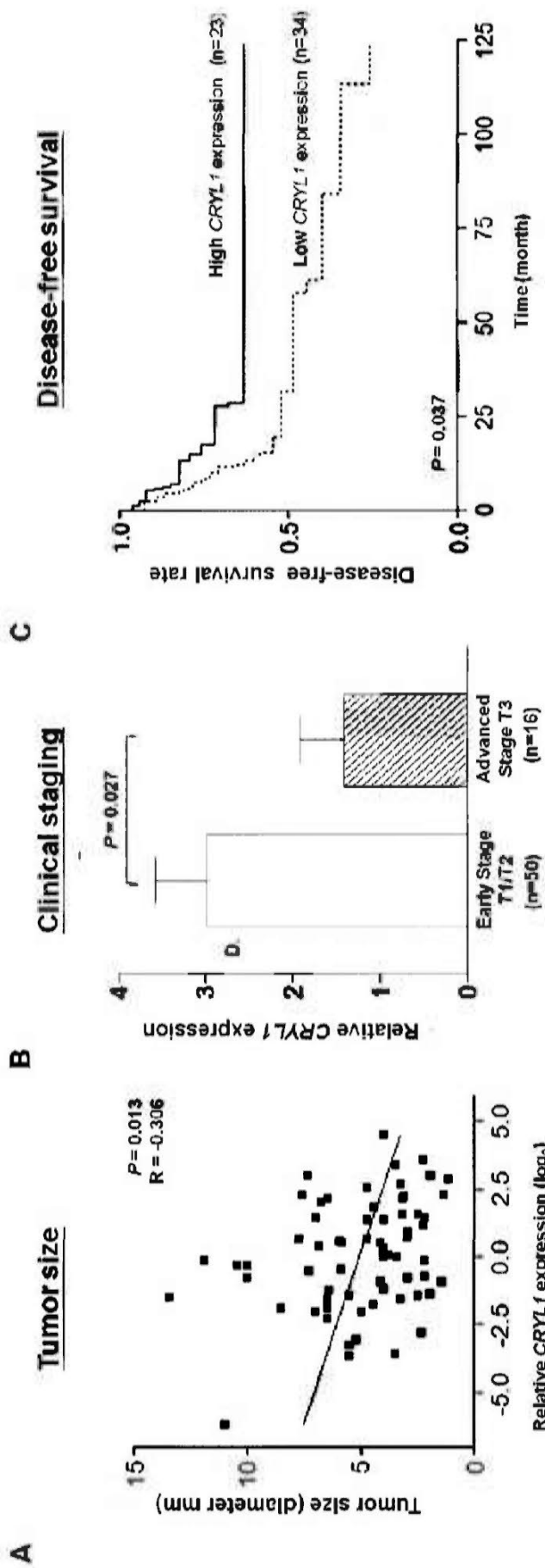


Figure 3.6 Clinicopathological correlations of *CRYL1* expression in HCC

(A) An inverse relationship between *CRYL1* expression and tumor size was found. Low *CRYL1* expression correlated with bigger tumor size. (B) *CRYL1* expressions in advanced Stage T3 tumors were markedly lower than early stage HCCs. (C) Kaplan-Meier analysis was performed on HCC patients who had tumors with *CRYL1* over-expression ($\log_2 \geq 1.5$) and patients with low *CRYL1* expression ($\log_2 \leq -0.4$). Disease-free survival of patients who had low *CRYL1* expression was evidently shorter.

3.2.2 Functional effects of *CRYLI*

Transfection of *CRYLI* in SK-HEP1, a cell line with HD of *CRYLI*, led to marked inhibition on cell viability. At day 6 post-transfection, pcDNA3.1-*CRYLI* transfected cells showed an approximate 45% reduction in total cell viability compared control vector ($P < 0.0001$; Figure 3.7A). In estimating the SK-HEP1 cell growth, there was an exponential increase in cell number in vector transfected cells from day 4 onwards, whilst cells transfected with pcDNA3.1-*CRYLI* showed no significant changes in cell number over the period of monitoring (Figure 3.7B). On day 6, a significant reduction in cell number was suggested in *CRYLI* transfected cells compared to vector control ($P = 0.0015$). The effect of *CRYLI* on cell growth was also confirmed from colony formation analysis. A differential cell growth between stable *CRYLI* transfectant and control group was also readily observed at 2-weeks after G418 selection. The control group showed significant increase in colony number and enlarged colony size compared to *CRYLI* expressing cells ($P = 0.029$) (Figure 3.7C). There was approximately 40% difference in the number of colonies formed between the 2 groups.

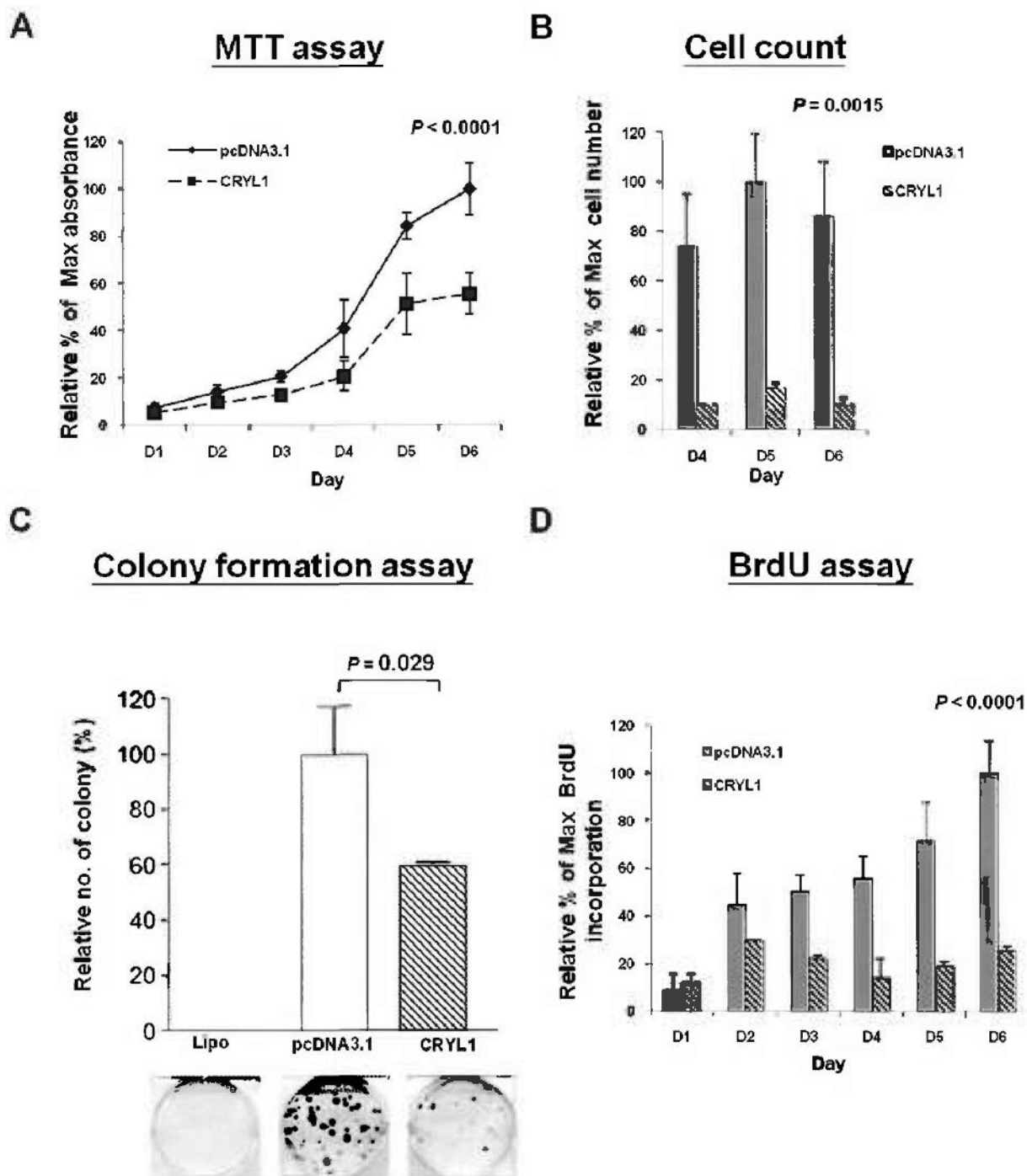


Figure 3.7 Functional effects of *CRYL1* on cell growth and proliferation

(A) MTT assay showed *CRYL1* transfected SK-HEP1 (dash line) has significantly lower cell viability than the control vector (solid line). (B) Cell growth as assessed by cell number estimation showed that the cell number in *CRYL1* transfected group (striped bar) was significantly less than the control group (solid bar) over the 6 days of monitoring. Data on day 4 to day 6 were shown. (C) In colony formation assay, *CRYL1* transfected group showed much reduced in number and smaller size of colonies compared to the vector pcDNA3.1 control group. (D) Examination of cell proliferation by BrdU incorporation showed the percentage of actively dividing cells in *CRYL1* transfected group (striped bar) was significantly lower than that in the control group (solid bar).

3.2.3 Effect of *CRYLI* on cell-cycle

To determine whether the effect on cell number was due to a hindered cell replication, BrdU incorporation assays were carried out. Result showed that *CRYLI* expression induced about 75% less actively dividing cells than control ($P < 0.0001$) (Figure 3.7D). It is therefore plausible that a lower percentage of cells taking part in cell division had impinged upon the overall cell growth. In this regard, undertook cell cycle analysis and apoptosis assays were further carried out to examine the underlying mechanistic effect of *CRYLI*.

Nocodazole synchronized vector and *CRYLI* transfected SK-HEP1 cells were studied for cell-cycle changes. Cell-cycle histogram at 0 hr showed about 80% of the vector or *CRYLI* transfected cells were successfully arrested in G₂-M phase due to nocodazole treatment (Figure 3.8A). At 10 hr and 12 hr following the removal of nocodazole, cell-cycle histograms showed an increased proportion of *CRYLI* transfected cells in G₂-M phase compared to vector control. The *CRYLI* transfected cells failed to re-gain entry to normal cell cycle leading to a significant decrease of cells in G₀-G₁ phase with time, a corresponding increase of cells at G₂-M phase was readily observed, which reached the optimum level with an average of 15% (sem \pm 4.36%) by 12 hr ($P < 0.05$) (Figure 3.8A). After nocodazole release, the whole cell lysate were collected every 2 hr up to 24 hr for Western blot examinations of the key regulators of G₂-M transition. The results indicated that there was a gradual accumulation of the cyclinB2 protein in *CRYLI*-treated cells after nocodazole release, which peaked at 10 hr and 12 hr. On the other hand, the level of Cdc2 remained largely unchanged over the same period (Figure 3.8B).

The effect of *CRYLI* expression on apoptosis was also investigated. By Annexin V-PI staining, the percentage apoptotic cells (pre-apoptotic + dead cells) in

CRYLI transfected group were higher than that of the control group. An average 25% increase in apoptotic cells was found in *CRYLI* transfected SK-HEP1 cells ($P = 0.017$) (Figure 3.9A). There was also an increase in the cleaved PARP, apoptosis marker, in *CRYLI* transfected cells compared to control group by Western blot analysis (Figure 3.9B).

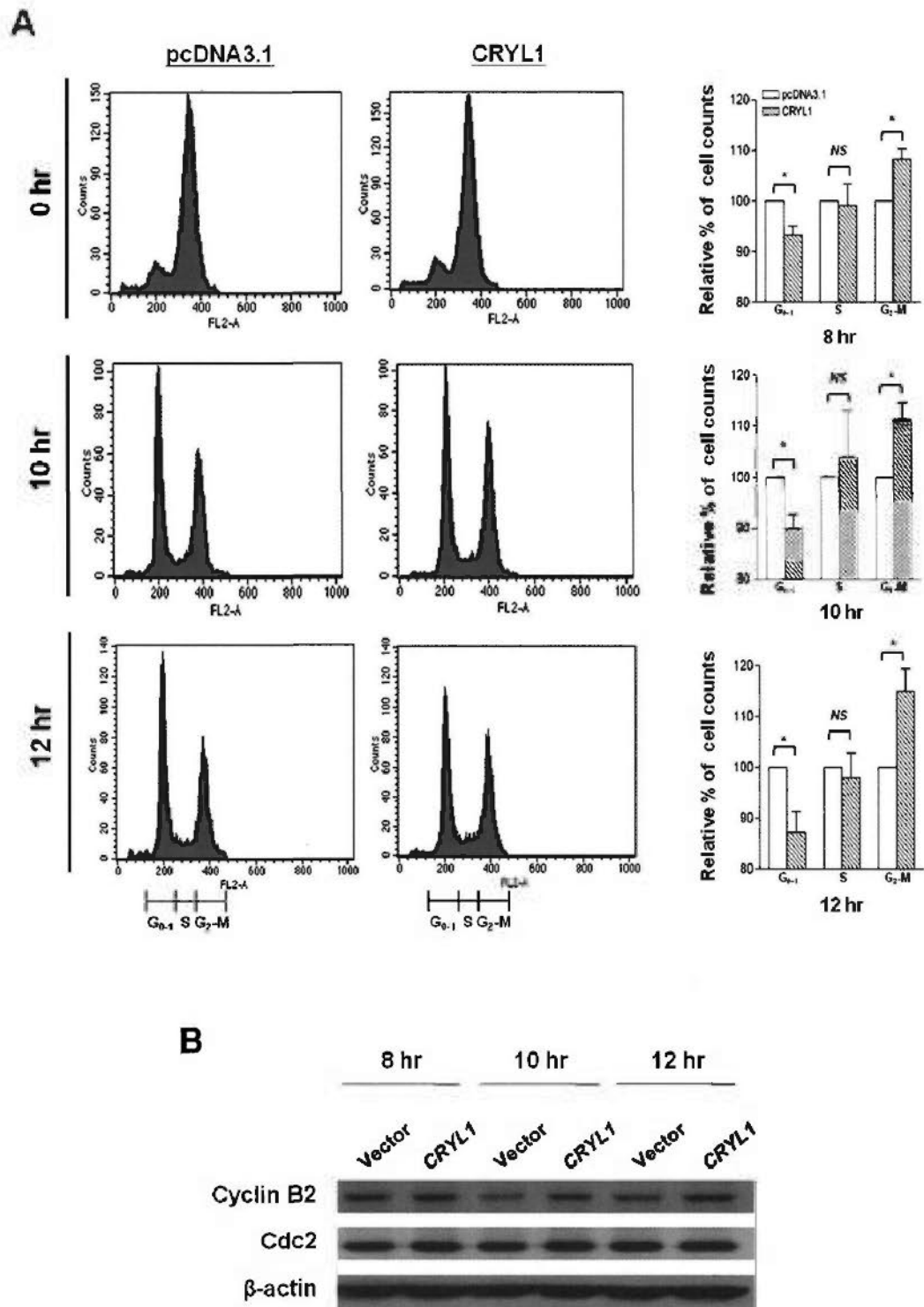


Figure 3.8 Functional effects of *CRYL1* on cell cycle arrest

(A) Cell-cycle histogram on the left panel of 0 hr showed about 80% of cells were successfully arrested in G₂-M phase in nocodazole treatment. The bar charts on the right panel showed the percentage of vector or *CRYL1* transfected cells in each phase from 8 hr to 12 hr. The effect of *CRYL1* caused a significant increase in cell population in G₂-M phase with time, which reached 15% (sem ± 4.36%) by 12 hr, and a corresponding decrease in G₀-G₁ phase was also observed (*P ≤ 0.05). (B) Western blot analysis for lysate harvested at 8 hr, 10 hr and 12 hr showed that there was a gradual accumulation of cyclin B2 in *CRYL1* transfected lysate that peaked at 10 hr to 12 hr when compared to vector transfection. The amount of Cdc2 remained similar over the period of 24 hr collection.

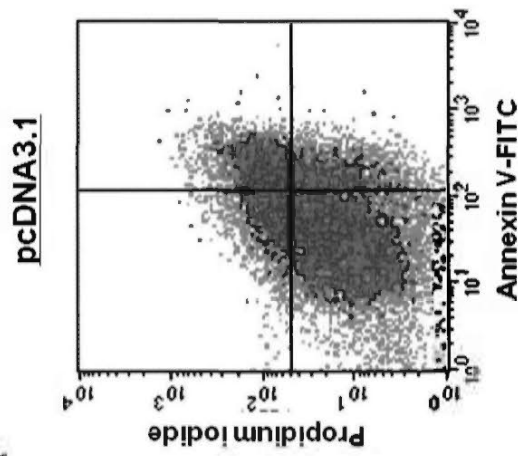
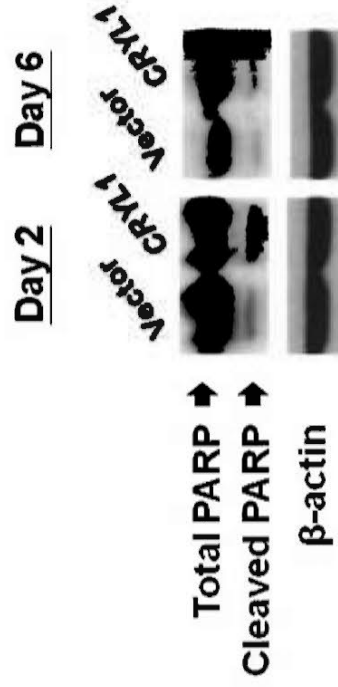
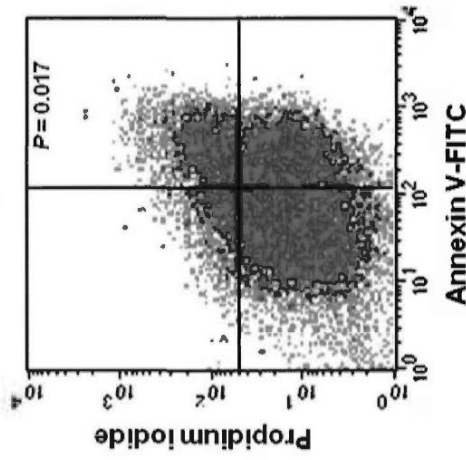
A**B**

Figure 3.9 Functional effects of *CRYL1* on apoptotic pathway

(A) Annexin V-PI staining indicated apoptotic cells [pre-apoptotic (lower right quadrant) + dead cells (upper right quadrant)] was 25% higher following *CRYL1* transfection compared to vector transfected cells. (B) The western blot analysis at day 2 and day 6 post-transfection showed an increase in the PARP cleavage in *CRYL1* transfected cells compared to control group.

3.2.4 Inactivating mechanisms of *CRYLI*

It is hypothesized that copy number loss is a major cause of *CRYLI* down-regulations in HCC. In 25 HCC specimens that displayed losses or down-regulations of *CRYLI*, qPCR analysis of *CRYLI* exons 1 to 9 showed the presence of HDs in as much as 36% of cases. Recurrent HDs were identified on exons 1, 5 and 8 (Figure 3.10). A corresponding down-regulation of *CRYLI* with mono-allelic loss or presence of HD was detected in 72% of cases, suggesting a strong association for genomic loss in the reduced gene expression. Nevertheless, other inactivating mechanism(s) in the suppression of *CRYLI* is likely present in the remaining discordant cases.

Since the promoter region of *CRYLI* harbours one closely resided CpG-island on 55-478bp upstream to the start codon, bisulfite conversion and methylation specific PCRs (MSP) were firstly performed on 12 cell lines and 40 primary tumors to examine if promoter hypermethylation contributed to *CRYLI* repression. Distinct methylation band was observed in MSP experiment of 3 cell lines and 5 primary cases suggesting that their promoter regions of *CRYLI* were methylated (Figure 3.11A). The *CRYLI* expressions of these methylated cases were at least 1.5-fold down-regulated. Three cell lines, HKCI-2, HKCI-C1 and HKCI-C2, displayed promoter hypermethylation were subjected to single demethylating agent 5-Aza or single histone deacetylase inhibitor TSA, or combined treatment of 5-Aza and TSA. Single agent 5-Aza induced *CRYLI* re-expression in HKCI-C2 ($P = 0.0028$), while TSA augmented marked *CRYLI* expression in both HKCI-C1 ($P = 0.004$) and HKCI-C2 ($P < 0.0001$). The combined 5-Aza and TSA exposures, however, did not result in a further synergistic effect in these 2 cell lines (HKCI-C1: $P = 0.014$; HKCI-C2: $P < 0.0001$) (Figure 3.11B). The remaining cell line HKCI-2 was still

responsive towards 5-Aza or TSA, but the *CYRL1* re-expression was not statistically significant.

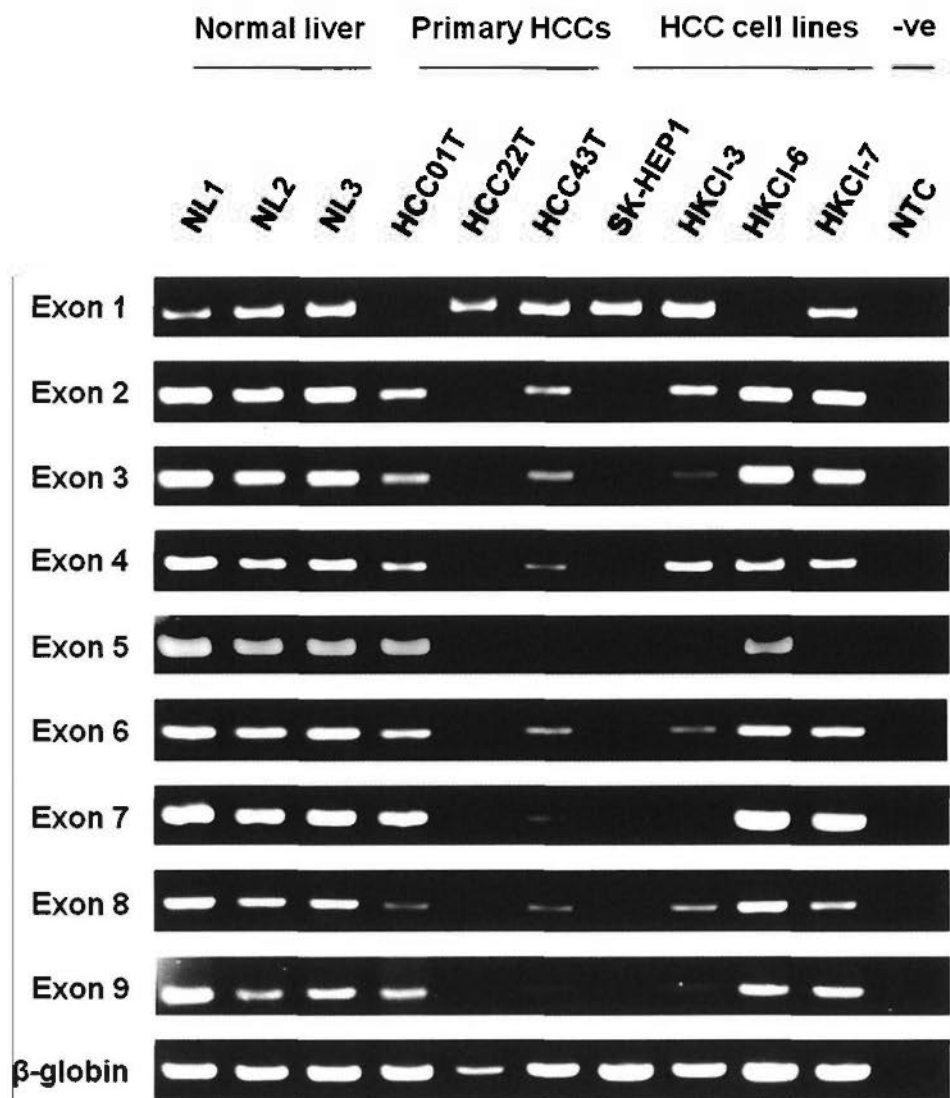
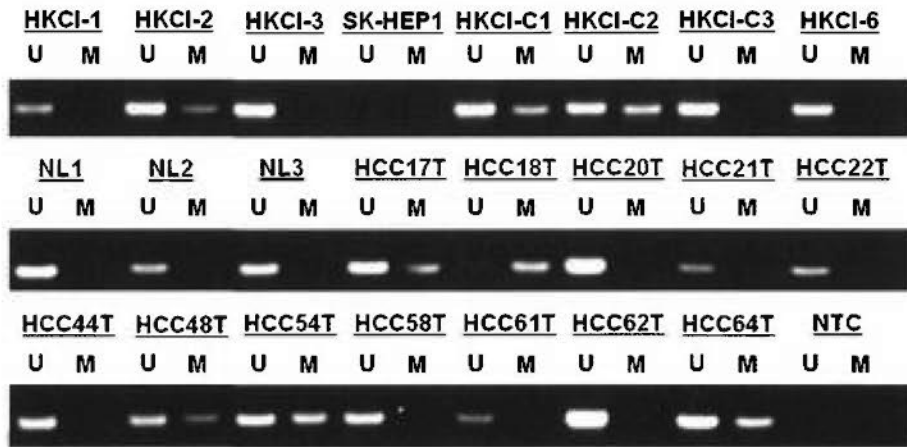


Figure 3.10 Genomic loss of *CRYL1*

Representative gel electrophoresis images of genomic PCR analysis on exons 1 to 9 of *CRYL1*. In HCC specimens that displayed loss or down-regulation of *CRYL1* expression, frequent HDs were detected on exons 1, 5 and 8. (NL: Normal Liver; NTC: No template control)

A



B

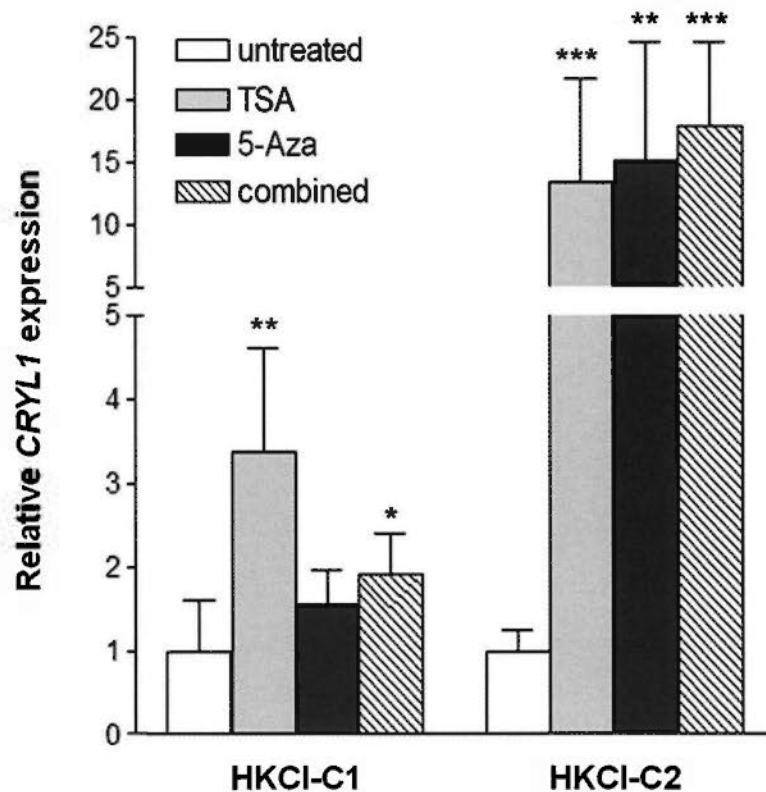


Figure 3.11 Epigenetic inactivation of *CRYL1*

(A) MSP analysis of *CRYL1* in 8/12 cell lines and 12/40 primary tumors were shown. The methylated band was observed in 3 cell lines and 5 primary cases showing that their promoter regions of *CRYL1* were methylated. (B) Cell lines HKCI-2, HKCI-C1 and HKCI-C2 were subjected to single agent 5-Aza or TSA, or a combined 5-Aza and TSA treatment. HKCI-C1 showed significant *CRYL1* re-expression in response to TSA exposure and in combinatorial treatment. *CRYL1* expression in HKCI-C2 was readily inducible by all three treatments (* $P < 0.02$; ** $P < 0.005$; *** $P < 0.0001$).

3.3 DISCUSSION

The current paucity on HDs in HCC has led to the screening on a panel of HCC cell lines in this study. Positional mapping by array-CGH highlighted genome-wide HD regions in HCC and underlined a number of potential tumor suppressor genes. Systemic validations at the genomic and mRNA levels revealed crystalline Lambda 1 (*CRYL1*; on chr.13q12.11), a novel crystallin enzyme, to exhibit distinct down-regulations in HCC. It is known that diminutions on chr.13q are common in HCC and have been implicated as one of the most important carcinogenetic events in the liver tumorigenesis (Poon TC *et al*, 2006; Hertz S *et al*, 2008). Early allelic mapping on chr.13q has further suggested the existence of 3 smallest overlapping regional (SOR) deletions, all of which might hold inference in the hepatocarcinogenesis (Lin YW *et al*, 1999). In particular, the sub-chromosomal SOR at chr.13q12-14 displayed significant associations with clinicopathological features, where a relation with advanced stage HCC and more aggressive tumor behaviors have been shown (Wong CM *et al*, 2002). Two well-known TSGs, *RBI* (at chr.13q14) and *BRCA2* (at chr.13q13), are thought to be the likely target genes of the region. However, no strong evidence has emerged to support a significant role of *BRCA2* in the induction of liver tumorigenicity (Rider MA *et al*, 2002). Moreover, the lack of evidence for genetic alterations in *RBI* in HCC suggested the possible involvement of other mechanism(s) in the disruption of the gene expression. In fact, it is becoming apparent that *RBI* is mainly inactivated in HCC by ubiquitin degradation at the protein level consequential from binding to a liver oncoprotein Gankyrin, which is a component of the 26S proteasome (Higashitsuji H *et al*, 2000). Recent discovery of *DLC2* (on chr.13q12.3) although has been shown to induce a growth suppressive function *in-vitro*, was only under-expressed in 18% of human HCC

tumors (Ching YP *et al*, 2003). These reports would invariably suggest the *bona fide* TSG(s) resultant from the genomic losses of chr.13q12-14 remained to be discovered in HCC.

In line with the reported clinicopathological relations of regional chr.13q12-14 losses in HCC, the findings on *CRYLI* suggested a strong inverse relationship with tumor size, and a more profound repression in the advanced stage HCC. Moreover, low expressions of *CRYLI* also held prognostic implication in predicting a shorter disease-free survival in HCC patients. A considerable incidence of *CRYLI* down-regulations (53%) was found in the series of tumors analyzed. This repression was also discriminatory between tumors and adjacent non-tumoral cirrhotic liver, which is also considered the putative pre-malignant lesion of HCC. Consistent with this finding, two earlier reports have also described on a reduced *CRYLI* expression in 50-60% of HCC (Chen J *et al*, 2003; Chen CF *et al*, 2005). However, these studies failed to address the functional significance of *CRYLI* and its potential association with tumor features. In this study, it was demonstrated, for the first time, profound inhibitory effects of *CRYLI* on HCC cell growth and proliferation. The findings showed that loss of *CRYLI* conferred significant growth advantages to HCC cells, which were abolished upon gene re-expression. The expression of *CRYLI* induced a delay in the G₂-M transition of the cell cycle and a concomitant increase in apoptotic cells. Similar to the finding here, another member of the crystalline family, βγ-crystalline domain of AIM1, has also been shown to exert tumor suppressive effects in inhibiting the cell proliferation of melanoma cells through a delay of G₂-M phase transition (Ray ME *et al*, 1997; He YY *et al*, 2008). It is postulated that the Cdc2/cyclin B2 complex, the key regulators of the G₂-M transition, can be affected by the *CRYLI*-induced cell-cycle blockade. Immunoblotting analysis showed a

gradual accumulation of the cyclin B2 protein over the period of investigation, whereas the level of Cdc2 remained steady. The timely degradation of cyclin B2 ensues a smooth G₂-M exit, where upon accumulation may result in the retardation or arrest of the cell cycle (Smits VAJ *et al* 2000; Smits VAJ *et al*, 2001). This finding would therefore suggest *CRYLI* mediated a G₂-M blockade in HCC possibly through interrupting the cyclin B2 signaling path.

In summary, array-CGH identified in HCC a commonly homozygous deleted gene *CRYLI*, which is normally highly expressed in the liver (Chen J *et al*, 2003). Low expressions of *CRYLI* in HCC corroborated a poorer patient's prognosis and a functional role in the uncontrolled cell proliferation. It is also noteworthy that the *CRYLI* protein has two putative NAD and FAD domains which are thought to catalyze the β -oxidation of fatty acid (Mulders JW *et al*, 1988). Alterations in the fatty acid metabolism and chronic fatty changes (steatosis) in the liver have been implicated in the HCC development (Ockner RK *et al*, 1993; Yu S *et al*, 2003). In this context, besides affecting the cell-cycle progression, down-regulations of *CRYLI* might also cause interruption of normal fatty acid oxidation leading to an increase in plasma free fatty acids (FFA). Indeed, FFA in HCC patients has been reported to be significantly higher than control subjects (Li YZZY *et al*, 1997). It is also believed that these FFA could serve as metabolic substrates to cancer cells favouring cell survival and growth in tumor progression (Spector AA *et al*, 1967). Nevertheless, such postulation on the loss of *CRYLI* expression in the disruption of fatty acid metabolism leading to the development of HCC remained to be further investigated. The overall finding in this study suggests that *CRYLI* is likely a putative tumor suppressor gene at the proximal chr.13q12-q14 regional loss and the inactivation of

this gene via allelic losses and/or epigenetic controls may well have enhanced the tumor progression of HCC.

Chapter 4

***BOP1* plays an oncogenic role in HCC by promoting EMT**

4.1 INTRODUCTION

Gains of the chr.8q long-arm are frequently detected in human cancers, including HCC (Qin LX, 2002; Bucndia MA, 2002, Knuutila S *et al*, 1998). Early molecular investigations on different cancer types, *albeit* low-resolution, have defined a critical overlapping region to chr.8q24 (Knuutila S *et al*, 1998). Multiple independent studies further emphasized on the importance of this sub-chromosomal region in cancer development and progression (Horlings IIM *et al*, 2010; van Dekken H *et al*, 2003; Goel A *et al*, 2010). Our group and others have previously reported on recurrent chr.8q24 gains in 48%~77% of HCC cases (Wong N *et al*, 1999; Niketeghad F *et al*, 2001; Kusano N *et al*, 1999). Recent informatics analysis conducted on the genomic data of >150 HCC tumors further enabled us to underpin chr.8q24 gain as a major contributory event in the development of HCC (Poon TC *et al*, 2006). Using matrix-based CGH of BAC array analysis on a cohort of >65 HCC samples, German researchers were able to map more precisely the affected genomic loci in HCC, and refined the critical interstitial region of chr.8q24 to chr.8q24.23-24.3, which spanned an approx. 6.82Mb (Schlaeger C *et al*, 2008).

In this study, the chr.8q24.23-24.3 region was resolved for affect genes in HCC by high-resolution array-CGH. Distinct gains of the *BOP1* gene at chr.8q24.3 prompted our further investigations for its role in liver tumorigenesis. Frequent over-expression of *BOP1* (block of proliferation 1) in primary HCC tumors correlated with advance pathologic features and shorter survival of patients. The prognostic value was also examined in comparison to proto-oncogene *C-MYC* (at chr.8q24.21), which is also commonly up-regulated in HCC (Takahashi Y *et al*, 2007; Chan KL *et al*, 2004). The result on HCC suggested *BOP1* up-regulations were more frequent than *C-MYC*, and may represent an independent prognostic biomarker. This

study also revealed key functions of *BOP1* in promoting Epithelial-to-Mesenchymal Transition (EMT) and invasiveness of HCC cells, which may hold implications in metastasis of HCC.

4.2 RESULTS

4.2.1 *BOPI* is frequently up-regulated in HCC

Six cell lines and two primary HCC tumors with chr.8q24 gains from conventional CGH analysis were subjected to further array-CGH mapping. An example of array-CGH map of HKCI-9 on chr.8q24 is shown in Figure 4.1A. Among the candidate genes that showed copy number gain, consistent gains of *BOPI* were suggested in 8 out of 8 cases. Moreover, high-level gains of *BOPI* could be detected in 3/8 cases that ranked the highest scored event among all candidate genes (Figure 4.1B).

Validation by qRT-PCR confirmed up-regulations of *BOPI* in the six cell lines studied when compared to normal liver controls (n=6) with a high statistical significance ($P = 0.0001$) (Figure 4.2A). This corresponded to an increased protein expression of *BOPI* as demonstrated from Western blot (Figure 4.2B), which implicated that *BOPI* up-regulation at mRNA level in increased protein translation. It was also determined that an increased BOP1 protein could be found in primary HCC tumors relative to adjacent non-tumoral liver (Figure 4.2B). The mRNA level of *BOPI* was further examined in a cohort of 65 paired HCC tumors and their matching non-tumoral liver. Common up-regulation of *BOPI* (> 2 -fold) was identified in 84.6% tumors compared to adjacent non-tumoral liver (55/65; paired t-test $P < 0.0001$) (Figure 4.3A).

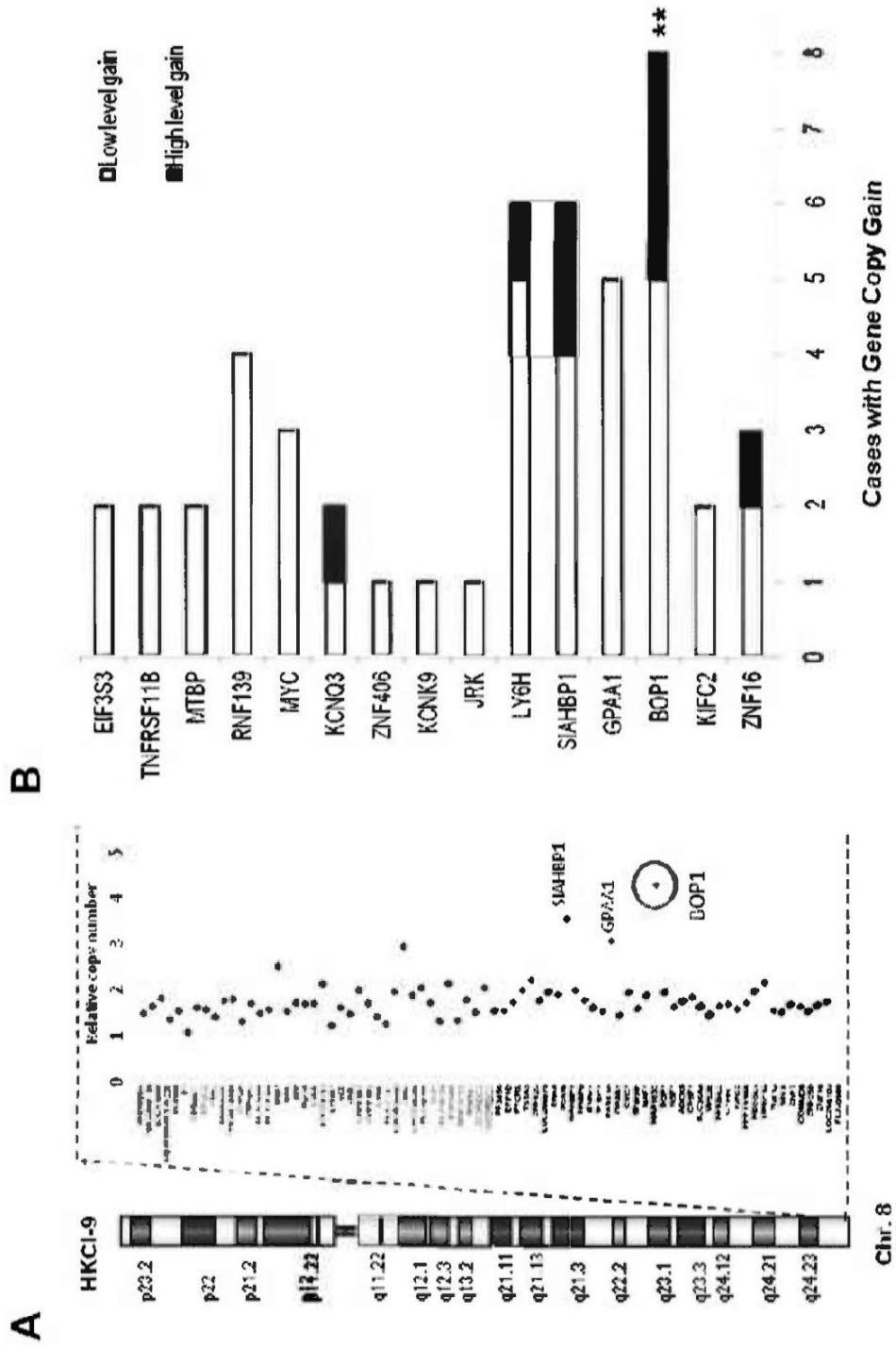


Figure 4.1 Array-CGH analysis on chr.8q24

(A) An example of array-CGH analysis on chr.8q24 in HKCI-9 shown. Vertical profile of DNA copy number with dots displacing towards the right of balanced region (line labeled as "1") correspond to relative copy gain. (B) Genes that displayed ≥ 1.8 -fold gain were regarded as low level gain, while high level gain was defined at ≥ 3.5 -fold. **In 8/8 cases analyzed, *BOP1* showed copy number gain, in which 3 cases displayed high level gains.

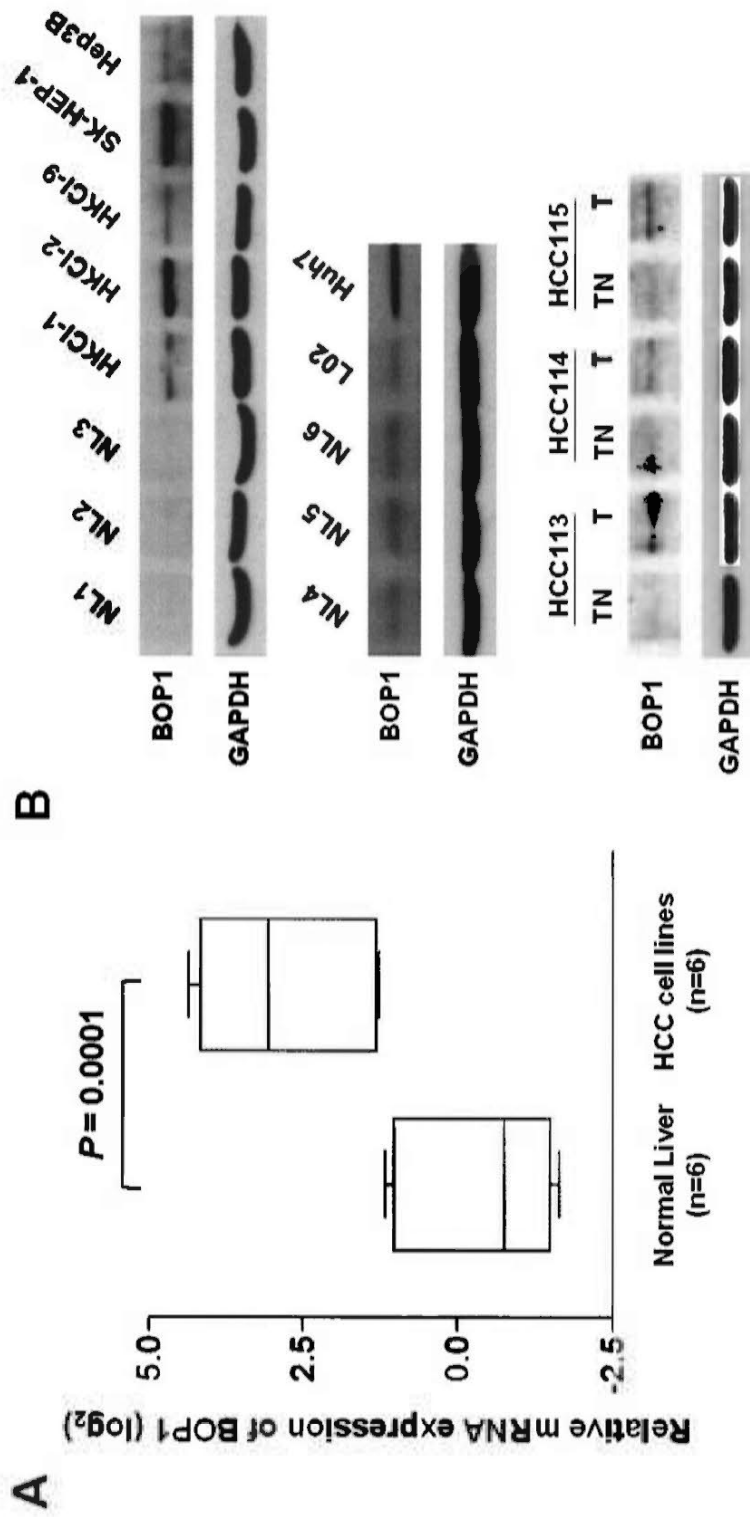


Figure 4.2 Over-expression of BOP1 in HCC

(A) The expression of *BOP1* was verified by qRT-PCR in 6 HCC cell lines that were subjected to array-CGH analysis. Significant up-regulations of *BOP1* were suggested when compared to normal liver controls ($n=6$) ($P = 0.0001$). (B) Up-regulated *BOP1* corresponded to elevated protein level. Western blot analysis showed low or negligible *BOP1* protein in normal livers (NL1-NL6), immortalized hepatocyte L02 and tumor adjacent non-tumoral livers (TN) relative to much increased levels of *BOP1* protein in HCC cell lines and primary tumors (T).

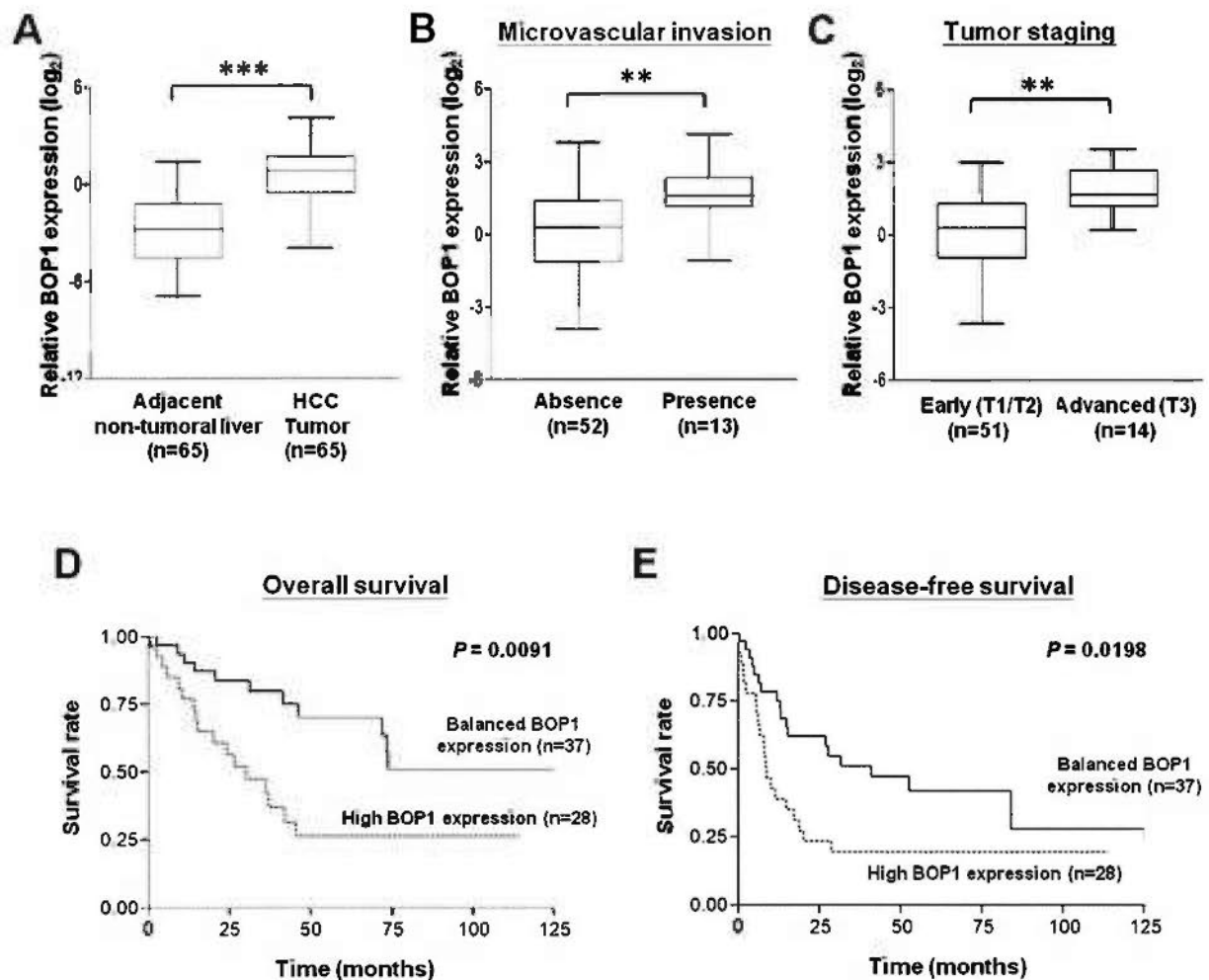


Figure 4.3 Clinicopathologic correlations of *BOP1* expression in HCC

(A) Significant up-regulation of *BOP1* mRNA expression was suggested in HCC tumors relative to adjacent non-tumoral liver (n=65) (***) paired t-test $P < 0.0001$) (B-C) Elevated *BOP1* expression also showed marked association with tumors bearing microvascular invasion and patients with advanced staged tumors (** $P < 0.006$). (D-E) Kaplan-Meier analyses were performed according to *BOP1* mRNA expression on HCC patients. High *BOP1* was regarded as ≥ 2 -fold up-regulation relative to the mean expression of 6 normal liver RNA samples. Overall ($P = 0.0091$) and disease-free survival ($P = 0.0198$) of patients who had high *BOP1* expression was evidently shorter.

4.2.2 Prognostic value of *BOPI*

Correlative analysis of *BOPI* mRNA levels with clinicopathologic features suggested significant association between increased *BOPI* expression and the histologic presence of microvascular invasion ($P = 0.0059$) (Figure 4.3B) and advance tumor stage (Stage T3, $P = 0.0042$) (Figure 4.3C). Up-regulation of *BOPI* was also found to predict shorter overall ($P = 0.0091$) and disease-free survival of patients ($P = 0.0198$) (Figure 4.3D-E). Multivariate survival analysis using the Cox proportional hazards model further indicated that *BOPI* up-regulation correlated with a higher hazard ratio and worse clinical outcomes (for overall survival, $P = 0.009$, hazard ratio = 3.075; for disease free-survival, $P = 0.025$, hazard ratio = 2.160) (Table 4.1).

To further establish the prognostic value of *BOPI*, the expression of *C-MYC*, a recognized oncogene generally assumed to be the target gene from the chr.8q24 region, was simultaneously examined in the same series of specimens that were subjected to *BOPI* evaluations. Limited by RNA availability, only 57 paired tumor and adjacent non-tumoral liver were studied. Increased expressions of *C-MYC* were suggested in 47.4% cases but, unlike *BOPI*, significant correlations could not be established with clinicopathologic features including microvascular invasion and tumor staging (Figure 4.4A-C) and the survival of patients (Figure 4.4D-E). In addition, Cox regression analysis did not suggest correlation of *C-MYC* expression with the hazard ratio and clinical outcomes (for overall survival, $P = 0.681$, hazard ratio = 1.202; for disease free-survival, $P = 0.754$, hazard ratio = 1.123) (Table 4.1). Collectively, these data would strongly implicate *BOPI* an independent prognostic biomarker in HCC.

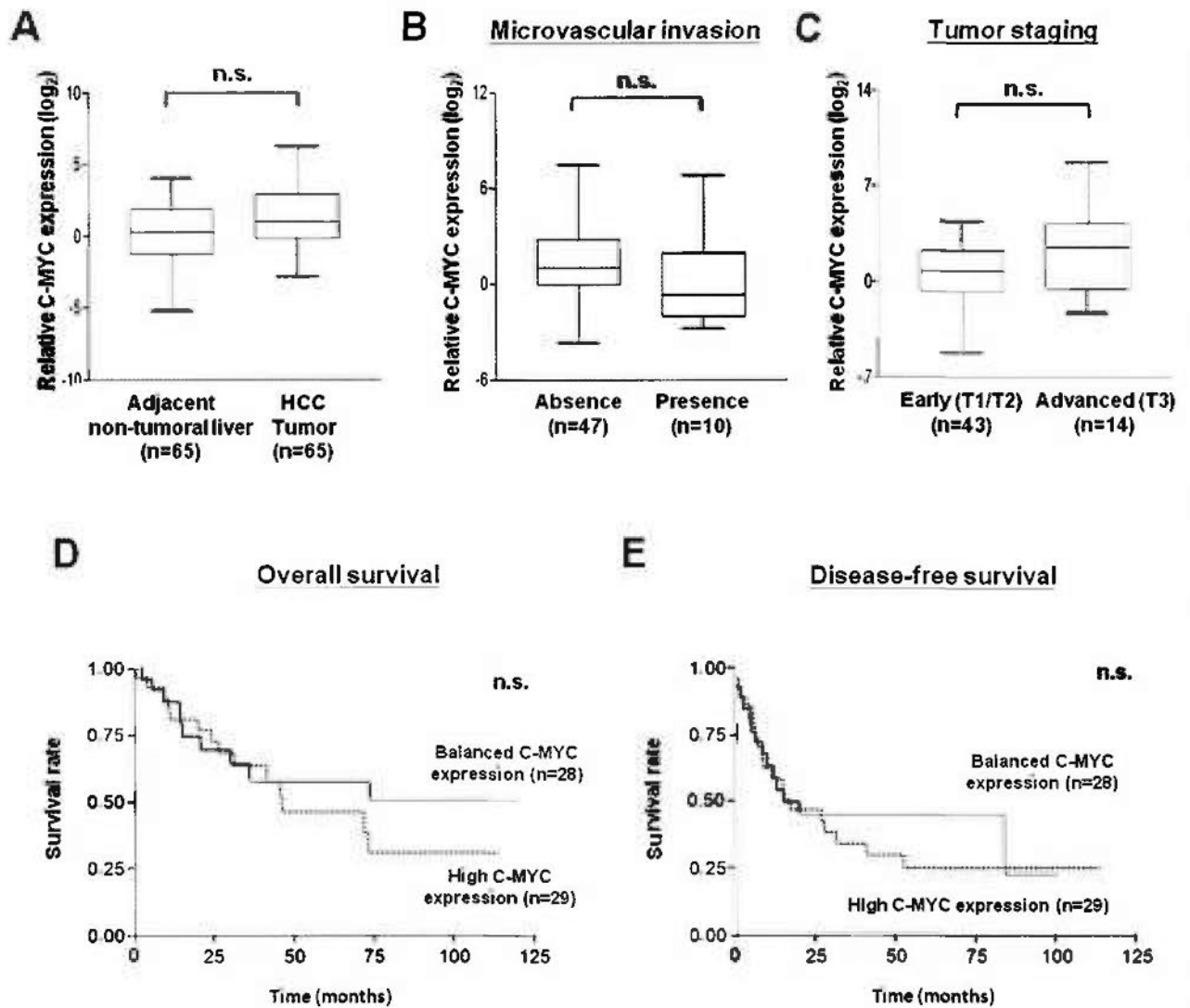


Figure 4.4 Clinicopathologic correlations of C-MYC expression in HCC

(A-C) Expression of *C-MYC* in primary HCC tumors neither showed significant up-regulations compared to adjacent non-tumoral livers, nor correlated with clinicopathologic features, including microvascular invasion and tumor staging. (D-E) Kaplan-Meier analyses were performed according to *C-MYC* mRNA expression on HCC patients. High *C-MYC* was regarded at ≥ 2 -fold up-regulation relative to the mean expression of 6 normal liver RNA samples. Up-regulation of *C-MYC* was not associated with the disease outcome. (n.s.: non significant)

Table 4.1. Multivariate Cox regression analysis of *BOP1* and *C-MYC* expressions in HCC

BOP1 Variables	Overall survival			Disease free survival		
	Hazard Ratio	95% CI	P-value	Hazard Ratio	95% CI	P-value
<i>BOP1</i> expression	3.075	1.323 to 7.144	*0.009	2.160	1.105 to 4.223	*0.025
Cirrhosis	1.910	0.634 to 5.753	0.252	1.129	0.532 to 2.399	0.753
Gender	0.743	0.174 to 3.171	0.690	0.734	0.242 to 2.228	0.587
HbsAg ^a	4.297	0.549 to 33.620	0.167	1.020	0.348 to 2.993	0.971
Macro-vascular invasion ^b	0.538	0.097 to 2.993	0.481	0.467	0.102 to 2.142	0.329
Micro-vascular invasion ^b	1.621	0.560 to 4.696	0.375	1.129	0.425 to 3.000	0.808
Clinical stage ^c	2.837	0.738 to 10.907	0.131	1.786	0.622 to 5.128	0.283

C-MYC Variables	Overall survival			Disease free survival		
	Hazard Ratio	95% CI	P-value	Hazard Ratio	95% CI	P-value
<i>C-MYC</i> expression	1.202	0.502 to 2.872	0.681	1.123	0.545 to 2.314	0.754
Cirrhosis	2.067	0.648 to 6.592	0.222	1.233	0.549 to 2.770	0.614
Gender	0.958	0.171 to 5.379	0.962	1.179	0.348 to 3.998	0.793
HbsAg ^a	2.621	0.304 to 22.626	0.383	1.175	0.252 to 5.478	0.838
Macro-vascular invasion ^b	0.606	0.082 to 4.489	0.626	0.729	0.121 to 4.395	0.732
Micro-vascular invasion ^b	2.109	0.640 to 6.952	0.223	0.913	0.253 to 3.293	0.890
Clinical stage ^c	1.852	0.398 to 8.609	0.434	1.230	0.361 to 4.186	0.742

^a HbsAg: HBV positive vs HBV negative

^b Macro-vascular invasion; micro-vascular invasion; cirrhosis: Presence vs absence

^c Clinical stage: early vs advanced stage

4.2.3 Functional role of *BOP1* in cell migration and invasion

In functional examinations of *BOP1*, siRNA-mediated suppression in Hep3B and HKCI-9 showed ~80% knockdown of *BOP1* mRNA level by qRT-PCR analysis (Figure 4.5A and Figure 4.6A). *BOP1* depletions in both Hep3B and HKCI-9 did not suggest an effect on cell viability from MTT assay and neither cell proliferation from BrdU incorporation study (Figure 4.5B-C and Figure 4.6B-C). However, marked inhibitory effects on cell invasion through Matrigel and transwell motility were readily observed. Depletion of *BOP1* in both Hep3B and HKCI-9 showed significant reductions in the number of cells invaded ($P = 0.0021$ and $P = 0.0009$, respectively) and migrated ($P = 0.0475$ and $P = 0.0327$, respectively) (Figure 4.5D-E and Figure 4.6D-E). The reduction was more profound in the invasion assay, in which more than 50% reduction in the percentage of invaded cells was observed upon *BOP1* depletion. To further support a role for *BOP1* in promoting cell motility, ectopic expression of pcDNA3.1-*BOP1* or empty vector in immortalized hepatocyte cell line L02 was performed. Ectopic transfection of *BOP1* in L02 cells induced expression by ~30-fold compared to vector transfected cells as shown in Figure 4.7A. *BOP1* over-expression showed marked stimulation on cell invasion and migration, where >50% increase in the percentage invaded and migrated cells were detected ($P < 0.0001$) (Figure 4.7D-E). In concordance with knockdown study, ectopically expressed *BOP1* in L02 did not show an effect on both cell viability and proliferation (Figure 4.7B-C).

Hep3B

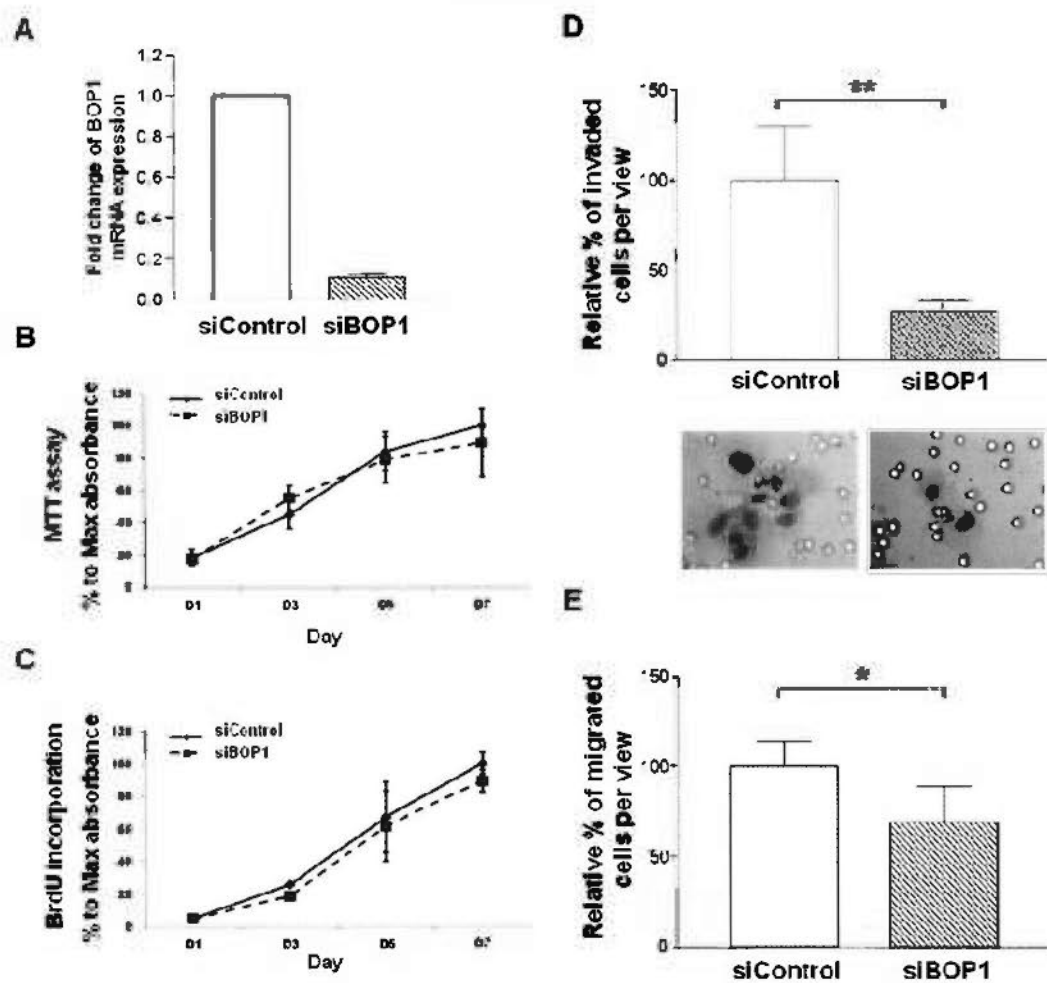


Figure 4.5 Functional effects of *BOP1* on Hep3B cell migration and invasion

(A) Expression of *BOP1* was suppressed by >80% in Hep3B upon *siBOP1* knockdown. (B-C) MTT and BrdU assays in Hep3B cells showed no apparent effects upon *BOP1* depletion (dash line) compared to siControl transfected cells (solid line). (D-E) Migration and invasion assays in Hep3B showed that the relative migrated and invaded cells in *siBOP1* transfected groups (striped bars) were significantly suppressed compared to the control groups (solid bars) (paired t-test; * $P < 0.05$; ** $P < 0.005$). Representative images of invaded cells in Hep3B shown.

HKCI-9

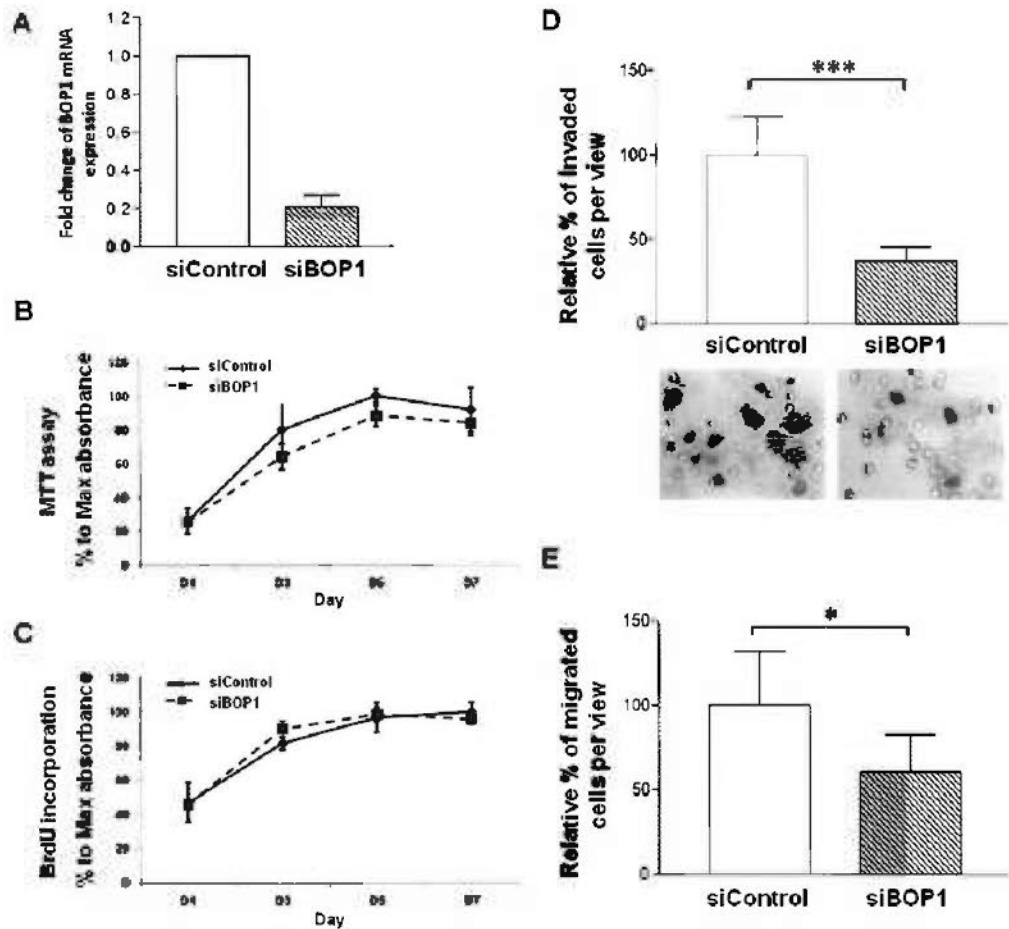


Figure 4.6 Functional effects of *BOP1* on HKCI-9 cell migration and invasion

(A) Expression of *BOP1* was suppressed by ~80% in HKCI-9 upon siBOP1 knockdown. (B-C) MTT and BrdU assays in HKCI-9 cells showed no apparent effects upon *BOP1* depletion (dash line) compared to siControl transfected cells (solid line). (D-E) Migration and invasion assays in HKCI-9 showed that the relative migrated and invaded cells in siBOP1 transfected groups (striped bars) were significantly suppressed compared to the control groups (solid bars) (paired t-test; * $P < 0.05$; *** $P < 0.001$). Representative images of invaded cells in HKCI-9 shown.

L02

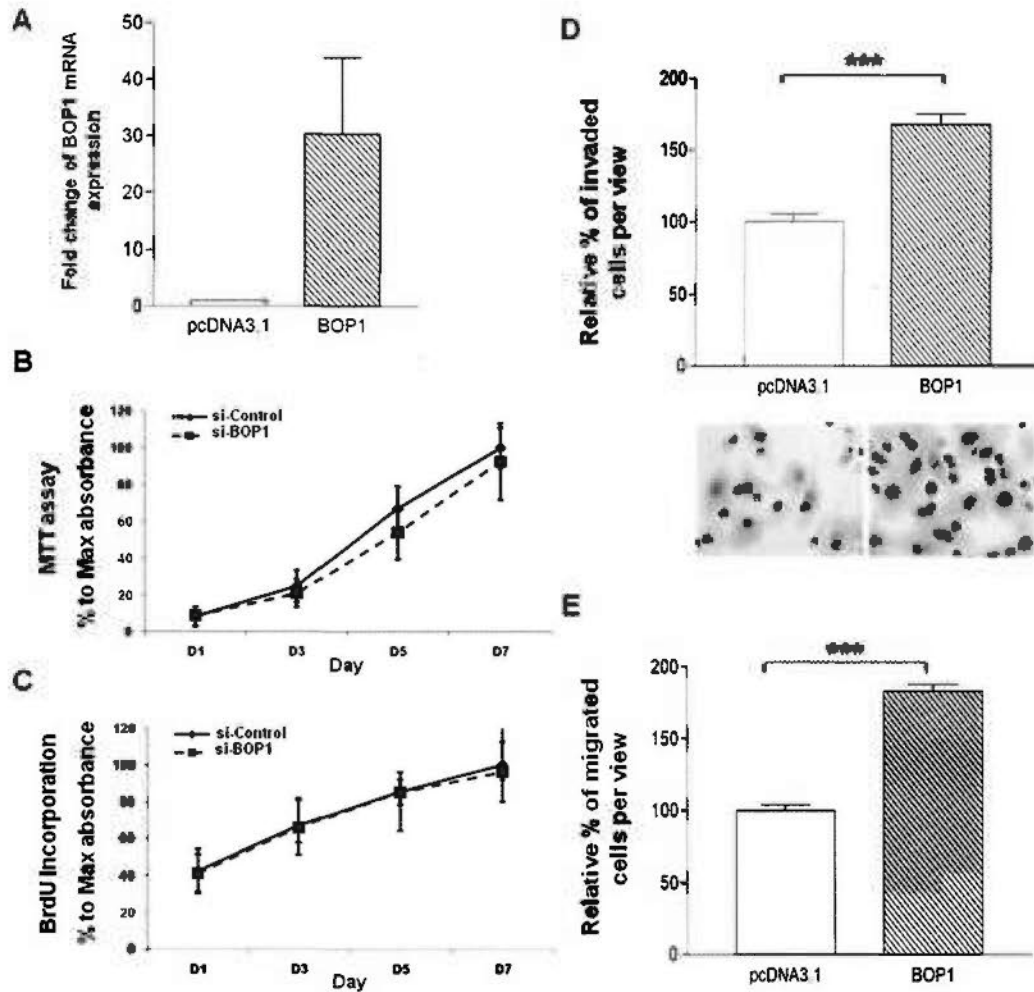


Figure 4.7 Ectopic expression of *BOP1* in immortalized liver cell line, L02

(A) Ectopic transfection of *BOP1* in immortalized L02 cells induced expression by ~30-fold compared to vector transfected cells. (B-C) MTT and BrdU assays in L02 cells showed no growth advantage in *BOP1* expressing cells (dash line) compared to vector control (solid line). (D-E) Migration and invasion assays showed that *BOP1* transfected cells (striped bars) exhibited higher migratory and invasive abilities compared to vector control (solid bars) (paired t-test; *** $P < 0.0001$). Representative images of invaded cells in L02 shown.

4.2.4 BOP1 promotes HCC cell motility through EMT induction

Previous studies on *BOP1* have proposed a role for this WD40 protein in mediating maturation of large ribosomal subunits in mammalian cells, specifically in the formation of mature 28S and 5.8S ribosomal RNAs (rRNAs) (Strezoska Z *et al*, 2000; Pestov DG *et al*, 2001). To rule out possible involvement of ribosomal biogenesis in the functional phenotypes observed in HCC, rRNA analysis in *BOP1* knockdown cells was carried out. In si-*BOP1* transfected Hep3B and HKCI-9 cells, Northern blotting did not indicate differences in the maturation of ribosomal proteins compared to siControl cells (Figure 4.8). Since noticeable changes in the rRNA processing in HCC could not be detected despite perturbed *BOP1* activities, it is tempting to speculate that *BOP1* has other cancer-related functions that are yet to be determined.

Given that up-regulated *BOP1* correlated with enhanced cell migratory abilities of HCC cells, EMT was next examined as an underlying mechanism. In si*BOP1* treated cells, re-expressions of cohesive epithelial markers, E-cadherin, cytokeratin 18 and γ -catenin, was revealed from Western blotting in Hep3B and HKCI-9. This was accompanied by a corresponding down-regulation of mesenchymal markers, fibronectin and vimentin (Figure 4.9). In addition, immuno-staining of cytokeratin 18 showed prominent remodelled organizations in the cytoplasm of si*BOP1* transfected cells compared to cells treated with siControl (Figure 4.10). These findings would imply a loss of mesenchymal-like features and re-acquisition of epithelial characteristics in *BOP1* depleted HCC cells. The involvement of EMT was further supported by the augmentation of mesenchymal markers in *BOP1* transfected L02 cells. In *BOP1* over-expressing cells, expression of mesenchymal markers, fibronectin and vimentin, elevated above the levels in vector transfected cells, while

epithelial markers cytokeratin 18 and γ -catenin were found to be down-regulated (Figure 4.9). A reduced expression of cytokeratin 18 was also confirmed from immuno-fluorescence analysis (Figure 4.10).

In promoting the mesenchymal motile phenotype during EMT, circumferential F-actin fibres of the cytoskeleton are replaced by a network of actin fibers polymerization (Yilmaz M *et al*, 2009; Thiery JP *et al*, 2009). Using phalloidin staining for F-actin, much reduced F-actin polymerizations and stress fibers disassembly were found in *BOP1* depleted Hep3B cells, which would signify an effect of actin cytoskeleton remodelling on the motile inhibition observed. In contrast, ectopic expression of *BOP1* in L02, increased polymerization of F-actin was observed (Figure 4.11).

The RhoA GTPase is known to play a regulatory role in the F-actin fiber rearrangements, including the formation of stress fibers (Narumiya S *et al*, 2009; Etienne-Manneville S *et al*, 2002). The endogenous RhoA status under the influence of *BOP1* was therefore examined. Results obtained from *in vitro* GTP-pull-down assay in Hep3B and L02 indicated that *BOP1* could directly affect the level activation of RhoA GTPase, and would likely represent a downstream effector of *BOP1* in promoting actin stress fibers polymerisation (Figure 4.12A).

To establish an association between RhoA activation and *BOP1* expression, the effect of RhoA knockdown in *BOP1* expressing cells was further investigate. In *BOP1*-expressing L02 cells, siRNA knockdown against RhoA readily reduced L02 cell invasion by 40% ($P = 0.006$) and migration by 60% ($P = 0.021$) when compared to siControl experiments (Figure 4.12B). The effect of RhoA knockdown in vector transfected L02 cells, on the other hand, showed similar behavior to siControl assays and did not suggest significant changes in cell motility and invasion ($P > 0.05$).

These findings would suggest that the *BOP1*-mediated cellular invasiveness and motility was dependent on the activation of RhoA pathway.

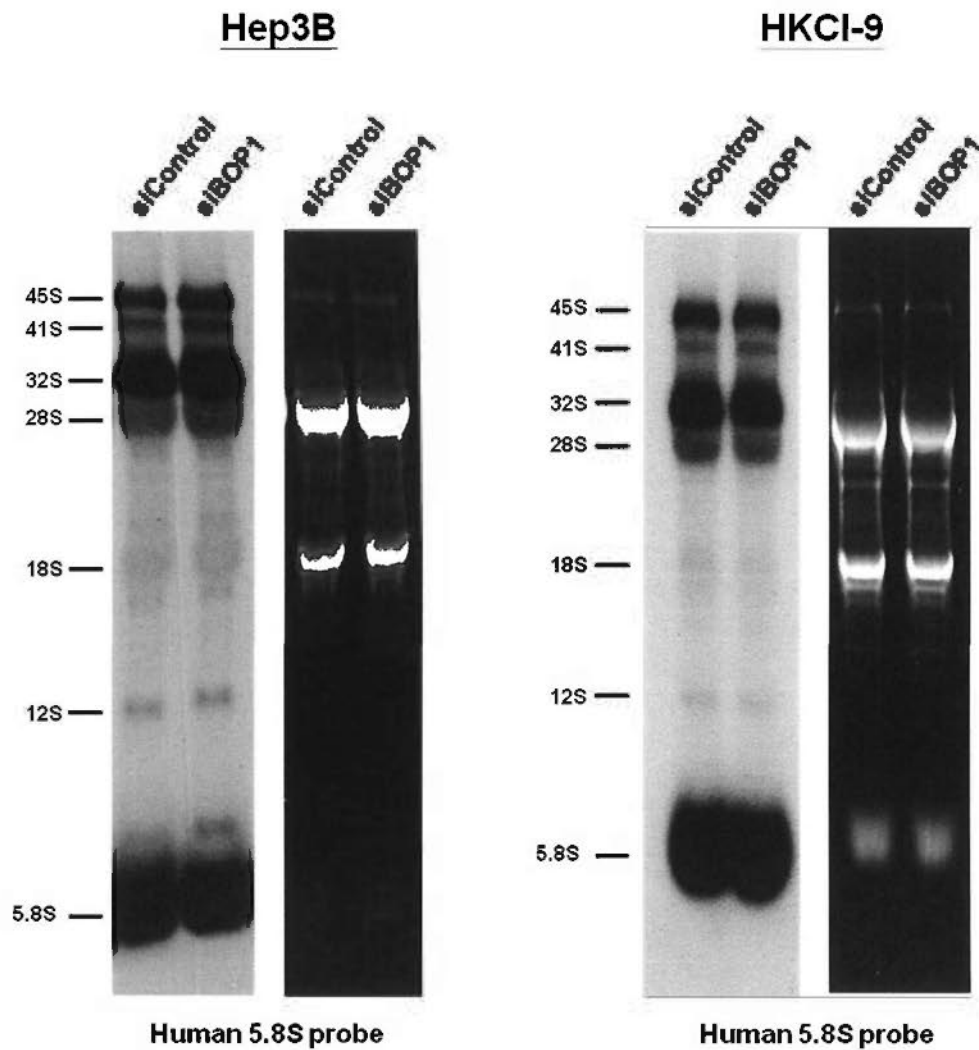


Figure 4.8 Effect of *BOP1* on rRNA maturation in HCC

Northern blot analysis for 5.8S and 28S rRNAs was performed using a 40-mer oligonucleotide complementary to nt 68-108 of the human 5.8S rRNA. *BOP1* knockdown in both Hep3B and HKCI-9 did not suggest apparent changes in the synthesis of 5.8S and 28S rRNAs compared to siControl transfected cells.

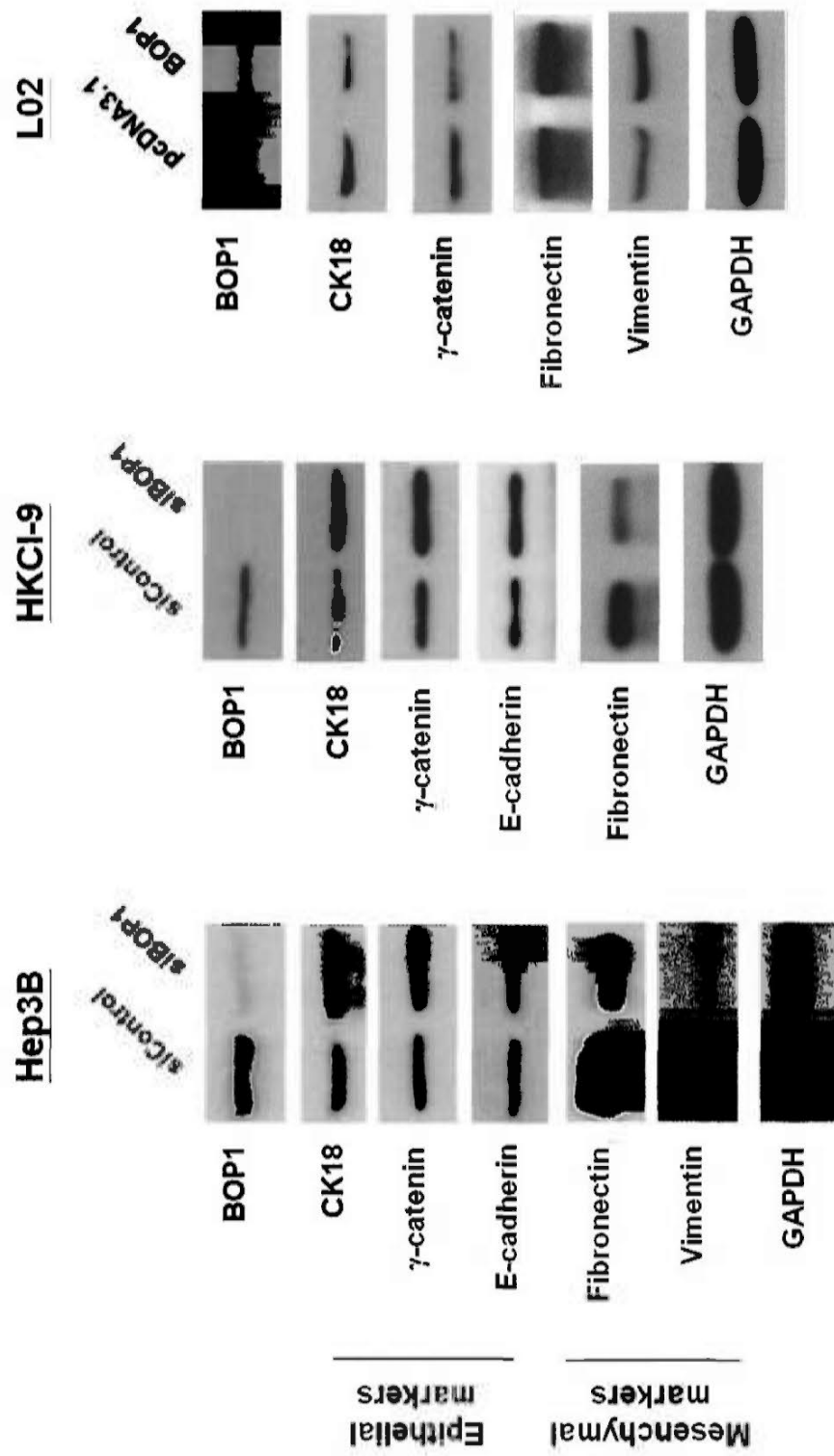


Figure 4.9 *BOP1* promotes HCC motility through EMT

Western blot analysis showed a significant increase in epithelial markers, cytokeratin 18 (CK18), E-cadherin and γ -catenin, and decrease in mesenchymal markers, fibronectin and vimentin, in *BOP1* depleted cells compared to siControl transfected cells (left and middle panels) (HKCI-9 showed negligible endogenous expression of vimentin). Ectopic expression of *BOP1* in L02 suppressed cytokeratin 18 (CK18) and γ -catenin expressions (epithelial markers) and increased fibronectin and vimentin expressions (mesenchymal markers) (right panel) (L02 showed negligible expression of E-cadherin).

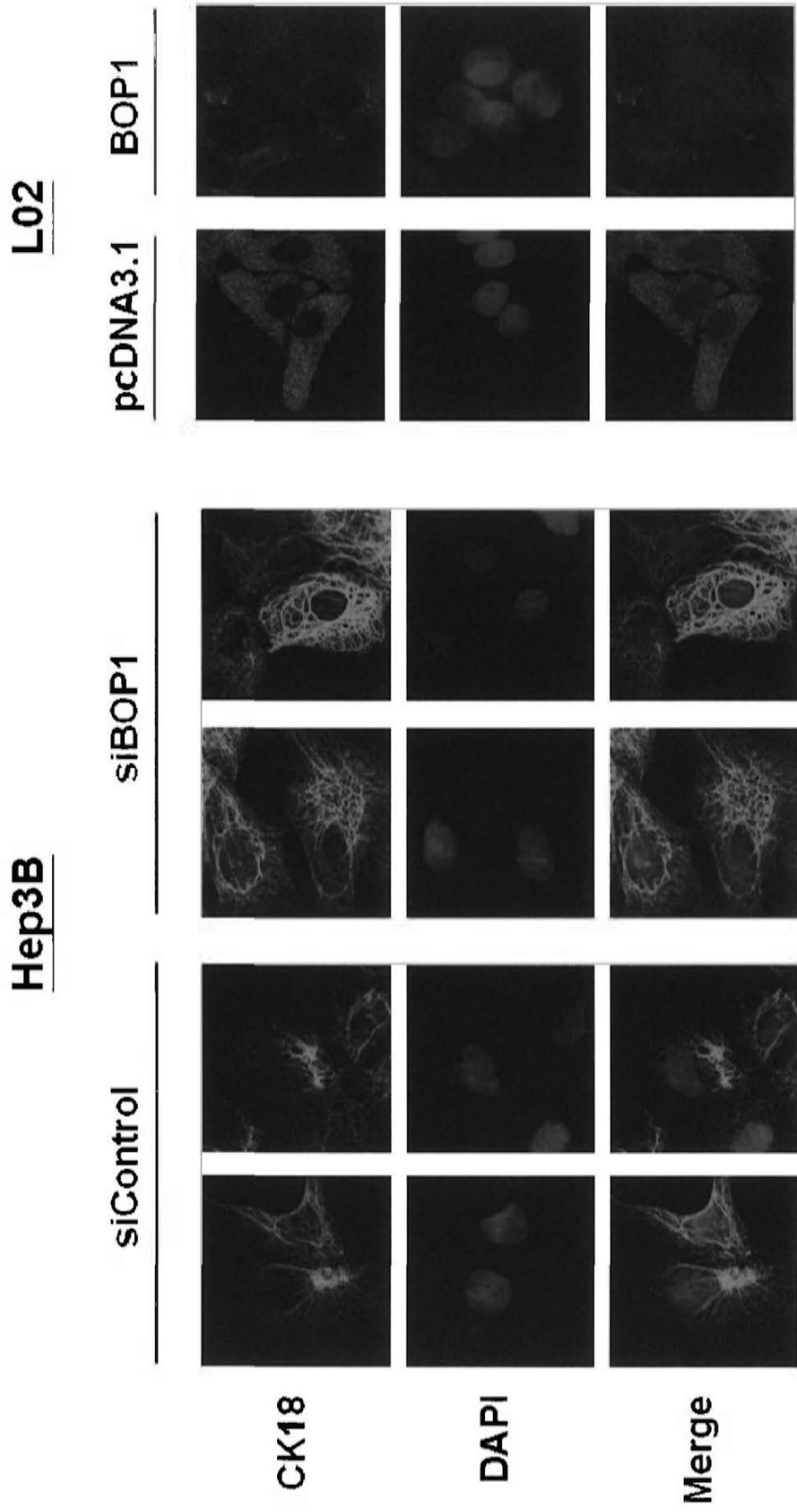


Figure 4.10 *BOP1* reduces the expression of cytokeratin 18

Immuno-staining of cytokeratin 18 (CK18) (green) was shown to be up-regulated with remodelled organizations in the cytoplasm of si*BOP1* transfected Hep3B cells compared to siControl transfection (left and middle panels) Lower expression of CK18 in *BOP1* ectopic expressing cells of L02 was observed compared to that in vector control (right panel).

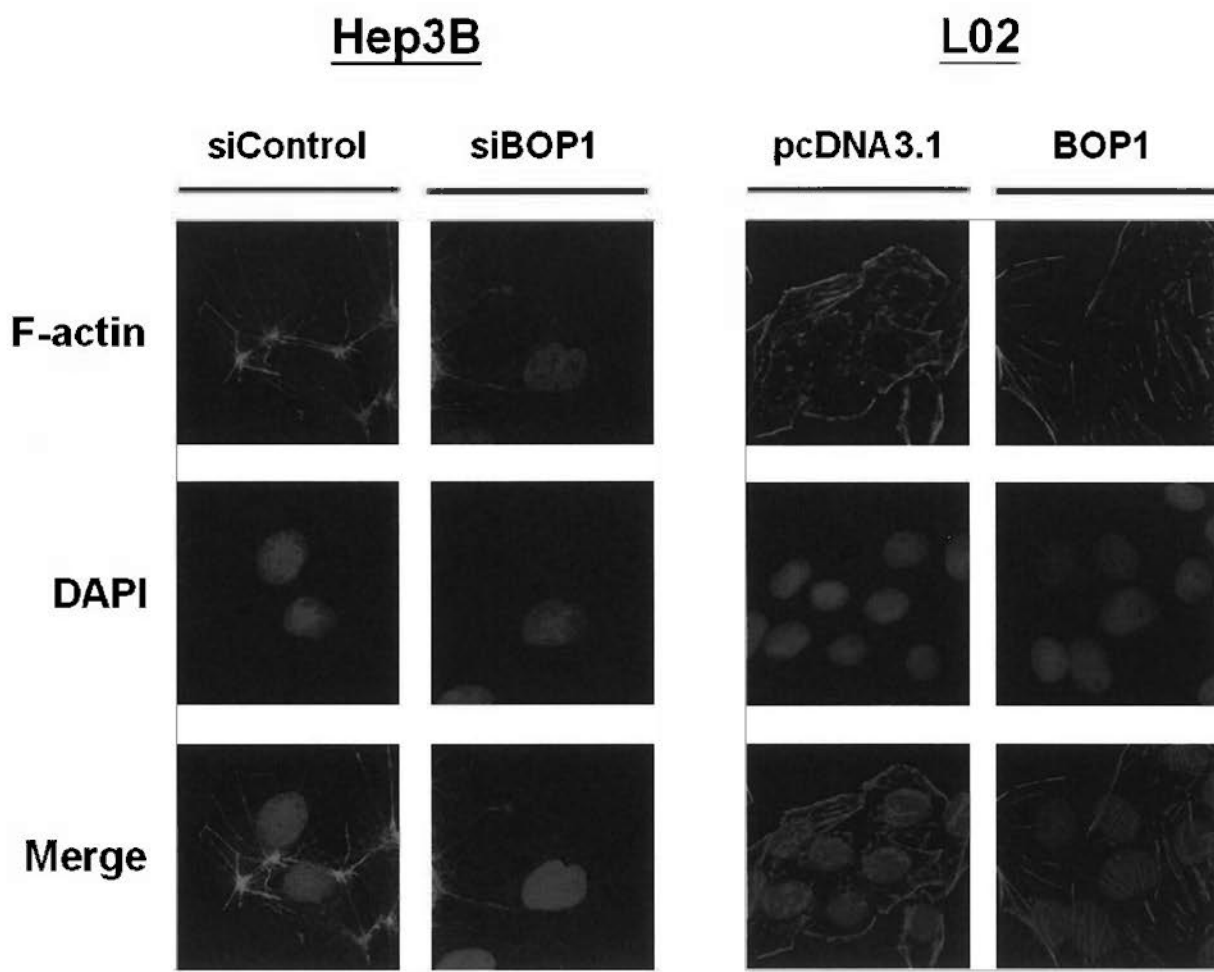


Figure 4.11 BOP1 induced stress fibre formation

Phalloidin staining (red) in the siBOP1 transfected cells showed a reduced short-branched actin stress fibers filaments (*left panel*). Intensified polymerization of stress fibres in BOP1 ectopic expressing cells of L02 was observed compared to that in vector control (*right panel*).

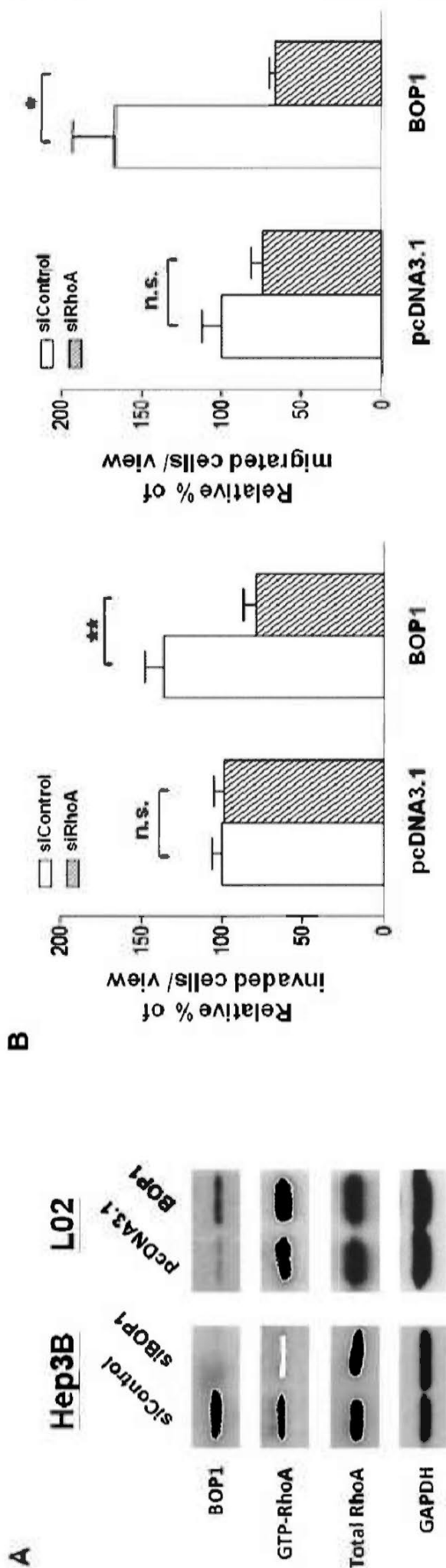


Figure 4.12 *BOP1* induces stress fibres formation and HCC motility through RhoA

(A) *BOP1* depletion in Hep3B corresponded to a decrease in the amount of active GTP-bound RhoA, while the ectopic expression of *BOP1* in L02 showed increased level of active GTP-RhoA providing that the level of total RhoA remained unchanged in both experiments. (B) RhoA depletion in *BOP1* over-expressing cells of L02 significantly inhibited the cell invasion and migration compared to siControl transfected cells (paired t-test; * $P < 0.03$; ** $P < 0.01$), while the RhoA depletion exhibited insignificant effect on cell migration and cell invasion in pcDNA3.1 transfected L02 cells (n.s.: non significant).

4.3 DISCUSSION

In this study, *BOP1* was identified as a target oncogene within the common over-represented region chr.8q24 in HCC. A functional role for this gene as a contributory factor in EMT and invasiveness of HCC cells was also established. The gene *BOP1* is a WD40 protein that was first isolated from the cDNA library screening for growth-related sequences in mouse embryonic fibroblasts (Pestov DG *et al*, 1998). Studies on mouse fibroblasts had in fact laid much of the earlier groundwork on the role of *BOP1*, which implicated *BOP1* as an integral component of the rRNA processing machinery (Strezoska Z *et al*, 2000; Pestov DG *et al*, 2001; Rohmoser M *et al*, 2007). Nevertheless, recent publications have begun to reveal the existence of extra-ribosomal activities of *BOP1*. In yeast, *BOP1* was shown to play in a role in maintaining the genomic integrity through its function in the accurate chromosome segregation and mitosis at the metaphase/anaphase transition (Killian A *et al*, 2004). Studies on colorectal cancers indicated common *BOP1* over-expressions in cases with chr.8q gain, and demonstrated that deregulation of *BOP1* would likely disrupt vital pathways contributory to the colorectal tumorigenesis (Lips EH *et al*, 2008; Killian A *et al*, 2006). It was also reported in colorectal cancer that gene dosage increase of *BOP1* was independent from that of *C-MYC*, and was more frequently occurring than *C-MYC* (Killian A *et al*, 2006). In line with this finding, the results on HCC also suggested more frequent up-regulations of *BOP1* (84.6%) compared to *C-MYC* (47.4%). Moreover, contrary to the results obtained from *C-MYC*, it was able to establish significant *BOP1* up-regulations in HCC tumors relative to adjacent non-tumoral livers, and a positive correlation between *BOP1* expression and advance clinicopathologic features. In addition, multivariate Cox regression analysis

highlighted *BOP1* may represent an independent prognostic biomarker in predicting the overall and disease-free survival of HCC patients.

Functional analysis by RNAi-mediated gene suppression of *BOP1* in over-expressing HCC cell lines showed marked reductions on cell invasion and migration but not cell proliferation. In concordance with the knockdown studies, ectopic expression of *BOP1* in immortalized hepatocytes L02 promoted cell migratory and invasive abilities. The lack of detectable function for ribosomal biogenesis in these phenotypes prompted our investigation for alternate mechanism in the *BOP1*-mediated cell motility. It was found that *BOP1* depletion caused rapid regression of EMT features, where a gain in the expression of epithelial cell adhesion molecules, such as E-cadherin, and re-organization of cytoplasmic cytokeratin 18 were revealed. In *BOP1* transfected L02 cells, a striking increase in the expression of mesenchymal markers (vimentin and fibronectin) concurred with the enhanced cell motile and invasive phenotypes. Cumulating evidence has indicated that EMT mediates tumor progression including local invasion, dissemination from the primary tumor, intravasation into blood circulation and metastasis (Thiery JP *et al*, 2009; Thiery JP, 2002). EMT is a complex process requiring extensive changes in cell adhesion and morphology, and activation of signaling paths, the experimental findings here suggested that *BOP1* may represent an upstream molecule that can induce this transition. It is well recognized that RhoA plays an oncogenic role in enhancing cell contractility through actin rearrangements and stress fibers formation (Narumiya S *et al*, 2009; Etienne-Manneville S *et al*, 2002; Hall A, 2009). Considerable depolymerizations of the actin stress fibers was found upon *BOP1* knockdown, which coincided with a reduced RhoA-GTPase activity. Furthermore, RhoA depletion experiments in *BOP1*-expressing L02 cells showed much reduced

cell motile and invasive phenotypes, which further implicates RhoA as a downstream effector of *BOP1*. Our findings would highly suggest a role of RhoA-GTPase activation in mediating the functional effects of *BOP1*.

Proteins containing WD40 repeats can be found a range of regulatory proteins that cover a wide variety of physiological functions, including signal transduction, RNA processing and cytoskeletal dynamics (Neer EJ *et al*, 1994; Li D *et al*, 2001, Smith TF, 2008). *BOP1* is an evolutionary conserved gene that contains seven WD40 repeats in human. Recent studies began to suggest a role for *BOP1* in tumorigenesis (Lips EH *et al*, 2008; Killian A *et al*, 2006) and microtubule dynamics by interacting with end-binding protein (EB1) (Kim J *et al*, 2008), which is also a well-known binding partner of the APC tumor suppressor (Morrison EE *et al*, 2009). Here, it was able to define oncogenic functions of *BOP1* in promoting HCC cell migratory and invasive activities through the induction of EMT, which is a key regulatory program activated during cancer invasion and metastasis under ribosome-independent mechanism. The possibility that *BOP1* may exert an effect on cancer invasion machinery as revealed in this study suggests that there are as yet undescribed cancer-related functions of *BOP1*. The fact that *BOP1* is also commonly over-expressed in a majority of HCC tumors and hold prognostic significance, further elucidation of *BOP1*'s capacity in coordinating protein-protein interactions and cellular processes would have much implication in therapy designs and inhibition of HCC metastasis.

Chapter 5

**Frequent over-expression of *GEF-H1*,
on chr.1q22, promotes EMT and
enhances cell motility in HCC**

5.1 INTRODUCTION

As discussed in Chapter 1, chr.1q gain is one of the most frequent genomic aberrations in HCC. Moreover, our group has previously demonstrated by SOTA analysis that chr.1q gain is a causative genomic event in the early HCC development (Poon TC *et al*, 2006). Specifically, amplification of the small interstitial chromosome region of 1q21-22 is frequent in HCC (~40% of advanced metastatic cases) (Wang Y *et al*, 2002). Cytogenetic evidence confers much importance on this amplicon, where an association with advanced metastatic tumors has been implicated (Wang Y *et al*, 2002). Due to its implication in tumorigenesis, much effort has been devoted to define target oncogenes within this amplicon.

Our group has previously shown 3 amplification loci within the chr.1q21-22 region in HCC by fluorescent *in situ* hybridization (FISH) (Wong N *et al*, 2003). The genomic map of these 3 regions represented by YACs, 955E11 (Peak a), 876B11 (Peak b) and 945D5 (Peak c) is shown in Figure 5.1. The FISH mapping analysis showed 3 peaks of maxima that entailed the chr.1q21.1, chr.1q21.2, chr.1q21.3-1q22 regions (Figure 5.2). Recently, *CHD1L* at chr.1q21.1, located within Peak a, has been identified as a potent oncogene favouring cellular transformation, G₁-S transition and cell motility (Ma NF *et al*, 2008; Chen L *et al*, 2010). Here, I describe the finding of another putative oncogene *GEF-H1* (Rho/Rac guanine nucleotide exchange factor H1), which is located in the proximity of Peak c at chr.1q22.

By high resolution array-CGH analysis on cases that display chr.1q21-22 gains, several candidate genes were identified. Among 19 genes, amplification of the *GEF-H1* gene ranked most profound. Both *GEF-H1* mRNA and protein were found to be frequently up-regulated in HCC tumors compared to the adjacent non-tumoral livers. Its up-regulation was found to be associated with microvascular invasion and

advanced staging of HCC patients. High *GEF-H1* level also holds prognostic value in predicting shorter disease-free and overall patient survival. In functional studies, it was found that *GEF-H1* could promote invasiveness of HCC cells through the modulation of EMT. It is possible that *GEF-H1* represents another proto-oncogene which may work in concert with other target genes (e.g. *CHDIL*) in leading to the development of HCC.

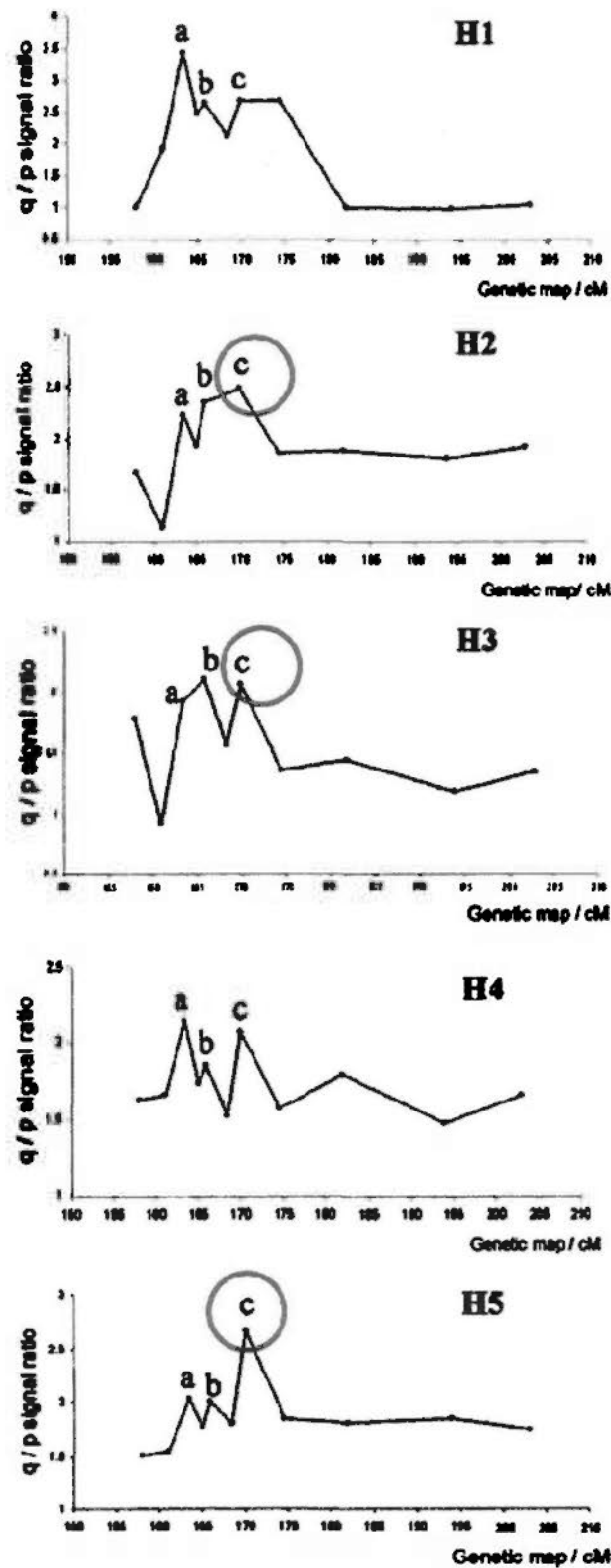


Figure 5.2 Mapping analysis on HCC cases displaying chr.1q21-22 amplicon

The average signal ratios of q-arm test probes to p-arm reference probe are plotted against the genetic distances represented by the YACs probes examined. Three peaks of amplification maxima at a, b and c represented by YAC clones 955E11, 876B11 and 945D5, respectively, were identified. The cases with copy number at Peak c greater than Peak a were represented in red circles.

Figure adapted from Wong N *et al*, 2003.

5.2 RESULTS

5.2.1 GEF-H1 is frequently up-regulated in HCC

Six HCC cell lines and three primary tumors that displayed chr.1q21-22 genomic gains were subjected to array-CGH analysis. Nineteen candidate genes were identified as shown in Table 5.1. These genes were selected based on copy number gain in more than 6 cases. Some genes identified, for example *CCT3* and *CROCA4* (Table 5.4), had been previously examined by our group and found to show only marginal significance in terms of their up-regulations in HCC tumors (Wong N *et al*, 2003). Among the 19 genes, *GEF-H1* on chr.1q22 was the only gene displaying gross amplification (\log_2 ratio ≥ 2) in one-third of the cases (3/9). An example of array CGH profile on chr.1q21-22 suggesting high copy number gains of *GEF-H1* is shown in Figure 5.3.

The mRNA expressions of *GEF-H1* in 13 HCC cell lines (HKCI-1, -2, -3, -6, -7, -9, -11, C1, C2, C3, SK-HEP1, Hep3B and Huh7) were examined by qRT-PCR. Frequent up-regulation of *GEF-H1* was observed in 92% of HCC cell lines (12/13) compared to that of normal livers samples ($P < 0.0001$) (Figure 5.4A). The *GEF-H1* expression was further examined in a cohort of 100 primary HCC tumors and their matching non-tumoral livers. Up-regulation (≥ 2 -fold) of *GEF-H1* was suggested in 64% tumors compared to adjacent non-tumoral liver (64/100; paired *t*-test $P < 0.0001$) (Figure 5.4B). There was a corresponding increase in the protein level of GEF-H1 in primary HCC tumors relative to adjacent non-tumoral livers, and HCC cell lines (Figure 5.4C).

Table 5.1 Candidate genes showing frequent copy number gain from array-CGH analysis

Chromosomal region	Candidate genes	No. of cases with low level gain	No. of cases with high level gain
1q21	GJA5	7	0
	ANXA9	6	0
	AF1Q	6	0
	TCFL1	6	1
	SNX27	7	0
	RORC	6	0
	SPRR1A	7	0
	SPRR1B	7	0
	S100A7	8	0
	ATP8B2	7	1
1q22	RUSC1	6	0
	THC2128963	7	0
	GEF-H1	7	3
	THC2216346	6	1
	SEMA4A	6	0
	CCT3	8	1
	CROC4	7	1
	IQGAP3	8	1
	GPATC4	6	0

In a total of 9 cases analysed by array-CGH, genes were shortlisted when copy number gain was found in 6 cases or more.

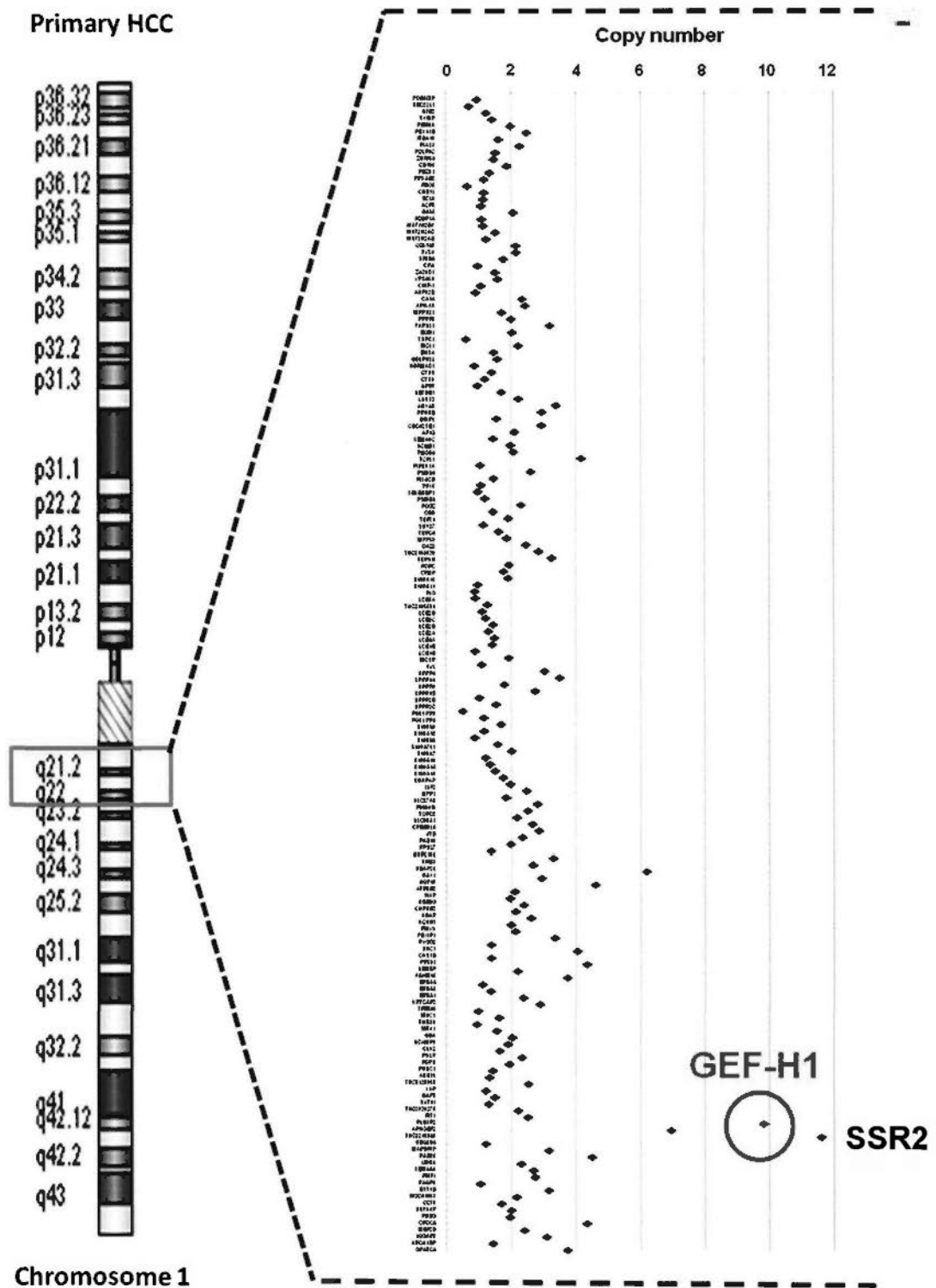


Figure 5.3 Array-CGH analysis of chromosome 1 on Primary HCC

High-resolution profile of chr.1q21-22 is shown with copy number fold-change relative to normal liver. Copy number amplification of *GEF-H1* (highlighted in red circle) was identified.

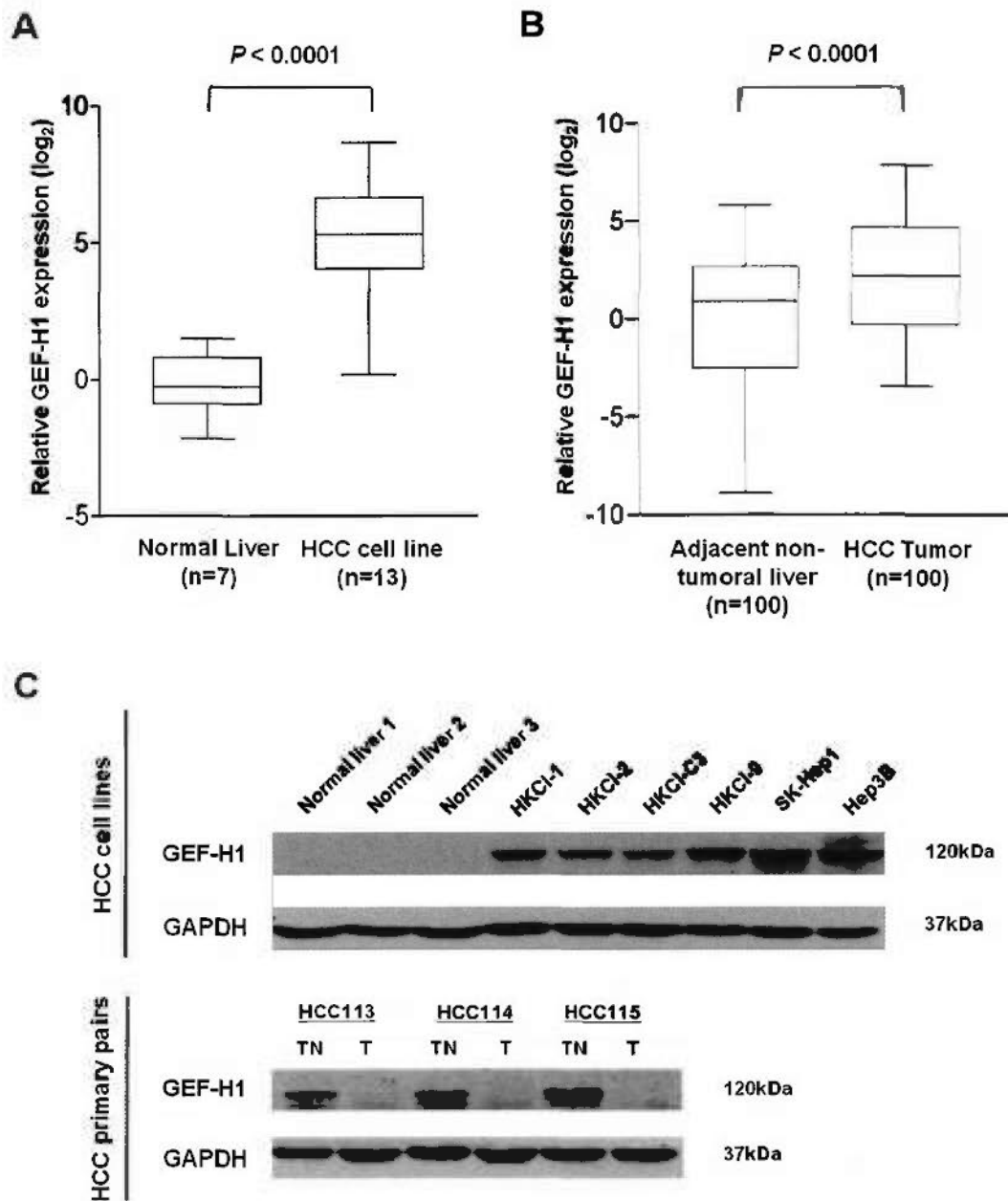


Figure 5.4 GEF-H1 is frequently up-regulated in HCC

The mRNA levels (**A and B**) and protein levels (**C**) of GEF-H1 were significantly up-regulated in HCC cell lines compared to the normal liver samples and in HCC tumors compared to the adjacent non-tumoral livers.

5.2.2 Prognostic value of *GEF-HI*

Correlative analysis of *GEF-HI* mRNA levels with patients' clinicopathological features is shown in Table 5.2. Up-regulations of *GEF-HI* was found to be significantly associated with the presence of microvascular invasion ($P = 0.049$) and advanced stage HCC (Stage T3, $P = 0.048$). Increased *GEF-HI* expression (relative gene expression ≥ 2 -fold) was also found to correlate with shorter disease-free ($P = 0.022$) and overall survival ($P = 0.026$) of HCC patients (Figure 5.2). Multivariate survival analysis using the Cox proportional hazards model further supported that *GEF-HI* over-expression is strongly associated with a higher hazard ratio and adverse clinical outcomes (for disease free-survival, $P = 0.017$, hazard ratio = 2.206; for overall survival, $P = 0.016$, hazard ratio = 2.752). Nevertheless, the presence of microvascular invasion represents a stronger prognostic marker (Table 5.3).

Table 5.2 Clinicopathological correlations of *GEF-H1* expression in HCC

Clinicopathological features (n=100)	Relative <i>GEF-H1</i> expression median (inter-quartiles)	<i>P</i>-value
<u>Gender</u>		
Male (n=86)	3.614 (1.628 – 16.19)	0.398
Female (n=14)	1.779 (0.624 – 7.349)	
<u>Age</u>		
≤ 40 (n=12)	3.444 (1.221 – 11.56)	0.7044
> 40 (n=88)	3.564 (1.305 – 10.87)	
<u>AJCC Staging (6th Edition)</u>		
Early T1 (n=64)	2.897 (1.072 – 7.583)	*0.048
Advanced T2/T3 (n=36)	5.348 (2.303 – 16.19)	
<u>Macro-vascular invasion</u>		
Presence (n= 8)	5.546 (2.208 – 37.25)	0.220
Absence (n=92)	3.564 (1.166 – 9.267)	
<u>Micro-vascular invasion</u>		
Presence (n=21)	5.348 (2.966 – 19.64)	*0.049
Absence (n=79)	3.403 (1.166 – 10.87)	
<u>Tumoral lesion</u>		
Solitary (n=73)	3.403 (1.337 – 11.94)	0.466
Multiple (n=27)	4.812 (1.095 – 17.52)	
<u>Viral HBV infection</u>		
Positive (n=91)	3.564 (1.382– 16.19)	0.142
Negative (n=9)	2.144 (0.862 – 4.926)	
<u>Liver cirrhosis</u>		
Presence (n=70)	3.564 (1.243 – 14.25)	0.824
Absence (n=30)	3.564 (1.144 – 12.81)	

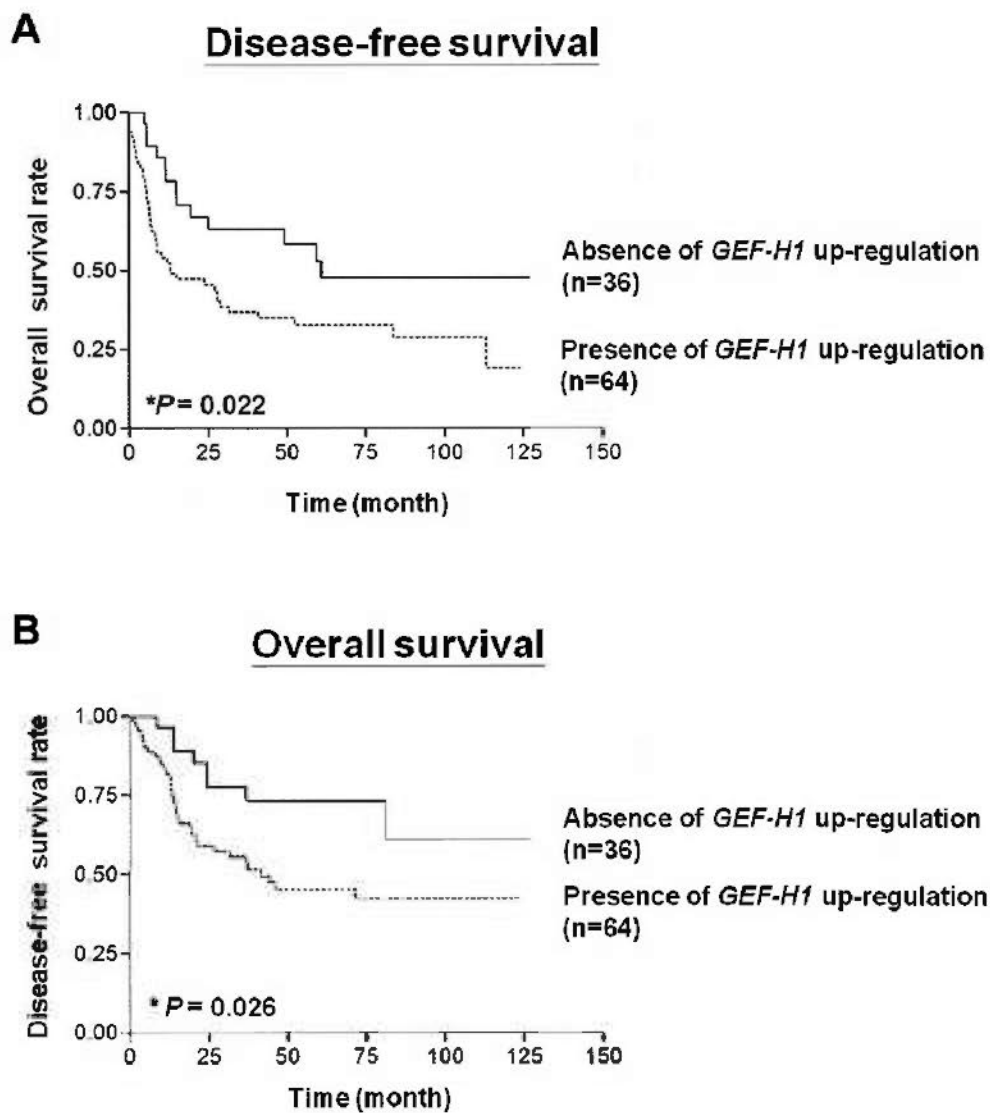


Figure 5.5 Kaplan-Meier analysis of *GEF-H1* expression in HCC

(A) Disease-free survival (B) Overall survival

The group of presence of *GEF-H1* up-regulation (n=64) contained the HCC tumors harbouring *GEF-H1* expression ≥ 2 -fold increase relative to normal livers samples.

Table 5.3 Multivariate Cox regression analysis of *GEF-H1* expression in HCC

Variables	Disease free survival		
	Hazard Ratio	95% CI	<i>P</i> -value
<i>GEF-H1</i> expression	2.206	1.154 to 4.216	*0.017
Gender	0.746	0.267 to 2.089	0.579
Age ^a	1.018	0.990 to 1.048	0.214
Tumoral lesion ^b	2.204	0.952 to 5.104	0.066
Liver cirrhosis ^c	1.833	0.899 to 3.738	0.097
Macro-vascular invasion ^c	1.457	0.467 to 4.542	0.519
Micro-vascular invasion ^c	3.897	1.828 to 8.306	*0.0005
HbsAg ^d	0.651	0.217 to 1.951	0.445
Clinical stage ^e	0.935	0.496 to 1.763	0.836

Variables	Overall survival		
	Hazard Ratio	95% CI	<i>P</i> -value
<i>GEF-H1</i> expression	2.752	1.216 to 6.229	*0.016
Gender	0.468	0.125 to 1.747	0.261
Age ^a	1.030	0.994 to 1.067	0.106
Tumoral lesion ^b	2.299	0.885 to 5.974	0.089
Liver cirrhosis ^c	1.527	0.661 to 3.527	0.324
Macro-vascular invasion ^c	0.834	0.250 to 2.786	0.770
Micro-vascular invasion ^c	5.280	2.233 to 12.484	*0.0002
HbsAg ^d	0.428	0.141 to 1.301	0.137
Clinical stage ^e	1.078	0.543 to 2.139	0.832

^a Age: patients aged ≤ 40 vs patients aged > 40

^b Tumoral lesion: solitary vs multiple

^c Liver cirrhosis; macro-vascular invasion; micro-vascular invasion:
Presence vs absence

^d HbsAg: HBV positive vs HBV negative

^e Clinical stage: early vs advanced stage

5.2.3 Functional studies of *GEF-H1* upon *GEF-H1* depletion by siRNA

siRNA was used to suppress the expression of *GEF-H1* in Hep3B and SK-HEP1 which were the two cell lines displaying high *GEF-H1* expression. The knockdown of *GEF-H1* expression was affirmed by qRT-PCR and Western blot analysis (Figure 5.6).

In functional investigations, significant inhibition of cell invasiveness was found in siGEF-H1 treated cells ($P = 0.0005$ for Hep3B; $P = 0.003$ for SK-HEP1), when compared to siControl treated group. In addition, significant decrease in cell migration was also observed in siGEF-H1 treated HCC cells compared to control experiments ($P = 0.028$ for Hep3B; $P = 0.035$ for SK-HEP1) (Figure 5.7). Besides, the migratory ability of Hep3B and SK-HEP1 cells in wound healing assay was impeded when *GEF-H1* was knockdown (Figure 5.8). Upon 24 hr incubation after the introduction of wound, siGEF-H1 treated cells showed a slower migration ability compared to siControl treated cells. After 48 hr incubation, wound closure in the control treatments was completed, whereas in *GEF-H1* depleted cells, an opening could still be clearly observed in both Hep3B and SK-HEP1.

GEF-H1 suppression, however, did not suggest apparent effects on cell viability and cell proliferation in both Hep3B and SK-HEP1 relative to siControl treated cells or cells incubated with lipofectamine alone (Lipo) (Figure 5.9).

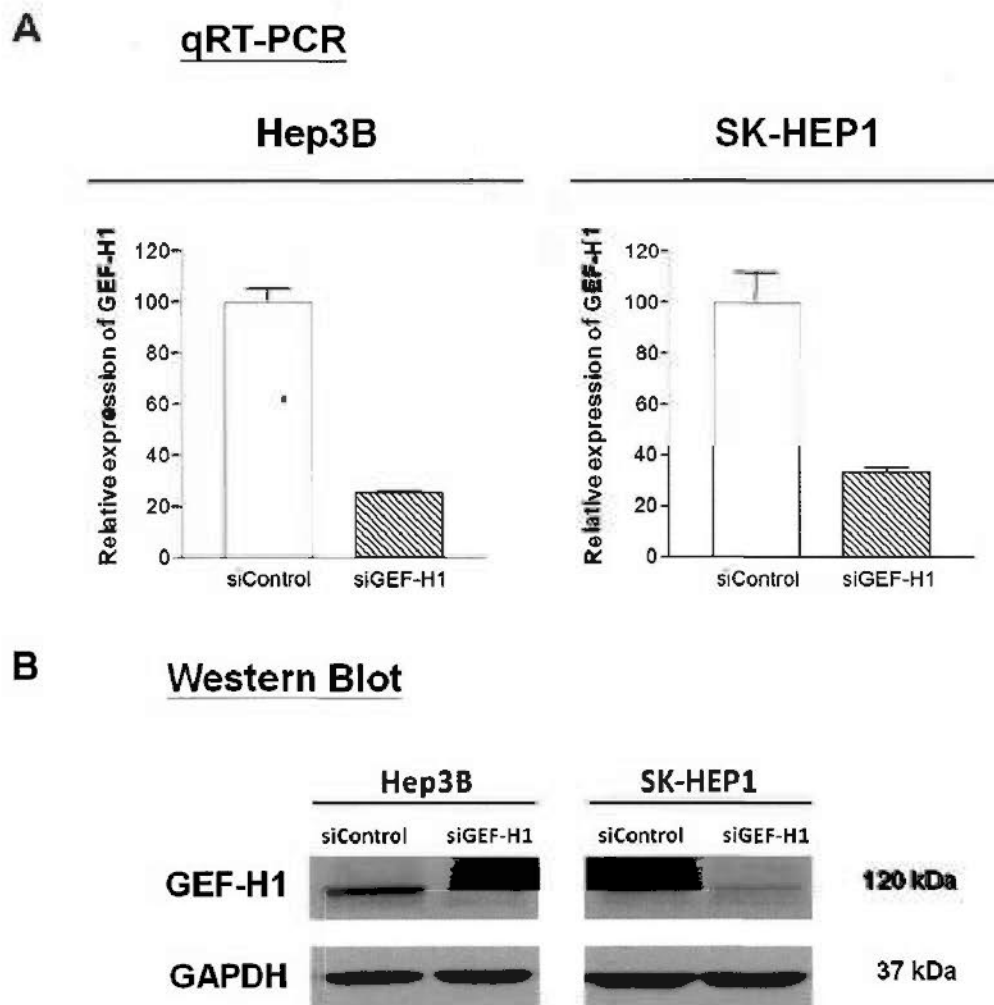


Figure 5.6 GEF-H1 expression of Hep3B and SK-HEP1 cells in knockdown experiments

(A) There were 80% and 70% suppression of *GEF-H1* mRNA level found in Hep3B cells and SK-HEP1 cells. (B) Significant suppression of GEF-H1 proteins was confirmed by Western blot in both cell lines.

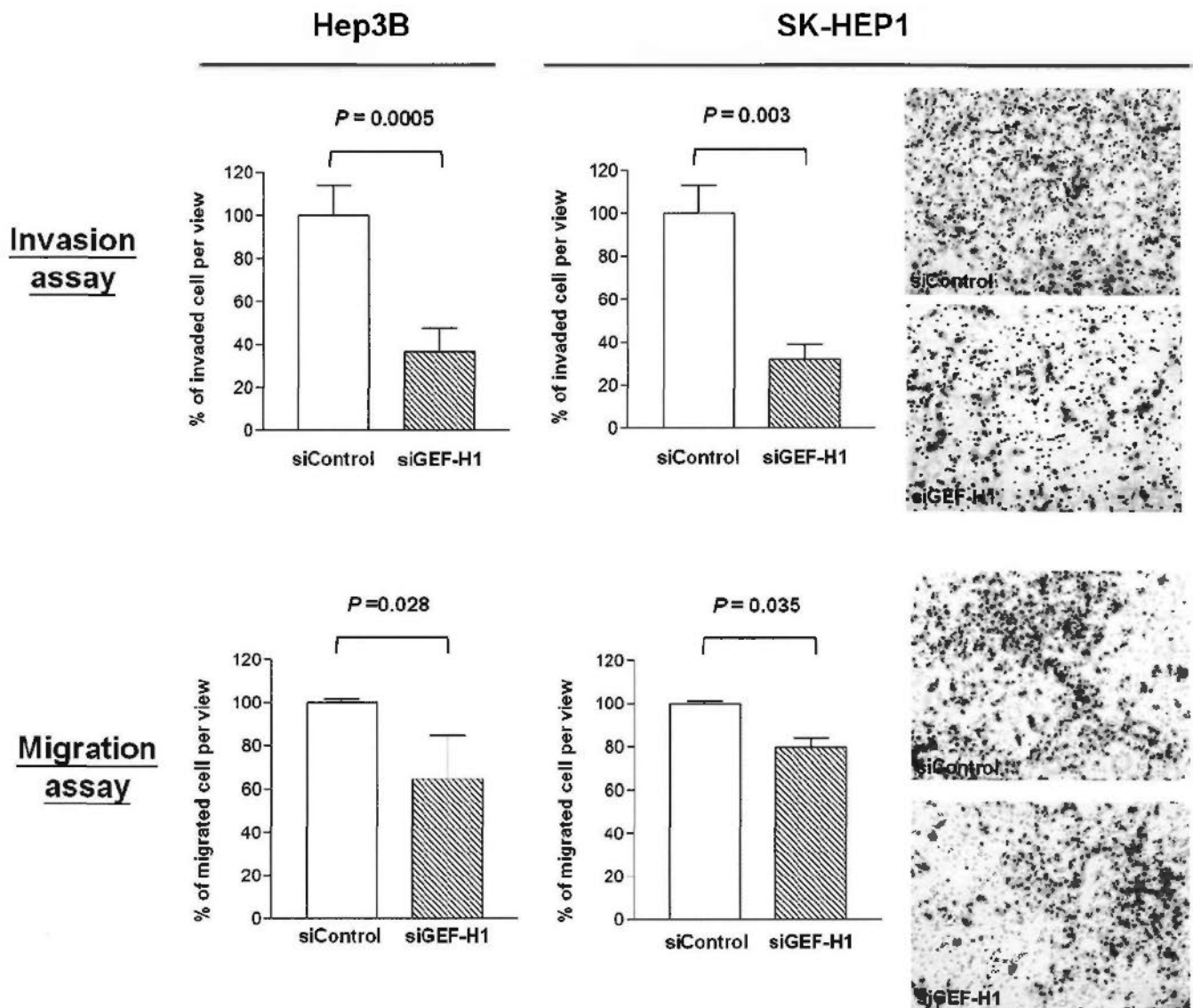


Figure 5.7 mRNA suppression of *GEF-H1* inhibits the cell invasiveness and cell migratory ability in Hep3B and SK-HEP1

Significant inhibition of invasion and migration upon *GEF-H1* depletion was demonstrated in Hep3B and SK-HEP1. Representative images of invaded and migrated SK-HEP1 cells with siGEF-H1 or siControl transfection are shown on the right panel.

Wound Healing assay

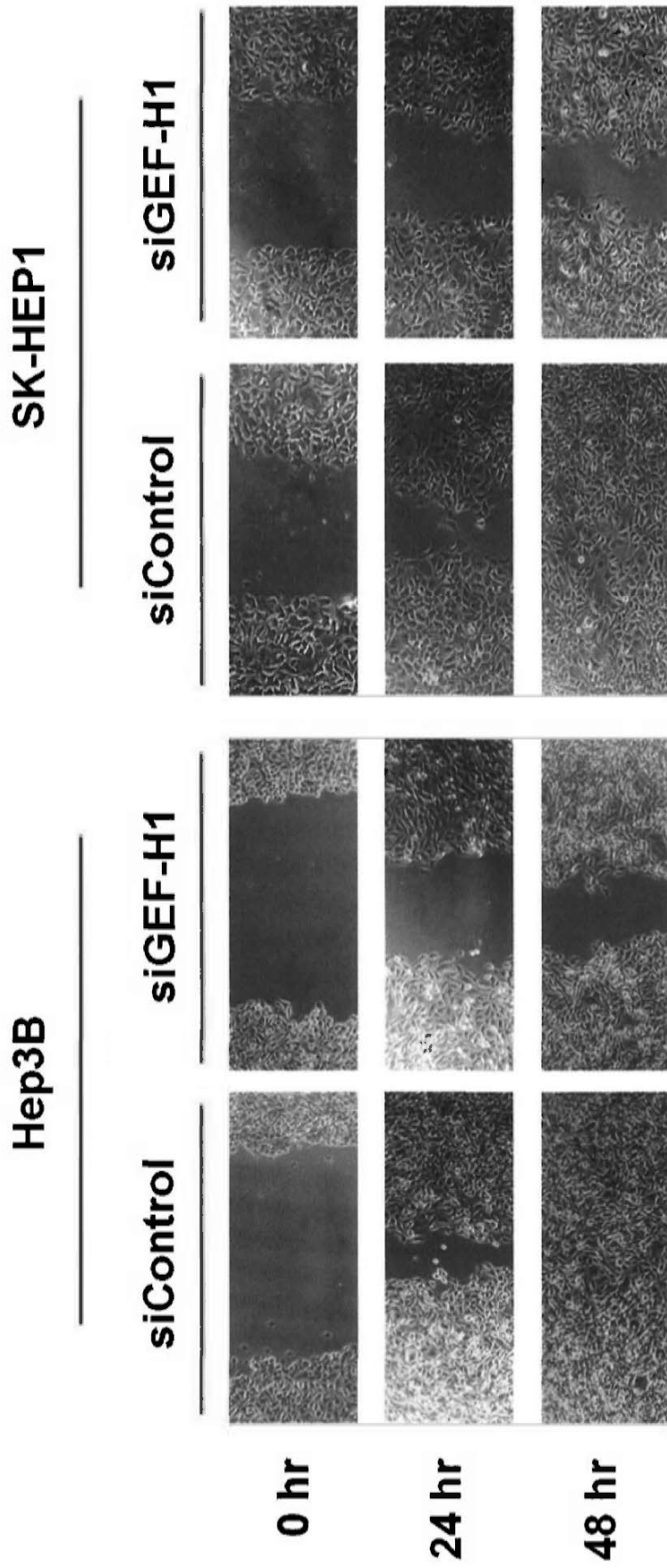


Figure 5.8 Wound healing assay suggested mRNA suppression of *GEF-H1* inhibits cell migratory ability in Hep3B and SK-HEP1

The migratory ability of Hep3B and SK-HEP1 cells were found to be impeded following knockdown of *GEF-H1* expression.

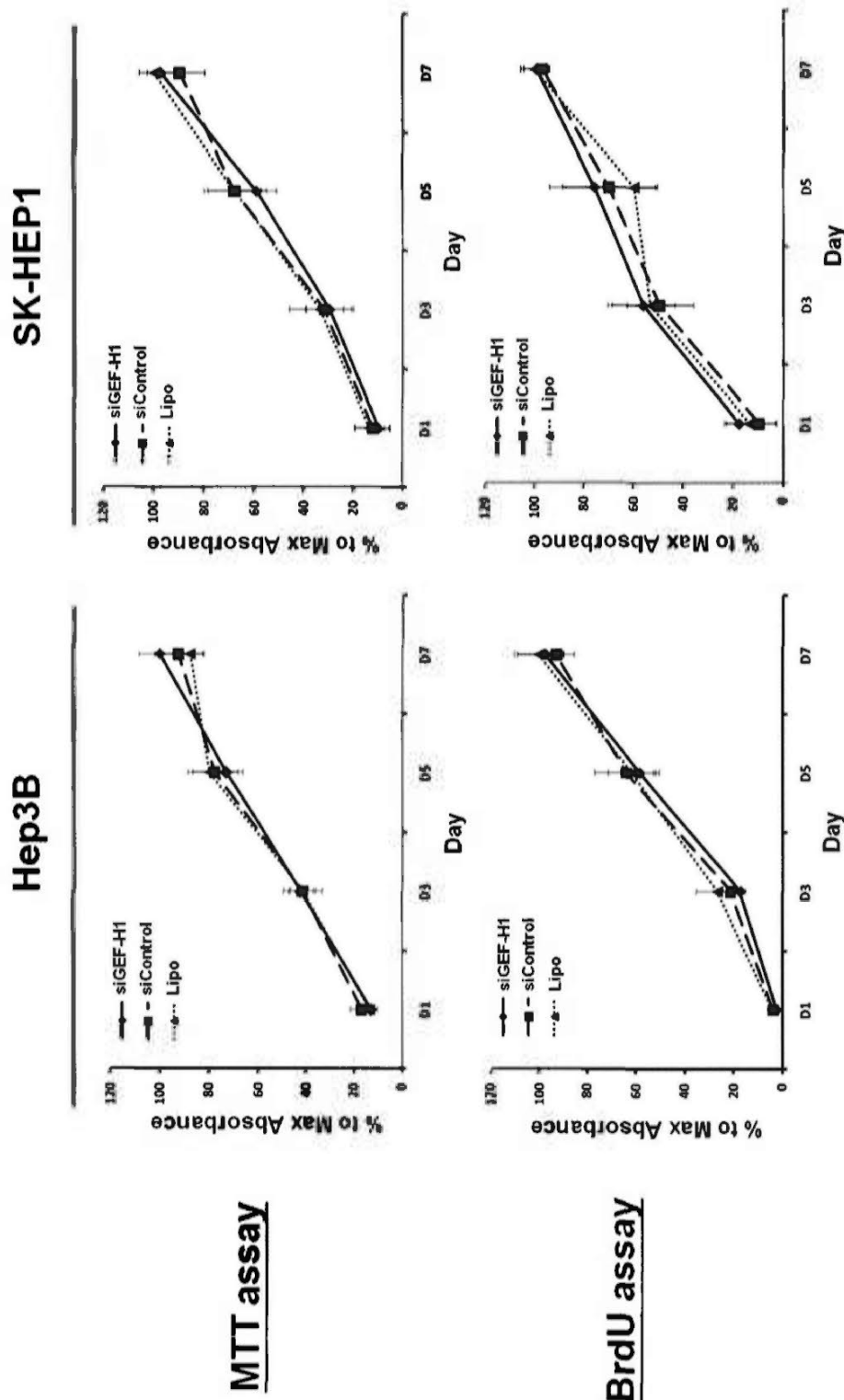


Figure 5.9 mRNA suppression of *GEF-H1* does not affect the cell viability and cell proliferation in Hep3B and SK-HEP1

GEF-H1 depletion did not suggest any effects in cell viability and cell proliferation in both Hep3B and SK-HEP1 when compared to siControl treated cells or cells incubated with lipofectamine alone (Lipo) demonstrated in the MTT and BrdU assays.

5.2.4 GEF-H1 depletion restores the epithelial phenotype of HCC cells through reversing EMT process

EMT normally occurs during embryonic development in many animal species including mesoderm formation, neural crest and heart valve development. (Yang J *et al*, 2008). It is a highly conserved cellular program that allows polarized, immotile epithelial cells to convert to motile mesenchymal cells. Accumulating evidence has showed that EMT programme gives rise to the dissemination of primary cancer cells to the secondary sites, which is a first step in the metastasis process (Thiery JP *et al*, 2006; Thiery JP *et al*, 2009). It is hypothesized here that EMT would be induced upon *GEF-H1* up-regulation. By Western blot analysis, it was demonstrated that knockdown of *GEF-H1* in Hep3B and SK-HEP1 showed substantial decrease in the mesenchymal markers (N-cadherin, vimentin and fibronectin), along with a corresponding increase of epithelial markers (E-cadherin, cytokeratin 18, α -catenin and γ -catenin) (Figure 5.10). To further confirm the mesenchymal to epithelial (MET) phenotype, immuno-fluorescence analysis of EMT markers on siGEF-H1 or siControl transfected cells was performed. The *GEF-H1* depleted Hep3B and SK-HEP1 cells showed much reduced mesenchymal phenotype with only weak expressions of vimentin and N-cadherin compared to the abundant expression of these mesenchymal markers in the control groups (Figure 5.11). The elicitation of epithelial phenotype by the re-expression of cytokeratin 18 in *GEF-H1* depleted cells was also observed in both cell lines, while only low expression cytokeratin 18 was found in siControl transfected cells. Besides, the tight-junction protein E-cadherin was found to relocate to the cell membrane forming the cell-cell adhesion, while in siControl Hep3B cells E-cadherin was mainly localized in the cytosol (Figure 5.12).

The SK-HEP1 cells showed negligible expression of E-cadherin in both Western blot and immuno-fluorescence experiments and hence cannot be confidently interpreted.

During the execution of EMT program, many genes involved in cell adhesion, mesenchymal differentiation, cell migration and invasion are transcriptionally altered. The best-studied transcriptional modulation during EMT involved the E-cadherin gene. The interaction of well-known EMT transcriptional regulators (namely SNAIL1, SLUG, ZEB1, ZEB2, TWIST1 and TCF3) and the E-box elements residing on the promoter of E-cadherin are responsible for its transcriptional repression (Girolodi LA *et al*; 1997; Hennig G *et al*, 1995). These E-cadherin repressors were studied to further understand the EMT process under the influence of *GEF-H1*. In Hep3B and SK-HEP1 cells, transcript levels of SNAIL1 ($P = 0.018$), ZEB1 ($P = 0.0006$) and TCF3 ($P = 0.035$) were significantly down-regulated in *GEF-H1* depleted Hep3B cells while significant down-regulations of ZEB1 ($P = 0.007$), ZEB2 ($P = 0.009$) and TCF3 ($P = 0.006$) were found in *GEF-H1* depleted SK-HEP1 cells (Figure 5.13).

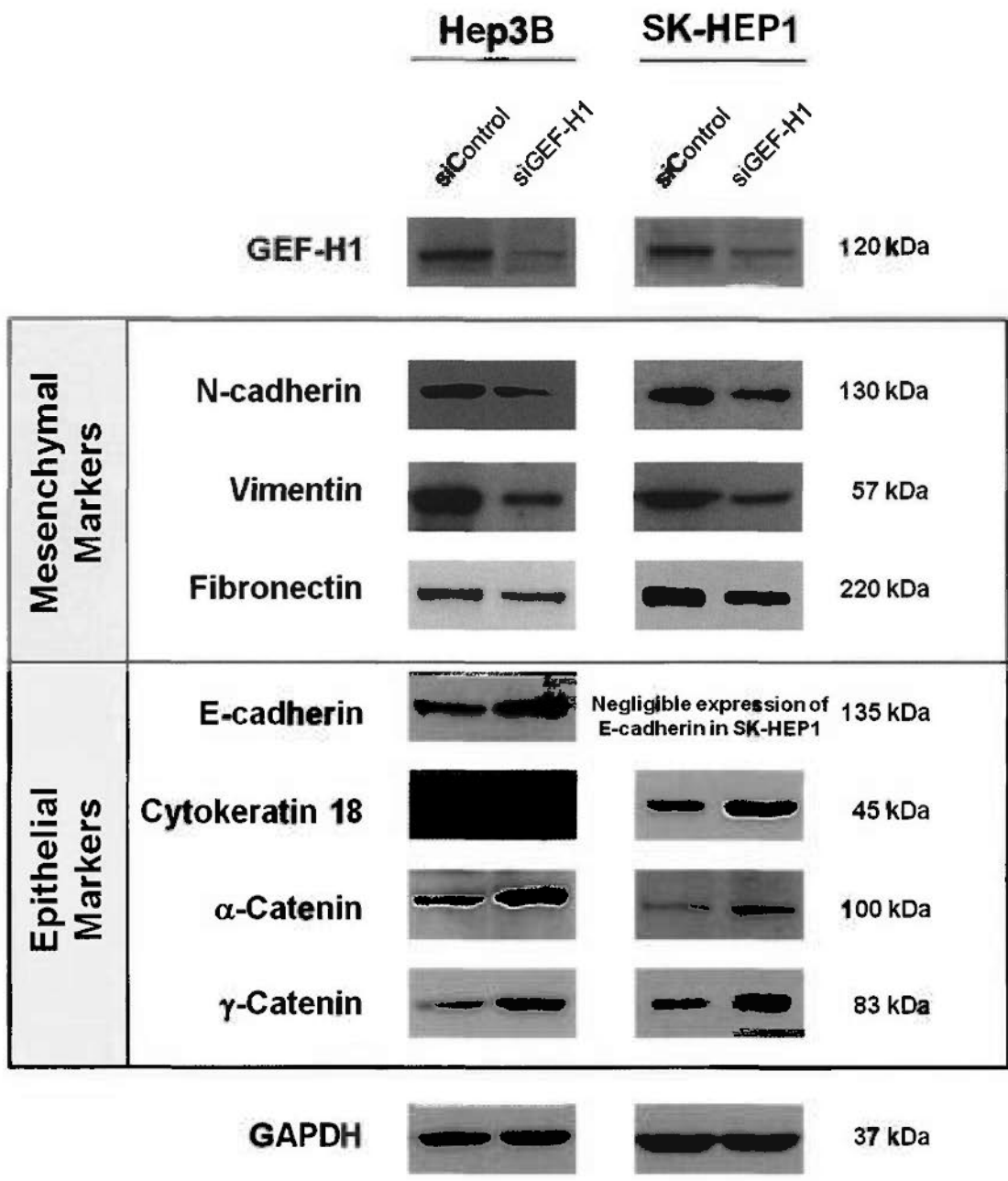


Figure 5.10 Western blot of EMT markers upon *GEF-H1* depletion

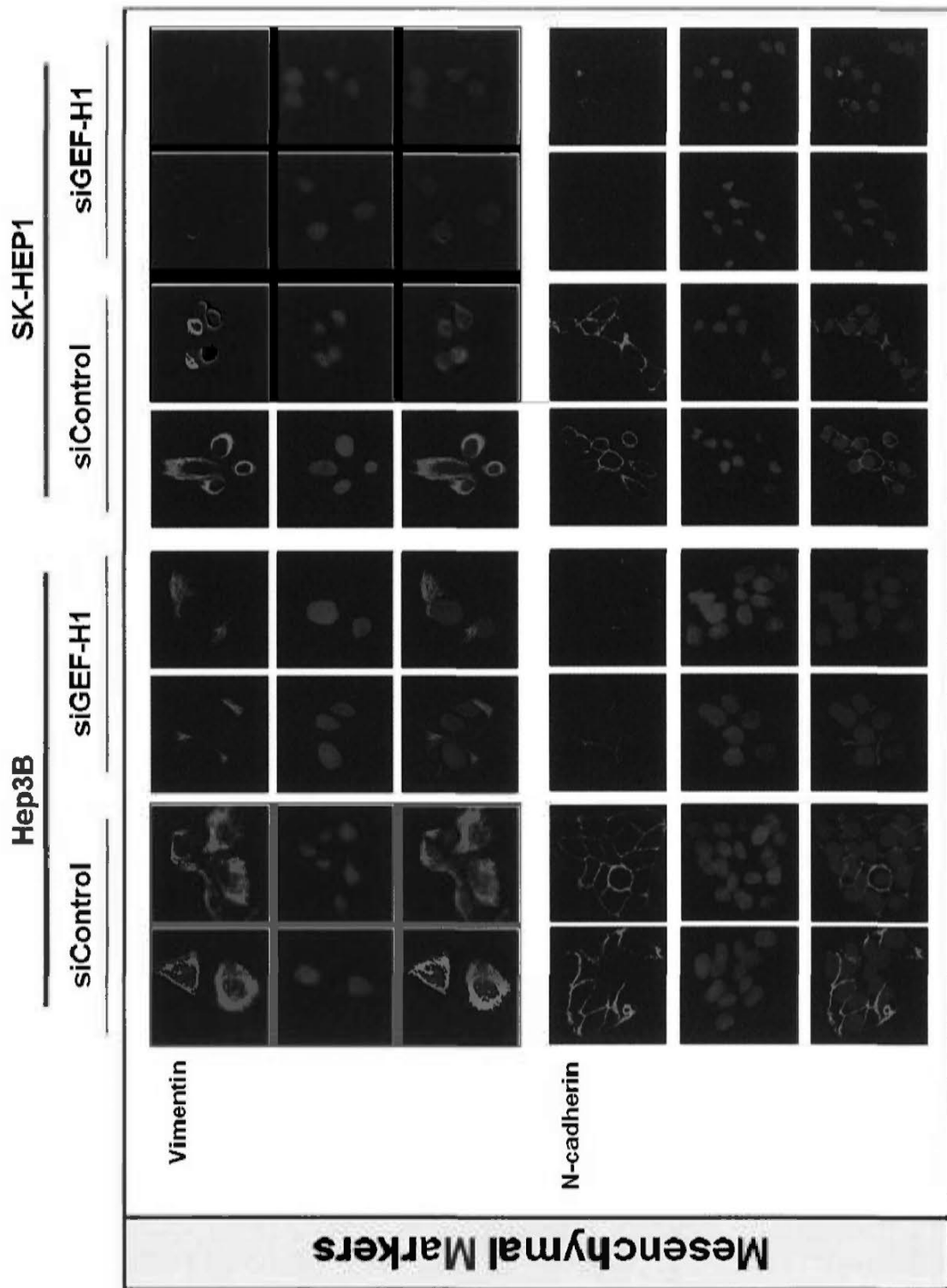


Figure 5.11 Immuno-fluorescence images of mesenchymal markers in *GEF-H1* knockdown experiment

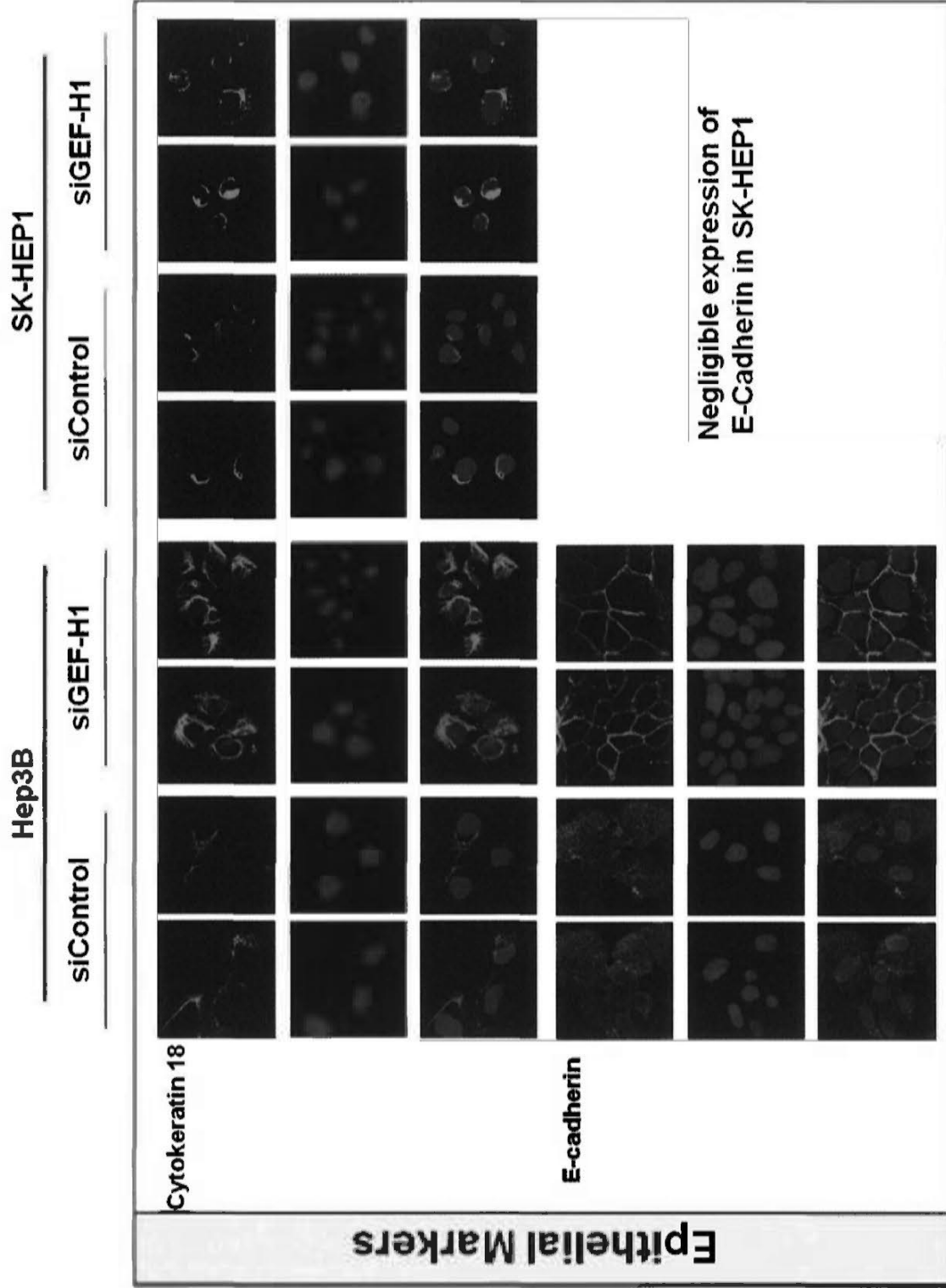


Figure 5.12 Immuno-fluorescence images of epithelial markers in *GEF-H1* knockdown experiment

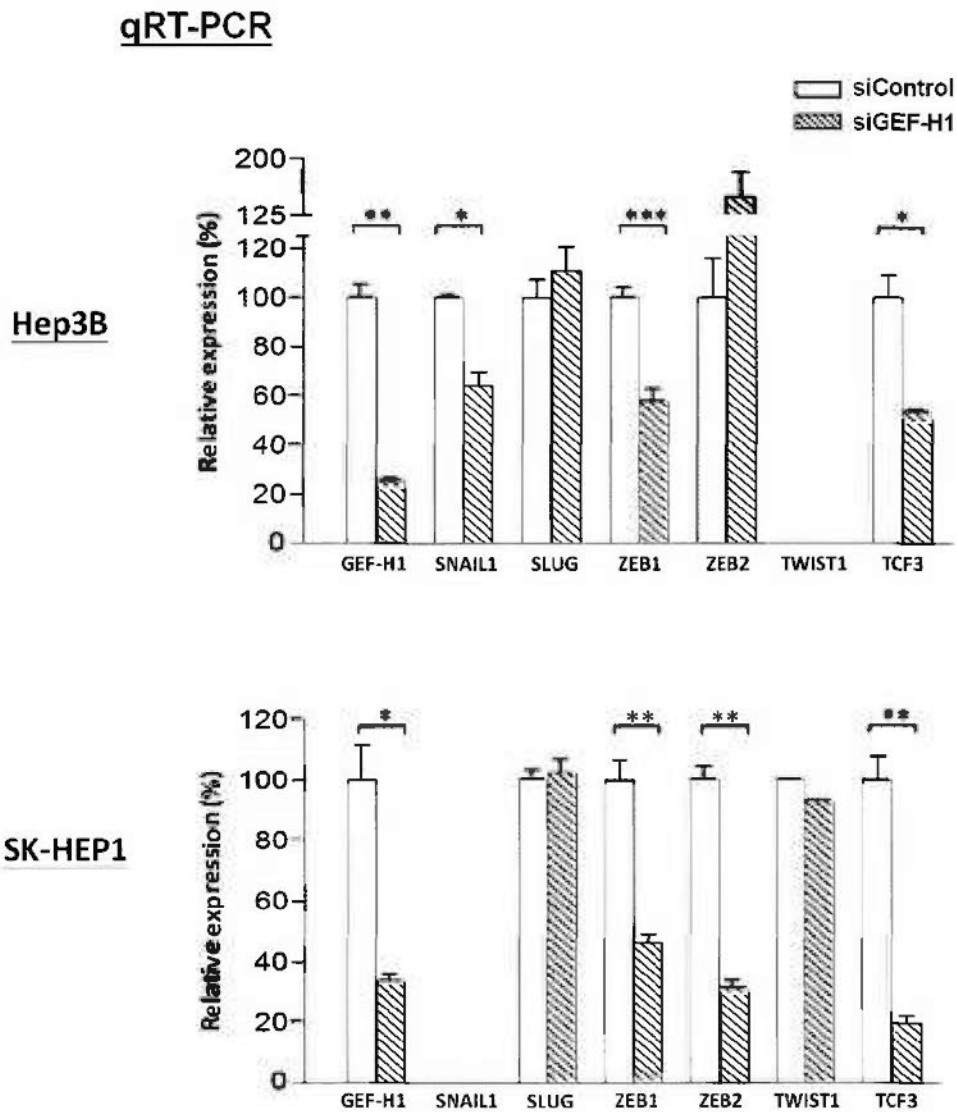


Figure 5.13 Decreased in mRNA and protein levels of E-cadherin transcription repressors were observed in Hep3B and SK-HEP1 cells upon *GEF-H1* depletion by qRT-PCR and Western blot analysis

(A) Significant down-regulations of SNAIL1, ZEB1, TCF3 were found in *GEF-H1* depleted Hep3B cells while significantly down-regulations of ZEB1, ZEB2 and TCF3 were found in *GEF-H1* depleted SK-HEP1 cells (* $P < 0.05$; ** $P < 0.01$; *** $P < 0.001$).

5.2.5 GEF-H1 depletion abolishes Rho pathway activation and inhibits stress

fibre formation

GEF-H1 is a microtubule-associated Rho-GEF that has emerged as a crucial player in coupling microtubule dynamics to Rho-GTPase activation in variety of normal biological processes including cytoskeletal organizations, gene transcription, signal transductions and differentiation (Ren Y *et al*, 1998; Jaffe AB *et al*, 2005; Burrige K *et al*, 2004). The zinc finger at the N-terminal and the coiled coil motif at C-terminal of *GEF-H1* are responsible for the microtubule binding which acts as the negative regulator and the free active form of GEF-H1 is released only upon microtubule depolymerisation (Krendel M, *et al*, 2002). The unbound form of GEF-H1 would induce the replacement of GDP to GTP on Rho GTPases especially on RhoA and Rac1, which belong to the Rho GTPase family. To determine whether the depletion of *GEF-H1* would affect the GTP/GDP binding status of Rho GTPases, the GTP bound RhoA, Rac1 and Cdc42 were investigated by Rhotekin Rho binding domain (RBD) and PAK p21 binding domain (PBD) pull down assay. As shown in Figure 5.14, the level of GTP-RhoA was significantly decreased upon *GEF-H1* depletion at both 24 hr and 48 hr post-transfection in Hep3B cells while a reduction was observed at 48 hr in SK-HEP1 cells. Hence, the depletion of *GEF-H1* affected the amount of active GTP-RhoA level, while the protein level of total RhoA (including the GTP- and GDP-RhoA) remained unchanged.

The active form of GTP-Rac1 and GTP-Cdc42 were also examined. Contrary to RhoA-GTP findings, the level of GTP-Rac1 was increased in siGEF-H1 treated Hep3B cells at both 24 hr and 48 hr while a prominent increase of GTP-Rac1 in siGEF-H1 transfected SK-HEP1 cells was observed at 24 hr. Similar to RhoA, the

total protein level of Rac1 was not affected. For Cdc42, the pulled GTP forms were weak and the level seemed to be independent of the presence of *GEF-H1* in both cell lines (Figure 5.14).

Next, it was hypothesized that the RhoA pathway would be inactivated upon *GEF-H1* depletion through the down-regulation of GTP-RhoA, that led to inhibition of cell invasion and migration. To explore the key players in RhoA pathway, the direct RhoA downstream effector, ROCK1 (Rho kinase 1) protein were investigated. ROCK1 itself exerts an autoinhibition machinery through interaction between its C-terminal inhibitory pleckstrin homology (PH) domain and N-terminal kinase region. The active GTP-RhoA binds to the RBD on ROCK1 which results in the open conformation of the kinase and frees the catalytic activity to carry out serine/threonine phosphorylations (Riento K *et al*, 2003). Following the decrease of active GTP-RhoA of siGEF-H1 treated Hep3B and SK-HEP1 cells, the protein levels of cleaved-ROCK1 (active form) were found to be significantly decreased in both cell lines, while the total ROCK1 proteins among the siGEF-H1 or siControl transfected cells were similar (Figure 5.15). In addition, the phosphorylated form of myosin light chain 2 (MLC2), one of the direct phosphorylated targets of ROCK1, was also found to be significantly decreased in *GEF-H1* depleted cells, while the total MLC2 level remained unchanged.

It is well-known that the active RhoA pathway is responsible for many cellular processes including gene transcription, cell growth and differentiation, especially on cytoskeletal dynamics and cell motility through stress fibre formation (Pellegrin S *et al*, 2007). To determine whether the inactivation of RhoA-ROCK1-MLC2 pathway upon *GEF-H1* depletion would bring about an inhibition of stress fibre formation, the siGEF-H1 or siControl transfected Hep3B and SK-HEP1 cells were examined with

TRITC-conjugated Phalloidin staining which is a group of toxin that actively and specifically binds to the F-actin. As shown in figure 5.16, the stress fibres in siControl treated cells of both cell lines appeared as extensive parallel bundles which were densely stained in a well-organized manner. The stress fibre architecture, however, was disrupted in siGEF-H1 treated cells. The F-actin was loosely organized and randomly dispersed in these cells. It is plausible that down-regulation of *GEF-H1* in HCC cells directly decreased the active GTP-RhoA protein leading to the inactivation of the downstream RhoA effectors including the decreased cleaved-ROCK1 level and reduced active phosphorylated-MLC2. The latter MLC2 with less ATPase activity would reduce actomyosin contraction and stress fibre formation, eventually leading to a retardation of cell motility in *GEF-H1* depleted cells.

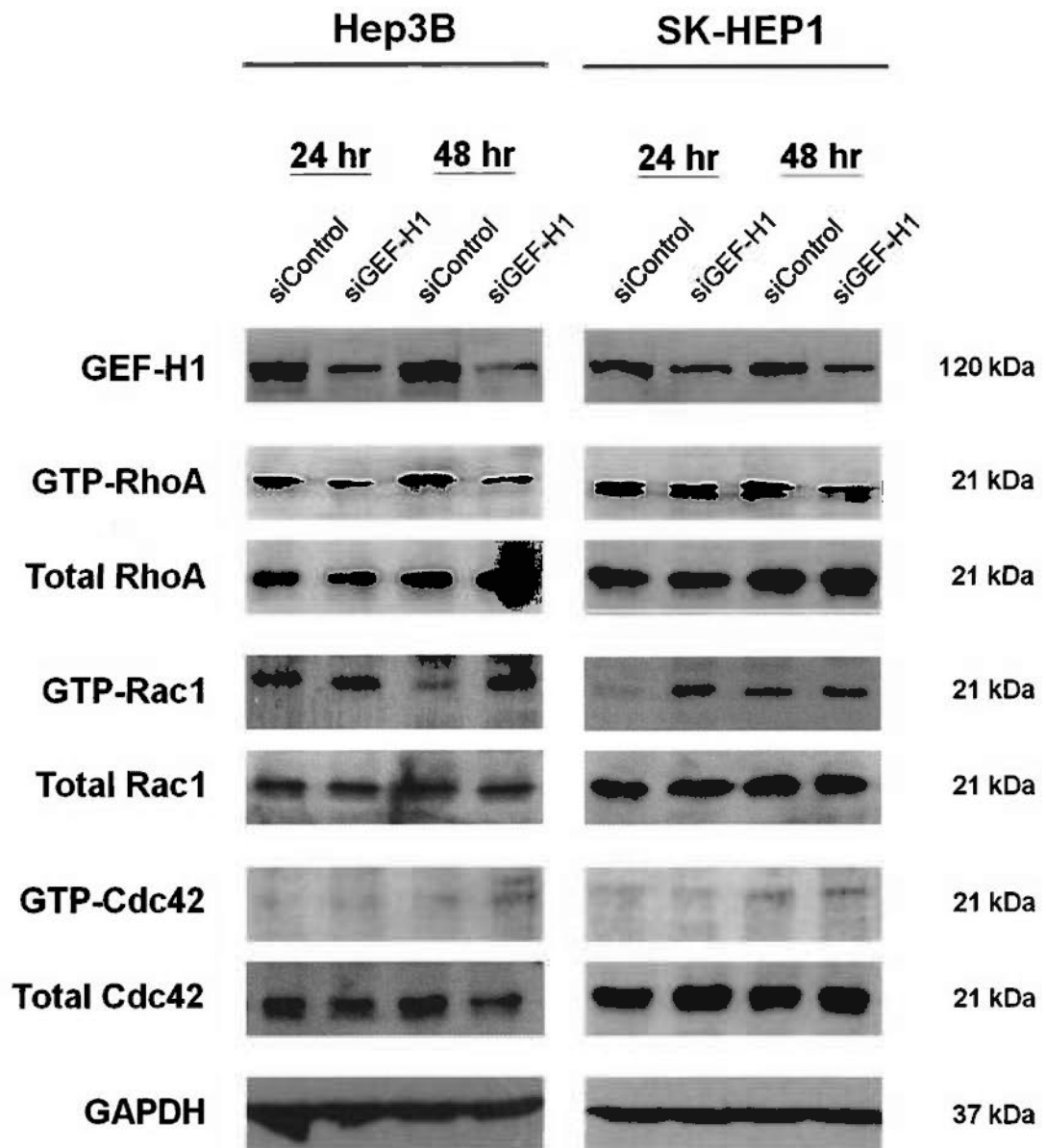


Figure 5.14 The effect on GTPase guanine nucleotide binding status of RhoA, Rac1 and Cdc42 upon *GEF-H1* depletion in Hep3B and SK-HEP1

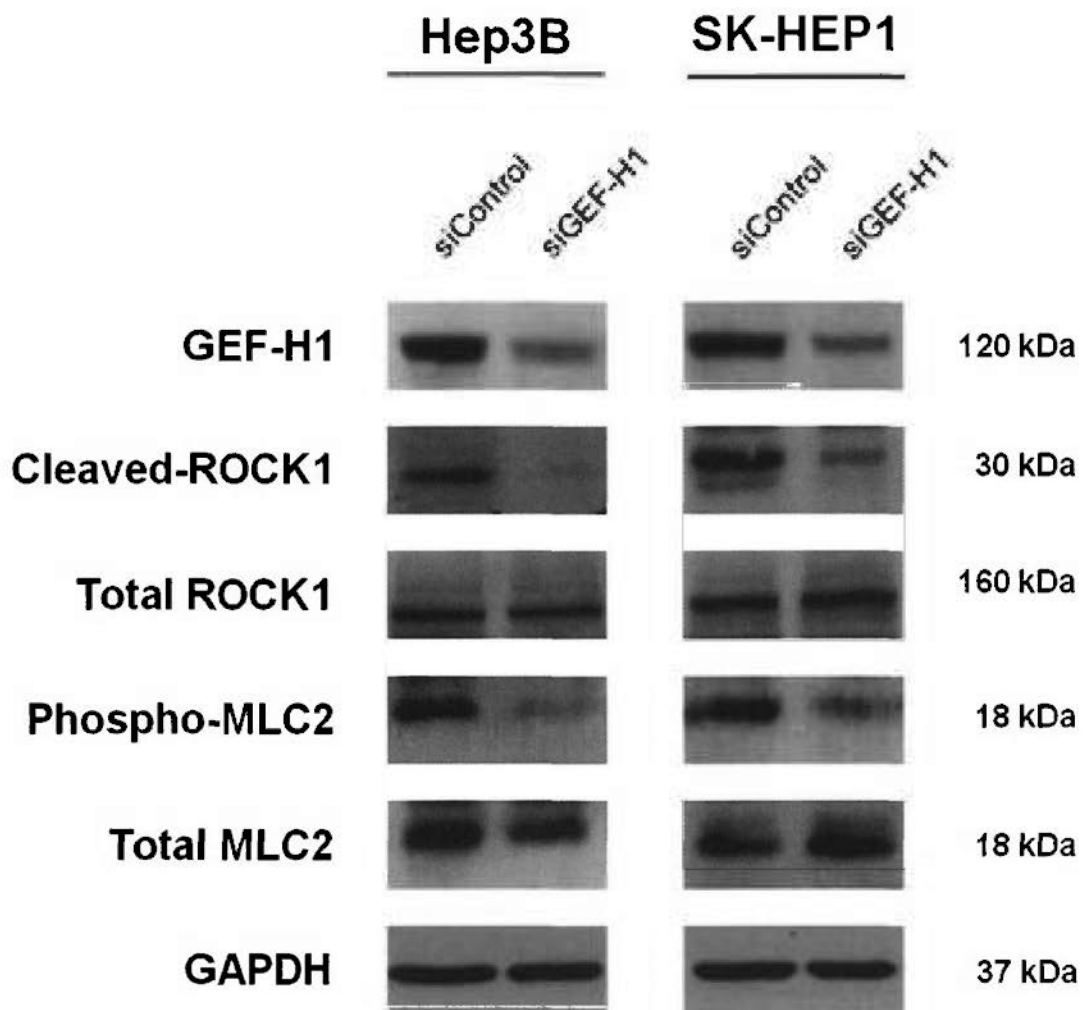


Figure 5.15 The effect on the downstream effectors of RhoA in Hep3B and SK-HEP1 upon *GEF-H1* depletion

Hep3B

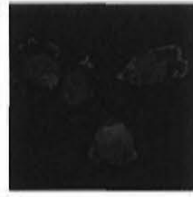
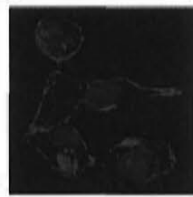
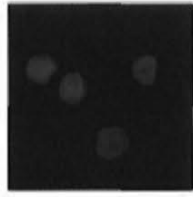
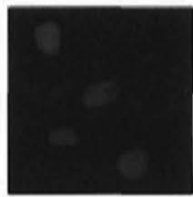
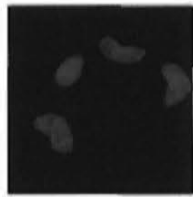
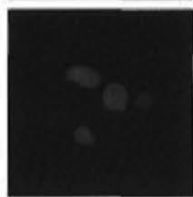
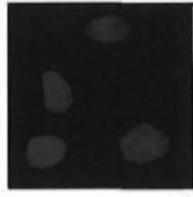
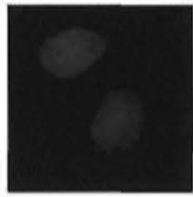
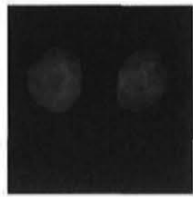
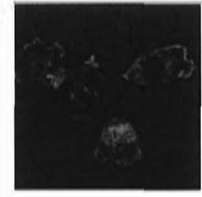
SK-HEP1

siControl

siGEF-H1

siControl

siGEF-H1



F-actin

DAPI

Merged

Figure 5.16 Inhibition of stress fibre formation upon *GEF-H1* depletion

The actin filaments were visualized with TRITC-conjugated phalloidin

5.3 DISCUSSION

In an attempt to delineate chr.1q21-q22 for affected gene(s), array-CGH analysis defined *GEF-H1* as a novel proto-oncogene located at chr.1q22. Common up-regulation of *GEF-H1* was found in 64% of HCC tumors compared to the adjacent non-tumoral livers. Gain in *GEF-H1* expression not only holds prognostic significance in predicting shorter disease-free and overall patient survival, but also association with advance-staged HCC and presence of microvascular invasion. Besides, functional examinations of *GEF-H1* in 2 HCC cell lines (SK-HEP1 and Hep3B) suggested that *GEF-H1* conferred profound promotional effects on cellular motility and invasiveness. Correlative studies carried out would hence suggest *GEF-H1* expression could serve as a predictive marker in HCC patients for high metastatic potential.

To further understand the underlying mechanisms of *GEF-H1* activity in promoting cellular motility and invasiveness, the Rho GTPase pathway was investigated based on the fact that *GEF-H1* is a Rho-GEF protein. It is known that Rho GTPases, belonging to Ras superfamily, play an important role in the regulation of many cellular processes, including cytoskeletal dynamics and cell motility, gene expression and cell-cycle progression (Ren Y *et al*, 1998; Jaffe AB *et al*, 2005; Burridge K *et al*, 2004). Their GTP-binding / GTP hydrolysis cycle is tightly controlled by guanine nucleotide exchange factors (GEFs) and GTPase-activating proteins (GAPs). GEFs catalyze the exchange of GDP to GTP, thereby switching Rho GTPase to an active conformation. GAPs are responsible for the GTP hydrolysis to induce Rho inactivation. In the current study, *GEF-H1* identified is a specific GEF for RhoA activation. It was found that *GEF-H1* depletion would significantly decrease RhoA-GTP level. Reduced levels of downstream effectors of RhoA

including the active forms of cleaved-ROCK1 and phosphorylated MLC2 were also significantly shown in *GEF-H1*-depleted HCC cells. Deleted in liver cancer 1 (*DLC1*) is a Rho-GAP that is frequently down-regulated in HCC. *DLC1* resided on recurrent regional loss of chr.8p21.3-22 has been reported to show allelic loss in 44-50% of HCC tumors by Loss of Heterozygosity (LOH) analysis. Down-regulation of *DLC1*, on the other hand, can be detected in 20-68% of HCC cases (Ng IO *et al*, 2000; Wong CM *et al*, 2003). The loss of *DLC1* expression abolishes its GTP-hydrolytic function on RhoA leading to an excessive accumulation of the active RhoA-GTP levels. This leads to the activation of downstream signaling through ROCK1 and MLC2 resulting in the enhancement of cell motility and invasiveness. The novel finding on *GEF-H1* here suggested that the activation of RhoA signaling pathway is not solely dependent on the loss of the hydrolytic arm of GTP-binding cycle of RhoA, but also the gain of the catalytic arm of GTP loading on RhoA. The possible activation mechanisms of RhoA by *GEF-H1* and *DLC1* are summarized in Figure 5.17. At the moment, whether the increased RhoA-GTP level in HCC has been due to the loss of *DLC1* or gain of *GEF-H1* or both proteins exerting their function in a synergistic manner require further investigations.

Besides regulating the activity of RhoA, *GEF-H1* depletion was also found to increase the Rac1-GTP form in the current study. This phenomenon may hold implication in the metastasis behaviour or cell motility as it has been reported that RhoA and Rac1 function in antagonistic manner. For example, the occurrence of Rac1 up-regulation and RhoA down-regulation was found when cells reach full confluence and assembling of cell-cell junctions (Zondag GC *et al*, 2000; Fukata M *et al*, 2001). Moreover, Ras-induced transformation would cause Rac1 inactivation and RhoA activation (Zondag GC *et al*, 2000; Sahai E *et al*, 2001). In addition, it was

shown in a wide variety of mammalian cell types as well as in yeast, flies and worms that activated Rac1 promoted cell spreading and reduced the number of actin stress fibres, while activated RhoA increased cell contractility and enhanced stress fibre formation (Aspenström P, 1999; Etienne-Manneville S *et al*, 2002). Recently, it has been reported that activation of RhoA and ROCK suppressed Rac1 activation at the leading edge while inhibition of ROCK switched Rac1 as the dominant Rho GTPase driving protrusion in carcinoma cells (El-Sibai M *et al*, 2008). It has also been shown in neuronal cells that the high level of Rho-GTP induced ROCK activation and actomyosin contractility, whereas the low level of Rho-GTP preferentially activated mDia1 and induced Rac activation, resulting in neurite retraction and elongation, respectively (Arakawa Y *et al*, 2003; Narumiya S *et al*, 2009). The significance of the opposite working pattern of RhoA and Rac1 in the *GEF-H1*-mediated HCC motility requires further elucidation.

EMT is a highly conserved cellular program that allows polarized, immotile epithelial cells to convert to motile mesenchymal cells. It is a fundamental process initially recognized during several critical stages of embryonic development such as mesoderm formation, neural crest development, heart valve development and secondary palate formation (Yang J *et al*, 2008). The phenotypic changes include the loss of cell-cell adhesion, the loss of cell polarity and the acquisition of migratory and invasive properties. EMT not only occurs during embryonic development, but also proposed as an important process in carcinoma aggressiveness and metastasis (Gotzmann J *et al*, 2004; Polyak K *et al*, 2009; Thiery JP *et al*, 2006). In this study, *GEF-H1* depletion in HCC cells would also cause the reverse of EMT features (re-gaining of epithelial phenotypes and loss of mesenchymal phenotypes). In addition, it was found that the EMT mediated by *GEF-H1* in HCC was probably due

to the activation of several E-cadherin transcription repressors including SNAIL1, ZEB1, ZEB2 and TCF3. However, the exact action of GEF-H1 on the activation of these transcriptional repressors is unclear. Nevertheless, many studies showed that there is a close association between RhoA pathway and EMT through the disruption of cell-cell tight junction including the down-regulation of E-cadherin suppression, breakdown of cell-basement membrane (Tang DJ *et al*, 2010; Hutchison N *et al*, 2009; Nakaya Y *et al*, 2008; Patel S *et al*, 2005), also through the remodelling of actin cytoskeleton (Lu J *et al*, 2001; Wicki A *et al*, 2006). Therefore, it is plausible that the induction of EMT by *GEF-H1* could be through RhoA activation.

It is reported here for the first time that the over-expression of *GEF-H1*, a key element for continuously loading the GTP molecule on RhoA, was responsible for the constitutive activation of RhoA and EMT pathway in HCC followed by the downstream metastatic phenotypes. Since EMT plays a central role in physiological and pathological processes, further defining the gene regulatory networks of *GEF-H1* during EMT in the liver carcinogenesis will be fundamental to help assign molecular features that underline the metastatic potentials of HCC tumors.

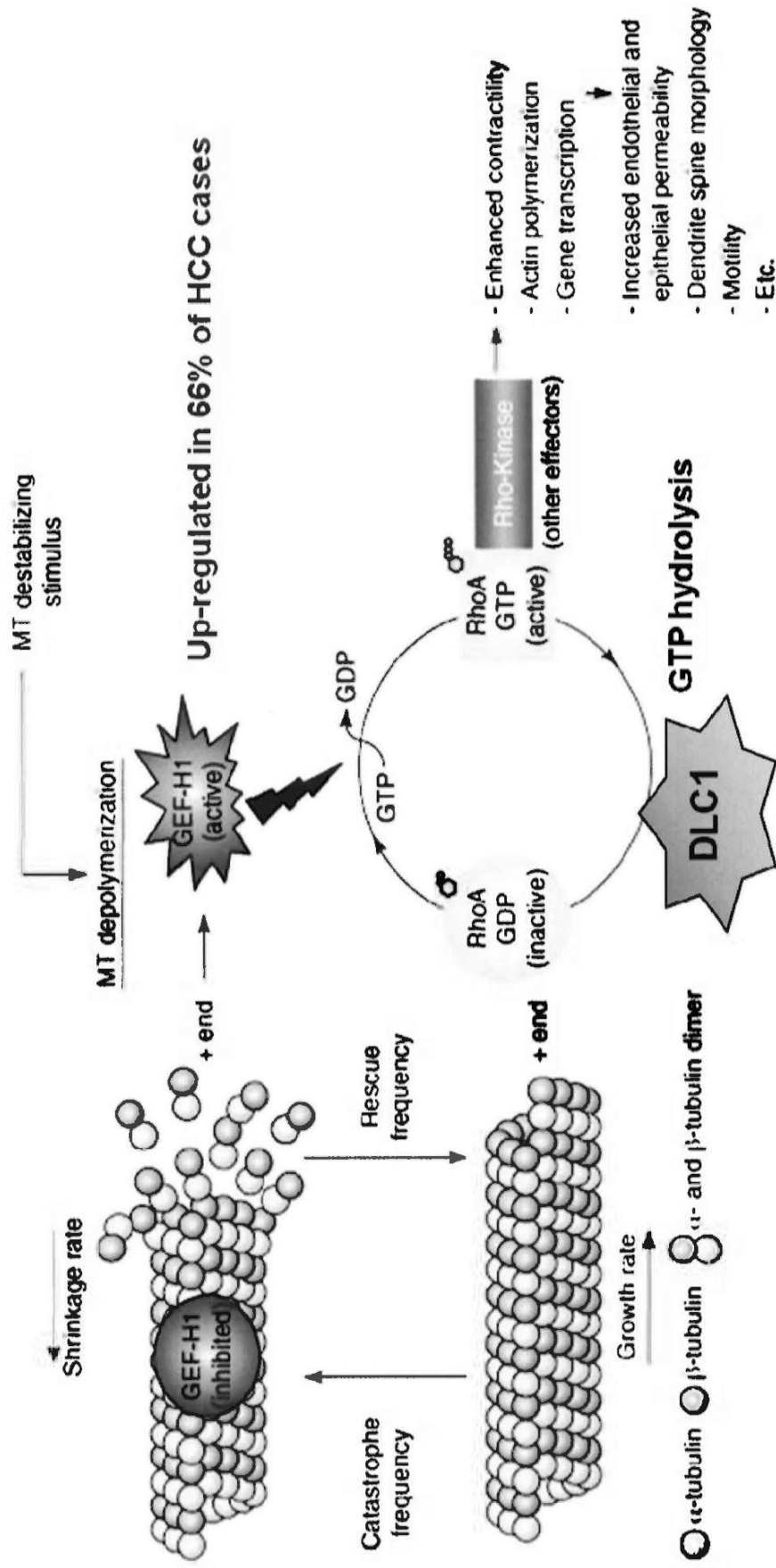


Figure 5.17 Regulation of RhoA activity through GEF-H1 (RhoGEF) and DLC1 (RhoGAP)

Figure modified from Birkenfeld J *et al.*, 2008.

Chapter 6

Conclusions and proposed future studies

6. CONCLUSIONS AND PROPOSED FUTURE STUDIES

With the advent of microarray technologies, the use of array-CGH has circumvented many problems associated with conventional genome positional mappings, such as resolution, precision and throughput. In this thesis, array-CGH was deployed to provide a comprehensive analysis on DNA copy number changes on specific chromosomal loci and define target genes associated with HCC development. Particularly this thesis focused on the mapping of HD regions and the over-representations of chr.8q24 and chr.1q21-22, which are classified as early important events in HCC carcinogenesis (Poon TC *et al*, 2006).

BOPI (chr.8q24) and *GEF-HI* (chr.1q22) identified are functionally characterized and represent novel oncogenes which might confer metastatic advantage in malignant hepatocytes. In addition, clinicopathological significance of *BOPI/GEF-HI* up-regulations was established in correlation with shorter patient survival and the presence of micro-vascular invasion. Since both intra- and extra-hepatic metastases are major factors that contribute to the inferior prognosis in individuals diagnosed with HCC, *BOPI* and *GEF-HI* may well be causal genes in underlining HCC metastasis. Together with the findings of EMT induction and RhoA activation, it is plausible that *BOPI* and/or *GEF-HI* may be deregulated in the initial stage of HCC carcinogenesis and confer the metastatic potentials to the malignant hepatocytes for later metastatic development, since it is not necessary to harbour the metastasis-related alterations only at late stage of tumor development (Ramaswamy S *et al*, 2003).

Both *BOPI* and *GEF-HI* were found to regulate the cell motility through RhoA pathway. No doubt that RhoA pathway is well-known and vital in regulating stress fibre formation, thereby providing contractional force in cell motility. In the

functional studies of *BOP1* and *GEF-H1*, more profound effects on cellular invasion were observed compared to cell migration. Therefore, it is plausible that *BOP1* and *GEF-H1* regulate not only cell contractility, but also invasion-related features such as digestion of the extracellular matrix by proteases as well as extravasation and intravasation characterization.

In the future lines of investigations, one proposes it will be worth elucidating the various signaling pathways that are under the influence of *BOP1* and *GEF-H1*. To achieve a comprehensive overview on affected genes, expression array profiling on *BOP1/GEF-H1* ectopic expressing clones in immortalized normal liver cell line and *BOP1/GEF-H1* depleted cells can be performed. The common deregulated genes can be further analyzed by ontology programmes to delineate the potential affected pathways mediated by BOP1 and GEF-H1.

Due to their similar functional behavior, BOP1 and GEF-H1 may cooperative interact, especially in view that BOP1 has protein-binding properties. Immuno-precipitation (IP) of BOP1 and GEF-H1 protein can be performed in BOP1 or GEF-H1 expressing HCC cells in attempt to identify their interacting relationship.

In addition, the immuno-precipitated targets of BOP1 and GEF-H1 can be further analyzed by mass spectrophotometry to identify possible interacting proteins. Together with the expression array data, mechanistic information on the function of BOP1 and GEF-H1 can be further delineated.

Chapter 7

References

7. REFERENCES

- Arakawa Y, Bito H, Furuyashiki T, Tsuji T, Takemoto-Kimura S, Kimura K, Nozaki K, Hashimoto N, Narumiya S. Control of axon elongation via an SDF-1alpha/Rho/mDia pathway in cultured cerebella granule neurons. *J Cell Biol* 2003; **161**:381-391.
- Aspenström P. The Rho GTPases have multiple effects on the actin cytoskeleton. *Exp Cell Res* 1999; **246**:20-25.
- Balsara BR, Pei J, De Rienzo A, Simon D, Tosolini A, Lu YY, Shen FM, Fan X, Lin WY, Buetow KH, London WT, Testa JR. Human hepatocellular carcinoma is characterized by a highly consistent pattern of genomic imbalances, including frequent loss of 16q23.1–24.1. *Genes Chromosomes Cancer* 2001; **30**:245-253.
- Battaglia S, Benzoubir N, Nobilet S, Charneau P, Samuel D, Zignego AL, Atfi A, Bréchet C, Bourgeade MF. Liver cancer-derived hepatitis C virus core proteins shift TGF-beta responses from tumor suppression to epithelial-mesenchymal transition. *PLoS ONE* 2009; **42**:e4355.
- Becker U, Deis A, Sørensen TIA, Grønbaek M, Borch-Johnsen K, Müller CF, Schnohr P, Jensen G. Prediction of risk of liver disease by alcohol intake, sex, and age: a prospective population study. *Hepatology* 1996; **23**:1025-1029.
- Birkenfeld J, Nalbant P, Yoon SH, Bokoch GM. Cellular functions of GEF-H1, a microtubule-regulated Rho-GEF: is altered GEF-H1 activity a crucial determinant of disease pathogenesis? *Trends Cell Biol* 2008; **18**:210-219.
- Bressac B, Kew M, Wands H, Ozturk M. Selective G to T mutations of p53 gene in hepatocellular carcinoma from southern Africa. *Nature* 1991; **350**:429-431.
- Buendia MA. Genetic alterations in hepatoblastoma and hepatocellular carcinoma: common and distinctive aspects. *Med Pediatr Oncol* 2002; **39**:530-535.
- Bugianesi E. Non-alcoholic steatohepatitis and cancer. *Clin. Liver Dis* 2007; **11**:191-207.
- Burrige K, Wennerberg K. Rho and Rac take center stage. *Cell* 2004; **116**:167-179.
- Calle EE, Rodriguez C, Walker-Thurmond K, Thun MJ. Overweight, obesity, and mortality from cancer in a prospectively studied cohort of US adults. *N Engl Med* 2003; **348**:1625-1638.
- Chan KL, Guan XY, Ng IO. High-throughput tissue microarray analysis of c-myc activation in chronic liver diseases and hepatocellular carcinoma. *Hum Pathol* 2004; **35**:1324-1331.
- Chan KY, Wong N, Lai PB, Squire JA, Macgregor PF, Beheshti B, Albert M, To KF, Johnson PJ. Transcriptional profiling on chromosome 19p indicated frequent downregulation of ACP5 expression in hepatocellular carcinoma. *Int J Cancer* 2005; **114**:902-908.
- Chang J, Kim NG, Piao Z, Park C, Park KS, Paik YK, Lee WJ, Kim BR, Kim H. Assessment of chromosomal losses and gains in hepatocellular carcinoma. *Cancer Lett* 2002; **182**:193-202.
- Chen CF, Yeh SH, Chen DS, Chen PJ, Jou YS. Molecular genetic evidence supporting a novel human Hepatocellular carcinoma tumor suppressor locus at 13q12.11. *Genes Chromosomes Cancer* 2005; **44**:320-328.
- Chen CJ, Yang HI, Su J, Jen CL, You SL, Lu SN, Huang GT, Iloeje UH. Risk of hepatocellular carcinoma across a biological gradient of serum hepatitis B virus DNA level. *JAMA* 2006; **295**:65-73.

- Chen CL, Yang HI, Yang WS, Liu CJ, Chen PJ, You SL, Wang LY, Sun CA, Lu SN, Chen DS, Chen CJ. Metabolic factors and risk of hepatocellular carcinoma by chronic hepatitis B/C infection: a follow-up study in Taiwan. *Gastroenterology* 2008; **135**:111-121.
- Chen J, Yu L, Li D, Gao Q, Wang J, Huang X, Bi G, Wu H, Zhao S. Human CRYL1, a novel enzyme-crystallin overexpressed in liver and kidney and downregulated in 58% of liver cancer tissues from 60 Chinese patients, and four new homologs from other mammals. *Gene* 2003; **302**:103-113.
- Chen L, Chan TH, Yuan YF, Hu L, Huang J, Ma S, Wang J, Dong SS, Tang KH, Xie D, Li Y, Guan XY. CHD1L promotes hepatocellular carcinoma progression and metastasis in mice and is associated with these processes in human patients. *J Clin Invest* 2010; **120**:1178-1191.
- Ching YP, Wong CM, Chan SF, Leung TH, Ng DC, Jin DY, Ng IO. Deleted in liver cancer (DLC) 2 encodes a RhoGAP protein with growth suppressor function and is underexpressed in hepatocellular carcinoma. *J Biol Chem* 2003; **278**:10824-10830.
- Chiu CM, Yeh SH, Chen PJ, Kuo TJ, Chang CJ, Chen PJ, Yang WJ, Chen DS. Hepatitis B virus X protein enhances androgen receptor-responsive gene expression depending on androgen level. *Proc Natl Acad Sci USA* 2007; **104**:2571-2578.
- Cho J, Baek W, Yang S, Chang J, Sung YC, Suh M. HCV core protein modulates Rb pathway through pRb down-regulation and E2F-1 up-regulation. *Biochim Biophys Acta* 2001; **1538**:59-66.
- Choi YW, Choi JS, Zheng LT, Lim YJ, Yoon HK, Kim YH, Wang YP, Lim Y. Comparative genomic hybridization array analysis and real time PCR reveals genomic alterations in squamous cell carcinomas of the lung. *Lung Cancer* 2007; **55**:43-51.
- Cooper JA. Effects of cytochalasin and phalloidin on actin. *J Cell Biol* 1987; **105**:1473-1478.
- Database of Genomic Variants Website: <http://projects.tcag.ca/variation> (Assessed: January 2007).
- Deng L, Nagano-Fujii M, Tanaka M, Nomura-Takigawa Y, Ikeda M, Kato N, Sada K, Hotta H. NS3 protein of Hepatitis C virus associates with the tumour suppressor p53 and inhibits its function in an NS3 sequence-dependent manner. *J Gen Virol* 2006; **87**:1703-1713.
- Di Lorenzo G, Imbimbo M, Leopardo D, Marciano R, Federico P, Buonerba C, Salvatore B, Marinelli A, Palmieri G. A long-lasting response to Sorafenib treatment in an advanced hepatocellular carcinoma patient. *Int J Immunopathol Pharmacol* 2010; **23**:951-954.
- Ding J, Huang S, Wu S, Zhao Y, Liang L, Yan M, Ge C, Yao J, Chen T, Wan D, Wang H, Gu J, Yao M, Li J, Tu H, He X. Gain of miR-151 on chromosome 8q24.3 facilitates tumour cell migration and spreading through downregulating RhoGDI. *Nat Cell Biol* 2010; **12**:390-399.
- Donato F, Gelatti U, Limina RM, Fattovich G. Southern Europe as an example of interaction between various environmental factors: a systemic review of the epidemiologic evidence. *Oncogene* 2006; **25**:3756-3770.
- Donato F, Tagger A, Gelatti U, Parrinello G, Boffetta P, Albertini A, Decarli A, Trevisi P, Ribero ML, Martelli C, Porru S, Nardi G. Alcohol and hepatocellular carcinoma: the effect of lifetime intake and hepatitis virus infections in men and women. *Am J Epidemiol* 2002; **155**:323-331.

- Dumenco L, Oguey D, Wu J, Messier N, Fausto N. Introduction of a murine p53 mutation corresponding to human codon 249 into a murine hepatocyte cell line results in growth advantage, but not in transformation. *Hepatology* 1995; **22**(Part 1):1279-1288.
- Dyson N, Howley PM, Munger K, Harlow E. The human papilloma virus-16 E7 oncoprotein is able to bind to the retinoblastoma gene product. *Science* 1989; **243**:934-937.
- Edamoto Y, Hara A, Biernat W, Terracciano L, Cathomas G, Riehle HM, Matsuda M, Fujii H, Scoazec JY, Ohgaki H. Alterations of RB1, p53 and Wnt pathways in hepatocellular carcinomas associated with hepatitis C, hepatitis B and alcoholic liver cirrhosis. *Int J Cancer* 2003; **106**:334-341.
- El Gammal AT, Brüchmann M, Zustin J, Isbarn H, Hellwinkel OJ, Köllermann J, Sauter G, Simon R, Wilczak W, Schwarz J, Bokemeyer C, Brümmendorf TH, Izbicki JR, Yekebas E, Fisch M, Huland H, Graefen M, Schlomm T. Chromosome 8p deletions and 8q gains are associated with tumor progression and poor prognosis in prostate cancer. *Clin Cancer Res* 2010; **16**:56-64.
- El-Serag HB, Rudolph KL. Hepatocellular carcinoma: epidemiology and molecular carcinogenesis. *Gastroenterology* 2007; **132**:2557-2576.
- El-Sibai M, Pertz O, Pang H, Yip SC, Lorenz M, Symons M, Condeelis JS, Hahn KM, Backer JM. RhoA/ROCK-mediated switching between Cdc42- and Rac1-dependent protrusion in MTLn3 carcinoma cells. *Exp Cell Res* 2008; **314**:1540-1552.
- Essigmann JM, Green CL, Croy RG, Fowler KW, Buchi GH, Wogan GN. Interactions of aflatoxin B1 and alkylating agents with DNA: structural and functional studies. *Cold Spring Harb Symp Quant Biol* 1983; **1**:327-337.
- Etienne-Manneville S, Hall A. Rho GTPases in cell biology. *Nature* 2002; **420**:629-635.
- Fan JG, Farrell GC. Epidemiology of nonalcoholic fatty liver disease in China. *J Hepatol* 2009; **50**:204-210.
- Fang Y, Guan X, Guo Y, Sham J, Deng M, Liang Q, Li H, Zhang H, Zhou H, Trent J. Analysis of genetic alterations in primary nasopharyngeal carcinoma by comparative genomic hybridization (CGH). *Genes Chromosomes Cancer* 2001; **30**:254-260.
- Farrell GC, Larter CZ. Nonalcoholic fatty liver disease: from steatosis to cirrhosis. *Hepatology* 2006; **43**:S99-112.
- Fattovich G, Giustina G, Realdi G, Corrocher R, Schalm SW. Long-term outcome of hepatitis B e antigen-positive patients with compensated cirrhosis treated with interferon- α . *Hepatology* 1997; **26**:1338-1342.
- Feitelson MA, Lee J. Hepatitis B virus integration, fragile sites, and hepatocarcinogenesis. *Cancer Lett* 2007; **252**:157-170.
- Feitelson MA, Reis HM, Lale Tufan N, Sun B, Pan J, Lian Z. Putative roles of hepatitis B x antigen in the pathogenesis of chronic liver disease. *Cancer Lett* 2009; **286**:69-79.
- Feo F, Frau M, Tomasi ML, Brozzetti S, Pascale RM. Genetic and epigenetic control of molecular alterations in hepatocellular carcinoma. *Exp Biol Med (Maywood)* 2009; **234**:726-736.
- Ferlay J, Shin HR, Bray F, Forman D, Mathers C, Parkin DM. Estimates of worldwide burden of cancer in 2008: GLOBOCAN 2008. *Int J Cancer* 2010; *Epub ahead of print*.

- Friedman SL, Arthur MJ. Activation of cultured rat hepatic lipocytes by Kupffer cell conditioned medium. Direct enhancement of matrix synthesis and stimulation of cell proliferation via induction of platelet-derived growth factor receptors. *J Clin Invest* 1989; **84**:1780-1785.
- Fukata M, Kaibuchi K. Rho-family GTPases in cadherin-mediated cell-cell adhesion. *Nat Rev Mol Cell Biol* 2001; **2**:887-897.
- Giroldi LA, Binguier PP, de Weijert M, Jansen C, van Bokhoven A, Schalken JA. Role of E boxes in the repression of E-cadherin expression. *Biochem Biophys Res Commun* 1997; **241**:453-458.
- Goel A, Boland CR. Recent insights into the pathogenesis of colorectal cancer. *Curr Opin Gastroenterol* 2010; **26**:47-52.
- Gotzmann J, Mikula M, Eger A, et al. Molecular aspects of epithelial cell plasticity: implications for local tumor invasion and metastasis. *Mutat Res* 2004; **566**:9-20.
- Gronwald J, Störkel S, Holtgreve-Grez H, Hadaczek P, Brinkschmidt C, Jauch A, Lubinski J, Cremer T. Comparison of DNA gains and losses in primary renal clear cell carcinomas and metastatic sites: importance of 1q and 3p copy number changes in metastatic events. *Cancer Res* 1997; **57**:481-487.
- Guan XY, Fang Y, Sham JS, Kwong DL, Zhang Y, Liang Q, Li H, Zhou H, Trent JM. Recurrent chromosome alterations in hepatocellular carcinoma detected by comparative genomic hybridization. *Genes Chromosomes Cancer* 2000; **29**:110-116.
- Guerrero RB, Roberts LR. The role of hepatitis B virus integrations in the pathogenesis of human hepatocellular carcinoma. *J Hepatol* 2005; **42**:760-777.
- Hahn SA, Schutte M, Hoque AT, Moskaluk CA, da Costa LT, Rozenblum E, Weinstein CL, Fischer A, Yeo CJ, Hruban RH, Kern SE. DPC4, a candidate tumor suppressor gene at human chromosome 18q21.1. *Science* 1996; **271**:350-353.
- Hall A. The cytoskeleton and cancer. *Cancer Metastasis Rev* 2009; **28**:5-14.
- Hanna RF, Aguirre DA, Kased N, Emery SC, Peterson MR, Sirlin CB. Cirrhosis-associated hepatocellular nodules: correlation of histopathologic and MR imaging features. *Radiographics* 2008; **28**:747-769.
- Harrison SA. Liver disease in patients with diabetes mellitus. *J Clin Gastroenterol* 2006; **40**:68-76.
- Hassan M, Selimovic D, Ghazlan H, Abdel-kader O. Hepatitis C virus core protein triggers hepatic angiogenesis by a mechanism including multiple pathways. *Hepatology* 2009; **49**:1469-1482.
- He YY, Liu SB, Lee WH, Zhang Y. Melanoma cell growth inhibition by $\beta\gamma$ -CAT, which is a novel non-lens betagamma-crystallin and trefoil factor complex from frog *Bombina maxima* skin. *Toxicol* 2008; **52**:341-347.
- Hennig G, Behrens J, Truss M, Frisch S, Reichmann E, Birchmeier W. Progression of carcinoma cells is associated with alterations in chromatin structure and factor binding at the E-cadherin promoter in vivo. *Oncogene* 1995; **11**:475-484.
- Hertz S, Rothämel T, Skawran B, Giere C, Steinemann D, Flemming P, Becker T, Flik J, Wiese B, Soudah B, Kreipe H, Schlegelberger B, Wilkens L. Losses of chromosome arms 4q, 8p, 13q and gain of 8q are correlated with increasing chromosomal instability in hepatocellular carcinoma. *Pathobiology* 2008; **75**:312-322.
- Higashitsuji H, Itoh K, Nagao T, Dawson S, Nonoguchi K, Kido T, Mayer RJ, Arai S, Fujita J. Reduced stability of retinoblastoma protein by gankyrin, an oncogenic ankyrin-repeat protein overexpressed in hepatomas. *Nat Med* 2000; **6**:96-99.

- Hijikata M, Kato N, Ootsuyama Y, Nakagawa M, Shimotohno K. Gene mapping of the putative structural region of the hepatitis C virus genome by in vitro processing analysis. *Proc Natl Acad Sci USA* 1991; **88**:5547-5551.
- Hirai M, Yoshida S, Kashiwagi H, Kawamura T, Ishikawa T, Kaneko M, Ohkawa H, Nakagawara A, Miwa M, Uchida K. 1q23 gain is associated with progressive neuroblastoma resistant to aggressive treatment. *Genes Chromosomes Cancer* 1999; **25**:261-269.
- Horikawa I, Barrett JC. Cis-activation of the human telomerase gene (hTERT) by the hepatitis B virus genome. *J Natl Cancer Inst* 2001; **93**:1171-1173.
- Horlings HM, Lai C, Nuyten DS, Halfwerk H, Kristel P, van Beers E, Joosse SA, Klijn C, Nederlof PM, Reinders MJ, Wessels LF, van de Vijver MJ. Integration of DNA copy number alterations and prognostic gene expression signatures in breast cancer patients. *Clin Cancer Res* 2010; **16**:651-663.
- Huibregtse J, Nomoto A, Lemon SM. Hepatitis C virus induces E6AP-dependent degradation of the retinoblastoma protein. *PLoS Pathog* 2007; **3**:1335-1347.
- Hutchison N, Hendry BM, Sharpe CC. Rho isoforms have distinct and specific functions in the process of epithelial to mesenchymal transition in renal proximal tubular cells. *Cell Signal* 2009; **21**:1522-1531.
- Ikeguchi M, Hirooka Y. Expression of c-myc mRNA in hepatocellular carcinomas, noncancerous livers, and normal livers. *Pathobiology* 2004; **71**:281-286.
- Inagaki Y, Yasui K, Endo M, Nakajima T, Zen K, Tsuji K, Minami M, Tanaka S, Taniwaki M, Itoh Y, Arii S, Okanoue T. CREB3L4, INTS3, and SNAPAP are targets for the 1q21 amplicon frequently detected in hepatocellular carcinoma. *Cancer Genet Cytogenet* 2008; **180**:30-36.
- Ishido S, Fujita, T, Hotta, H. Complex formation of NS5B with NS3 and NS4A proteins of hepatitis C virus. *Biochem. Biophys Res Commun* 1998; **244**:35-40.
- Jaffe AB, Hall A. Rho GTPases: biochemistry and biology. *Annu Rev Cell Dev Biol* 2005; **21**:247-269.
- Jones S, Chen WD, Parmigiani G, Diehl F, Beerenwinkel N, Antal T, Traulsen A, Nowak MA, Siegel C, Velculescu VE, Kinzler KW, Vogelstein B, Willis J, Markowitz SD. Comparative lesion sequencing provides insights into tumor evolution. *Proc Natl Acad Sci USA* 2008; **105**:4283-4288.
- Kamb A, Gruis NA, Weaver-Feldhaus J, Liu Q, Harshman K, Tavitgian SV, Stockert E, Day RS 3rd, Johnson BE, Skolnick MH. A cell cycle regulator potentially involved in genesis of many tumor types. *Science* 1994; **264**:436-440.
- Kaposi-Novak P, Libbrecht L, Woo HG, Lee YH, Sears NC, Coulouarn C, Conner EA, Factor VM, Roskams T, Thorgeirsson SS. Central role of c-Myc during malignant conversion in human hepatocarcinogenesis. *Cancer Res* 2009; **69**:2775-2782.
- Kasprzak A, Adamek A. Role of hepatitis C virus proteins (C, NS3, NS5A) in hepatic oncogenesis. *Hepatol Res* 2008; **38**:1-26.
- Kawate S, Fukusato T, Ohwada S, Watanuki A, Morishita Y. Amplification of c-myc in hepatocellular carcinoma: Correlation with clinicopathologic features, proliferative activity and p53 overexpression. *Oncology* 1999; **57**:157-163.
- Killian A, Le Meur N, Sesboué R, Bourguignon J, Bougeard G, Gautherot J, Bastard C, Frébourg T, Flaman JM. Inactivation of the RRB1-Pescadillo pathway involved in ribosome biogenesis induces chromosomal instability. *Oncogene* 2004; **23**:8597-8602.
- Killian A, Sarafan-Vasseur N, Sesboué R, Le Pessot F, Blanchard F, Lamy A, Laurent M, Flaman JM, Frébourg T. Contribution of the BOP1 gene, located on

- 8q24, to colorectal tumorigenesis. *Genes Chromosomes Cancer* 2006; **45**:874-881.
- Kim CM, Koike K, Saito, I, Miyamura T, Jay G. HBx gene of hepatitis B virus induces liver cancer in transgenic mice. *Nature* 1991; **351**:317-320.
- Kim J, Sim S, Yong TS, Park SJ. Interaction of BOP1, a protein for ribosome biogenesis, with EB1 in *Giardia lamblia*. *Parasitol Res* 2008; **103**:1459-1464.
- Kim TM, Yim SH, Shin SH, Xu HD, Jung YC, Park CK, Choi JY, Park WS, Kwon MS, Fiegler H, Carter NP, Rhyu MG, Chung YJ. Clinical implication of recurrent copy number alterations in hepatocellular carcinoma and putative oncogenes in recurrent gains on 1q. *Int J Cancer* 2008; **123**:2808-2815.
- Knuutila S, Björkqvist AM, Autio K, Tarkkanen M, Wolf M, Monni O, Szymanska J, Larramendy ML, Tapper J, Pere H, El-Rifai W, Hemmer S, Wasenius VM, Vidgren V, Zhu Y. DNA copy number amplifications in human neoplasms: review of comparative genomic hybridization studies. *Am J Pathol* 1998; **152**:1107-1123.
- Kremsdorf D, Soussan P, Paterlini-Brechot P, Brechot C. Hepatitis B virus-related hepatocellular carcinoma: paradigms for viral-related human carcinogenesis. *Oncogene* 2006; **25**:3823-3833.
- Krendel M, Zenke FT, Bokoch GM. Nucleotide exchange factor GEF-H1 mediates cross-talk between microtubules and the actin cytoskeleton. *Nat Cell Biol* 2002; **4**:294-301.
- Kudoh K, Takano M, Koshikawa T, Hirai M, Yoshida S, Mano Y, Yamamoto K, Ishii K, Kita T, Kikuchi Y, Nagata I, Miwa M, Uchida K. Gains of 1q21-q22 and 13q12-q14 are potential indicators for resistance to cisplatin-based chemotherapy in ovarian cancer patients. *Clin Cancer Res* 1999; **5**:2526-31.
- Kusano N, Okita K, Shirahashi H, Harada T, Shiraishi K, Oga A, Kawauchi S, Furuya T, Sasaki K. Chromosomal imbalances detected by comparative genomic hybridization are associated with outcome of patients with hepatocellular carcinoma. *Cancer* 2002; **94**:746-751.
- Kusano N, Shiraishi K, Kubo K, Oga A, Okita K, Sasaki K. Genetic aberrations detected by comparative genomic hybridization in hepatocellular carcinomas: their relationship to clinicopathological features. *Hepatology* 1999; **29**:1858-62.
- Kwong D, Lam A, Guan XY, Law S, Tai A, Sham J. Chromosomal aberrations in esophageal squamous cell carcinoma among Chinese: gain of 12p predicts poor prognosis after surgery. *Human Pathol* 2004; **35**:309-316.
- Lan KH, Sheu ML, Hwang SJ, Yen SH, Chen SY, Wu JC, Wang YJ, Kato N, Omata M, Chang FY, Lee SD. HCV NS5A interacts with p53 and inhibits p53-mediated apoptosis. *Oncogene* 2002; **21**:4801-4811.
- Larsson SC, Wolk A. Excess body fatness: an important cause of most cancers. *Lancet* 2008; **371**:536-537.
- Lee SG, Rho HM. Transcriptional repression of the human p53 gene by hepatitis B viral X protein. *Oncogene* 2000; **19**:468-471.
- Lee JO, Russo AA, Pavletich NP. Structure of the retinoblastoma tumour-suppressor pocket domain bound to a peptide from HPV E7. *Nature* 1998; **391**:859-865.
- Li D, Roberts R. WD-repeat proteins: structure characteristics, biological function, and their involvement in human diseases. *Cell Mol Life Sci* 2001; **58**:2085-2097.
- Li J, Yen C, Liaw D, Podsypanina K, Bose S, Wang SI, Puc J, Miliareis C, Rodgers L, McCombie R, Bigner SH, Giovanella BC, Ittmann M, Tycko B, Hibshoosh H, Wigler MH, Parsons R. PTEN, a putative protein tyrosine phosphatase gene

- mutated in human brain, breast, and prostate cancer. *Science* 1997; **275**:1943-1947.
- Li ND, Lu FZ, Zhang SW, Mo R, Sun XD. Trends and prediction in malignant tumors mortality in past 20 years in China. *Chin J Oncol* 1997; **19**:3-9.
- Li YZZY, Wang CH. The analysis of serum free fatty acid spectrum in 33 patients with primary hepatocellular carcinoma. *Journal of Dalian Medical University* 1997; **19**:134-136.
- Liaw YF. Natural history of chronic hepatitis B virus infection and long-term outcome under treatment. *Liver Int* 2009; **29**:100-107.
- Lin C, Lindenbach BD, Pragai BM, McCourt DW, Rice CM. Processing in the hepatitis C virus E2-NS2 region: identification of p7 and two distinct E2-specific products with different C termini. *J Virol* 1994; **68**:5063-5073.
- Lin SM, Yu ML, Lee CM, Chien RN, Sheen IS, Chu CM, Liaw YF. Interferon therapy in HBeAg-positive chronic hepatitis reduces progression to cirrhosis and hepatocellular carcinoma. *J Hepatol* 2007; **46**:45-52.
- Lin YW, Sheu JC, Liu LY, Chen CH, Lee HS, Huang GT, Wang JT, Lee PH, Lu FJ. Loss of heterozygosity at chromosome 13q in hepatocellular carcinoma: identification of three independent regions. *Eur J Cancer* 1999; **35**:1730-1734.
- Lips EH, van Eijk R, de Graaf EJ, Oosting J, de Miranda NF, Karsten T, et al. Integrating chromosomal aberrations and gene expression profiles to dissect rectal tumorigenesis. *BMC Cancer* 2008; **8**:314.
- Liu CJ, Chen BF, Chen PJ, Lai MY, Huang WL, Kao JH, Chen DS. Role of hepatitis B viral load and basal core promoter mutation in hepatocellular carcinoma in hepatitis B carriers. *J Infect Dis* 2006; **193**:1258-1265.
- Llovet JM, Ricci S, Mazzaferro V, Hilgard P, Gane E, Blanc JF, de Oliveira AC, Santoro A, Raoul JL, Forner A, Schwartz M, Porta C, Zeuzem S, Bolondi L, Greten TF, Galle PR, Seitz JF, Borbath I, Häussinger D, Giannaris T, Shan M, Moscovici M, Voliotis D, Bruix J, SHARP Investigators Study Group. Sorafenib in advanced hepatocellular carcinoma. *N Engl J Med* 2008; **359**:378-390.
- Lu J, Landerholm TE, Wei JS, Dong XR, Wu SP, Liu X, Nagata K, Inagaki M, Majesky MW. Coronary smooth muscle differentiation from proepicardial cells requires rhoA-mediated actin reorganization and p160 rho-kinase activity. *Dev Biol* 2001; **240**:404-418.
- Ma NF, Hu L, Fung JM, Xie D, Zheng BJ, Chen L, Tang DJ, Fu L, Wu Z, Chen M, Fang Y, Guan XY. Isolation and characterization of a novel oncogene, amplified in liver cancer 1, within a commonly amplified region at 1q21 in hepatocellular carcinoma. *Hepatology* 2008; **47**:503-510.
- Ma WL, Hsu CL, Wu MH, Wu CT, Wu CC, Lai JJ, Jou YS, Chen CW, Yeh S, Chang C. Androgen receptor is a new potential therapeutic target for the treatment of hepatocellular carcinoma. *Gastroenterology* 2008; **135**:947-955.
- Majumder M, Ghosh AK, Steele R, Ray R, Ray RB. Hepatitis C virus NS5A physically associates with p53 and regulates p21/waf1 gene expression in a p53-dependent manner. *J Virol* 2001; **75**:1401-1407.
- Marchio A, Meddeb M, Pineau P, Danglot G, Tiollais P, Bernheim A, Dejean A. Recurrent chromosomal abnormalities in hepatocellular carcinoma detected by comparative genomic hybridization. *Genes Chromosomes Cancer* 1997; **18**:59-65.

- Marusawa H, Hijikata M, Chiba T, Shimotohno K. Hepatitis C virus core protein inhibits Fas-and tumor necrosis factor alpha-mediated apoptosis via NF-kappaB activation. *H Virol* 1999; **73**:4713-4720.
- Matsuzaki K. Modulation of TGF-beta signaling during progression of chronic liver diseases. *Front Bioscience* 2009; **14**:2923-2934.
- McKillop IH, Moran DM, Jin X, Koniaris LG. Molecular Pathogenesis of Hepatocellular Carcinoma. *J Surg Res* 2006; **136**:125-135.
- Midorikawa Y, Tsutsumi S, Nishimura K, Kamimura N, Kano M, Sakamoto H, Makuuchi M, Aburatani H. Distinct chromosomal bias of gene expression signatures in the progression of hepatocellular carcinoma. *Cancer Res* 2004; **64**:7263-7270.
- Miller EC. Some current perspectives on chemical carcinogenesis in humans and experimental animals: Presidential Address. *Cancer Res* 1978; **38**:1479-1496.
- Moinzadeh P, Breuhahn K, Stützer H, Schirmacher P. Chromosome alterations in human hepatocellular carcinomas correlate with aetiology, and histological grade-results of an explorative CGH meta-analysis. *Br J Cancer* 2005; **92**:935-941.
- Mollenhauer J, Wiemann S, Scheurlen W, Korn B, Hayashi Y, Wilgenbus KK, von Deimling A, Poustka A. DMBT1, a new member of the SRCR superfamily, on chromosome 10q25.3-26.1 is deleted in malignant brain tumours. *Nat Genet* 1997; **17**:32-39.
- Moradpour D, Penin F, Rice CM. Replication of hepatitis C virus. *Nat Rev Microbiol* 2007; **5**:453-563.
- Morgan TR, Mandayam S, Jamal MM. Alcohol and hepatocellular carcinoma. *Gastroenterology* 2004; **127**:S87-96.
- Moriya K, Fujie H, Shintani Y, Yotsuyanagi H, Tsutsumi T, Ishibashi K, Matsuura Y, Kimura S, Miyamura T, Koike K. The core protein of hepatitis C virus induces hepatocellular carcinoma in transgenic mice. *Nat Med* 1998; **4**:1065-1067.
- Morrison EE. The APC-EB1 interaction. *Adv Exp Med Biol* 2009; **656**:41-50.
- Mulders JW, Hendriks W, Blankesteyn WM, Bloemendal H, De Jong WW. Lambda-crystallin, a major rabbit lens protein, is related to hydroxyacyl-coenzyme A dehydrogenases. *J Biol Chem* 1988; **263**:15462-15466.
- Munakata T, Nakamura M, Liang Y, Li K, Lemon SM. Down-regulation of the retinoblastoma tumor suppressor by the hepatitis C virus NS5B RNA-dependent RNA polymerase. *Proc Natl Acad Sci USA* 2005; **102**:18159-18164.
- Murakami Y, Saigo K, Takashima H, Minami M, Okanoue T, Bréchet C, Paterlini-Bréchet P. Large scaled analysis of hepatitis B virus (HBV) DNA integration in HBV related hepatocellular carcinomas. *Gut* 2005; **54**:1162-1168.
- Nakaya Y, Sukowati EW, Wu Y, Sheng G. RhoA and microtubule dynamics control cell-basement membrane interaction in EMT during gastrulation. *Nat Cell Biol* 2008; **10**:765-775.
- Narumiya S, Tanji M, Ishizaki T. Rho signaling, ROCK and mDia1, in transformation, metastasis and invasion. *Cancer Metastasis Rev* 2009; **28**:65-76.
- Neer EJ, Schmidt CJ, Nambudripad R, Smith TF. The ancient regulatory-protein family of WD-repeat proteins. *Nature* 1994; **371**:297-300.
- Ng IO, Liang ZD, Cao L, Lee TK. DLC-1 is deleted in primary hepatocellular carcinoma and exerts inhibitory effects on the proliferation of hepatoma cell lines with deleted DLC-1. *Cancer Res* 2000; **60**:6581-6584.

- Niketeghad F, Decker HJ, Caselmann WH, Lund P, Geissler F, Dienes HP, Schirmacher P. Frequent genomic imbalances suggest commonly altered tumour genes in human hepatocarcinogenesis. *Br J Cancer* 2001; **85**:697-704.
- Nishimura T, Nishida N, Itoh T, Komeda T, Fukuda Y, Ikai I, Yamaoka Y, Nakao K. Discrete breakpoint mapping and shortest region of overlap of chromosome arm 1q gain and 1p loss in human hepatocellular carcinoma detected by semiquantitative microsatellite analysis. *Genes Chromosomes Cancer* 2005; **42**:34-43.
- Nishimura T, Nishida N, Itoh T, Kuno M, Minata M, Komeda T, Fukuda Y, Ikai I, Yamaoka Y, Nakao K. Comprehensive allelotyping of well-differentiated human hepatocellular carcinoma with semiquantitative determination of chromosomal gain or loss. *Genes Chromosomes Cancer* 2002; **35**:329-339.
- Nordenstedt H, White DL, El-Serag HB. The changing pattern of epidemiology in hepatocellular carcinoma. *Dig Liver Dis* 2010; **3(Suppl)**:S206-214.
- Ockner RK, Kaikous RM, Bass NM. Fatty-acid metabolism and the pathogenesis of hepatocellular carcinoma: review and hypothesis. *Hepatology* 1993; **18**:669-676.
- Okamoto H, Yasui K, Zhao C, Arii S, Inazawa J. PTK2 and EIF3S3 genes may be amplification targets at 8q23-q24 and are associated with large hepatocellular carcinomas. *Hepatology* 2003; **38**:1242-1249.
- Okuno M, Kojima S, Akita K, Matsushima-Nishiwaki R, Adachi S, Sano T, Takano Y, Takai K, Obora A, Yasuda I, Shiratori Y, Okano Y, Shimada J, Suzuki Y, Muto Y, Moriwaki Y. Retinoids in liver fibrosis and cancer. *Front Biosci* 2002; **1**:d204-218.
- Pang E, Wong N, Lai PB, To KF, Lau WY, Johnson PJ. Consistent chromosome 10 rearrangements in four newly established human hepatocellular carcinoma cell lines. *Cancer Genet Cytogenet* 2002; **33**:150-159.
- Patel S, Takagi KI, Suzuki J, Imaizumi A, Kimura T, Mason RM, Kamimura T, Zhang Z. Rho GTPase activation is a key step in renal epithelial mesenchymal transdifferentiation. *J Am Soc Nephrol* 2005; **16**:1977-1984.
- Pellegrin S, Mellor H. Actin stress fibres. *J Cell Sci* 2007; **120(Pt 20)**:3491-3499.
- Pestov DG, Grzeszkiewicz TM, Lau LF. Isolation of growth suppressors from a cDNA expression library. *Oncogene* 1998; **17**:3187-3197.
- Pestov DG, Stockelman MG, Strezoska Z, Lau LF. *ERB1*, the yeast homolog of mammalian *Bop1*, is an essential gene required for maturation of the 25S and 5.8S ribosomal RNAs. *Nucleic Acids Res* 2001; **29**:3621-3630.
- Petersen S, Aninat-Meyer M, Schluns K, Gellert K, Dietel M, Petersen I. Chromosomal alterations in the clonal evolution to the metastatic stage of squamous cell carcinomas of the lung. *Br J Cancer* 2000; **82**:65-73.
- Pinzani M, Milani S, Herbst H, DeFranco R, Grappone C, Gentilini A, Caligiuri A, Pellegrini G, Ngo DV, Romanelli RG, Gentilini P. Expression of platelet-derived growth factor and its receptors in normal human liver and during active hepatic fibrogenesis. *Am J Pathol* 1996; **148**:785-800.
- Polesel H, Zucchetto A, Montella M, DalMaso L, Crispo A, La Vecchia C, Serraino D, Franceschi S, Talamini R. The impact of obesity and diabetes mellitus on the risk of hepatocellular carcinoma. *Ann Oncol* 2009; **20**:352-357.
- Polyak K, Weinberg RA. Transitions between epithelial and mesenchymal states: acquisition of malignant and stem cell traits. *Nat Rev Cancer* 2009; **9**:265-273.
- Ponchel F, Puisieux A, Tabone E, Michot JP, Fröschl G, Morel AP, Frébourg T, Fontanière B, Oberhammer F, Ozturk M. Hepatocarcinoma-specific mutant

- p53-249ser induces mitotic activity but has no effect on transforming growth factor beta 1-mediated apoptosis. *Cancer Res* 1994; **54**:2064-2068.
- Poon TC, Wong N, Lai PB, Rattray M, Johnson PJ, Sung JJ. A tumor progression model for hepatocellular carcinoma: bioinformatics analysis of genomic data. *Gastroenterology* 2006; **131**:1262-1270.
- Puisieux A, Lim S, Groopman J, Ozturk M. Selective targeting of p53 gene mutational hotspots in human cancers by etiologically defined carcinogens. *Cancer Res* 1991; **51**:6185-6189.
- Qian Y, Fan JG. Obesity, fatty liver and liver cancer. *Hepatobiliary Pancreat Dis Int* 2005; **4**:173-177.
- Qin LX. Chromosomal aberrations related to metastasis of human solid tumors. *World J Gastroenterol* 2002; **8**:769-776.
- Qin LX, Tang ZY, Sham JS, Ma ZC, Ye SL, Zhou XD, Wu ZQ, Trent JM, Guan XY. The association of chromosome 8p deletion and tumor metastasis in human hepatocellular carcinoma. *Cancer Res* 1999; **59**:5662-5665.
- Ramaswamy S, Ross KN, Lander ES, Golub TR. A molecular signature of metastasis in primary solid tumors. *Nat Genet* 2003; **33**:49-54.
- Ray ME, Wistow G, Su YA, Meltzer PS, Trent JM. AIM1, a novel non-lens member of the betagamma-crystallin superfamily, is associated with the control of tumorigenicity in human malignant melanoma. *Proc Natl Acad Sci USA* 1997; **94**:3229-3234.
- Ray RB, Lagging LM, Meyer K, Steele R, Ray R. Transcriptional regulation of cellular and viral promoters by the hepatitis C virus core protein. *Virus Res* 1995; **37**:209-220.
- Rehermann B, Nascimbeni M. Immunology of hepatitis B virus and hepatitis C virus infection. *Nature Rev Immunol* 2005; **5**:215-229.
- Ren Y, Li R, Zheng Y, Busch H. Cloning and characterization of GEF-H1, a microtubule-associated guanine nucleotide exchange factor for Rac and Rho GTPases. *J Biol Chem* 1998; **273**:34954-34960.
- Rehnan AG, Tyson M, Egger M, Heller RF, Zwahlen M. Body-mass index and incidence of cancer: a systematic review and meta-analysis of prospective observational studies. *Lancet* 2008; **371**:569-578.
- Rider MA, Butz GM, Ricketts SL, Newberry ST, Grisham JW, Coleman WB. Suppression of tumorigenicity of rat liver tumor cells by human chromosome 13: evidence against the involvement of pRB and BRCA2. *Int J Oncol* 2002; **20**:235-245.
- Riento K, Ridley AJ. Rocks: multifunctional kinases in cell behaviour. *Nat Rev Mol Cell Biol* 2003; **4**:446-456.
- Röcken C, Carl-McGrath S. Pathology and pathogenesis of hepatocellular carcinoma. *Dig Dis* 2001; **19**:269-278.
- Rohrmoser M, Hölzel M, Grimm T, Malamoussi A, Harasim T, Orban M, et al. Interdependence of Pes1, Bop1, and WDR12 controls nucleolar localization and assembly of the PeBoW complex required for maturation of the 60S ribosomal subunit. *Mol Cell Biol* 2007; **27**:3682-3694.
- Rudolph KL, Chang S, Millard M, Schreiber-Agus N, DePinho RA. Inhibition of experimental liver cirrhosis in mice by telomerase gene delivery. *Science* 2000; **287**:1253-1258.
- Sahai E, Olson MF, Marshall CJ. Cross-talk between Ras and Rho signalling pathways in transformation favours proliferation and increased motility. *EMBO J* 2001; **20**:755-766.

- Sakakura C, Hagiwara A, Taniguchi H, Yamaguchi T, Yamagishi H, Takahashi T, Koyama K, Nakamura Y, Abe T, Inazawa J. Chromosomal aberrations in human hepatocellular carcinomas associated with hepatitis C virus infection detected by comparative genomic hybridization. *Br J Cancer* 1999; **80**:2034-2039.
- Schlaeger C, Longerich T, Schiller C, Bewerunge P, Mehrabi A, Toedt G, Kleeff J, Ehemann V, Eils R, Lichter P, Schirmacher P, Radlwimmer B. Etiology-dependent molecular mechanisms in human hepatocarcinogenesis. *Hepatology* 2008; **47**:511-520.
- Seitz HK, Stickel F. Risk factors and mechanisms of hepatocarcinogenesis with special emphasis on alcohol and oxidative stress. *Biol Chem* 2006; **387**:349-360.
- Shachaf CM, Kopelman AM, Arvanitis C, Karlsson A, Beer S, Mandl S, Bachmann MH, Borowsky AD, Ruebner B, Cardiff RD, Yang Q, Bishop JM, Contag CH, Felsher DW. MYC inactivation uncovers pluripotent differentiation and tumour dormancy in hepatocellular cancer. *Nature* 2004; **431**:1112-1117.
- Shadeo A, Lam WL. Comprehensive copy number profiles of breast cancer cell model genomes *Breast Cancer Res* 2006; **8**:R9.
- Sham JST, Tang TCM, Fang Y, Sun L, Qin LX, Xie D, Guan XY. Recurrent chromosome alterations in primary ovarian carcinoma of Chinese women. *Cancer Genet Cytogenet* 2002; **133**:39-44.
- Sharp TV, Al-Attar A, Foxler DE, Ding L, de A Vallim TQ, Zhang Y, Nijmeh HS, Webb TM, Nicholson AG, Zhang Q, Kraja A, Spendlove I, Osborne J, Mardis E, Longmore GD. The chromosome 3p21.3-encoded gene, LIMD1, is a critical tumor suppressor involved in human lung cancer development. *Proc Natl Acad Sci USA* 2008; **10**:19932-19937.
- Shin JY, Hur W, Wang JS, Jang JW, Kim CW, Bae SH, Jang SK, Yang SH, Sung YC, Kwon OJ, Yoon SK. HCV core protein promotes liver fibrogenesis via up-regulation of CTGF with TGF-beta1. *Exp Mol Med* 2005; **37**:138-145.
- Shiraishi K, Okita K, Kusano N, Harada T, Kondoh S, Okita S, Ryozaawa S, Ohmura R, Noguchi T, Iida Y, Akiyama T, Oga A, Fukumoto Y, Furuya T, Kawauchi S, Sasaki K. A comparison of DNA copy number changes detected by comparative genomic hybridization in malignancies of the liver, biliary tract and pancreas. *Oncology* 2001; **60**:151-161.
- Smedile A, Bugianesi E. Steatosis and hepatocellular carcinoma risk. *Eur Rev Med Pharmacol Sci* 2005; **9**:291-293.
- Smela ME, Currier SS, Bailey EA, Essigmann JM. The chemistry and biology of aflatoxin B(1): from mutational spectrometry to carcinogenesis. *Carcinogenesis* 2001; **22**:535-545.
- Smith TF. Diversity of WD-repeat proteins. *Subcell Biochem* 2008; **48**:20-30.
- Smits VAJ, Klompmaker R, Arnaud L, Rijkssen G, Nigg EA, Medema RH. Polo-like kinase-1 is a target of the DNA damage checkpoint. *Nat Cell Biol* 2000; **2**:672-676.
- Smits VAJ, Medema RH. Checking out the G₂/M transition. *Biochim Biophys Acta* 2001; **1519**:1-12.
- Sorrell MF, Belongia EA, Costa J, Gareen IF, Grem JL, Inadomi JM, Kern ER, McHugh JA, Petersen GM, Rein MF, Strader DB, Trotter HT. National Institutes of Health consensus development conference statement: management of hepatitis B. *Hepatology* 2009; **49**(5 Suppl):S4-12.
- Spector AA. The importance of free fatty acid in tumor nutrition. *Cancer Res* 1967; **27**:1580-1586.

- Stelolwagen RH, Cole RD. Chromosomal proteins. *Ann Rev Biochem* 1969; **38**:951.
- Strezoska Z, Pestov DG, Lau LF. Bop1 is a mouse WD40 repeat nucleolar protein involved in 28S and 5.8S rRNA processing and 60S ribosome biogenesis. *Mol Cell Biol* 2000; **20**:5516-5528.
- Stroffolini T, Andreone P, Andriulli A, Ascione A, Craxi A, Chiaramonte M, Galante D, Manghisi OG, Mazzanti R, Medaglia C, Pilleri G, Rapaccini GL, Albanese M, Taliani G, Tosti ME, Villa E, Gasbarrini G. Gross pathologic types of hepatocellular carcinoma in Italy. *Oncogene* 1999; **56**:189-192.
- Tai AW, Chung RT. Treatment failure in hepatitis C: mechanisms of non-response. *J Hepatol* 2009; **50**:412-420.
- Takahashi Y, Kawate S, Watanabe M, Fukushima J, Mori S and Fukusato T. Amplification of c-myc and cyclin D1 genes in primary and metastatic carcinomas of the liver. *Pathol Int* 2007; **57**:437-442.
- Taniguchi H, Kato N, Otsuka M, Goto T, Yoshida H, Shiratori Y, Omata M. Hepatitis C virus core protein upregulates transforming growth factor-beta 1 transcription. *J med Virol* 2004; **72**:52-59.
- Tang DJ, Dong SS, Ma NF, Xie D, Chen L, Fu L, Lau SH, Li Y, Li Y, Guan XY. Overexpression of eukaryotic initiation factor 5A2 enhances cell motility and promotes tumor metastasis in hepatocellular carcinoma. *Hepatology* 2010; **51**:1255-1263.
- Teo EK, Fock KM. Hepatocellular carcinoma: an Asian perspective. *Dig Dis* 2001; **19**:263-268.
- The Hepatitis virus database website:
<http://www.ibibiobase.com/projects/hepatitis/index.htm>.
- Thiagalingam S, Lisitsyn NA, Hamaguchi M, Wigler MH, Willson JK, Markowitz SD, Leach FS, Kinzler KW, Vogelstein B. Evaluation of the FHIT gene in colorectal cancers. *Cancer Res* 1996; **56**:2936-2939.
- Thiery JP. Epithelial-mesenchymal transitions in tumour progression. *Nat Rev Cancer* 2002; **2**:442-454.
- Thiery JP, Acloque H, Huang RY, Nieto MA. Epithelial-mesenchymal transitions in development and disease. *Cell* 2009; **139**:871-890.
- Thiery JP, Sleeman JP. Complex networks orchestrate epithelial-mesenchymal transitions. *Nat Rev Mol Cell Biol* 2006; **7**:131-142.
- Tong WM, Lee MK, Galendo D, Wang ZQ, Sabapathy K. Aflatoxin-B exposure does not lead to p53 mutations but results in enhanced liver cancer of Hupki (human p53 knock-in) mice. *Int J Cancer* 2006; **119**:745-749.
- Turner PC, Sylla A, Diallo MS, Castegnaro JJ, Hall AJ, Wild CP. The role of aflatoxins and hepatitis viruses in the etiopathogenesis of hepatocellular carcinoma: a basis for primary prevention in Guinea-Conakry, West Africa. *J Gastroenterol Hepatol* 2002; **17**:S441-418.
- van Dekken H, Alers JC, Damen IA, Vissers KJ, Krijtenburg PJ, Hoedemaeker RF, Wildhagen MF, Hop WC, van der Kwast TH, Tanke HJ, Schröder FH. Genetic evaluation of localized prostate cancer in a cohort of forty patients: gain of distal 8q discriminates between progressors and nonprogressors. *Lab Invest* 2003; **83**:789-796.
- Wang XW, Gibson MK, Vermeulen W, et al. Abrogation of p53-induced apoptosis by the hepatitis B virus X gene. *Cancer Res* 1995; **55**:6012-6016.

- Wang Y, Wu MC, Sham JS, Zhang W, Wu WQ, Guan XY. Prognostic significance of c-myc and AIB1 amplification in hepatocellular carcinoma. A broad survey using high-throughput tissue microarray. *Cancer* 2002; **95**:2346-2352.
- Watashi K, Hijikata M, Tagawa A, Doi T, Marusawa H, Shimotohno K. Modulation of retinoid signalling by a cytoplasmic viral protein via sequestration of Sp110b, a potent transcriptional corepressor of retinoic acid receptor, from the nucleus. *Mol Cell Biol* 2003; **23**:7498-7509.
- Weiner A, Erickson AL, Kansopon J, Crawford K, Muchmore E, Hughes AL, Houghton M, Walker CM. Persistent hepatitis C virus infection in a chimpanzee is associated with emergence of a cytotoxic T lymphocyte escape variant. *Proc Natl Acad Sci USA* 1995; **92**:2755-2759.
- Whyte P, Buchkovich KJ, Horowitz JM, Friend SH, Raybuck M, Weinberg RA, Harlow E. Association between an oncogene and an anti-oncogene: the adenovirus E1A proteins bind to the retinoblastoma gene product. *Nature* 1988; **334**:124-129.
- Wicki A, Lehembre F, Wick N, Hantusch B, Kerjaschki D, Christofori G. Tumor invasion in the absence of epithelial-mesenchymal transition: podoplanin-mediated remodeling of the actin cytoskeleton. *Cancer Cell* 2006; **9**:261-272.
- Wolk A, Gridley G, Svensson M, Nyrén O, McLaughlin JK, Fraumeni JF, Adam HO. A prospective study of obesity and cancer risk (Sweden). *Cancer Causes Control* 2001; **12**:13-21.
- Wong CM, Lee JM, Ching YP, Jin DY, Ng IO. Genetic and epigenetic alterations of DLC-1 gene in hepatocellular carcinoma. *Cancer Res* 2003; **63**:7646-7651.
- Wong CM, Lee JM, Lau TC, Fan ST, Ng IO. Clinicopathological significance of loss of heterozygosity on chromosome 13q in hepatocellular carcinoma. *Clin Cancer Res* 2002; **8**:2266-2272.
- Wong N, Chan A, Lee SW, Lam E, To KF, Lai PB, Li XN, Liew CT, Johnson PJ. Positional mapping for amplified DNA sequences on 1q21-q22 in hepatocellular carcinoma indicates candidate genes over-expression. *J Hepatol* 2003; **38**:298-306.
- Wong N, Chan KY, Macgregor PF, Lai PB, Squire JA, Beheshti B, Albert M, Leung TW. Transcriptional profiling identifies gene expression changes associated with IFN-alpha tolerance in hepatitis C-related hepatocellular carcinoma cells. *Clin Cancer Res* 2005; **11**:1319-1326.
- Wong N, Lai P, Lee SW, Fan S, Pang E, Liew CT, Sheng Z, Lau JW, Johnson PJ. Assessment of genetic changes in hepatocellular carcinoma by comparative genomic hybridization analysis: relationship to disease stage, tumor size, and cirrhosis. *Am J Pathol* 1999; **154**:37-43.
- Yang J, Weinberg RA. Epithelial-mesenchymal transition: at the crossroads of development and tumor metastasis. *Dev Cell* 2008; **14**:818-829.
- Yang YF, Zhao W, Zhong YD, Xia HM, Shen L, Zhang N. Interferon therapy in chronic hepatitis B reduces progression to cirrhosis and hepatocellular carcinoma: a meta-analysis. *J Viral Hepat* 2009; **16**:265-271.
- Yilmaz M, Christofori G. EMT, the cytoskeleton, and cancer cell invasion. *Cancer Metastasis Rev* 2009; **28**:15-33.
- Yoshizawa H. Hepatocellular carcinoma associated with hepatitis C virus infection in Japan: projection to other countries in the foreseeable future. *Oncology* 2002; **62**(suppl 1):8-17.

- Yu DY, Moon HB, Son JK, Jeong S, Yu SL, Yoon H, Han YM, Lee CS, Park JS, Lee CH, Hyun BH, Murakami S, Lee KK. Incidence of hepatocellular carcinoma in transgenic mice expressing the hepatitis B virus X-protein. *J Hepatol* 1999; **31**:123-132.
- Yu MW, Chen CJ. Elevated serum testosterone levels and risk of hepatocellular carcinoma. *Cancer Res* 1993; **287**:1253-1258.
- Yu MW, Yang YC, Yang SY, Cheng SW, Liaw YF, Lin SM, Chen CJ. Hormonal markers and hepatitis B virus-related hepatocellular carcinoma risk: a nested case-control among men. *J Natl Cancer Inst* 2001; **93**:1644-1651.
- Yu S, Rao S, Reddy JK. Peroxisome proliferator-activated receptors, fatty acid oxidation, steatohepatitis and hepatocarcinogenesis. *Curr Mol Med* 2003; **3**:561-572.
- Yuen MF, Tanaka Y, Fong DYT, Fung J, Wong DKH, Yuen JCH, But DYK, Chan AOO, Wong BCY, Mizokami M, Lai CL. Independent risk factors and predictive score for the development of hepatocellular carcinoma in chronic hepatitis B. *J Hepatol* 2009; **50**:80-88.
- Zondag GC, Evers EE, ten Klooster JP, Janssen L, van der Kammen RA, Collard JG. Oncogenic Ras downregulates Rac activity, which leads to increased Rho activity and epithelial-mesenchymal transition. *J Cell Biol* 2000; **149**:775-782.